MOLECULAR BASIS OF ENE-REDUCTASES REACTIVITY AND SELECTIVITY TOWARDS NICOTINAMIDE COENZYMES

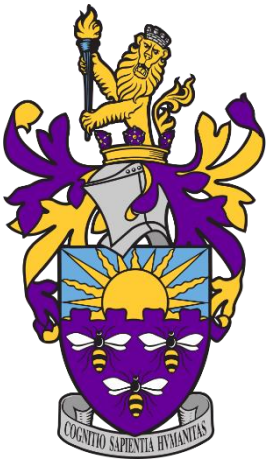

A THESIS SUBMITTED TO THE UNIVERSITY OF MANCHESTER FOR THE DEGREE OF

DOCTOR OF PHILOSOPHY

IN THE FACULTY OF SCIENCE AND ENGINEERING

2019

ANDREEA I. IORGU

SCHOOL OF CHEMISTRY

Contents

Word count: 46,767

List of figures

List of tables

Abstract

Understanding the physical basis of enzyme catalysis is critical for deciphering the physiological function of enzymes, and for driving developments in contemporary areas of research, including *de novo* enzyme design for biotechnology and synthetic biology applications. The increasing knowledge of enzyme structure and mechanisms has led to a shift in the production of fine chemicals from traditional synthetic methods to more environmentally friendly and sustainable approaches. One of the most widely employed chemical reaction in industry for which biocatalytic routes are greatly explored is the asymmetric reduction of activated C=C bonds, which can be catalysed by members of the Old Yellow Enzyme family of ene-reductases. One such member is pentaerythritol tetranitrate reductase (PETNR), a flavin mononucleotide (FMN)-dependent enzyme that uses NADPH (and, less efficiently, NADH) as ancillary hydride donor. Previous kinetic studies of PETNR have inferred that quantum mechanical tunnelling and fast protein dynamics contribute to the enzymatic hydride transfer step from NAD(P)H to the FMN cofactor. Herein, the molecular basis of PETNR reactivity and specificity towards nicotinamide coenzymes is addressed using a wide range of experimental techniques, including mutagenesis, stopped-flow rapid kinetics, X-ray crystallography, temperature dependence/kinetic isotope effect studies of reaction rates, and NMR spectroscopy. ^{1}H, ^{15}N and ^{13}C backbone resonance assignments of PETNR are reported, along with NMR studies evaluating the differences in binding modes of NADPH and NADH coenzymes to PETNR. An investigation of H-transfer mechanism in PETNR through mutagenesis of second sphere 'noncatalytic' residues (L25 and I107) is also presented, and it is the first study probing the role of (rather distal) hydrophobic side chains and dynamics in controlling rates of enzymatic H-transfer catalysed by PETNR. The last section details kinetic studies of rationally designed variants of PETNR and morphinone reductase (MR), another member of the OYE family, which enabled determination of the basis of coenzyme recognition in these two ene-reductases. The approaches developed herein should find wider application in related studies of enzymatic H-transfer reactions and coenzyme specificity studies of other OYE ene-reductases.

Declaration

No portion of the work referred to in the thesis has been submitted in support of an application for another degree or qualification of this or any other university or other institute of learning.

Copyright statement

i. The author of this thesis (including any appendices and/or schedules to this thesis) owns certain copyright or related rights in it (the "Copyright") and s/he has given The University of Manchester certain rights to use such Copyright, including for administrative purposes.

ii. Copies of this thesis, either in full or in extracts and whether in hard or electronic copy, may be made only in accordance with the Copyright, Designs and Patents Act 1988 (as amended) and regulations issued under it or, where appropriate, in accordance with licensing agreements which the University has from time to time. This page must form part of any such copies made.

iii. The ownership of certain Copyright, patents, designs, trademarks and other intellectual property (the "Intellectual Property") and any reproductions of copyright works in the thesis, for example graphs and tables ("Reproductions"), which may be described in this thesis, may not be owned by the author and may be owned by third parties. Such Intellectual Property and Reproductions cannot and must not be made available for use without the prior written permission of the owner(s) of the relevant Intellectual Property and/or Reproductions.

iv. Further information on the conditions under which disclosure, publication and commercialisation of this thesis, the Copyright and any Intellectual Property and/or Reproductions described in it may take place is available in the University IP Policy (see http://documents.manchester.ac.uk/DocuInfo.aspx?DocID=24420), in any relevant Thesis restriction declarations deposited in the University Library, The University Library's regulations (see http://www.library.manchester.ac.uk/about/regulations/) and in The University's policy on Presentation of Theses.

Acknowledgements

First and foremost, I would like to express my gratitude to my main supervisor, **Prof. Nigel Scrutton**, for granting me a position in his lab, and offering me the opportunity to work on an exciting enzymology project. I would like to thank Nigel for his guidance and support throughout this project, and for providing a working environment that allowed me to develop myself and grow as a scientist. You have given me the freedom to pursue my own ideas and work in a rather independent manner, but always made yourself available when I required guidance, and I thank you for that! I am happy that when you selected me for this project, you overlooked my slightly divergent scientific background, and you have provided the support and help for me to learn (and become enthusiastic) about biology-related disciplines. At the end of this project, I feel that I've become a jack of all trades, and master of none (which I would argue is better than a master of one).

Secondly, I am also very grateful to my co-supervisors, **Prof. Jon Waltho** and **Dr. Sam Hay**, for their fruitful discussions and contributions to my project, from assisting with experiment design to helping with manuscript preparation. A special thanks to Sam, for offering me the opportunity to work and continue research in his lab following the end of my PhD funding (Sam, please know that I bear a reasonable amount of guilt for not being able to keep the writing of this thesis completely "out of hours", and thank you for understanding).

I would like to thank **Dr. Matt Cliff** and **Dr. Nicky Baxter** for their advice and help concerning all aspects of NMR spectroscopy. Thank you Matt for assisting me to set up NMR experiments, and for the numerous tips and suggestions that enabled me to become (a little) confident with protein NMR spectroscopy. Thank you Nicky for sharing your vast expertise related to my project and for your constructive comments that brought improvements to the work presented herein. I would also like to thank **Dr. Colin Levy** for the crystallographic work presented in this thesis.

I would like to extend my acknowledgements to all past and present members of the Scrutton, Hay, Munro, Leys and Waltho groups for their warm welcome upon my

arrival in Manchester and making this PhD journey an enjoyable experience. During the last four years, we had many animated discussions, and sometimes one too many pints of beer. I would like to thank **Dr. Stefan Görlich**, **Dr. Derren Heyes** and **Michiyo Sakuma** for their support regarding many aspects of lab work. Thank you Michiyo for all the guidance regarding general lab practices, and **Dr. Alex Geddes** for walking me through protein expression and purification principles at the beginning of my studies. Particular thanks should be given to Stefan for many tips and tricks that enabled me to conduct my experiments faster (I regret you moved to Dresden shortly after we started talking and sharing many ideas, struggles, laughs and beers). Thank you Derren for being cool (I think that says it all, no description needed)! Special thanks to **Dr. Hanan Messiha** for her kind nature and to **Lesley-Ann Miller** for good chats. I would also like to thank **Sylwia Czarnota**, **Dr. Zhalgas Serimbetov** and **Dr. Stanislava Panova** for the many exciting discussions regarding NMR spectroscopy and for the energising group bantering about how protein NMR projects are *the hardest*.

I must acknowledge the generous funding provided for this project by the EU Seventh Framework Programme through the Marie Curie Initial Training Network MAGIC, and I am very grateful to **Dr. Dearg Brown** for being so approachable and providing astonishing support for the whole MAGIC network.

Many people have contributed to my personal and professional development during my previous studies (long before my arrival in Manchester four years ago), which ultimately enabled me to take become a PhD candidate and made me decide I want to pursue a scientific career. Many thanks to **Prof. Ileana Popescu (Diriga)** and **Prof. Costel Gheorghe (Dl. Director)** for putting up with me during my high school years and extending their help much above their responsibilities. I owe a good appreciation of scientific rigour to **Prof. Daniela Berger** and **Prof. Cristian Matei**. It was your welcoming nature, excitement towards scientific experiments and many hours spent in your lab that made me appreciate the academic world. I would like to thank my closest friends, **Blonda** (only the codename is needed) and **Cristina**, for always being there for me. Thank you **Mariana** and **Călin** for the support you have given me in the years preceding my PhD studies.

Last, I would like to thank my partner, **Dr. Tobias Hedison (Toby)**, for sharing every moment of this PhD journey with me. Thank you Toby for the extraordinary emotional support, patience and endless motivational speeches you have offered me. Thank you for sacrificing your time to always be there and accompany me on every path I've taken in the last four years. Thank you for all the scientific discussions and help provided with every aspect of my project, and for the evenings you waited for me to finish my experiments before we could go home. Thank you for enduring the stress that writing of this thesis inflicted at times, and for celebrating all the success of this project with me. It was amazing to take on this journey along you, during which we grew together as a couple, as people, and as scientists.

Last, to my family, thank you for always supporting my education and unquestionably assuming that I'm capable of achieving anything I've set myself up to do. This thesis is dedicated to my grandma, **Mamanu**, for the unconditional love and care she has given me from the day I was born, and for being an inspiration to me in all the ways. **Mulțumesc, Mamanu, pentru că ţi-ai sacrificat fiecare clipă a vieţii din ziua în care m-am născut pentru a îmi oferi cea mai bună educaţie posibilă.**

Preface and thesis structure

This thesis is presented in the Journal Format style with permission from The University of Manchester. Section 1 is a general introductory chapter, while the four experimental chapters (Sections 2-5) are all manuscripts published/submitted/to be submitted for publication in peer reviewed journals. Sections 6 provides a conclusion to the overall work reported in the thesis. Some aspects of Sections 2-5 might differ from the final published version of the papers in order to ensure consistency throughout the thesis.

Individual contributions to the experimental chapters are as follows:

Section 2: Isotopically labelled flavoenzymes and their uses in probing reaction mechanisms

Publication status: *under review*

Authors: Andreea I. Iorgu, Nigel S. Scrutton, Sam Hay

Contributions: A.I.I. wrote the paper, with contributions from all authors. The manuscript is a methods-focused paper, written as an invited contribution for publication in *Methods Enzymol*. A.I.I. performed all original research experiments and developed all methodologies described in this section, unless otherwise conveyed through referencing. S.H. and N.S.S. supervised the project.

Section 3: ^{1}H, ^{15}N and ^{13}C backbone resonance assignments of pentaerythritol tetranitrate reductase from *Enterobacter cloacae* PB2

Publication status: *this manuscript is published in Biomolecular NMR Assignments* **2018**, 12, 1, 79-83.

Authors: Andreea I. Iorgu, Nicola J. Baxter, Matthew J. Cliff, Jonathan P. Waltho, Sam Hay, Nigel S. Scrutton

Contributions: A.I.I. wrote the paper, with contributions from all authors. A.I.I. conducted all experiments, with help from M.J.C and N.J.B. for NMR data acquisition and interpretation. J.P.W., S.H. and N.S.S. conceived and supervised the project.

Section 4: Nonequivalence of second sphere 'noncatalytic' residues in pentaerythritol tetranitrate reductase in relation to local dynamics linked to H-transfer in reactions with NADH and NADPH coenzymes

Publication status: *a revised version of this manuscript is published in ACS Catalysis* **2018**, 8, 12, 11589-11599

Authors: Andreea I. Iorgu, Nicola J. Baxter, Matthew J. Cliff, Colin Levy, Jonathan P. Waltho, Sam Hay, Nigel S. Scrutton

Contributions: A.I.I. wrote the paper, with contributions from all authors. A.I.I. conducted all experiments and analysed all the data, except for the crystallography (which was performed by C.L.). N.J.B. and M.J.C. helped with NMR data acquisition and interpretation. J.P.W., S.H. and N.S.S. designed and supervised the project.

Section 5: Selectivity through discriminatory induced fit enables switching of NAD(P)H coenzyme specificity in Old Yellow Enzyme ene-reductases

Publication status: *under review*

Authors: Andreea I. Iorgu, Tobias M. Hedison, Sam Hay, Nigel S. Scrutton

Contributions: A.I.I. wrote the paper, with contributions from all authors. A.I.I. conducted all experiments and data analysis. T.M.H. helped A.I.I. with data analysis and interpretation. A.I.I. designed the project, under supervision of S.H. and N.S.S.

1. Introduction

Understanding the physical basis of enzyme catalysis is a central goal of modern enzymology, and it could further development in contemporary areas of research, such as biotechnology and synthetic biology. Much or our understanding of enzyme function is derived from traditional biochemical kinetic studies, and it is now exponentially amplified by the large availability of novel cell biology, spectroscopic and crystallographic techniques. We are getting closer and closer to develop (bio)physical models that provide answers to the central fundamental question that concerns every enzymologist: *What makes enzymes Nature's best catalysts?* However, is it likely that the answer might not be universal, as a growing number of studies are unravelling an expanding complexity of physical phenomena governing enzyme catalysis. This thesis is only a small contribution towards understanding the physical basis of enzyme catalysis (and, naturally, adding a bit more complexity to it), and dives into using this understanding for contemporary goals, such as developing better biocatalysts. In particular, the thesis addresses the molecular basis of ene-reductases reactivity and specificity towards nicotinamide coenzymes. This introductory section, far from being exhaustive, provides general context to the experimental work undertaken.

1.1. Background

Proteins are one of the four classes of biomacromolecules essential for life. Acting as sophisticated molecular machines, proteins are involved in virtually every biological process, from maintaining the electrochemical potential across cell membranes[1] to catalysing a myriad of chemical reactions that make up the cellular metabolism.[2,3] At primary level, proteins can be defined as a series of L-amino acids sequentially linked through peptide bonds in a definite sequence. Almost universally, this amino acid sequence, and mainly the arrangement of the amino acid side chains, determines the unique three-dimensional (3-D) structure of each protein, also known as the native state of the protein (*i.e.* the folded operative form that provides the protein function).[4] Protein folding happens concomitantly to protein synthesis (translation)

at the ribosome, and it is characterised by a specific conformational sampling processes through a rugged energy landscape, which allows for the energy-rich, disordered polypeptide chain to adopt a defined 3-D structure characterised by a free energy minimum.[5–9] The molecular understanding of protein folding, structure and function was revolutionized by the seminal X-ray crystallography studies performed on myoglobin, the first globular protein for which a 3-D model was proposed in 1958.[10] Apart from being a stepping stone to a whole new field of structural protein studies by X-ray diffraction, this pivotal work anticipated the intricacies of protein folding that are still baffling scientists. Referring to the structure of the small globular myoglobin protein, Kendrew *et al*. wrote: "Perhaps the most remarkable features of the molecule are its complexity and its lack of symmetry. The arrangement seems to be almost totally lacking in the kind of regularities which one instinctively anticipates, and it is more complicated than has been predicated by any theory of protein structure".[10] Since the first pioneering insights into the tertiary and quaternary features of proteins,[10–12] the development of state-of-the-art X-ray crystallographic methods and equipment, as well as the advances in novel structural biology techniques, such as nuclear magnetic resonance spectroscopy (NMR) and electron microscopy, have furthered our understanding of protein structure. However, despite this wealth of structural data (> 100,000 protein structures in the Protein Data Bank[13]), the prediction of protein folding from amino acid sequence is still a major challenge for structural and computational biologists.[14] Moreover, the prediction of protein function from structure is equally challenging.[15,16]

A particularly important class of proteins are the enzymes, which provide the essential role of catalysing chemical reactions in cells. Enzymes are able to catalyse biochemical reactions with extraordinary selectivity and specificity and, in some cases, with extreme efficiency (rates > 10^{21} order of magnitude higher than for the non-catalysed solution reaction have been reported).[17–19] Intrinsically, understanding the physical basis of enzyme catalysis is critical for deciphering the physiological function of enzymes, and for broader scope, such as in drug discovery and for driving developments in contemporary areas of research, including *de novo* enzyme design for biotechnology and synthetic biology applications. Similar to all

protein-ligand interactions, the mechanism of interaction of an enzyme with its substrate has been historically described by two main models. The “lock-and-key” model, which was initially proposed by Fischer in 1894, emphasized the importance of shape complementarity between the two structures.[20] However, the observed structural changes between the bound form of a protein and the unbound, ligand-free form, indicated the invalidity of this early model of enzymatic catalysis, and led to the proposition of the “induced fit” model by Koshland in 1958.[21] This latter model accounts for this type of plasticity (flexible binding of proteins), in which the ligand is postulated to induce a conformational change at the interaction site upon binding. Although the latter accounts for protein conformational changes, both models suppose that proteins exist in a single, defined stable conformation. However, proteins have been observed to sample a vast ensemble of conformations,[22] and are now accepted to have inherent “dynamic personalities”.[23–32] Thus, the alternative “conformational selection” model for protein-ligand interactions has emerged, which accounts for the conformational heterogeneity of proteins in solution, and proposes that higher energy conformations (though less populated) could be responsible for ligand recognition.[33] Overall, this shift in concept illustrates the gradual recognition of dynamic contributions to protein function and enzyme catalysis.[34–38]

When it comes to understanding the (sometimes astonishing) efficiency of enzymes at catalysing chemical reactions, Pauling’s transition state (TS) theory is the best known model of enzyme action.[39] The trajectory of a chemical reaction, i.e. substrate-to-product transformation, is accepted to (almost always) involve passing through a transition state, which can be defined as an unstable structure poised between the chemical structures of the substrates and products.[40] The TS can be regarded as the configuration along the reaction coordinate that bears the highest potential energy. Enzymes are recognised to work by lowering the activation energy of a chemical reaction (Figure 1.1), and their mechanism of action is known to involve stabilization of the transition state through electrostatic contributions and hydrogen bonding.[41–43]

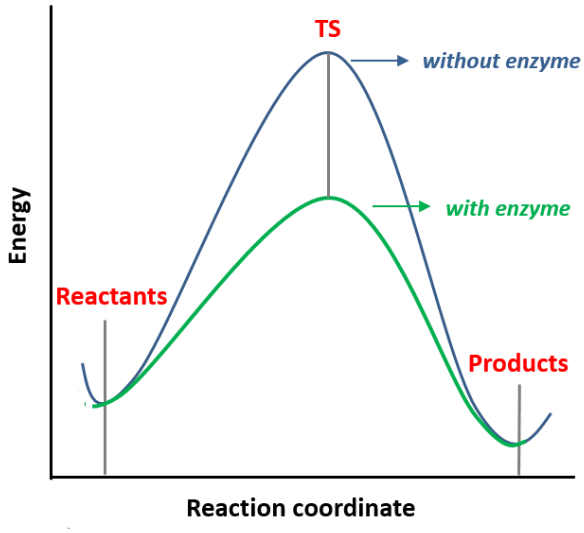

Figure 1.1. The classical transition state theory model of catalysis. The curves represent a two-dimensional potential energy surface for an enzymatic catalysed reaction (green) and for the same chemical reaction in solution (blue). The energy maxima along the reaction coordinate is the transition state (denoted TS). According to the TS theory, the enzyme contributes to catalysis by stabilizing the TS, thus lowering the energy required by the reactants to reach TS.

The transition state is thought to be essential for the biological function of enzymes, so the design of TS analogues as powerful enzymatic inhibitors is one of the most researched avenues in pharmaceutical industries (as up to one-third of current drugs act as enzyme inhibitors).[44–46] Enzyme transition states are, however, very short lived, having typically femtoseconds (fs) lifetimes (the time required for bond breaking/formation and electron distribution),[47,48] while the functional turnover number of an enzyme is usually 10^{12} longer, often on the millisecond (ms) timescale.[44] While characterisation of the catalytic turnover of an enzyme can be done effortlessly in most of the cases, the very short lived nature of the TS makes it highly challenging to trap actual enzymatic TS complexes using available crystallographic techniques (though a recent study making use of genetically encoded noncanonical amino acids exemplifies the direct observation of the TS for biphenyl bond ration in a computationally designed protein[49]).

From the first proposition in 1958 by Koshland of the “induced fit” model for protein-ligand interactions,[21] a growing number of experimental studies (often supported by computation) have indicated the contribution of protein dynamics in enzyme

turnover.[50–59] However, the study of protein dynamics is still a challenging area of research, as conformational changes can occur over a broad range of timescales and directionalities, and no single spectroscopic method can cover the whole fs-s array whilst allowing atomic visualisation of a molecule (Figure 1.2).

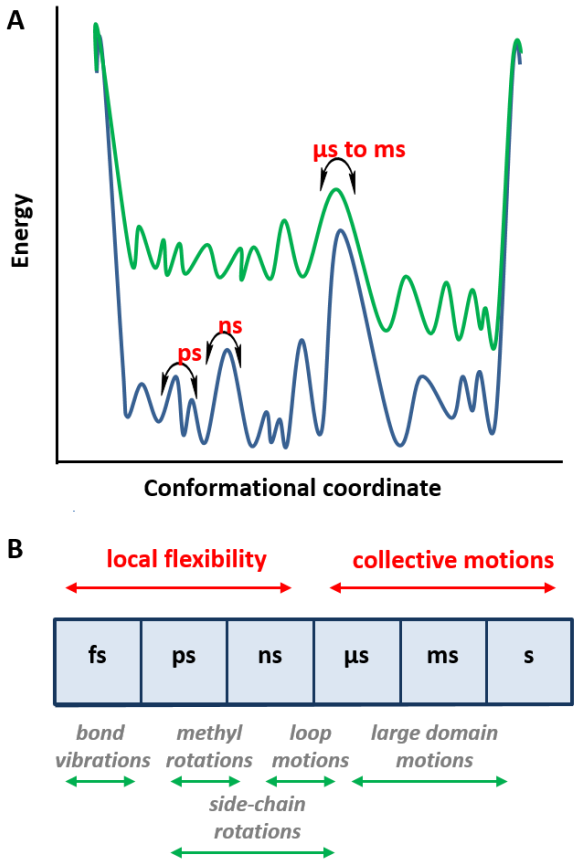

Figure 1.2. The energy landscape of a protein represented through the amplitude and timescale of protein motions. (A) One-dimensional cross section of the multidimensional energy landscape of a protein. The equilibrium between two conformational states (depicted herein in blue and green) can be perturbed by temperature, pressure, mutagenesis, ligand binding, etc. (B) Timescale of dynamic processes in proteins.

Slow (ms-s) protein conformational transitions have been shown to facilitate gating of chemical steps and substrate binding/products release steps, through productive positioning of cofactors, catalytic residues or inorganic ions. These type of motions, often attributed to large-scale protein domain motions, have been often identified using NMR methodologies.[60,61] In contrast, the role of fast protein motions, occurring on the picosecond-nanosecond (ps-ns) timescale, in enzymatic catalysis is more

contentious, as currently available spectroscopic probes are not allowing their direct observation. Therefore, direct coupling of fast (fs-ns) dynamics to chemistry is mostly inferred from kinetic isotope effect (KIE) studies and predicted by computational analysis such as transition path sampling,[62–67] but this area of research is still under intensive debate (with others questioning the validity of models of catalysis involving dynamic contributions[68–70]). Regardless, it is becoming rather apparent that our inability to predict protein folding from amino acid sequence or protein function and enzymatic mechanisms from structure is highly related to our limited understanding of the contribution of protein dynamics to all these (bio)chemical events.

1.2. Fast protein dynamics and biological hydride transfer

Hydrogen transfer is one of the most ubiquitous biological reactions. In recent years, particular attention has been given to assess relative contributions of protein dynamics to enzymatic catalysis involving hydrogen transfer steps. Biological hydrogen transfer can refer to the transfer of a hydride, a hydrogen atom or a proton. Hydride transfer (further denoted as H-transfer) is usually defined as the transfer of two electrons and one proton from a donor molecule to an acceptor molecule. This definition distinguishes hydride transfer from two other similar biological reactions, hydrogen atom transfer (involving transfer of one proton and one electron from a donor to an acceptor) and proton-coupled electron transfer (PCET, involving the coupled transfer of protons and electrons coming from different donors to an acceptor).[71] The properties of hydrogen, relating to the wave-particle duality of matter and largely dictated by its small mass, enable effects such as quantum mechanical tunnelling (QMT) to play important roles in H-transfer catalysis. Tunnelling can be described as a phenomenon in which a particle crosses the energy barrier between the reactant and products without needing to acquire the energy required to reach the TS (Figure 1.3). Tunnelling is a mass-dependent phenomenon often investigated through KIE studies, the measure of ratio of reaction rates using different isotopes (e.g. hydrogen/deuterium).[72]

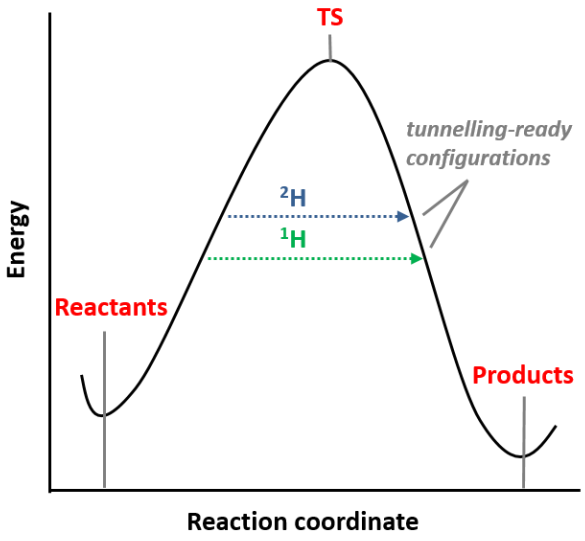

Figure 1.3. Simplified illustration of quantum mechanical tunnelling in enzymatic H-transfer. The classical view of TS theory considers reactions proceed by overcoming an energy barrier, equal to the difference between the energy of the TS and the ground state of the reactants. Thus, the rate determining factor is given by this energy difference (the height of the potential energy barrier). Contrary, QMT supposes the crossing of a particle through the potential energy barrier, as an effect of the wave-particle duality formalism, making the width of the barrier the key determinant of the reaction rate. As a mass dependent phenomenon, tunnelling is less likely for a heavy isotope (^{2}H, blue dashed line) than for a ^{1}H (green dashed line). Thus, QMT explains what gives rise to elevated KIEs. The ensemble of reactants that achieve the energetics and distances compatible with tunnelling is often referred to as "tunnelling-ready" configurations.

The enhancement of enzymatic reaction rates as a results of significant QMT contributions cannot be readily explained by the TS theory, which led to the emergence of many theories that consider QMT of the transferred particle.[73] It is now widely accepted that quantum mechanical tunnelling (QMT) plays an important role in enzymatic reactions.[74] In recent years, new theoretical frameworks that couple QMT with protein motions have been developed.[75–78] Temperature dependence studies of kinetic isotope effects (KIEs) for many biological reactions have shown that KIE values exhibited cannot be explained by corrected transition states theories that take into account QMT. Thus, new models such as the environmentally coupled hydrogen tunnelling models have been developed, which take into consideration the contribution of protein dynamics to the reaction rate.[78] Although there is a general acceptance (with few exceptions[79]) of the contribution

of H-tunnelling to the reaction rate of enzymatic reactions, the role of protein motions in catalysis is still under debate.[69,70]

The majority of studies that infer a direct coupling between fast (fs-ns) protein dynamics and reaction chemistry are based on the interrogation of reaction mechanisms through the use of kinetic isotope effects (KIE), and are often supported by computational analysis such as transition path sampling. Overall, experimental work involves perturbation of dynamics modes through mutagenesis and through mass perturbation. The use of isotopically labelled substrates to probe reaction mechanism has the major advantage of offering special resolution, as deviations in kinetics can be directly attributed to perturbation induced by the isotopically substituted atom. Moreover, the temperature dependence of KIEs on reaction kinetics is the most widely used probe of quantum mechanical tunnelling (QMT) in H-transfer reactions. Some interpretations of the temperature dependence of KIEs have inferred a role for distance sampling dynamical contributions to facilitate the tunnelling reaction.[65–67,80,81] The temperature dependence of the KIE has also been attributed to modulation of donor-acceptor distance (DAD) distributions and perturbation of high-frequency motions, or disruption of dynamic networks that extend to remote residues within the enzyme.[82,83] Many of these studies involved variant enzymes, which have also been used to perturb active site structure and probe effects on reaction mechanism/dynamical contributions using a number of enzyme systems. Several studies have addressed these topics, and model enzyme systems that have been probed through mutagenesis include dihydrofolate reductase, soybean lipoxygenase-1, thymidylate synthase and morphinone reductase.[84–88] More recently, experimental KIE measurements have been diversified through the use of high pressure and “heavy enzymes” (^{2}H, ^{13}C, and/or ^{15}N isotopically labelled enzymes).[89–96] For the particularities of H-transfer reactions, it can be observed that the debates regarding the role of protein dynamics in these reactions are only challenging the development of better experimental and theoretical tools to address this topic.[64,97]

1.3. The versatility of flavin cofactors and flavoenzymes

A vast proportion of enzymes require cofactors to be functional. Cofactors can thus be defined as "co-catalysts" that are required for the activity of an enzyme, and can be broadly classified in two groups: coenzymes (organic non-protein molecules that are released during the catalytic cycle, e.g. NAD(H) and NADP(H)) and prosthetic groups (small molecules bound to the protein, often in a non-covalent manner). With an estimated 1% of the total eukaryotic and prokaryotic genome encoding flavin-binding proteins, flavin cofactors are one of the most prevalent prosthetic groups found in proteins.[98–100] Flavin-binding proteins are at the heart of a plethora of biological redox reactions, and are recognised to be involved in a wide variety of biological processes, such as protein folding, cell signalling, cell metabolism, immune defence, drug and xenobiotic metabolism, chromatin modification, biodegradation, DNA repair, energy production, light sensing and apoptosis.[99,101–105]

Flavins cofactors are derived from riboflavin (vitamin B2) and have a yellow colour in their oxidised state. The two well-characterised flavin cofactors are flavin mononucleotide (FMN) and flavin adenine dinucleotide (FAD),[105,106] with their structure shown in Figure 1.4. More recently, a third type of flavin cofactor (prenyl-FMN) has been discovered.[107–109] Prenyl-FMN is used by members of the UbiD family of reversible decarboxylases, which have been observed to be involved in ubiquinone biosynthesis, biological decomposition of lignin, and biotransformation of aromatic compounds.[110] The catalytic core of flavin cofactors is the tricyclic dimethyl-isoalloxazine ring, with the N5, C4a, C10a and N1 atoms as catalytically reactive positions (Figure 1.4), while the additional functional groups are typically responsible for anchoring the cofactor in the active site of the protein. Both FMN and FAD contain the flavin, ribitol and phosphate moieties, with FAD having an additional adenosine monophosphate (AMP) moiety. Even though they share the same catalytic core (the flavin isoalloxazine ring system), flavoenzymes are highly distinct from other cofactor-dependent enzymes, as they are involved in varied biological processes (while other cofactor-dependent systems are known to catalyse similar type of chemical reactions). This versatility of flavins is a result of the interaction of the

molecule with the active site of the protein. Flavins are typically found in non-covalent attachment to their respective apoproteins, but covalent interactions between active-site residues (tyrosine, histidine or cysteine) and the flavin cofactor have also been observed.[105]

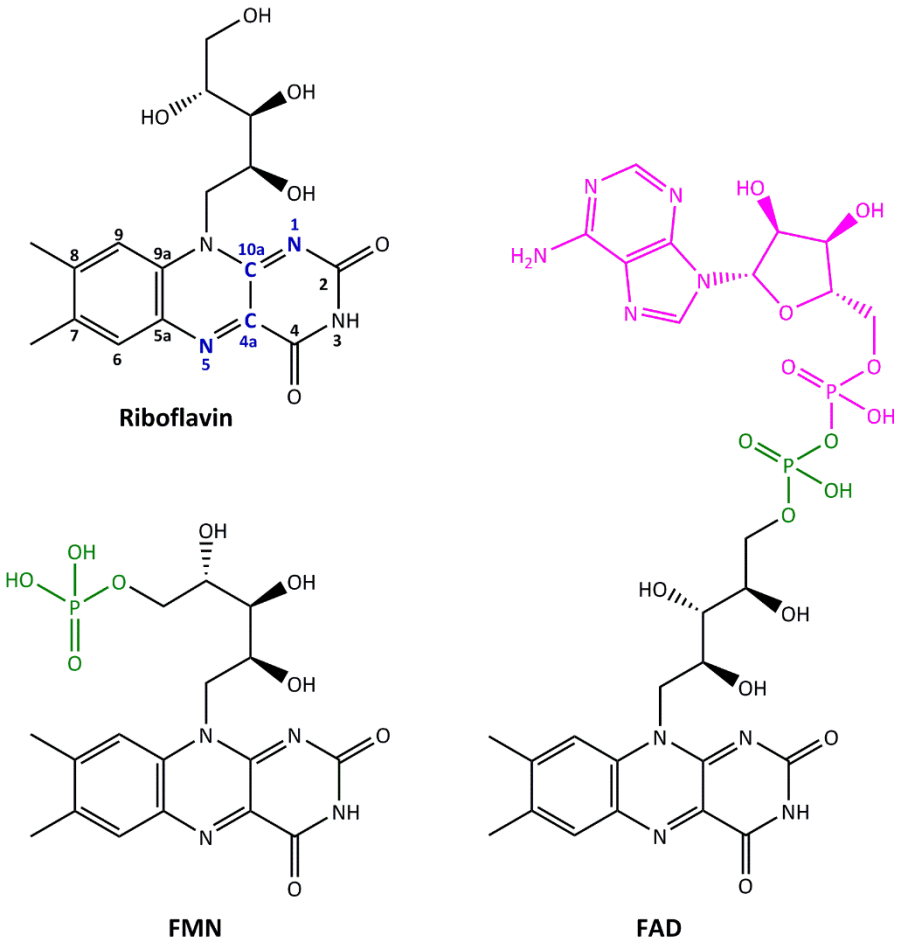

Figure 1.4. The structure of natural flavins. The atomic numbering of the isoalloxazine ring (oxidized state) is shown on the riboflavin structure and the most relevant reactive atoms are highlighted in blue. The differentiating moieties of FMN and FAD cofactors are shown in green and pink, respectively.

Flavoenzymes have been traditionally defined as oxidoreductases that require the flavin prosthetic group for their biological activity. While it is true that, for most of flavin-bound enzymes, the catalytic cycle consists of the oxidation of substrate, followed by the reaction of the reduced flavin with an electron-accepting substrate, (e.g. oxygen, which regenerates the oxidized state), the definition of flavoenzymes as oxidoreductases might be an oversimplification, given the broad variability of this

redox model. Regardless, a general catalytic cycle for flavoenzymes can be described by two half-reactions – a reductive and an oxidative half reaction, during which the flavin alternates between oxidized and reduced states (Figure 1.5).[111] Typically, in the reductive half reaction (RHR), an electron/hydride donor (e.g. NADH) reduces the flavin cofactor, while the oxidative half reaction (OHR) involves electron/hydride transfer from the reduced flavin to an electron accepting partner (e.g. molecular oxygen). Depending on the substrate, enzyme and environmental factors (such as pH), the catalytic cycle of flavoenzymes can occur either through a ternary complex or a bi-bi ping-pong mechanism.[98] In the ternary complex, the electron acceptor reacts with the enzyme-product complex of the RHR, while the ping-pong mechanism involves reaction of the electron acceptor species after subsequent to product release.

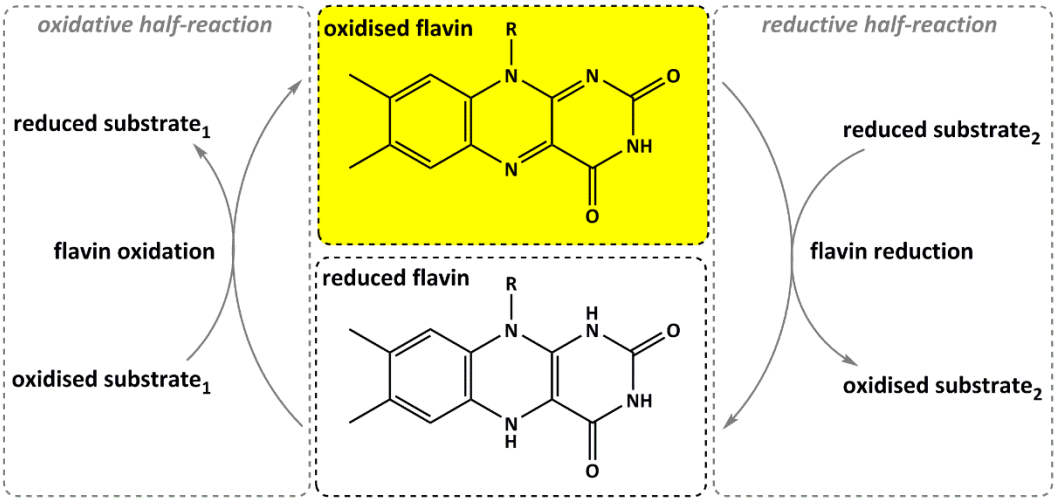

Figure 1.5. The general catalytic cycle of flavoenzymes, comprising of a reductive half-reaction and an oxidative half-reaction.

The versatility of flavins could be considered intriguing, given they all share the same isolloxazine ring system. However, it is the complexity of the isoalloxazine heterocycle that enables flavoenzymes to accept so many diverse substrates and perform such distinct reaction chemistries, coupled with the ability of the flavin molecule to exist in various redox and protonation states (Figure 1.6).[112,113] This diversity is also augmented by the protein environment surrounding the flavin

cofactor, with hydrogen bonding, π-stacking, hydrophobic interactions and solvent accessibility ultimately governing flavin chemistry.[98,114]

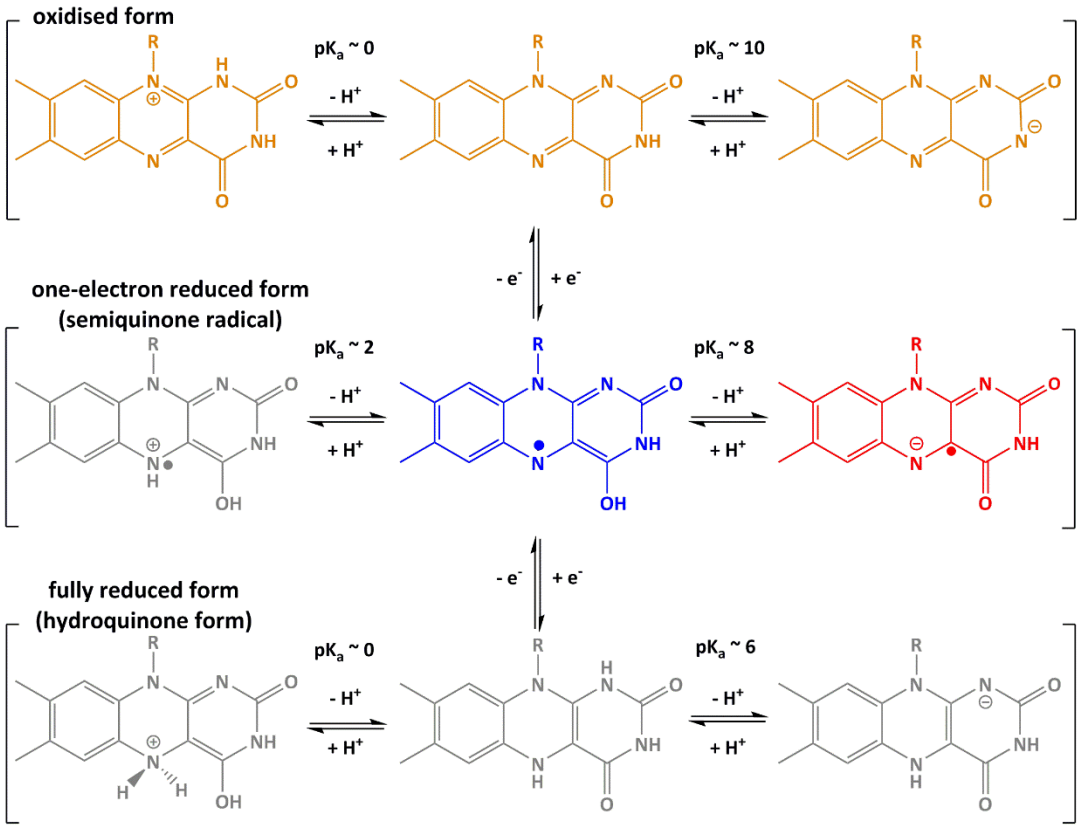

Figure 1.6. The different redox and protonation states of flavin cofactors.

Another special feature of flavin chemistry is their ability to react with molecular oxygen.[115] Thus, flavoproteins have been traditionally classified based on their reactivity towards molecular oxygen, and three main groups are defined based on the rate of reaction with O_2 and the nature of the product. The first group comprises the flavin-dependent dehydrogenases/reductases, which do not react with O_2, or react very slowly to form H_2O_2 (or less often, a superoxide anion such as $O_2^{-\bullet}$) as reaction product.[115] The second and third groups comprise of the oxidases and monooxygenases, which readily react with molecular oxygen to form the oxidised flavoprotein and convert their substrates (typically amino acids or amines). Flavin-dependent oxidases use O_2 as an electron acceptor to produce H_2O_2, while monooxygenases react with O_2 to yield a C(4a)−(hydro)peroxide flavin intermediate, which is subsequently used to insert an oxygen atom in the substrate, while

concurrently reducing the other oxygen atom to water.[115] Compared to the latter classes, the lack of sensitivity of flavin-dependent dehydrogenases/reductases towards molecular oxygen enables these enzymes to catalyse complex redox reaction without the formation of radical oxygen species.

Apart from being involved in a plethora of vital biological processes, which has driven a lot of research into understanding mechanistic aspects of catalysis, flavoenzymes are highly important for more contemporary scopes, as their versatility indicates suitability for use in biocatalytic processes.[114] In particular, ene-reductases from the Old Yellow Enzyme family of oxidoreductases are one of the classes of flavin-dependent proteins widely studied for their biocatalytic potential, and more details regarding their structure and mechanism is provided in the following subsection.

1.4. The Old Yellow Enzyme family of ene-reductases

Several families of enzymes are able to catalyse the stereoselective reduction of alkenes bearing an electron-withdrawing group (EWG). These enzyme families are known under the umbrella term of "ene-reductases" (ERs).[116–118] The large majority of ERs belong to the NAD(P)H-dependent (NADPH- or/and NADH- dependent), FMN-containing Old Yellow Enzyme (OYE) family of oxidoreductases.[118] OYEs possess a very broad substrate scope, and preferentially catalyse the reduction of α,β-unsaturated compounds bearing aldehydes, ketones or nitro functions as EWG.[118] The oxygen-sensitive clostridial enoate reductases (which contains FAD- and [4Fe−4S]- prosthetic groups) are another family of ERs, which show high specificity for substrates with carboxyl or ketone functionalities (rather weak EWG).[119,120] Other known ERs are flavin-independent enzymes that belong to the leukotriene B4 dehydrogenase subfamily of medium-chain dehydrogenases/reductases and the salutaridine/menthone reductase-like subfamily of short-chain dehydrogenases/reductases, enzymes that prefer aromatic and monocyclic alkenes bearing aldehydes or ketones EWG as substrates.[121,122]

The asymmetric reduction of activated C=C bonds is a widely employed chemical reaction in industry for which biocatalytic routes are intensively explored. This shift

from traditional synthetic methods to more environmentally friendly and sustainable approaches in the production of chemicals has been driven by increasing knowledge of enzyme structure and mechanisms, augmented by developments in metabolic engineering and synthetic biology techniques.[123–126] Therefore, extensive research has been dedicated to the use of ERs for the manufacture of fine chemicals. More and more studies have investigated the use of ERs as potential catalysts in individual biocatalytic reactions[127], as part of enzymatic and chemo-enzymatic cascade reactions,[128–133] , in whole cell biotransformation reactions, and in integrated synthetic biology pathways.[134–136] ERs have also been the subject of many studies dedicated to improving the chemo-, regio-, and stereoselectivity of target compounds, or expanding the substrate scope for asymmetric bioreductions through site-directed mutagenesis.[137–146]

As mentioned above, the majority of known ene-reductases are homologues of the OYE family of oxidoreductases. This family of ERs is named after its first discovered member, known as old yellow enzyme (OYE1), which was isolated from *Saccharomyces pastorianus* in 1932.[147] OYEs are a large family of FMN-dependent enzymes that use NADH or NADPH nicotinamide coenzymes as ancillary hydride donors (see Figure A1 in Appendix for chemical structures of the coenzymes). Phylogenetic analysis of 63 members of this family[148] revealed that OYEs can be classified in three classes (an updated view compared to the previous thermophilic-like' and 'classical' OYEs classification[149]). Class I consists mainly of monomeric OYEs originating from plants and bacteria that prefer α-methylated enones as substrates. Members of this class include pentaerythritol tetranitrate reductase (PETNR) from *Enterobacter cloacae* PB2 and morphinone reductase (MR, name given for its ability to reduce morphinone, see Figure A2 in Appendix) from *Pseudomonas putida* M10 (both classified as EC 1.6.99.1). Based on this classification, class II OYEs are mainly derived from fungal species (e.g. OYE1), and suggested to have developed in a co-driven evolution from class I. The last class comprises mostly of thermophilic-like and mesophilic OYEs (such as thermophilic old yellow enzyme, TOYE, from *pseudethanolicus* E39) that could have evolved convergent to class I/II, preferring maleimides as substrates and forming high oligomeric species in solution.[148]

OYEs share a common $(\alpha,\beta)_8$-barrel structural scaffold (a tertiary fold consisting of an 8-fold repeat of linked α-helix and β-sheet structures), also known as triosephosphate isomerase (TIM) barrel.[106,150,151] The particular features of this fold are represented by the radial arrangement of the α,β-units around a central axis, with the α-helices located on the outside of the barrel structure (being mainly solvent-exposed) and the β-sheets creating an inner hydrophobic cavity (Figure 1.7). The wide-open active site pocket of OYEs is mainly assembled with aromatic residues and it is located at the C-terminal end of this hydrophobic cavity, which contains the non-covalently bound FMN cofactor.[152,153] The *re* side of the flavin prosthetic group is in contact with strand β1 and facing the protein (completely hidden from the active site), while the *si* side is facing the solvent access channel comprising the active site.[154] Homologues of this family also share another structural feature, consisting of a large polypeptide excursion between β3 strand and α3 helix of the TIM barrel structure (Figure 1.7). This latter feature is, however, less conserved in terms of structural identity (with variants encompassing β-hairpin structural motifs or limited helical features[148]), but is theorised to regulate substrate entry to the active site.

Despite sharing a highly conserved monomer architecture (the TIM barrel fold), OYEs members show rather diverse oligomeric states (ranging from monomeric solution states to dodecameric quaternary arrangements), and possess limited conservation of sequence identity (with < 15% residues conversed across all three classes).[116,118,148] However, the residue similarity is more accentuated in the active site pocket. For example, the FMN cofactor is tethered by an extensive network of hydrogen bonds with the side chains of Thr/Cys26, His191, Arg243 and Arg348 in OYE1, and similar residues can be identified in the majority of OYE homologues.[154] Moreover, the His191/Asn194 pair (OYE1 numbering) is known to be involved in binding of both the reductive and oxidative substrates.[155] The His191 residue is fully conserved across all OYEs, while the Asn194 (present in OYE1 and MR) is replaced with a histidine for other homologues, such as PETNR.[148] Other moderately conserved residues include Tyr196, observed to function as the proton donor for the oxidative half-reaction in some cases (e.g. in the catalytic cycle of OYE1[156]).

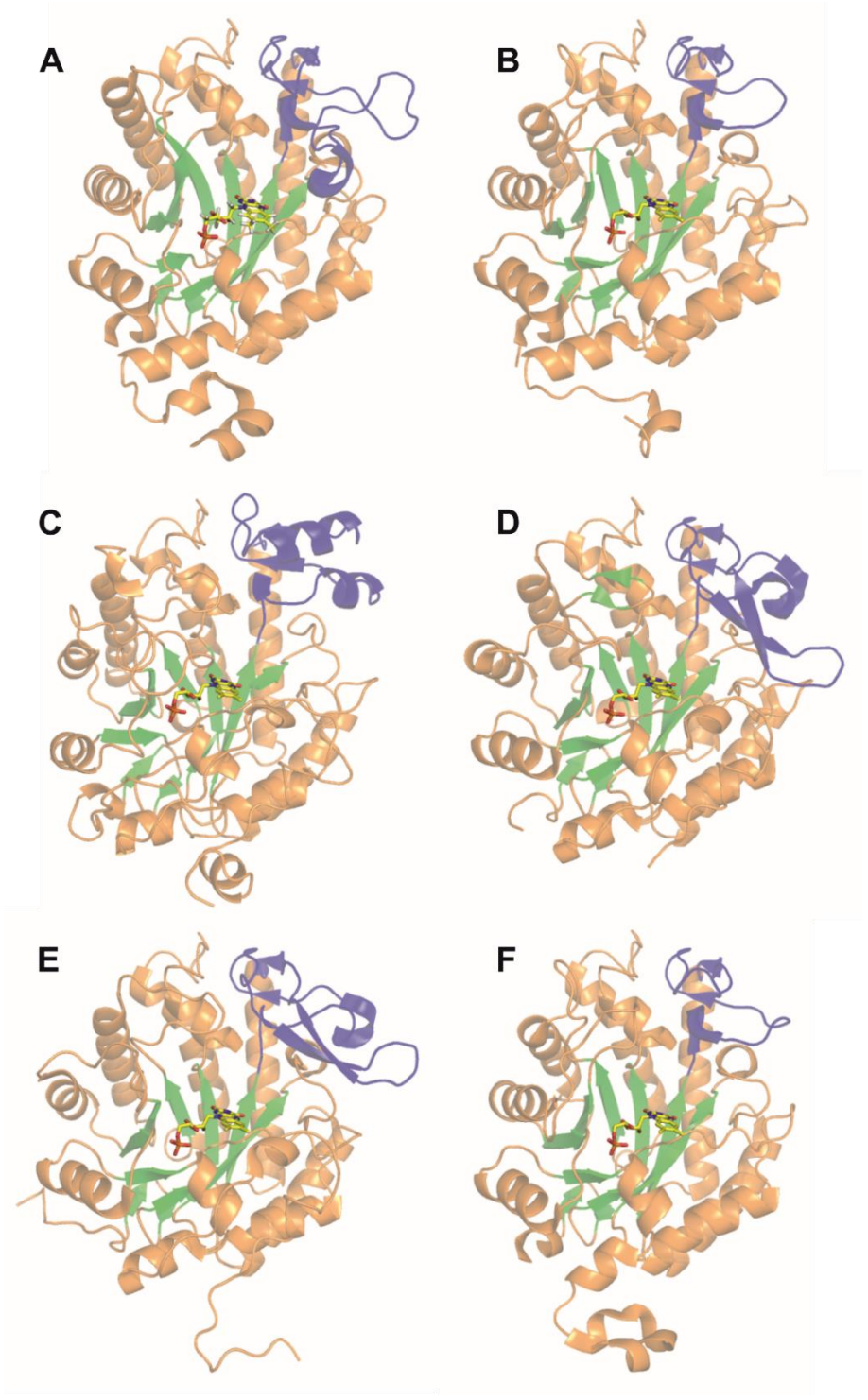

Figure 1.7. Structural architecture of OYE ene-reductases. Several representative enzymes from this family are shown: (A) XenA (PDB:3L5L), (B) YqjM (PDB:1Z41), (C) OYE1 (PDB:1OYA), (D) PETNR (PDB:5LGX), (E) MR (PDB:1GWJ) and (F) TOYE (PDB:3KRU). The structure of the OYEs is illustrated in cartoon form (coloured orange, with the β-sheets shown in green, highlighting the TIM-barrel architectural fold). The FMN cofactor is shown as yellow sticks, and the polypeptide excursion between the β3 strand and α3 helix of the TIM barrel is shown in blue.

The catalytic cycle of OYEs occurs by a single-site ping-pong mechanism, comprising of a reductive half-reaction and an oxidative half-reaction, in the same manner as described in Section 1.3 for all flavoenzymes. In particular, the RHR in OYEs consists of hydride transfer from the C4 *pro*-R hydrogen atom of the NAD(P)H coenzyme to the N5 atom of the FMN cofactor,[157] while the OHR comprises transfer of reducing equivalents from FMN to an oxidizing substrate, typically an α,β-unsaturated alkene (Figure 1.8).

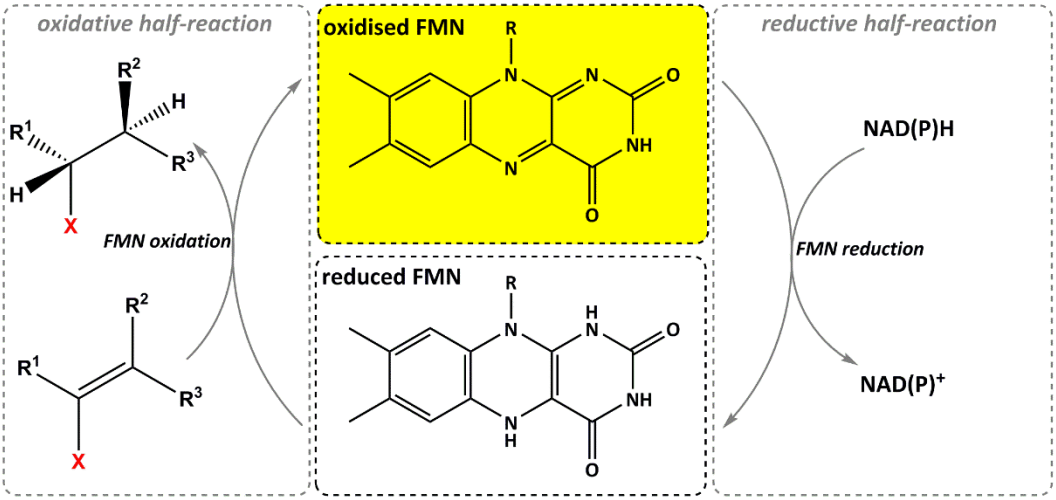

Figure 1.8. General catalytic cycle of OYE ene-reductases, comprising of a reductive half-reaction and an oxidative half-reaction. The RHR is represented by H-transfer from a nicotinamide coenzyme to the flavin cofactor, while the OHR comprises of asymmetric hydrogenation of an α,β-unsaturated substrate bearing an electron-withdrawing group (denoted as X).

The catalytic mechanism has been thoroughly investigated in many OYEs, as many of these steps can be readily observed using UV-vis spectroscopic techniques (in particular, stopped-flow spectroscopy), given the colour transition of the FMN cofactor from yellow (in oxidized form) to almost colourless (in reduced form). Briefly, the initial step of coenzyme binding can be observed by the formation of a charge (CT) transfer complex that absorbs light in the 520-600 nm range when rapidly mixing an OYE with the NAD(P)H.[158–160] The increase in absorbance at ~ 555 nm upon coenzyme binding can be tracked experimentally, enabling determination of the rates of CT complex formation (which are normally > 100 s^{-1}).[159] Moreover, the relative change in the extinction coefficient at 555 nm was reported to correlate with changes in the donor-acceptor distance in the enzyme:coenzyme complex, which

enables deeper understanding of the reaction chemistry.[161] Upon formation of the CT complex, the hydride transfer between coenzyme and the FMN cofactor takes place, which can be kinetically resolved from the decay in absorbance at 464 nm, the spectral characteristic maxima for protein-bound FMN.[158,160] Prior to the OHR, dissociation of the $NAD(P)^+$ from the active site takes place. Next, hydride transfer from the reduced FMN cofactor (along with proton transfer from an active site residue or bulk solvent) to the α,β-unsaturated substrate closes the catalytic cycle, restoring the oxidised form of the enzyme.

The versatility of OYEs comes from their remarkable ability to accept a very wide range of oxidising substrates. The main requirement for the substrate is the presence of activating electron-deficient group. OYEs have been observed to drive the reduction of α,β-unsaturated aldehydes, ketones, carboxylic acids, and other substrates, such as nitrate esters, nitroaromatic explosives and cyclic triazines.[117,149] During reduction of an α,β-unsaturated substrate, the activating EWG facilitates the asymmetric reduction of the C=C bond, with a *trans*-addition of 2 H: the proton from the N5 atom of the reduced FMN is transferred to the Cβ of the substrate and a protein/solvent-derived proton is transferred to the Cα atom.[149] This step is the slowest in the reaction cycle, and considered rate-limiting in the catalytic turnover of OYEs.

1.5. Pentaerythritol tetranitrate reductase

PETNR is a monomeric 40 kDa flavoenzyme and is one of the well-characterised members of the Old Yellow Enzyme family of ene-reductases. PETNR was originally isolated from an *Enterobacter cloacae* PB2 strain, a bacteria that was thriving on soil contaminated with explosives.[162] The name of the enzyme was given upon observation of its ability to degrade nitrate esters, such as pentaerythritol tetranitrate (PETN, see Figure A2 in Appendix), and to use these explosive substrates as sole source of nitrogen. Similar to the OYE class of enzymes, catalysis by PETNR takes place via a ping-pong mechanism, using NADPH as the preferred hydride donor source. However, PETNR has dual-specificity, as it can also be reduced by NADH (although less efficiently). As for the majority (if not all) of the enzymes belonging to

the OYE family, the specific biological role and physiological substrate for PETNR are unknown. Nevertheless, PETNR possesses a broad substrate specificity, and it can catalyse the reduction of a wide variety of α,β-unsaturated compounds, often with high enantioselectivity towards desired products.[138,163,164] The substrate scope includes 2-cyclohexenone (a highly generic target for many OYEs, see Figure A2 in Appendix), several steroids, cyclic triazines, various explosives (e.g. PETN, trinitrotoluene) and nitrate esters (e.g. nitroglycerin).[145] Moreover, several studies have shown that broadening of the substrate scope for asymmetric bioreductions, as well as improvements in the chemo-, regio- and stereoselectivity of target compounds, can be achieved through mutagenesis of relevant active-site residues.[138] This versatility of PETNR, along with its high stability and ease of production, offers it high potential to be used in biocatalytic processes.

The crystal structure of PETNR has been elucidated and is highly representative of the TIM barrel fold characteristic to all OYEs (Figure 1.7 and 1.9). The distinguishing feature is the presence of a β-hairpin motif that is capping the active-site channel, which is located along the polypeptide excursion between the β3 strand and α3 helix of the TIM barrel.

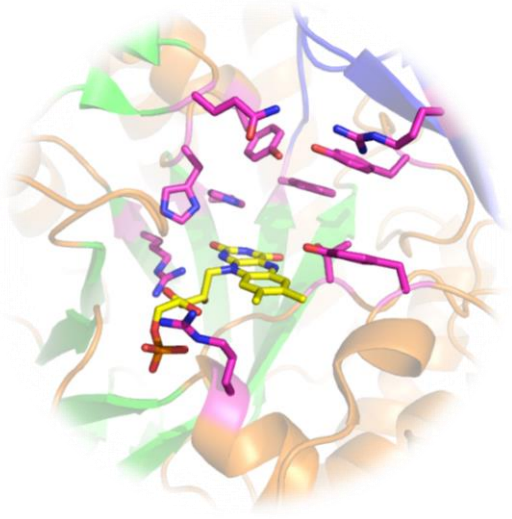

Figure 1.9. Active site of PETNR flavoenzyme. The FMN cofactor and relevant active-site residues are shown as sticks (yellow and pink carbons, respectively), with secondary structural features shown as cartoons (PDB:5LGX).

Initial studies of the reductive half-reaction of PETNR have shown that the hydride transfer proceeds ~15X slower when NADH is used as coenzyme instead of NADPH, even though the binding mechanism is thought to be almost identical for both substrates.[159] Temperature and pressure dependence studies of primary KIEs suggest that the H-transfer from NADPH is facilitated by a "soft" promoting vibration, while in the case of NADH reaction, there is either a "hard" promoting vibration or there is no vibration connected to the reaction coordinate.[95] The existence of promoting vibrations that assist H-tunnelling in the hydride transfer from NADPH to the flavin in PETNR is inferred from the temperature dependent KIE values and also from the pressure dependence data, which presents a positive curvature in the KIE.[165] Furthermore, the role of fast protein dynamics in H-transfer reactions can also be probed by comparing temperature dependencies of KIEs between a wild-type enzyme and its corresponding "heavy" (^{13}C, ^{15}N, and ^{2}H) isotope labelled variant, as the overall structure of the protein and the reaction geometry is not affected by isotope labelling. The KIE temperature dependence for FMN reduction with NADPH is perturbed in the case of heavy labelled PETNR, with a direct correlation between mass of the enzyme and the temperature dependence of KIEs, which accounts for a direct coupling between protein vibrations and the reaction coordinate.[166] A recent study involving PETNR isotopologues (in which the protein and/or the FMN cofactor are ^{2}H, ^{15}N, and ^{13}C isotopically labelled) suggests that vibrations local to the active site play a role in the H-transfer chemistry.[96] Moreover, fluorescence lifetime measurements of the FMN cofactor show differences between the different PETNR isotopologues ("light" *vs.* "heavy" enzyme) on the ns-ps timescale, suggesting isotope effects could arise from the contribution of protein vibrations on these fast timescales.[96]

1.6. The use of NMR to study protein structure and dynamics

Nuclear magnetic resonance spectroscopy is a powerful experimental technique for studying both protein structure and dynamics, as it covers a timescale of over 17 orders of magnitude (10^{-12} to 10^{5} s), enabling visualization of dynamics from fast backbone and side chain motions to large scale domain motions.[60] Using innovative labelling strategies, almost any atomic site can be probed by NMR and, most often, the kinetic and thermodynamic profile of the processes involved can be studied. The recent advances in NMR have made it possible to determine protein structures at a resolution comparable to that obtained from crystal structures, using higher dimensional techniques (2D, 3D and 4D NMR).[167,168] The main steps in structure determination by NMR consists of sequential resonance assignment, torsion angle determination, stereospecific assignment at chiral centres, identification of connectivities between protons through space and calculation of 3D structures using experimental NMR restraints.[169] Protein dynamics studies seek an in-depth understanding of the atomic vibrations that proteins undergo, from picosecond backbone and side chain fluctuations to slow breathing modes that occur on the second-minutes timescale. On the ps-ns timescale, fast backbone and side chain motions can be readily followed using spin relaxation techniques, by measuring the longitudinal relaxation rate (R_1), the transverse relaxation rate (R_2) and the Nuclear Overhauser Effect (NOE).[170] Moreover, relaxation dispersion NMR experiments can detect conformational exchange on a slower timescale, being able to grasp information about "excited" states (transient conformational species with <1% population and µs-ms lifetime) that are essential for protein function.[171] Another new tool used in NMR to study structure and function of proteins in solution is represented by residual dipolar couplings (RDCs). RDCs are complementary to the use of NOEs to provide structural insight and restraints in molecular dynamics simulations, providing information about long-range distance restraints, like angles between bond vectors.[172–175] Enzymes can be regarded as highly dynamics systems and NMR, as an ensemble technique, can provide a vast complexity of information in the current era of enzyme dynamics.

1.7. Aims of the thesis

The overarching objective of the project is to understand the molecular basis of ene-reductases specificity towards nicotinamide coenzymes. Specifically, the focus of these studies is on the reductive half-reaction of PETNR (with limited studies of MR presented in Section 5). The preferred reactivity and specificity of PETNR towards NADPH, when compared to NADH, is addressed using a wide range of experimental techniques, such as mutagenesis, stopped-flow rapid kinetics, X-ray crystallography, isotope/temperature dependence studies of reaction rates and NMR spectroscopy. Some of the work described in the thesis are developments of previous NMR and stopped-flow studies[176,177], and expand the array of methods used to probe H-tunnelling mechanism on PETNR (as detailed in Sections 1.3 and 1.5) through the use of NMR and mutagenesis probes. A more detailed depiction of the aims of the thesis, along with how these aims are covered in the following experimental sections (Sections 2-5), is provided below.

Section 2 presents methodologies for isotopic labelling of flavoenzymes and their use in probing reaction mechanisms through NMR and KIEs studies. The approaches described herein establish a strong foundation for the work undertaken in Sections 3-4. In particular, a detailed description of developed experimental strategies that ensure appropriate levels of back exchange of amide protium atoms for ^{2}H, ^{13}C, ^{15}N-labelled flavoenzymes can be found within this section.

Section 3 presents the ^{1}H, ^{15}N and ^{13}C backbone resonance assignments of PETNR. Backbone resonance assignment are the basis of any protein structural NMR study, and this is the first report of an NMR structural study of a member of the OYE family of ene-reductases. Near-complete, sequence-specific ^{1}H, $^{15}N_{H}$, $^{13}C_{\alpha}$, $^{13}C_{\beta}$ and $^{13}C'$ backbone resonance assignments of PETNR (holoenzyme form) are reported, with details regarding the methodology used, which involves the use of heteronuclear multidimensional NMR spectroscopy. This section provides a basis for Section 4, which conveys further structural and functional NMR studies of PETNR.

Section 4 presents the investigation of H-transfer mechanism in PETNR through mutagenesis of second sphere 'noncatalytic' residues (L25 and I107). The effect of mutagenesis on the RHR of PETNR is probed using a combination of experimental approaches that enable analysis of subtle kinetic changes. This is the first study of H-transfer mechanism in PETNR through mutagenesis, and discusses the role of (rather distal) hydrophobic side chains and dynamics in controlling rates of enzymatic H-transfer. The section exemplifies how the use of synergistic experimental approaches can aid interpretation of kinetic data and unmask kinetic complexities that are normally hidden in traditional H-transfer studies, such as those involving steady-state turnover measurements.

Section 5 addresses a central question regarding the OYE family: *What determines coenzyme specificity in this large family of ene-reductases?* Structural NMR data (presented in Sections 3-4) and previously reported X-ray crystallographic data are used to rationally design variants of PETNR and MR, two homologues belonging to the OYE family. Stopped-flow spectroscopic studies of the RHR of PETNR enable determination of the basis of coenzyme recognition in PETNR. Furthermore, the findings are used to rationally tune and switch coenzyme specificity by protein engineering in the related NADH-dependent morphinone reductase. The section illustrates how protein engineering can be used to tune coenzyme specificity across the OYE family of oxidoreductases to facilitate future applications in biocatalysis and cell factory engineering.

2. Isotopically labelled flavoenzymes and their uses in probing reaction mechanisms

Publication status: *under review*

Authors: Andreea I. Iorgu, Nigel S. Scrutton, Sam Hay

Running header: Isotopically labelled flavoenzymes

Contributions: A.I.I. wrote the paper, with contributions from all authors. The manuscript is a methods-focused paper, written as an invited contribution for publication in *Methods Enzymol*. A.I.I. performed all original research experiments and developed all methodologies described in this section, unless otherwise conveyed through referencing. S.H. and N.S.S. supervised the project.

2.1. Abstract

The incorporation of stable isotopes into proteins is beneficial or essential for a range of experiments, including NMR, neutron scattering and reflectometry, proteomic mass spectrometry, vibrational spectroscopy and “heavy” enzyme kinetic isotope effect (KIE) measurements. Here, we present detailed protocols for the stable isotopic labelling of pentaerythritol tetranitrate reductase (PETNR) *via* recombinant expression in *E. coli.* PETNR is an ene-reductase belonging to the Old Yellow Enzyme (OYE) family of flavoenzymes, and is regarded as a model system for studying hydride transfer reactions. Included is a discussion of how efficient back-exchange of amide protons in the protein core can be achieved and how the intrinsic flavin mononucleotide (FMN) cofactor can be exchanged, allowing the production of isotopologues with differentially labelled protein and cofactor. In addition to a thorough description of labelling strategies, we briefly exemplify how data analysis and interpretation of “heavy” enzyme KIEs can be performed.

2.2. Introduction

The substitution of natural abundance isotopes within a biomacromolecule with their heavier counterparts (such as ^{2}H, ^{3}H, ^{13}C, ^{14}C, ^{15}N, ^{18}O, etc.) has enabled a deeper understanding of the structure and function of a wealth of biological systems. The use of isotopically labelled proteins (and, in particular, of deuterated proteins) originated in the 1960s from the need to reduce complexity and increase resolution of nuclear magnetic resonance (NMR) spectra.[178–181] Starting as a necessity to access structural information from NMR studies, stable isotope labelling of biomacromolecules, along with developments in NMR methodologies, enabled an exponential expansion in the number of studies dedicated to the structure and function of proteins in solution. Concomitant with the advances in NMR techniques, developments in molecular biology resulted in *E. coli* becoming a preferred organism of choice for the production of recombinant proteins (or at least, for those proteins that do not require post-translational modifications). As one of the most characterised protein synthesis machineries, *E. coli* is also the most utilised system

for expressing isotopically labelled proteins, given its relatively rapid growth in minimal media, including $^{2}H_2O$ (D_2O) solutions.[182]

The necessity to study eukaryotic proteins that are not readily expressed in *E. coli* or other bacterial strains has recently driven developments in heavy atom labelling using insect cells or mammalian expression systems (such as adenoviral vector-based systems) as expression hosts.[183,184] Furthermore, a growing number of publications feature cell-free expression systems.[185,186] Apart from the now vast choice of expression hosts available that can incorporate heavy atoms, there are many variations in which proteins can be labelled with stable isotopes: uniform or partial isotopic labelling,[187] site-specific labelling,[188] selective labelling[92,189] and segmental labelling.[190] It seems that there is a lot of choice available when it comes to selecting methods of producing isotopically labelled proteins, and also types of labelling schemes, as required for particular techniques. Nevertheless, peculiarities still exist for each class of proteins, and it is not uncommon to notice that a highly established protocol for incorporating heavy atoms into one protein could not be readily replicated for another related protein.

While a wealth of developments has stemmed from the need to facilitate structural and dynamic NMR studies, the use of isotopic labelling schemes for proteins has expanded well beyond this primary scope. Isotopically labelled biomacromolecules are now commonly used in studies involving a large number of techniques, including small-angle neutron scattering, proteomic mass spectrometry, neutron reflectometry and site-directed vibrational spectroscopy.[188,191–193] Recently, the scope of isotopically labelled enzymes has extended even further, with “heavy” (primarily ^{2}H, ^{13}C and ^{15}N labelled) enzymes being now used to probe dynamical effects on the chemical step. This approach was popularised by Silva *et al*. in 2011, with the introduction of the concept of a Born-Oppenheimer enzyme.[91] A Born-Oppenheimer enzyme can be defined as an enzyme that is labelled with heavy atoms (^{2}H, ^{13}C and ^{15}N), and the isotopic substitution is postulated to reduce femtosecond bond vibration frequencies, while not affecting electrostatic properties of the enzyme. These experiments showed that, as computationally predicted, the increase

in the mass of the purine nucleoside phosphorylase (PNP) enzyme by isotopic substitution led to a decrease in the rate of the chemical step as a result of the decreased probability of transition-state barrier crossing.[91] The observation is consistent with coupling of the vibrational modes of the protein with the transition state, which is distorted in the "heavy" enzyme (compared to the "light", natural abundance unlabelled enzyme). Since this first study, more studies have been dedicated to probing the role of dynamics in the phosphorolysis step catalysed by PNP.[54,63,92,194] Moreover, several other enzyme systems catalysing diverse catalytic steps, such as proton transfer,[195] hydride transfer,[94,96,166,196,197] and hydrolysis[198,199] have been investigated using isotopically labelled enzymes, and measurements of the enzyme isotope effect have shown that catalytic rates are typically affected by isotopic substitution. The approaches used and the findings of these studies have been recently reviewed by Kholodar *et al*. and Swiderek *et al*.[200,201]

Herein, we will focus on discussing methodologies we have employed for the isotopic labelling of pentaerythritol tetranitrate reductase (PETNR), an ene-reductase from the Old Yellow Enzyme (OYE) family of flavoenzymes. PETNR is regarded as a model system for studying hydride transfer reactions, and is a flavin mononucleotide (FMN)-containing enzyme, which catalyses hydride transfer (H-transfer) from NAD(P)H to a wide range of activated α,β-unsaturated substrates *via* a bi-bi ping-pong mechanism that uses the FMN cofactor.[157,159,160] The H-transfer mechanism from NAD(P)H coenzyme to the FMN cofactor (known as the reductive half-reaction of the catalytic cycle, RHR) has been extensively studied using temperature and pressure dependence studies of coenzyme deuterium kinetic isotope effects (KIEs).[95,166] More recently, KIEs between "heavy" and "light" PETNR have been studied,[166] and differential labelling of the enzyme was used to study the different contribution of protein and cofactor vibrational modes to catalysis.[96] Moreover, PETNR is the first enzyme belonging to the OYE family of ene-reductases for which near-complete ^{1}H, ^{15}N and ^{13}C backbone resonance assignments have been reported, which opens new avenues for investigating functional dynamics through structural NMR studies.[202] In this chapter, we will describe experimental methods used for isotopic labelling of PETNR, from production of the labelled enzyme to efficient

methods used for FMN exchange, which enable kinetic studies of PETNR isotopologues (such as "light" apoenzyme-"heavy" FMN). We will also cover aspects regarding the distribution of "heavy" atoms in PETNR, and present methods for efficient deuterium-hydrogen (D-H) exchange of backbone amides, which are essential for structural NMR studies. These methods can be readily applied to other enzymes from the Old Yellow Enzyme (OYE) family of oxidoreductases, given their highly similar architecture,[118,148] and we expect that the protocols presented herein can be readily adapted for efficient labelling/cofactor exchange of other flavoenzymes. The last section of this chapter is dedicated to the recent applications of "heavy" PETNR in studying dynamical contribution to enzyme catalysis and will focus on data analysis and interpretation of KIEs when using "heavy" enzymes.

2.3. PETNR as a model flavoenzyme from the OYE family

PETNR is a monomeric 40 kDa enzyme that possesses broad substrate specificity, and it can catalyse the reduction of a wide variety of α,β-unsaturated compounds, often with high enantioselectivity towards desired products.[138,163,164] This promiscuity gives PETNR high potential to be used in biocatalytic processes. Moreover, PETNR is regarded as a model system for studying biological hydride transfer mechanisms. Several kinetic studies have indicated that quantum mechanical tunnelling contributes to the enzymatic hydride transfer step from NAD(P)H to the FMN cofactor, and fast (ps-ns) protein dynamics have been inferred to contribute to catalysis from the temperature and pressure dependence of the deuterium KIE on the RHR.[95,157,203] Recently, we developed an approach to generate isotopologues of PETNR in which the apoprotein and/or the FMN cofactor have been labelled with different isotopes.[96] These were studied using temperature dependence KIE studies along with fluorescence lifetime measurements in order to dissect whether dynamical contributions coupled with the H-transfer chemistry catalysed by PETNR arise from the apoenzyme alone and/or the FMN cofactor. These studies suggested that vibrations local to the active site (which appear to be on the 10-100 ps timescale) play a role in the H-transfer chemistry, with observed isotope effects arising from both the protein and FMN cofactor.[96] Having assigned the ^{1}H, $^{15}N_{H}$, $^{13}C_{\alpha}$, $^{13}C_{\beta}$ and $^{13}C'$

backbone resonances in the NMR spectra of PETNR to a great extent,[202] we are now on the cusp of unravelling more information regarding the role of functional dynamics in the H-transfer chemistry catalysed by PETNR, through more detailed NMR studies (Iorgu *et al*., in preparation). In the next sections, we will present details regarding the production of different PETNR isotopologues and strategies for determination of efficient conditions for D-H backbone amide exchange.

2.4. Expression and purification of isotopically labelled PETNR in *E. coli*

Throughout our studies, we used two different constructs for overexpression in *E. coli*. One expression system involves production of PETNR using the pBlueScript II SK(+) plasmid encoding the pONR1 gene. pBlueScript II SK(+) is a legacy plasmid, used since the first isolation of PETNR from soil contaminated with explosives in the mid-1990s.[162] Many of the early kinetic studies on this enzyme, along with the more recent NMR studies, were performed with recombinant PETNR expressed from this plasmid. More recently, we moved to use a more convenient expression plasmid (pET21a), from which a C-terminal His_8-tagged version of PETNR can be produced and easily purified *via* nickel-affinity chromatography. As we are now aware that there are no major differences in the kinetics and structure between PETNR and His-tagged PETNR,[96,137] we would suggest production (and, in particular, purification) of PETNR using the pET21a vector is more straightforward (and therefore, preferable) than using the pBlueScript II SK(+) plasmid. However, it is likely that, for other enzymes, a His tag is not desirable to be used, so we will describe herein both protocols. We will focus on the preparation and use of ^{2}H,^{13}C,^{15}N-labelled PETNR for NMR studies, which require a uniformly deuterated sample in which all backbone amides are back- exchanged (at least partially) to protium atoms (D-H exchange). As we have previously encountered difficulties in developing efficient methods for this D-H exchange, we aim to provide as many details as possible to perform backbone amide exchange on the PETNR system and, by extension, on other flavoenzymes.

Labelling of flavoenzymes with heavy atoms (such as ^{2}H, ^{13}C and ^{15}N) in *E. coli* can be done using well-established techniques that are applicable to a vast majority of soluble proteins. The common route for expression of isotopically labelled

flavoenzymes in *E. coli* involves the use of M9 minimal media (M9mm), which contains salts and trace elements required for bacteria growth. This basic M9mm is then supplemented with carbon and nitrogen sources, which can be either of natural abundance (leading to expression of unlabelled proteins) or isotopically labelled with specific heavy atoms. Expression of ^{2}H-lablled proteins is achieved using media prepared in D_2O (cf. H_2O). In the cases where uniform ^{2}H incorporation (perdeuteration) is required for the target protein, a ^{2}H-labelled carbon source is also required. The most common carbon source used for isotopic labelling in *E. coli* is $^{13}C_6$-D-glucose, which is replaced with $^{2}H_7$,$^{13}C_6$-D-glucose when expressing uniformly ^{2}H,^{13}C-labelled proteins.

2.4.1. Assembly of M9 minimal media for isotopic labelling of PETNR

The expression in *E. coli* of isotopically labelled PETNR involves the use of a modified M9mm, which is prepared following a combination of protocols developed for growth in supplemented minimal growth medium.[204,205] Strategies for the preparation of various isotopically labelled M9mm that we use for overexpression of PETNR are presented below.

^{15}N-labelled M9mm. First, 6 g Na_2HPO_4, 3 g KH_2PO_4 and 0.5 g NaCl are dissolved in ~900 mL double-distilled (dd) H_2O. The pH of the solution is then adjusted to 7.4 (using concentrated KOH), followed by dilution to 980 mL and sterilization (autoclave at 121 °C for 15 minutes). Under sterile conditions, the following components are further added to the 980 mL of M9mm salts solution: 1 mL ampicillin solution (0.1 g/mL), 500 µL 1M $MgSO_4$ solution, 500 µL thiamine solution (1 mg/mL), 100 µL 1M $CaCl_2$ solution, 200 µL trace metals solution, 3 g glucose (15 mL 20% (w/v) solution) and 1 g $^{15}NH_4Cl$ (5 mL 20% (w/v) solution). The overall composition of ^{15}N M9mm is detailed in Table 2.1. The trace metals solution (5000 × stock solution) is prepared using a combination of metal salts, as presented in Table 2.2. The stock solutions used above are prepared individually and filter-sterilised prior to use in M9mm assembly. The final concentration of antibiotic used in the medium is 0.1 mg/mL.

^{2}H,^{15}N-labelled M9mm. The preparation of ^{2}H,^{15}N-labelled M9mm is the same as for ^{15}N labelled M9mm, except $^{2}H_7$-D-glucose is used as a carbon source and all reagents are dissolved in D_2O (except for the 5000 × trace metals solution). The solution is sterilized by vacuum filtration using a vacuum filter system with a 0.2 µM pore size membrane, and is not autoclaved. Also, given the medium consists of D_2O solution, the pH is adjusted to pH_{read} = 6.99, as the actual pD of the solution is pD = pH_{read} + 0.41.

^{2}H,^{13}C,^{15}N-labelled M9mm. Preparation is the same as for ^{2}H,^{15}N-labelled M9mm, with the only difference being the use of $^{2}H_7$,$^{13}C_6$-D-glucose as a carbon source instead of $^{2}H_7$-D-glucose.

Table 2.1. Components for 1 litre of modified M9 minimal medium.

Component	Amount
Na_2HPO_4	6 g
KH_2PO_4	3 g
NaCl	0.5 g
$MgSO_4$	1 mL of 1M solution
thiamine	1 mL of 1 mg/mL solution
$CaCl_2$	100 µL of 1M solution
trace metals solution	200 µL
D-glucose	15 mL of 20% solution (3 g)
$^{15}NH_4Cl$	5 mL of 20% solution (1 g)

Table 2.2. Recipe for the preparation of 100 mL 5000 × trace metals solution.

Trace metal	Stock solution	Volume (mL)
Iron	0.1 M $FeCl_3$ in 0.1 M HCl	50
Manganese	1M $MnCl_2$	1
Zinc	1M $ZnSO_4$	1
Cobalt	0.2M $CoCl_2$	1
Copper	0.1M $CuCl_2$	2
Nickel	0.2M $NiCl_2$	1
Molybdenum	0.1 M Na_2MoO_4	2
Selenium	0.1M Na_2SeO_3	2
Boron	0.1M H_3BO_3	2
-	dd H_2O	38

2.4.2. Overexpression and purification of isotopically labelled PETNR

Our procedure for production of $^{2}H,^{13}C,^{15}N$-labelled PETNR, which is similar to the production of ^{2}H and $^{2}H,^{15}N$-labelled PETNR, is presented below.

1. The *E. coli* strain JM109 is transformed with 1-100 ng of pBlueScript II SK(+) plasmid encoding the pONR1 gene used for PETNR overexpression expression, following the protocols provided by the manufacturer. Cells are plated on LB agar containing ampicillin (0.1 mg/mL) and incubated at 37 °C for ~ 16h.

2. A single cell colony is selected from the plate and used to inoculate 5 mL of ^{15}N M9mm containing ampicillin (0.1 mg/mL). Cells are grown at 37 °C with shaking at 200 rpm, until an OD_{600} of >0.5 is reached. Following growth of the starting culture, 10-100 mL of $^{2}H,^{13}C,^{15}N$ M9mm (containing ampicillin) are inoculated in a 1:100 dilution with cells from the starting culture. Cells are further grown at 37 °C with shaking at 200 rpm until the OD_{600} reaches 0.8-1 (or overnight).

3. Final cultures, containing 500 mL of $^{2}H,^{13}C,^{15}N$ M9mm and ampicillin, are inoculated in a 1:50-1:100 dilution with cells from the intermediate culture, and grown at 37 °C with shaking at 200 rpm until the OD_{600} reaches 0.8-1. Overexpression of PETNR is then induced by addition of 0.5 mM isopropyl β-D-1-thiogalactopyranoside (IPTG, final concentration, added as 500 µL of freshly prepared and filter-sterilised 0.5 M IPTG stock in D_2O). At this point, the temperature is lowered to 25 °C. Cells are harvested after a further 24-36h growth by centrifugation at 3000 *g* for 10 min at 4 °C.

Purification of PETNR enriched with heavy atoms (^{2}H, ^{13}C and/or ^{15}N) is performed in the same manner as for unlabelled PETNR samples and is performed with buffers made in H_2O, not D_2O. The methodology for separating PETNR produced in JM109 cells has been previously described in detail,[153,162,202] and involves purification by affinity exchange chromatography, using a Mimetic Orange 2 column, followed by Source 15Q anion exchange chromatography. In the case of C-His_8 tagged PETNR expressed in NiCo(DE3) cells, purification of the target enzyme is performed using a HisTrap HP nickel-charged IMAC column. Usually, given that the yields are relatively

high (> 200 mg purified protein/L of culture), the C-His_8 tagged PETNR purification is performed with only one chromatographic step, and PETNR is found to be >95 % pure following purification, as judged by SDS-PAGE analysis. However, in line with the NiCo(DE3) cell user manual, if contaminants are found after nickel affinity purification, an extra step using chitin affinity chromatography can be added to remove the three well expressed *E.coli* proteins that contain sequences that bind to the chitin column. If purified proteins are being used for crystallography, enzymes from both purification methods (His-tagged or not) can be further purified using a gel filtration step. As all the purification steps are done in protiated buffers, the backbone amide groups that are solvent exposed in the ^2H labelled PETNR samples will undergo D-H exchange. If a completely ^2H labelled sample is required for further experiments, we would suggest that, rather than using expensive perdeuterated buffer solutions for purification, it would be more economical to purify the protein in protiated buffer and, following purification, exchange the solvent-exchangeable backbone amides back to ^2H by using a perdeuterated buffer in the last step.

Notes:

- For the production of C-His_8 PETNR, *E. coli* strain NiCo21(DE3) is transformed with 1-100 ng of pET21a plasmid encoding the C-His_8 PETNR gene, following the protocols provided by the manufacturer. All subsequent steps are identical for when the JM109 cells are used.

- We usually observe that expression yields are higher when the temperature is lowered to 20-25 °C following induction with IPTG (or, ideally, one-two hours before induction).

- Extra glucose (1-3 g/L culture) can be added at the IPTG induction stage to afford higher cell density and, therefore, higher yields of target protein.

- The main difference between using the NiCo21(DE3) and JM109 cells is related to the doubling time of the cells: JM109 cells grow about 2 × slower than NiCO21(DE3). Also, although it is well known cells grow slower in deuterated

medium, the time necessary to reach induction point, as compared to growth in rich supplemented medium, is specific to each cell line. JM109 *E. coli* cells grow 6 × slower in deuterated M9mm than in protiated M9mm: 36-40 hours for $^{2}H,^{15}N/^{2}H,^{13}C,^{15}N$-labelled M9mm to OD_{600} of 0.8-1.0, as compared to 5-6 hours for ^{15}N-labelled M9mm/LB Broth (growth from 1:100 dilution in final flasks). It was observed that deuteration influences both the timescale of growth, but also the maximal cell density (2-2.5 g of cell pellet/ L of $^{2}H,^{15}N$ or $^{2}H,^{13}C,^{15}N$ M9mm, as compared to 4.8 g/L ^{15}N media). Typical yields for PETNR production in JM109 and NiCo21(DE3) cells are commonly in the range of 70-100 and 200-250 mg of purified PETNR /L of culture, respectively.

- As yields of protein expression can be very high, especially when using NiCo21(DE3) cells for C-His_8 PETNR production, we often observe that a significant fraction of purified PETNR does not contain bound FMN. We suspect this arises through an inability of the host to produce sufficient quantities of FMN. Thus, FMN incorporation is required at the purification stage and can be done at the lysis stage: the lysis buffer is supplemented with 0.5-1 mM FMN, which will enable rapid incorporation of FMN into the apoenzyme following cell lysis, and the excess FMN will be washed off when loading the protein sample onto the column. It is worth nothing that this step should be done in this manner if the labelling of the FMN cofactor is not relevant for further experiments, as unlabelled FMN will be introduced (in some proportion) in the samples.

2.5. Spectral characteristics and quality control of isotopically labelled PETNR

An interesting observation for ^{2}H-labelled PETNR is the presence of a blue-shift of the FMN absorption (Figure 2.1). While the origin of this shift is uncertain, it indicates that there is a perturbation to the environment of the FMN cofactor in the deuterated samples. This could be an effect of deuteration on the hydrogen bonding interaction between the FMN cofactor and the enzyme, and must involve exchangeable protons, as the effect is lost following D-H exchange of backbone amides.

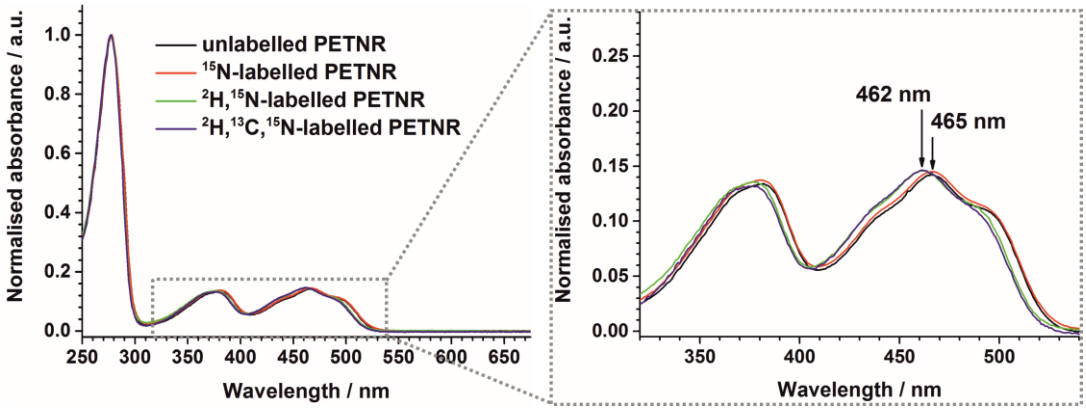

Figure 2.1. UV-Vis absorbance spectra of unlabelled, ^{15}N-labelled, ^{2}H,^{15}N-labelled and ^{2}H,^{13}C,^{15}N-labelled PETNR. The spectra are normalized to a maxima corresponding to the 277 nm peak. The insert shows the blue-shifted FMN absorbance in the deuterated samples.

The assessment of isotopic composition of a protein that was grown in media supplemented with heavy atoms is most commonly checked by mass spectrometry and/or ^{1}H-^{15}N TROSY NMR spectroscopy. While the first technique allows one to confirm the quantitative incorporation of the stable isotopes, the NMR spectra of a ^{2}H,^{13}C,^{15}N-labelled protein allows qualitative visualisation of the absence (or presence) of deuterium atoms in exchangeable backbone amide groups. Moreover, inspection of the ^{1}H NMR spectrum of the protein can indicate if a high degree of sample deuteration was achieved. As it can be observed in Figure 2.2., the region between -1 and 4 ppm in the 1D ^{1}H NMR spectrum of ^{15}N-labelled PETNR is highly populated with signals arising from the aliphatic region of the enzyme (e.g. protium atoms from side chain methyl groups), while in the case of ^{2}H,^{15}N and ^{2}H,^{13}C,^{15}N-labelled PETNR, this region has no visible signals present, suggesting effective incorporation of deuterium atoms into the enzyme.

Isotopic labelling of PETNR using the expression protocol discussed in Section 2.4.2. was also previously investigated using QTOF mass spectrometry, with mass increases of 9.8-10.3%, 5.3% and 1.3% observed for ^{2}H,^{13}C,^{15}N-labelled, ^{2}H,^{15}N-labelled and ^{15}N-labelled PETNR, respectively, when compared to “light” unlabelled PETNR.[96,166] These results are consistent with expected/calculated values of protein mass increase upon isotopic substitution, and similar values have been observed for several other systems.[200]

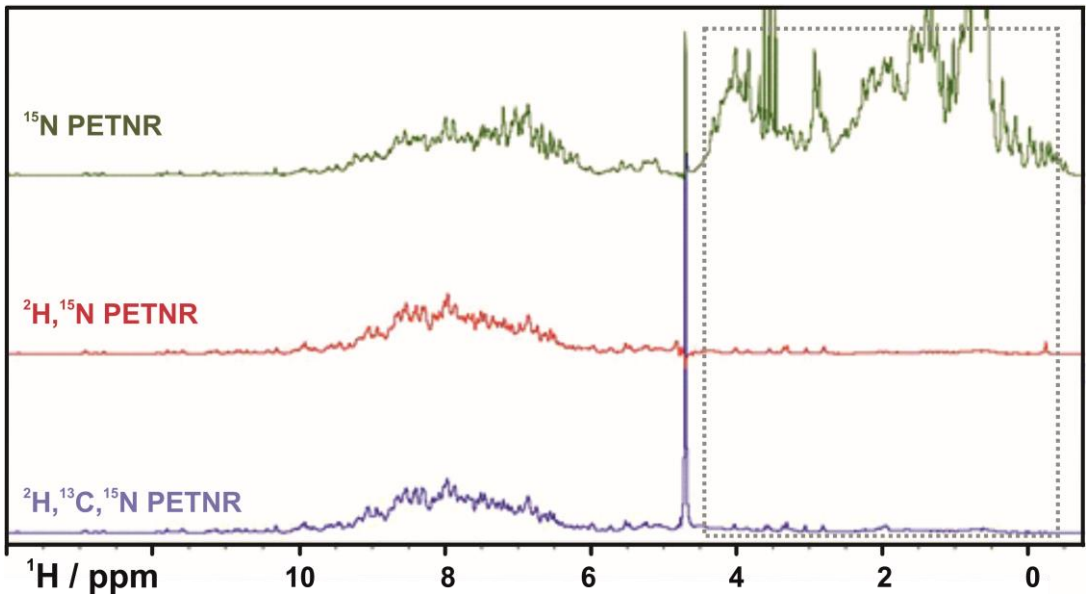

Figure 2.2. ^{1}H 1D NMR spectra of PETNR samples of various PETNR isotopologues. Spectra were recorded at 298 K on an 800 MHz Bruker Avance III spectrometer.

Apart from quantifying the degree of isotopic enrichment through the use of mass spectrometry, the conservation of the structural features and thermal stability of isotopically labelled enzymes, when compared to their corresponding "light" isotopologues, can be interrogated through the use of a range of methods including circular dichroism spectroscopy, differential scanning calorimetry, differential scanning fluorimetry and NMR spectroscopy. More details regarding the use of these techniques for assessing structural similarity (or otherwise) between "heavy" and "light" enzyme are summarised by Kholodar *et al*.[200] Comparison of the NMR temperature coefficients (the temperature dependencies of the backbone NH chemical shifts) is a powerful probe for structure perturbation. In the case of PETNR, we have previously shown evidence for the isostructural nature of ^{2}H,^{13}C,^{15}N-labelled PETNR and ^{15}N-labelled PETNR by correlating the NMR temperature coefficients for the backbone residues of both isotopologues.[166]

2.6. Analysis of deuterium-hydrogen exchange of backbone amides in PETNR

Large proteins (>25 kDa) require uniform deuteration in order to be structurally studied by NMR, as ^{2}H side-chain labelling increases significantly the sensitivity of 3D NMR experiments designed for backbone assignments.[206] However, maximum

sensitivity can only be achieved if complete re-protonation of all amide groups can be performed. With a molecular weight of 40 kDa, PETNR belongs to the class of relatively large proteins that require ^{2}H labelling for such measurements. The PETNR structure comprises of an $(\alpha,\beta)_8$-barrel structural scaffold, a tertiary fold consisting of an 8-fold repeat of linked α-helix and β-sheet structures, typical to all enzymes belonging to the OYE family.[148,207] This structural feature means the enzyme contains a highly hydrophobic, solvent-inaccessible core, with the *re* side of the flavin prosthetic group completely hidden from the active site, as it is located at the C-terminal end of this hydrophobic cavity. This structural feature makes exchange of amide backbone protons very slow. In order to anticipate and avoid problems in the sequential backbone assignment of the enzyme caused by lack of proton signals arising from deuteration, we initially analysed the ^{1}H-^{15}N TROSY spectrum of a protonated ^{15}N-labelled PETNR sample and studied its H-D exchange behaviour. We observed that more than 70 backbone amides (peaks) are essentially non-exchangeable over a period of 3 days (Figure 2.3). These peaks were later mapped, almost exclusively, to residues located in the β-barrel of the protein. The results indicated a necessity for the use of a denaturant that would enhance flexibility in the core of the enzyme. We thus studied the equilibrium unfolding curve of the enzyme in presence of guanidine hydrochloride in order to determine what conditions could be use that would enable efficient D-H exchange, while avoiding irreversible unfolding of the protein.

2.7. Spectroscopic characterisation of the equilibrium unfolding behaviour of PETNR

Initial trials to determine the unfolding-refolding behaviour of PETNR showed that after adding moderate concentrations of guanidine hydrochloride (GuHCl) solutions (2-4 M), irreversible precipitation of the protein occurs during the refolding step. Therefore, we decided to perform a thorough analysis of the unfolding behaviour of PETNR, monitoring the changes in UV-vis, fluorescence emission and circular dichroism spectral features when the enzyme is subjected to gradually increasing concentrations of GuHCl denaturant (Figure 2.4).

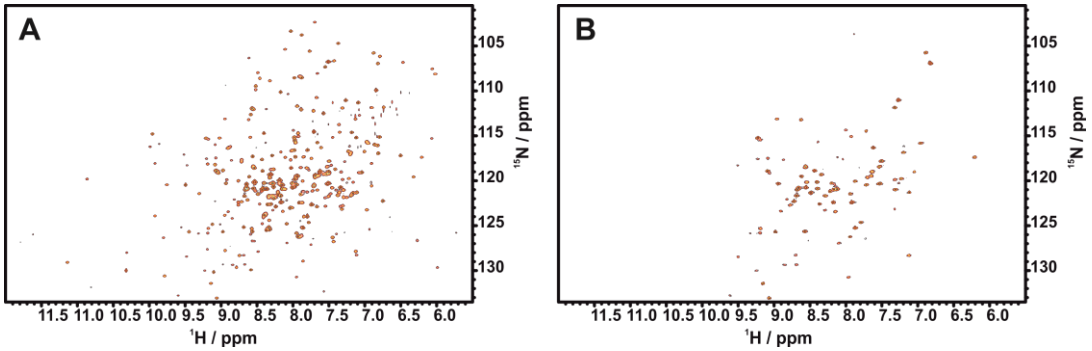

Figure 2.3. Comparison between ^{1}H-^{15}N TROSY spectra of ~1 mM ^{15}N-labelled PETNR recorded in A) standard buffer conditions (50 mM potassium phosphate buffer, pH 7.0, supplemented with 1mM NaN_3 and 10% D_2O) and B) 50 mM potassium phosphate buffer, pD 7.0, supplemented with 1 mM NaN_3, constituted in 100% D_2O. The spectrum in D_2O was recorded on an enzyme samples that was exchanged by repeated steps of concentrating by centrifugation into the desired deuterated buffer, starting from standard buffer conditions. Before recording the spectrum, the sample was left at 298 K for 72 hours to promote D-H exchange. The ^{15}N-labelled samples was expressed and purified as described for ^{2}H,^{13}C,^{15}N-labelled PETNR, except that unlabelled nitrogen and carbon sources were used during cell overexpression. Both spectra were recorded at 298 K on an 800 MHz Bruker Avance III spectrometer.

UV-vis absorption shows that FMN gradually loses the vibrational features characteristic of the bound flavin (peak with a maxima at 465 nm with two shoulders on both sides of the peak) with increasing concentrations of denaturant. At 1 M GuHCl concentration, the spectral features of the sample are suggestive of complete dissociation of the FMN into solution. The same pattern is observed in the fluorescence emission from the FMN, where a steep increase in fluorescence is observed when the denaturant concentration is above 0.75 M. This is in contrast to the fluorescence emission observed in the enzyme in the absence of any denaturant, in which case efficient quenching of the FMN is observed.[208] The circular dichroism data shows a gradual loss in the secondary structure of the enzyme as the GuHCl concentration is increased, and suggests that some secondary structure is present in the apoenzyme in 1M GuHCl.

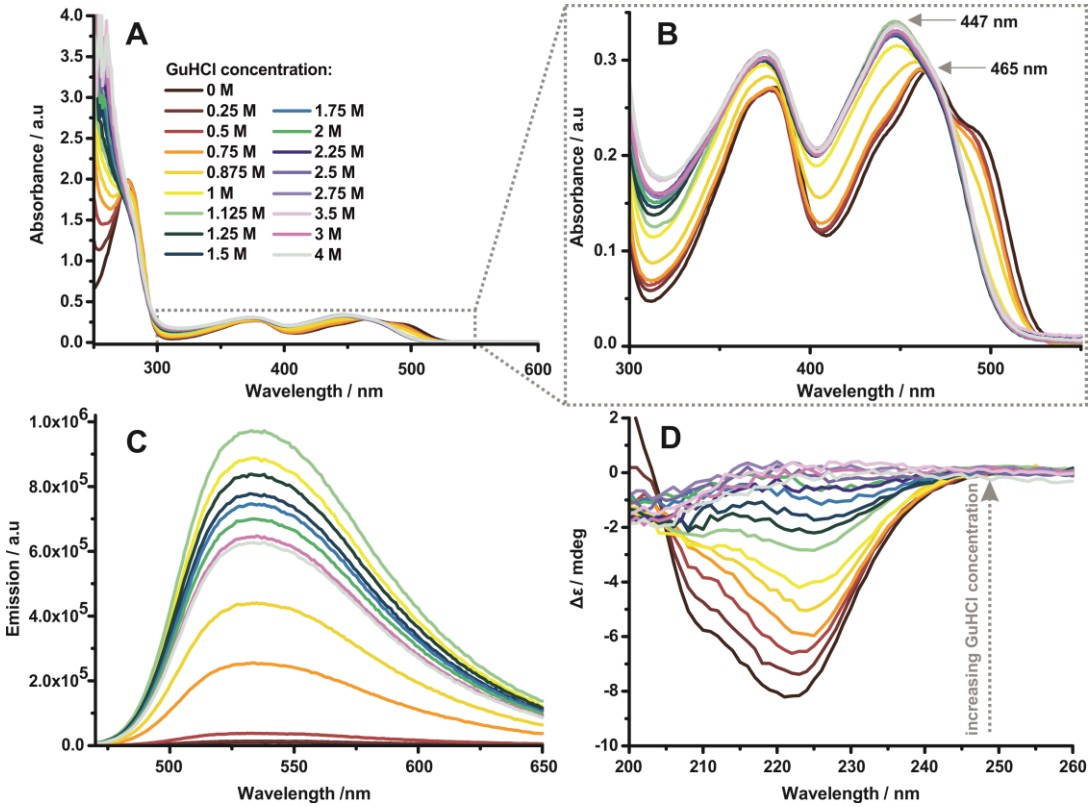

Figure 2.4. Characterisation of the behaviour of PETNR in the presence of gradually increasing concentrations (0-4 M) of guanidine hydrochloride. The equilibrium unfolding was monitored using UV-vis absorption (A and B), fluorescence emission upon excitation at 465 nm (C) and circular dichroism spectroscopy (D). The samples for UV-vis and CD spectroscopy contained 25 µM PETNR in a solution comprising 50 mM potassium phosphate buffer, pH 7.0 and various concentrations of GuHCl. A concentration of 8.3 µM PETNR was used for fluorescence experiments to prevent inner filter effects. UV-vis spectra were collected on a Cary 50 UV-vis spectrophotometer (Agilent Tech., UK), using a 1-cm two-window quartz cell. Fluorescence emission spectra of PETNR were recorded at 298 K using an FLS920 fluorescence spectrometer (Edinburgh Instruments, UK), with 1 nm excitation and 1 nm emission slit-widths in 1 mL quartz cells (1 cm excitation path length). Circular dichroism measurements were performed on an Applied Photophysics (Leatherhead, UK) Chirascan qCD spectrometer using a sealed cuvette with a 0.1 mm path length.

We also investigated how the samples behaved when subjected to the refolding procedure (fast dilution into native buffer) and found that the samples with concentrations of GuHCl higher than 0.875 M precipitated completely after dilution. Together, the data indicated that complete unfolding of the enzyme is unadvisable, as rapid refolding fails when the FMN cofactor is unbound. Therefore, we made a compromise, using 0.75 M GuHCl to promote back-exchange, which leads to a partial

D-H exchange. Overall, the main observation is that the loss of much of the secondary structure is concomitant with the loss of the bound FMN, which makes refolding difficult. Therefore, a successful unfolding-refolding procedure can only be performed by partially unfolding of PETNR under conditions where the FMN remains predominantly bound to the protein. Fortunately, this method enabled the partial protonation of all amide groups in the enzyme (all peaks were essentially visible in the ^{1}H-^{15}N TROSY spectra of back-exchanged ^{2}H,^{13}C,^{15}N-labelled PETNR when compared to the spectrum of protonated ^{15}N-labelled PETNR; data not shown), and ultimately enabled the near-complete sequential backbone assignment of PETNR, with 333 out of 344 non-proline residues successfully assigned in the ^{1}H–^{15}N TROSY experiment.[202]

2.8. Differential labelling of PETNR – exchanging the FMN cofactor

As mentioned in Section 1.3, we have recently developed a strategy to generate isotopologues of PETNR in which the protein and/or the intrinsic FMN cofactor are isotopically labelled.[96] This was achieved by binding the His_8-tagged PETNR to a HisTrap HP nickel-charged IMAC column, previously equilibrated with 50 mM sodium acetate, pH 5.5. Next, the FMN cofactor was removed by passing over the column a solution consisting of 2 M KBr, 50 mM sodium acetate, pH 5.5 until no yellow colour can be observed on the column and in the eluent. The apoenzyme (which was retained on the column) is then washed with 50 mM potassium phosphate, pH 7.0. PETNR is reconstituted with FMN by recirculating a solution of 0.1 mM FMN in 50 mM potassium phosphate, pH 7.0 through the column for several hours (until complete binding is observed). Next, the column is washed with 50 mM potassium phosphate, pH 7.0, in order to remove any unbound FMN prior to eluting the protein with 200 mM imidazole, 50 mM potassium phosphate, pH 7.0. This method enables almost complete incorporation of an unlabelled FMN cofactor into an isotopically labelled PETNR. It is possible to incorporate “heavy” labelled FMN into PETNR, but first the “heavy” FMN must be obtained by removing it from a “heavy” labelled PETNR sample as described above. This “heavy” FMN can then be incorporated into another sample by diluting the FMN-containing solution (which has 2 M KBr) by

approximately a third with non-denaturing buffer (50 mM potassium phosphate, pH 7.0). Thus, a lower concentration of KBr will enable subsequent rebinding of FMN.

2.9. Uses of isotopically labelled PETNR in probing biological hydride transfer mechanisms

"Heavy" isotopically labelled enzymes can be used to measure "heavy" enzyme KIEs. In this case, the KIE is simply the ratio of rate constants measured with two protein isotopologues and is expressed as KIE = $k_{"light"}/k_{"heavy"}$. "Heavy" enzyme KIEs have been measured in several enzymatic systems, including PNP,[54,63,92,194] HIV-1 protease,[198,199] alanine racemase,[195] dihydrofolate reductase,[94,196] and PETNR. The "heavy" enzyme KIEs are relatively small and it can be challenging to measure significant KIEs. The RHR of OYEs such as PETNR are particularly amenable to characterisation using anaerobic stopped-flow spectroscopy, which monitors the absorbance associated with the redox state of the bound FMN and/or the charge transfer complex formed between the FMN and NAD(P)H in the Michaelis complex.[95,157,159,160,166,203,209] In the case of PETNR, primary and secondary deuterium KIEs can be measured using this approach with a precision of 2-3%.[203] To date, the magnitude of the "heavy" enzyme KIEs measured on PETNR[96,166] and the homologue morphinone reductase (unpublished) have been typically no greater than 5% (0.95 - 1.05), which makes their individual significance questionable. However, by measuring the temperature dependence of these KIEs and by measuring primary KIEs (with deuterated NAD(P)H) with "heavy" enzymes, we can also consider the "heavy" enzyme KIEs on the apparent activation enthalpy and entropy ($\Delta H^{\ddagger}$ and $\Delta S^{\ddagger}$; Figure 2.5). By combining these data, we have made the case that isotopic labelling of the protein and/or FMN cofactor of PETNR leads to a measurable alteration in RHR kinetics, consistent with some vibrational coupling between protein, FMN and the reaction coordinate.[96]

Future work could include the specific uniform labelling of specific amino acid type(s) by adding labelled amino acid(s) to the expression medium, as recently employed by the Schramm *et al.*,[210] or in a cell-free expression system. More sophisticated experiments could employ specific incorporation of individual isotopically labelled

non-natural amino acid(s) using an orthogonal tRNA/aminoacyl-tRNA synthase pair encoded by an amber codon suppression.[211] In both cases, there is no apparent reason why such protocols could not be carried out using flavoenzymes such as PETNR.

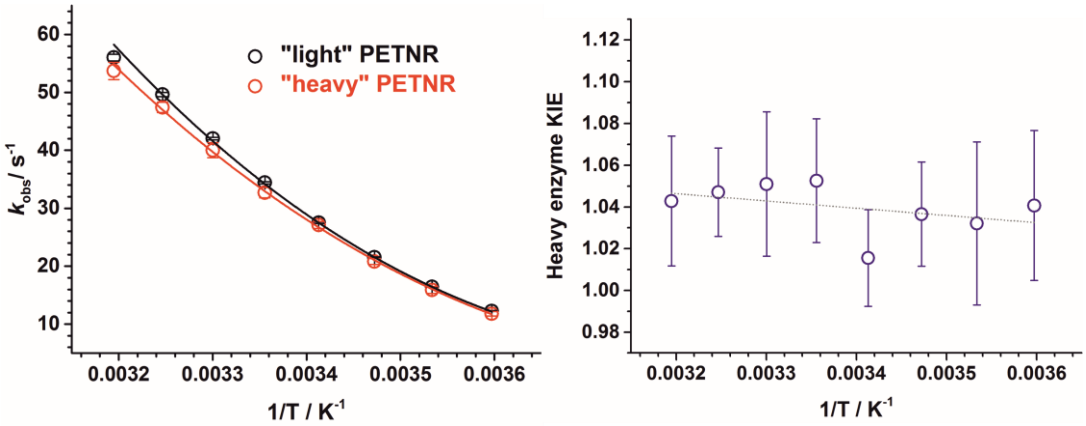

Figure 2.5. "Heavy" enzyme KIEs on the RHR of PETNR with NADPH. Left, the temperature dependence of the reaction of "light" and "heavy" ^{2}H,^{13}C,^{15}N-labelled PETNR with 5 mM NADPH fitted to the nonlinear Eyring-based equation,[212,213] yielding $\Delta H^{\ddagger}$ and $\Delta S^{\ddagger}$ = 6.0 ± 0.6 kJ mol^{-1} and 4.1 ± 1.9 J mol^{-1} K^{-1} for the "light" enzyme and 6.9 ± 0.9 kJ mol^{-1} and 7.8 ± 3.2 J mol^{-1} K^{-1} for the "heavy" enzyme. The heavy enzyme KIE calculated with these data is shown in the right panel. Data are taken from Longbotham *et al.*[96]

2.10. Conclusions

In summary, we have described some uses of stable isotopically labelled flavoenzymes, focusing on NMR and "heavy" enzyme KIE measurements with PETNR. Other experiments that require or benefit from such samples that are not discussed include neutron diffraction, proteomic mass spectrometry, and site-directed vibrational spectroscopy.[188,191–193] Detailed protocols for the preparation of isotopically labelled PETNR via recombinant expression in *E. coli* are provided with the hope they will be simply adapted to use with other flavoenzymes.

3. ^{1}H, ^{15}N and ^{13}C backbone resonance assignments of pentaerythritol tetranitrate reductase from *Enterobacter cloacae* PB2

Publication status: *this manuscript is published in Biomolecular NMR Assignments* 2018, 12, 1, 79-83

Authors: Andreea I. Iorgu, Nicola J. Baxter, Matthew J. Cliff, Jonathan P. Waltho, Sam Hay, Nigel S. Scrutton

Running Header: Backbone resonance assignments of PETNR

Contributions: A.I.I. wrote the paper, with contributions from all authors. A.I.I. conducted all experiments, with help from M.J.C and N.J.B. for NMR data acquisition and interpretation. J.P.W., S.H. and N.S.S. conceived and supervised the project.

3.1. Abstract

Pentaerythritol tetranitrate reductase (PETNR) is a flavoenzyme possessing a broad substrate specificity and is a member of the Old Yellow Enzyme family of oxidoreductases. As well as having high potential as an industrial biocatalyst, PETNR is an excellent model system for studying hydrogen transfer reactions. Mechanistic studies performed with PETNR using stopped-flow methods have shown that tunnelling contributes towards hydride transfer from the NAD(P)H coenzyme to the flavin mononucleotide (FMN) cofactor and fast protein dynamics have been inferred to facilitate this catalytic step. Herein, we report the near-complete ^{1}H, ^{15}N and ^{13}C backbone resonance assignments of PETNR in a stoichiometric complex with the FMN cofactor in its native oxidized form, which were obtained using heteronuclear multidimensional NMR spectroscopy. A total of 97% of all backbone resonances were assigned, with 333 out of a possible 344 residues assigned in the ^{1}H–^{15}N TROSY spectrum. This is the first report of an NMR structural study of a flavoenzyme from the Old Yellow Enzyme family and it lays the foundation for future investigations of functional dynamics in hydride transfer catalytic mechanism.

3.2. Biological context

Pentaerythritol tetranitrate reductase (PETNR, EC 1.6.99.1) is a monomeric flavoenzyme that possesses a broad substrate specificity and is a member of the Old Yellow Enzyme (OYE) family of oxidoreductases.[149] PETNR was originally isolated from an *Enterobacter cloacae* PB2 strain that was thriving on soil contaminated with explosives by exploiting nitrate esters as metabolic nitrogen sources.[162] The catalytic cycle of PETNR has been thoroughly investigated using stopped-flow techniques[157,160,214] and it is understood that the reaction chemistry takes place *via* a bi-bi ping-pong mechanism, with NADPH as the preferred coenzyme (NADH also supports catalysis, but in a less efficient manner). The first catalytic step, described as the reductive half-reaction, consists of the formation of a charge-transfer complex upon NAD(P)H binding, which enables subsequent hydride transfer from the nicotinamide ring C4 atom of NAD(P)H to the N5 atom of oxidized FMN (FMN_{ox}). The second step of the reaction, the oxidative half-reaction, is represented by hydride

transfer from the N5 atom of reduced FMN to an α,β-unsaturated substrate and, in some cases, additional proton transfer from a solvent molecule. The specific biological role of PETNR is unknown, as for all members of the OYE family of oxidoreductases.[207] However, whilst the biological substrate has yet to be discovered, many studies have unveiled the promiscuous nature of PETNR, as it catalyses the reduction of a wide variety of α,β-unsaturated compounds, often with high specificity and enantioselectivity towards desired products.[138] PETNR acts as an ene-reductase, by reducing 2-cyclohexenone and several steroids to their corresponding alkanes, but also catalyses the reduction of cyclic triazines, various explosives (*e.g.* pentaerythritol tetranitrate and trinitrotoluene) and nitrate esters (*e.g.* nitroglycerin). Several mutagenesis studies have highlighted the versatility of PETNR in the asymmetric reduction of C=C bonds, leading to an increased interest in understanding the physical basis of the catalytic power of this enzyme.[138,145,215]

As well as having high potential to be used in biocatalytic processes, PETNR is an excellent model system for studying hydride transfer reactions. Previous kinetic studies have revealed that quantum mechanical tunnelling contributes to the enzymatic hydride transfer step from NAD(P)H to the FMN cofactor, as the reaction manifests elevated kinetic isotope effects.[157] Moreover, fast protein dynamics have been inferred to contribute to catalysis from various temperature and pressure dependence studies, coupled with the use of different isotopic labelling strategies.[95,96,166] However, the difference in reactivity of PETNR towards NADPH and NADH is still not clearly understood and the role of fast protein dynamics in catalytic events requires an atomistic description of the enzyme, as kinetic data alone cannot pinpoint or specifically isolate time-resolved structural changes. Herein, we report the near-complete, sequence-specific ^{1}H, $^{15}N_{H}$, $^{13}C_{\alpha}$, $^{13}C_{\beta}$ and $^{13}C'$ backbone resonance assignments of PETNR in the PETNR:FMN_{ox} complex. The assignments provide a basis for further structural and functional studies by NMR spectroscopy, enabling more complex dynamic studies that can advance our understanding of enzymatic hydride transfer reactions.

3.3. Methods and experiments

All reagents were of analytical grade and were purchased from Sigma-Aldrich (UK), except for $^{15}NH_4Cl$ and $^{2}H_2O$ (>99.9% purity), which were procured from Goss Scientific Ltd. (UK) and $^{2}H_7$,$^{13}C_6$-D-glucose (>98% purity), which was purchased from Cambridge Isotope Laboratories (USA).

Recombinant PETNR is expressed and purified as a tight non-covalently bound PETNR:FMN_{ox} complex. A pBlueScript II SK(+) plasmid encoding the pONR1 gene was used for PETNR overexpression. The ^{2}H,^{13}C,^{15}N-labelled PETNR:FMN_{ox} complex (40 kDa) was expressed in JM109 *E. coli* cells grown in 100% $^{2}H_2O$ modified minimal media, using $^{15}NH_4Cl$ and $^{2}H_7$,$^{13}C_6$-D-glucose as nitrogen and carbon sources, respectively. Cells were incubated at 37 °C with shaking at 200 rpm, until OD_{600nm} = 0.8-1.0, after which the temperature was lowered to 25 °C and PETNR overexpression was induced by the addition of 0.5 mM isopropyl β-D-1-thiogalactopyranoside (IPTG). Cells were grown for a further 24 h before being harvested by centrifugation (6000 rpm for 15 min at 4 °C). All purification steps, which include affinity chromatography using a Mimetic Orange 2 column followed by Source 15Q anion exchange chromatography, were performed at 4 °C, as previously described.[152,162] A final yield of approximately 70 mg pure PETNR per litre of cell culture was obtained.

Following purification, back exchange to amide protium atoms in the ^{2}H,^{13}C,^{15}N-labelled PETNR:FMN_{ox} complex was promoted by mild destabilization using guanidine hydrochloride (GuHCl) as a denaturing agent, followed by rapid protein refolding. Partial unfolding of PETNR was initiated by mixing the sample (0.25 mM) in a 1:1 ratio with 1.5 M GuHCl solution in 50 mM potassium phosphate buffer (pH 7.0), followed by incubation at room temperature for 120 min. Refolding of PETNR was achieved by rapid 30-fold dilution into 50 mM potassium phosphate buffer (pH 7.0), under vigorous stirring. The resulting sample was filtered using a 0.2 µm filter-syringe to remove any precipitates, buffer-exchanged (to remove GuHCl) and concentrated using a Vivaspin 20 concentrator (10 kDa MWCO, Sigma-Aldrich, UK).

The concentration of the PETNR:FMN_{ox} complex was estimated by measuring the FMN-specific absorbance peak at 464 nm (ε = 11.3 mM^{-1} cm^{-1}).

All NMR experiments were conducted with samples containing 1 mM ^{2}H,^{13}C,^{15}N-labelled PETNR:FMN_{ox} complex in 50 mM potassium phosphate buffer (pH 7.0) supplemented with 1 mM NaN_3, 10% (v/v) $^{2}H_2O$ for the deuterium lock and 0.5% (v/v) trimethylsilyl propanoic acid (TSP) for chemical shift referencing. The samples (300 µL) were centrifuged for 10 min at 13,000 rpm before being transferred to 5-mm Shigemi tubes (Sigma-Aldrich, UK). All NMR experiments were recorded at 298 K on an 800 MHz Bruker Avance III spectrometer running TopSpin version 3.2, equipped with a 5-mm ^{1}H/^{13}C/^{15}N TCI cryoprobe and a Z-field gradient coil. The backbone resonance assignment of PETNR was achieved using standard Bruker ^{1}H-^{15}N TROSY and TROSY-based 3D HNCA, HNCACB, HN(CO)CACB, HN(CA)CO and HNCO triple resonance experiments.[168] The 3D experiments were acquired using non-uniform sampling with a sine-weighted multidimensional Poisson Gap scheduling strategy.[216] ^{1}H chemical shifts were referenced relative to the internal TSP signal, whereas ^{15}N and ^{13}C chemical shifts were referenced indirectly using nuclei-specific gyromagnetic ratios.[217] NMR data were processed using TopSpin software version 3.2 and analysed using CcpNmr Analysis software version 2.4.[218]

3.4. Resonance assignment and data deposition

Using conventional TROSY-based 3D heteronuclear experiments, sequential backbone assignment of PETNR in the PETNR:FMN_{ox} complex was achieved to a great extent, with 97% of backbone amide groups successfully assigned (333 out of 344 non-proline residues) in the ^{1}H-^{15}N TROSY spectrum (Figure 3.1). A similar degree of assignment (97%) was achieved for the corresponding $^{13}C_\alpha$, $^{13}C_\beta$ and $^{13}C'$ resonances: 354 out of all 364 C_α atoms, 320 out of all 330 C_β atoms and 354 out of all 364 C' atoms. The chemical shift assignments have been deposited in the Biological Magnetic Resonance Bank (BMRB: http//www.bmrb.wisc.edu/) under the accession number 27224.

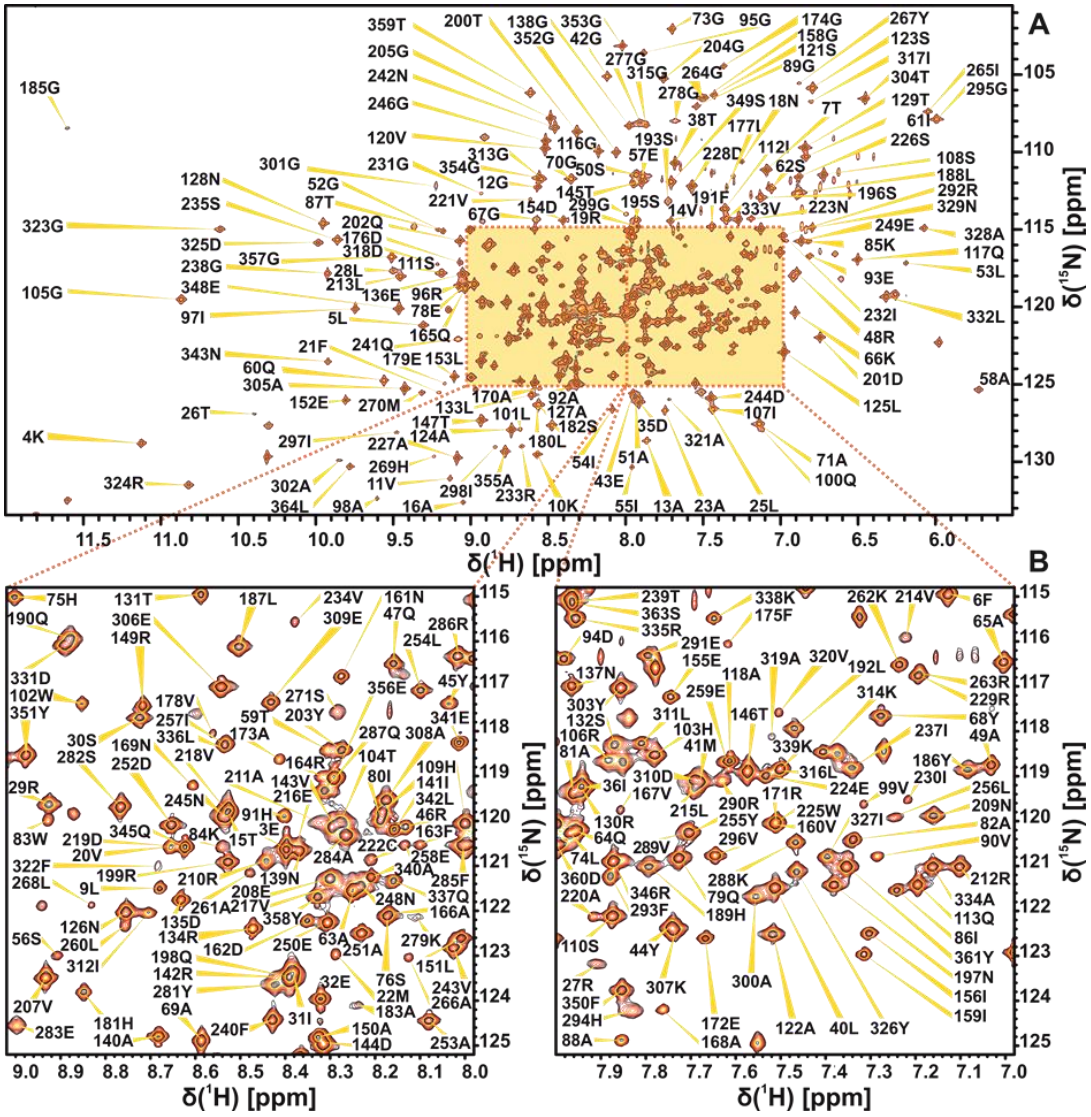

Figure 3.1. ^{1}H-^{15}N TROSY spectrum of 1 mM uniformly ^{2}H,^{13}C,^{15}N-labelled PETNR:FMNox complex in 50 mM potassium phosphate buffer (pH 7.0), recorded at 298 K on an 800 MHz spectrometer. The full spectrum (A) and two expansions of the crowded regions (B) are shown. The assignment of the backbone amide resonances are indicated by sequence number and residue type

The assignment extends the list of large molecular systems that have undergone essentially complete backbone assignment, at a time where limits are being pushed with studies of very large biological systems.[219] The assignment of PETNR was facilitated by the wide dispersion and favourable line shape of the resonances in the ^{1}H-^{15}N TROSY spectrum, attributed to the globular folded structure, isotopic labelling strategy and correlation time of the complex (21 ns). There are ten residues that remain unassigned in the ^{1}H-^{15}N TROSY spectrum (A2, G34, G115, H184, S206, E272, T273, D274, L275 and A276), which are mainly located in a mobile loop (E272-Y281),

at the N-terminus and in other solvent-exposed regions of PETNR (Figure 3.2). The E272-Y281 loop is located at the edge of the substrate-binding pocket of the active site, but is solvent exposed in the PETNR:FMN_{ox} complex and residues T273-A284 have high temperature factors and limited secondary structure, as it has been observed from crystallographic data.[152] Thus, both conformational exchange and solvent exchange are probably the source of signal attenuation beyond detection in the ^{1}H-^{15}N TROSY spectrum for residues E272, T273, D274, L275 and A276. Residue A2, located at the N-terminus, and residues G34, G115 and S206, located at the surface of PETNR, could not be assigned since their ^{1}H-^{15}N TROSY correlations are likely attenuated due to fast exchange with solvent. Residue H184 is known to be involved in substrate coordination[152] and, in the absence of bound substrate, will probably be undergoing conformational exchange on the millisecond timescale.

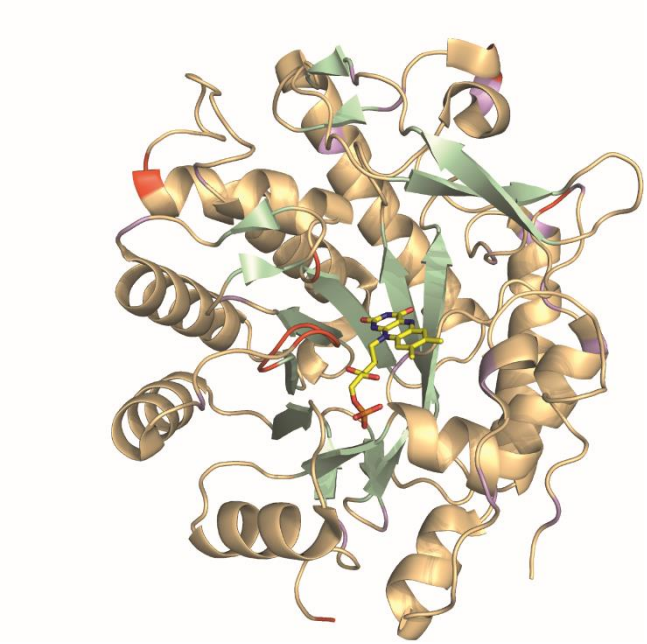

Figure 3.2. Cartoon representation of the crystal structure of the PETNR:FMN_{ox} complex (PDB: 5LGX [220]), highlighting the extent of backbone amide resonance assignments. Assigned residues are coloured *light orange* (for α-helices and loops) and *pale green* (for β-strands), with unassigned residues shown in *red* and proline residues in *purple*. The non-covalently bound FMN cofactor is depicted as *yellow sticks*

An empirical prediction of the secondary structure elements of PETNR in the PETNR:FMN_{ox} complex was performed by uploading the backbone $^{1}H_{N}$, ^{15}N, $^{13}C_{\alpha}$, $^{13}C_{\beta}$

and $^{13}C'$ chemical shift assignments to the TALOS-N webserver.[221] The results of the prediction are illustrated in Figure 3.3, along with a comparison of the secondary structure present in the crystal form of the complex. The prediction derived from the NMR data is in very good agreement with the crystallographic data, with all the specific elements of the eight-stranded α/β barrel (TIM barrel) predicted accurately. The results provide high confidence in the assignments of the PETNR:FMN_{ox} complex.

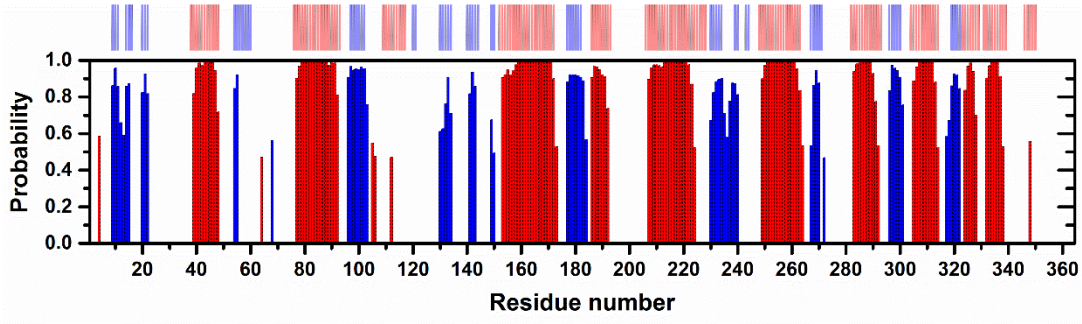

Figure 3.3. Backbone secondary structure prediction of PETNR in the PETNR:FMN_{ox} complex obtained with TALOS-N software[221] using the backbone $^{1}H_N$, ^{15}N, $^{13}C_\alpha$ $^{13}C_\beta$ and $^{13}C'$ chemical shifts. The secondary structure prediction is depicted as *red bars* and *blue bars* for α-helices and β-strands, respectively, with the height of the bars reflecting the probability of each element, as assigned by the software. As a comparison, the secondary structure observed in the crystal form of the PETNR:FMN_{ox} complex (PDB: 5LGX [220]) is shown at the *top* of the figure in the *same colour* representation

4. Nonequivalence of second sphere 'noncatalytic' residues in pentaerythritol tetranitrate reductase in relation to local dynamics linked to H-transfer in reactions with NADH and NADPH coenzymes

Publication status: *a revised version of this manuscript is published in ACS Catalysis* 2018, 8, 12, 11589-11599

Authors: Andreea I. Iorgu, Nicola J. Baxter, Matthew J. Cliff, Colin Levy, Jonathan P. Waltho, Sam Hay, Nigel S. Scrutton

Running header: Probing PETNR reactivity towards nicotinamide coenzymes

Contributions: A.I.I. wrote the paper, with contributions from all authors. A.I.I. conducted all experiments and analysed all the data, except for the crystallography (which was performed by C.L.). N.J.B. and M.J.C. helped with NMR data acquisition and interpretation. J.P.W., S.H. and N.S.S. designed and supervised the project.

4.1. Abstract

Many enzymes that catalyse hydride transfer reactions work *via* a mechanism dominated by quantum mechanical tunnelling. The involvement of fast vibrational modes of the reactive complex is often inferred in these reactions, as in the case of the NAD(P)H-dependent pentaerythritol tetranitrate reductase (PETNR). Herein, we interrogated the H-transfer mechanism in PETNR by designing conservative (L25I and I107L) and side-chain shortening (L25A and I107A) PETNR variants and using a combination of experimental approaches (stopped-flow rapid kinetics, X-ray crystallography, isotope/temperature dependence studies of H-transfer and NMR spectroscopy). X-ray data show subtle changes in the local environment of the targeted side-chains, but no major structural perturbation caused by mutagenesis of the two residues located along the reaction coordinate in PETNR:NAD(P)H complexes. However, temperature dependence studies of H-transfer revealed a coenzyme-specific and complex thermodynamic equilibrium between different reactive configurations in PETNR–coenzyme complexes. We find that mutagenesis of these second sphere 'noncatalytic' residues affects differently the reactivity of PETNR with coenzymes NADPH and NADH. We attribute this to subtle, dynamic structural change in the PETNR active site, the effects of which impact differently in the nonequivalent reactive geometries of PETNR:NADH and PETNR:NADPH complexes. This inference is confirmed through changes observed in the NMR chemical shift data for PETNR complexes with unreactive 1,4,5,6-tetrahydro-NAD(P) analogues. We show that H-transfer rates can (to some extent) be buffered through entropy-enthalpy compensation, but that use of 'sharp' experimental tools reveals hidden complexities that implicate a role for dynamics in this relatively simple H-transfer reaction. Similar approaches are likely to be informative in other enzymes to understand the relative importance of (distal) hydrophobic side-chains and dynamics in controlling the rates of enzymatic H-transfer.

4.2. Introduction

Understanding the physical basis of enzyme catalysis is important from a fundamental point of view, and also to drive applications in contemporary areas of research, such as biotechnology and synthetic biology. The development of sustainable and clean chemical manufacturing practices requires deep appreciation of the physical basis of enzyme catalysis that enables us to mimic and improve Nature's catalysts. Enzymes catalyse many chemical reactions with extraordinary selectivity and specificity and, in some cases, extreme efficiency.[17–19] Whilst it is difficult to pinpoint the exact origin of the catalytic effect for even one particular enzyme, the importance of electrostatic contributions,[222] i.e. stabilization of the transition state, and hydrogen bonding,[43] has long been recognized. Diverse experimental and theoretical methods have been used to probe chemical steps and have contributed to debates relating to physical models of catalysis, in some cases moving beyond traditional semi-classical frameworks for enzyme catalysis.[25,27,32,223] A fast-growing number of experimental studies indicate that protein dynamics might play a role in catalysis, across a hierarchy of timescales.[50–54] Beyond experimental approaches, the involvement of dynamics has been supported also by computation.[55–59] Slower (μs-ms) dynamics attributed to large-scale protein domain motions have been identified using NMR methodologies. Direct coupling of fast (fs-ns) dynamics to chemistry is mostly inferred from kinetic isotope effect (KIE) studies and supported by computational analysis such as transition path sampling.[62–64] The temperature dependence of KIEs is regarded as a "gold standard" for probing quantum mechanical tunnelling (QMT) for H-transfer reactions and some interpretations have inferred a role for distance sampling dynamical contributions to facilitate the tunnelling reaction[65–67,80,81] (although others have questioned these models[68,70,224]). Studies with variant enzymes have led to models in which the temperature dependence of the KIE has been attributed to modulation of donor-acceptor distance (DAD) distributions and perturbation of high-frequency motions,[82] or disruption of dynamic networks[83] that extend to remote residues within the enzyme. Mutagenesis has been used to perturb active site structure and probe effects on H-transfer and inferred dynamical contributions using a number of

enzyme systems (e.g. dihydrofolate reductase,[84] soybean lipoxygenase-1,[85] thymidylate synthase,[86] ene-reductases[87]). Experimental KIE measurements have also been extended to include the use of high pressure[89,90] and "heavy enzymes" (^{2}H, ^{13}C, and/or ^{15}N stable isotope-labelled),[91–96] to probe these effects further, and supported using computational simulations. Much of our current understanding of enzymatic catalysis has come from probing the effects of mutagenesis on catalytic rates and from computational simulations. For H-transfer reactions, this has opened up debates on the relative importance of dynamics in these reactions and challenged the community to develop integrated experimental[97] and theoretical[64] approaches to address this problem.

Old Yellow Enzymes (OYEs) are an intensively investigated class of ene-reductases, which catalyse the asymmetric reduction of a wide variety of activated α,β-unsaturated compounds, with high specificity for substrates bearing nitro- or keto-groups.[118] While their physiological role and natural substrates are often not known,[207] OYEs are particularly attractive to study from a mechanistic perspective, and for their biocatalytic potential. Pentaerythritol tetranitrate reductase (PETNR) is one such enzyme. PETNR has dual-specificity, and is reduced by both NADH and NADPH, but with a preference towards the latter coenzyme.[159] The basis of this dual specificity is not well understood. The catalytic cycle of PETNR follows a single-site ping-pong mechanism. The first step (the reductive half-reaction) involves hydride transfer from the C4 *pro*-R hydrogen atom of the NAD(P)H coenzyme to the N5 atom of the noncovalently-bound flavin mononucleotide (FMN) cofactor.[157] QMT contributes to this catalytic step[95], and several experimental studies have suggested an involvement of fast (ps-ns) dynamics in the H-transfer reaction[65,96,166]. Here, we interrogated the H-transfer mechanism in PETNR by designing four variants of two second sphere residues (L25 and I107), positioned axially either side of the FMN-NAD(P)H reaction coordinate (Figure 4.1), as inferred from the structure of PETNR in complex with the unreactive NADH analogue 1,4,5,6-tetrahydro-NAD.[95] L25 is located below the reaction coordinate, with the side-chain in van der Waals contact with the isoalloxazine ring of the FMN cofactor, while the side-chain of I107 is positioned above the nicotinamide ring of the coenzyme. These residues are 'non

catalytic' and are assumed not to contribute to major active site electrostatic effects. We have altered these residues by making conservative (L25I and I107L) and side-chain length shortening (L25A and I107A) variants of PETNR, with the objective of understanding how second sphere residues influence catalysis, H-tunnelling and any vibrational modes linked to H-transfer. We used X-ray crystallography to assess the impact of mutagenesis on overall structural properties and stopped-flow spectroscopy to analyse the kinetics of hydride transfer through a combination of concentration and temperature dependence studies with both coenzymes (NADPH and NADH). Building on the recent NMR work in which a full sequential backbone assignment of PETNR holoenzyme was undertaken,[202] we also used the coenzyme analogues 1,4,5,6-tetrahydro-NAD(P) (NAD(P)H_4, see Figure A3 in Appendix) to investigate coenzyme binding modes in the ground-state PETNR:NADPH_4 and PETNR:NADH_4 complexes. Our overall aim was to understand how localized dynamics can impact H-transfer in each of these complexes, and to investigate how perturbation of second sphere residues through mutagenesis impacts QMT and active site dynamics associated with this reaction with both NADPH and NADH.

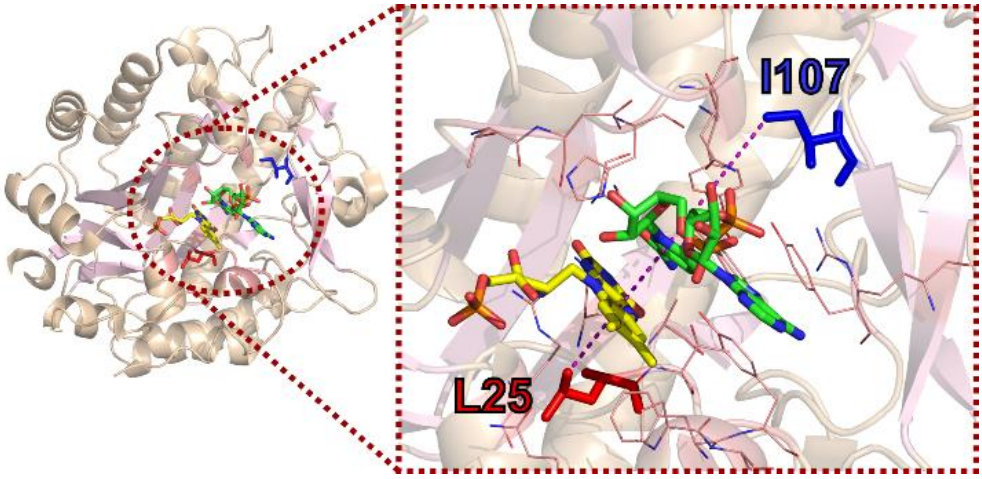

Figure 4.1. Crystal structure of the PETNR:NADH_4 complex (PDB: 3KFT),[95] showing the location of residues L25 (red) and I107 (blue), which have been targeted for mutagenesis. Residues located 5 Å away from the reaction coordinate are represented as wireframes in the right panel of the figure. Residue L25 is located at a ~4 Å distance from the FMN cofactor (yellow), with the side-chain pointing directly below the H-transfer coordinate, while I107 is located ~8 Å above the coenzyme site (green) and is positioned above two bulky side-chains (Y68 and Y186) that form one side of the active site hydrophobic cavity.

4.3. Results and discussion

First, to ensure that mutagenesis of PETNR had not influenced the coordination of the noncovalently bound FMN cofactor, we recorded UV-visible absorption spectra of the PETNR variants. All variants displayed the same spectroscopic features as wild-type PETNR (WT PETNR), with full FMN occupancy in the active site, and maintaining the characteristic PETNR-bound FMN spectral signature, with maxima at 380 nm and 465 nm (Figure S4.1). To assess any impact of mutagenesis on the general structure of the enzyme, we determined X-ray crystallographic structures for all variant forms isolated (Figures S4.2-S4.3 and Tables S4.1-S4.2). When compared to WT PETNR (PDB: 3P62), the RMSD values based on Cα positions corresponding to each variant were in the range 0.3-0.4 Å, indicating a high degree of similarity. No major reorientations occurred in the loops bearing the side-chain mutations and superpositions of all the structures indicates the tertiary TIM-barrel fold and external secondary features were largely unaffected by mutagenesis. Despite the overall structures of each of the four variants remaining largely unperturbed by mutagenesis some subtle shifts in side-chains are observed. One key shift in the I107A variant has led to a reorientation of the side-chain of Q241 (highlighted in Figure S4.2). Removal of the I107 side-chain bulk allows the side-chain of Q241 to rotate towards the vacated space, leading to a slight increase in the coenzyme binding pocket in this region. Altogether, the spectroscopic and structural evidence support the hypothesis that the targeted residues are not directly involved in FMN binding and that the mutations do not affect the overall architecture of the enzyme. Secondary impacts of these mutations resulting in subtle alterations within the active site are investigated below.

One of the benefits in using PETNR to study enzymatic hydride transfer mechanisms is that individual catalytic steps can be accessed by stopped-flow measurements that track changes in FMN absorbance during the reductive half-reaction of the enzyme catalytic cycle. The loss of FMN absorbance during reduction of PETNR by NAD(P)H reports directly on the hydride transfer step, which is essentially irreversible. The observed limiting rate constant (k_{red}) at saturating coenzyme concentration is

therefore the rate of hydride transfer, from which the intrinsic KIE values can also be obtained when using deuterated coenzyme (note that previously we have not observed evidence for other processes affecting the kinetics of H-transfer in OYEs, e.g. isomerization of the enzyme-substrate complex; we believe that the measured KIE is therefore an intrinsic value but we accept that the absence of evidence cannot be taken as proof).[209] This simplifies analysis compared to other enzymes, where studies of H-transfer are often performed under steady-state turnover conditions. For the PETNR variant enzymes, the coenzyme concentration dependencies of hydride transfer were recorded (Figure S4.4). H-transfer was monitored by following the quenching of PETNR-bound FMN absorbance at 465 nm when mixing the enzyme with NAD(P)H (for representative kinetic traces, see Figure 4.2), as described previously.[96,166] Limiting rate constants (k_{red}) and apparent saturation constants (K_S) at 25 °C for PETNR-catalysed hydride transfer are shown in Table 4.1. Although a plethora of data is available for WT PETNR from previous investigations, we re-examined all the kinetics of the WT enzyme for the purpose of this study to eliminate any possible disparities arising from slightly different conditions, coenzyme purity or experimental setup. We were able to confirm that there is no difference between the k_{red} and K_S values obtained in this study and those previously published for WT PETNR.[159]

The kinetic traces measured at 25 °C were adequately fit using a single exponential function for WT PETNR and for some variants. However, the behaviour of a number of variants was found to be more complex (*vide infra* for a more detailed analysis), with the majority of the reaction transients fitting to a double exponential function, comprising a fast rate (k_{obs1}) and a slow rate (k_{obs2} < 5 s^{-1}). The values presented in Table 4.1 reflect only the fast rate of the reaction, as extracted from the fits of the concentration dependence studies (Figure S4.4). By determining the saturation constant (K_S) for each variant, we noticed that there is no major difference in the apparent affinity for NADPH, with the I107L variant having the same affinity (107 ± 5 µM) as WT PETNR (103 ± 4 µM), while the other variants have slightly higher values for K_S, with the most prominent change for L25A PETNR, which exhibits a two-fold increase (K_S = 199 ± 6 µM).

Table 4.1. Observed rates of FMN reduction at 25 °C for PETNR variants with NADPH and NADH[a].

	k_{red} (s^{-1})	K_S (μM)	k_{red}/K_S (s^{-1} μM)
PETNR variant	NADPH		
WT	33.43 ± 0.22	103 ± 4	(3.25 ± 0.13)×10^{-1}
L25A	55.75 ± 0.35	199 ± 6	(2.80 ± 0.09)×10^{-1}
L25I	29.49 ± 0.49	130 ± 8	(2.27 ± 0.14)×10^{-1}
I107A	21.22 ± 0.25	130 ± 9	(1.63 ± 0.11)×10^{-1}
I107L	28.37 ± 0.20	107 ± 5	(2.65 ± 0.12)×10^{-1}
	NADH		
WT	2.03 ± 0.01	1067 ± 13	(1.90 ± 0.03)×10^{-3}
L25A	3.62 ± 0.04	2294 ± 91	(1.58 ± 0.06)×10^{-3}
L25I	1.74 ± 0.04	306 ± 40	(5.69 ± 0.94)×10^{-3}
I107A	2.05 ± 0.04	329 ± 37	(6.23 ± 0.71)×10^{-3}
I107L	1.94 ± 0.02	889 ± 36	(2.18 ± 0.09)×10^{-3}

[a]calculated from fitting data presented in Figure S4.4 to $k_{obs1} = k_{red}[NAD(P)H]/(K_S + [NAD(P)H])$; reaction conditions: 50 mM potassium phosphate buffer (pH 7.0), 20 μM enzyme concentration, [NAD(P)H] ranging 0.1 – 50 mM, 25 °C.

Analysing the limiting rate of reduction, we observed correlations between the size of the side-chain and the H-transfer rates: whilst the conservative (L25I and I107L) mutations have only a minor effect on the rate of FMN reduction, the alanine substitutions impose a markedly modified reaction rate. The rate of H-transfer is 60% faster for the L25A variant than for WT PETNR, while a 40% reduction in rate is observed for the I107A variant (Table 4.1). This suggests that an increase in the mobility of the FMN binding site, caused by shortening the L25 side-chain, is enhancing catalytic rates, while a larger void above the NADPH substrate, induced by truncation of I107 side-chain, is decreasing catalytic rates. While the L25A and L25I variants exhibit a very similar change in rate for the reaction with NADH (when compared to NADPH), the mutations introduced at the I107 site do not affect the limiting rate constant and, moreover, afford better binding of NADH. When comparing k_{red}/K_S (which reports, in this case, on the efficiency of each variant to perform the reductive half-reaction), we conclude that the increase in rate for L25A variants comes with a cost of lower binding affinity, leading to a slightly less efficient enzyme. We have noticed similar compensatory behaviour in the reaction of other OYEs with nicotinamide coenzyme biomimetics, where elevated catalytic rates are associated with inverse changes in binding affinity.[225] The I107A variant is more efficient in the reaction with NADH and is noticeably less efficient for performing H-

transfer from NADPH. Further, we performed temperature dependence studies of the rate of FMN reduction with both NADPH and NADH coenzymes, along with their corresponding deuterated forms, in the range of 5-40 °C. The unusual behaviour of the variants is first noticed through the shape of the transients observed, with all variants manifesting multiple kinetic phases at elevated temperatures (Figure 4.2). In general, the kinetic traces could be fitted to a single exponential function for low temperatures (<20 °C), while at higher temperatures the FMN reduction takes place with multiple resolvable kinetic phases.

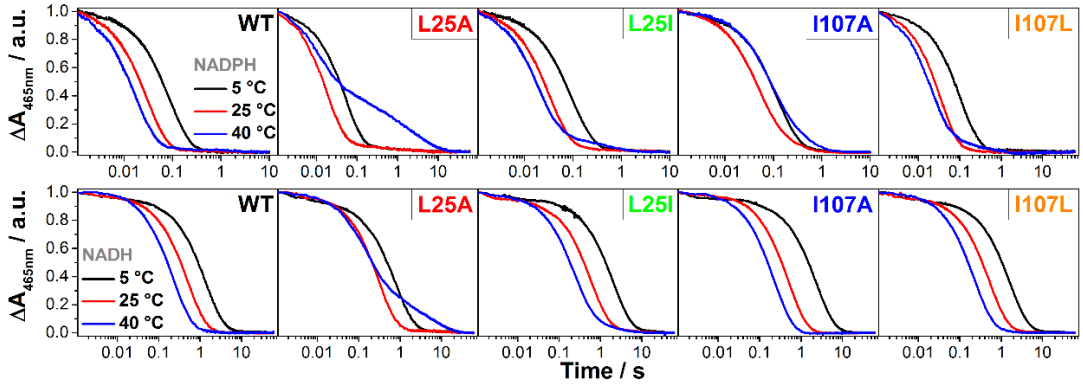

Figure 4.2. Stopped-flow kinetic traces showing FMN reduction for the PETNR variants with NADPH (top panel) and NADH (bottom panel), at selected representative temperatures (5, 25 and 40 °C). All absorbance values were normalised for a better comparison. Conditions: 50 mM potassium phosphate buffer (pH 7.0), 20 µM enzyme, 10 mM NADPH or 25 mM NADH (final concentrations).

It was observed that the amplitude of the slow kinetic components increases with increasing temperature (Figure 4.3), with the effect being more pronounced for the L25A and I107A variants in the case of PETNR reduction by NADPH (~40% of the total absorbance change attributed to k_{obs2} at 40 °C). The reduction with deuterated substrates follows closely that observed for NADPH (Figure S4.5 and Tables S4.3-S4.12). This suggests that the reaction chemistry (H *vs.* D transfer) is not kinetically controlled, and the differences observed are solely attributed to perturbations in the enzyme-coenzyme complex arising from mutagenesis of PETNR. FMN reduction follows the same trend with NADH for L25A and L25I variants, with multiple reactive configurations (MRCs) at elevated temperature and similar changes of amplitude contributions for each kinetic component. However, the mutagenesis of the I107 site

does not induce the formation of MRCs in reactions with NADH (the kinetic traces fit to a single exponential function across the studied temperature range, Figure 4.3 and S4.6), a contrasting behaviour when compared to reduction by NADPH. This indicates that truncation of I107 site has no detrimental effect on H-transfer from NADH coenzyme, whilst the NADPH reaction is noticeably affected. This suggests truncation of the I107 side-chain induces propagated effects (which extend beyond the tilting of the Q241 side-chain observed from X-ray data) on the structure (and dynamics) of the enzyme.

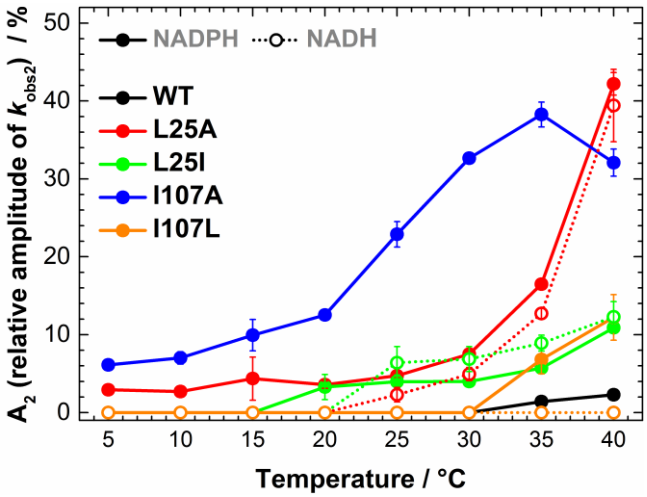

Figure 4.3. Manifestation of multiple reactive configurations as a function of temperature for investigated PETNR variants. For variants manifesting MRCs, the relative amplitude of the slow kinetic phase (k_{obs2}) during FMN reduction of PETNR variants by NADPH and NADH is increasing with temperature. The relative amplitude is reporting on the change in amplitude corresponding to the slow kinetic phase out of the total change in amplitude measured during FMN reduction. For L25A variant, the amplitude value at 40 °C represents the sum of two slow kinetic phases (k_{obs2} and k_{ob3}, see Tables S4.4 ad S4.9).

We have previously detected MRCs in the N189A variant of morphinone reductase (MR), another enzyme belonging to the OYE family, in which four detectable MRCs could be kinetically resolved.[87] Likewise, the data for the reduction of PETNR variants suggests that NADPH and NADH are able to bind in multiple conformations in the active site of PETNR variants, which leads to different competent states of the enzyme-coenzyme complex that are able to perform H-transfer, observed as multiple kinetic phases bearing KIEs (Figures S4.7-S4.8). While the k_{red} value is highest for L25A, this fast reactive conformation is very slowly interconverting (< 1 s^{-1}) with

another slow reactive conformation. In our previous work involving MR,[87] we were able to corroborate that the resolved kinetic phases represent different configurations of the enzyme-coenzyme complex using computational methods. Herein, we propose that our observations with PETNR are consistent with those we have reported previously with MR. This inference is consistent with the available evidence (KIEs observed on each kinetic phase for PETNR). However, we cannot exclude other explanations at this stage, e.g. a mechanism involving multiple free enzyme species that have different reactivities.

Given the KIE values at 25 °C are only slightly affected by mutagenesis, with small differences between the studied variants (Figure S4.7), we consider that a better way to interpret the data (as we have recently described elsewhere[96]) is by comparing the activation parameters (presented in Table 4.2). We analysed the thermodynamic parameters of the H-transfer reaction by fitting the Arrhenius plots of k_{obs1} (Figure 4.4) to the nonlinear Eyring-based function:

$$\ln k_{\mathrm{obs}} = \ln\left(\frac{k_{\mathrm{B}}T}{h}\right) - \frac{\Delta H^{\ddagger}_{T_0} + \Delta C^{\ddagger}_{\mathrm{p}}(T - T_0)}{RT} + \frac{\Delta S^{\ddagger}_{T_o} + \Delta C^{\ddagger}_{\mathrm{p}} \ln\left(\frac{T}{T_0}\right)}{R} \qquad (4.1)$$

where $\Delta H_{T0}^{\ddagger}$ and $\Delta S_{T0}^{\ddagger}$ are the apparent activation enthalpy and entropy, respectively, at a reference temperature (T0, 298 K in this study), $\Delta C_p^{\ddagger}$ is the difference in heat capacity between the reactant and transition states and k_B, h, and R are the Boltzmann, Planck, and ideal gas constants, respectively.[212,213]. This model has recently been used for interpreting curvatures observed in Eyring plots for a number of enzymes,[226,227] and recent computational work suggests changes in $\Delta C_p^{\ddagger}$ are related to dynamical changes during catalysis, and these changes are attributed from contributions of not only active site regions, but also distal domains of the enzyme (dynamical changes that are dispersed throughout the entire structure).[228]

Table 4.2. Extracted parameters from kinetic and thermodynamic studies.

PETNR variant	$\Delta H_{T0}^{\ddagger}$ (kJ mol^{-1})	$\Delta S_{T0}^{\ddagger}$ (J mol^{-1} K^{-1})	$\Delta C_p^{\ddagger}$ (kJ mol^{-1} K^{-1})	$\Delta H_{T0}^{\ddagger}$ (kJ mol^{-1})	$\Delta S_{T0}^{\ddagger}$ (J mol^{-1} K^{-1})	$\Delta C_p^{\ddagger}$ (kJ mol^{-1} K^{-1})
	NADPH			NADH		
WT	30.4 ± 0.3	-113.9 ± 0.9	-0.50 ± 0.05	35.4 ± 0.1	-120.5 ± 0.5	0.39 ± 0.03
L25A	23.3 ± 1.2	-133.7 ± 4.1	-0.92 ± 0.12	33.6 ± 0.5	-122.1 ± 1.7	0.28 ± 0.05
L25I	30.4 ± 0.6	-114.9 ± 2.0	-0.43 ± 0.07	42.7 ± 1.7	-97.7 ± 6.0	0.32 ± 0.18
I107A	17.8 ± 2.3	-160.2 ± 7.7	-1.08 ± 0.23	46.4 ± 1.1	-83.8 ± 3.6	-0.47 ± 0.22
I107L	31.5 ± 0.7	-111.6 ± 2.4	-0.44 ± 0.08	38.7 ± 0.2	-110.0 ± 0.8	0.23 ± 0.04
	(*R*)-[4-^{2}H]-NADPH			(*R*)-[4-^{2}H]-NADH		
WT	36.8 ± 0.3	-108.0 ± 0.1	-0.32 ± 0.04	40.3 ± 0.1	-120.4 ± 0.5	0.46 ± 0.02
L25A	31.9 ± 1.1	-120.5 ± 3.7	-0.78 ± 0.15	40.3 ± 1.1	-115.7 ± 3.8	0.42 ± 0.14
L25I	36.7 ± 0.5	-109.5 ± 1.6	-0.53 ± 0.09	44.9 ± 0.2	-106.8 ± 0.8	0.30 ± 0.07
I107A	19.0 ± 0.2	-172.6 ± 0.7	-1.43 ± 0.02	53.5 ± 1.7	-77.0 ± 5.6	0.17 ± 0.22
I107L	35.7 ± 0.4	-112.9 ± 1.4	-0.65 ± 0.07	45.4 ± 0.3	-103.9 ± 0.9	0.43 ± 0.07
	Isotope effect: (*R*)-[4-^{2}H]-NADPH - NADPH			Isotope effect: (*R*)-[4-^{2}H]-NADH - NADH		
WT	6.4 ± 0.4	5.8 ± 1.5	0.18 ± 0.06	4.9 ± 0.2	0.1 ± 0.7	0.07 ± 0.04
L25A	8.6 ± 1.27	13.3 ± 5.6	0.14 ± 0.19	6.6 ± 1.2	6.4 ± 4.2	0.13 ± 0.15
L25I	6.3 ± 0.7	5.4 ± 2.5	-0.11 ± 0.11	2.3 ± 1.8	-9.2 ± 6.0	-0.03 ± 0.19
I107A	1.2 ± 2.3	-12.3 ± 7.7	-0.35 ± 0.23	7.1 ± 2.0	6.8 ± 6.7	0.64 ± 0.31
I107L	4.2 ± 0.8	-1.3 ± 2.8	-0.22 ± 0.11	6.7 ± 0.4	6.1 ± 1.2	0.19 ± 0.08

For the reactions with NADPH and (*R*)-[4-^{2}H]-NADPH, the apparent activation enthalpy values for WT PETNR are identical with those previously reported, with a coenzyme isotope effect of 6.4 ± 0.4 kJ mol^{-1}, which we previously inferred to be an evidence of a "soft" promoting motion contributing to catalysis.[95] The kinetic isotope effect on the FMN reduction with NADH and (*R*)-[4-^{2}H]-NADH in WT PETNR manifests less temperature independence ($\Delta\Delta H_{T0}^{\ddagger}$ = 4.9 ± 0.2 kJ mol^{-1}) when compared with the KIE on the NADPH reaction (note that early work indicated a measurable temperature independent KIE, which we now believe was underestimated[95]). Overall, when comparing the apparent activation enthalpies and entropies for the PETNR variants, we observed a strong compensatory behaviour (Figure S4.9). This linear enthalpy-entropy compensation was recently observed in a study involving "heavy" PETNR isotopologues.[96] This compensation effect is closely observed for $\Delta\Delta H_{T0}^{\ddagger}$ and $\Delta\Delta S_{T0}^{\ddagger}$: changes in $\Delta\Delta H_{T0}^{\ddagger}$ values are reflected by similar changes in $\Delta\Delta S_{T0}^{\ddagger}$ (Figure 4.5A). Moreover, for the NADPH reaction, there is a strong correlation between the rate of the reaction and the coenzyme KIEs (differences in the apparent activation enthalpy, (*R*)-[4-^{2}H]-NADPH – NADPH), but there is no correlation for the NADH reaction (Figure 4.5B).

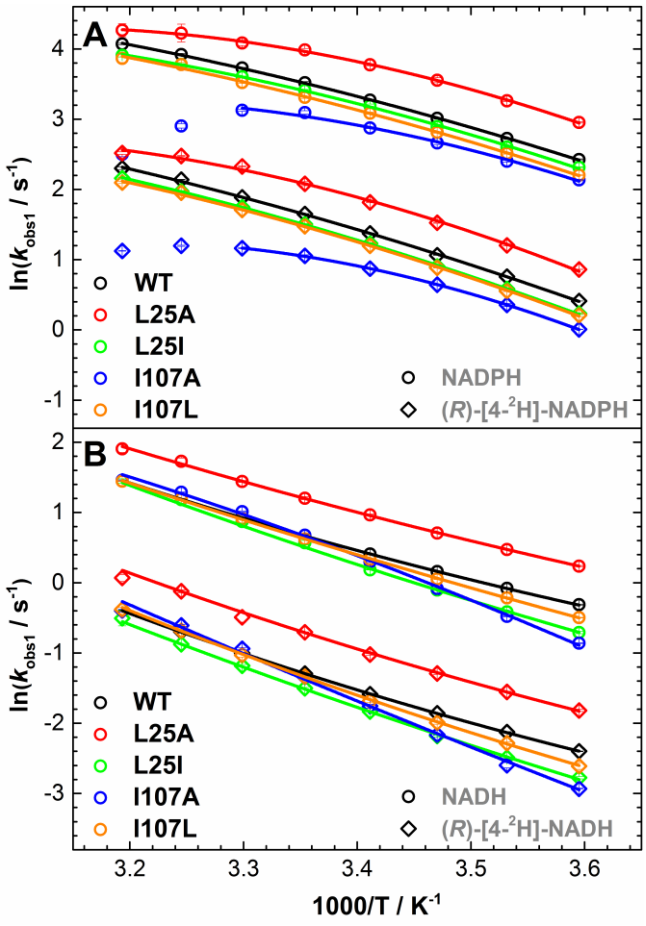

Figure 4.4. Arrhenius plots of the observed rate of hydride transfer from (A) NADPH and (*R*)-[4-^{2}H]-NADPH and (B) NADH and (*R*)-[4-^{2}H]-NADH to FMN in studied PETNR variants; plots of k_{obs1}, data from Tables S4.3-S4.12. See Table 4.2 for extracted parameters. *Note:* the decrease in k_{obs1} values for I107A PETNR reaction with NADPH and (*R*)-[4-^{2}H]-NADPH at 35-40 °C suggests a different mechanism at elevated temperatures, hence the data was omitted during the fitting.

The more prominent changes in $\Delta C_p^{\ddagger}$ are observed for the variants with side-chain truncations (L25A and I107A), which manifest a more negative $\Delta C_p^{\ddagger}$ when compared to WT PETNR. A recent study of ketosteroid isomerase and α-glucosidase MalL showed that the decrease in $\Delta C_p^{\ddagger}$ can be explained through significant dynamical contributions of regions remote from the active site.[228] In the case of PETNR, the effect of side-chain truncation on catalytic rates, enthalpy values, coupled with the nonequivalence in reactivity towards the two coenzyme and changes in $\Delta C_p^{\ddagger}$, could inform on vibrational coupling (previously observed in "heavy enzyme" studies[59,166]) that is extended beyond the mutagenesis site(s). While it is assumed that $\Delta C_p^{\ddagger}$ values are negative for enzyme systems in which the chemical reaction is rate limiting (as

the heat capacity for enzyme-substrate complex is larger than for the enzyme-transition state complex),[228] most of the data for PETNR reduction by NADH show negative values for $\Delta C_p^{\ddagger}$.

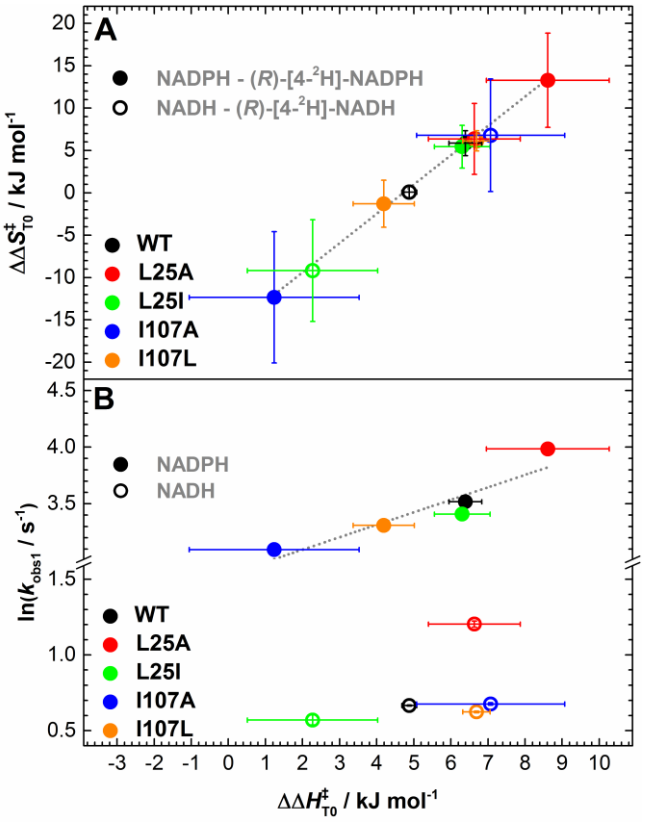

Figure 4.5. The relationship between the differences (coenzyme KIE) in apparent activation enthalpy ($\Delta\Delta H_{T0}^{\ddagger}$) and entropy (A) and correlations between $\Delta\Delta H_{T0}^{\ddagger}$ and observed rate constant (B) during H-transfer for the PETNR variants.

The kinetic and thermodynamic analysis of the reduction of FMN in the PETNR variants reveals coenzyme-specific perturbations to the H-transfer chemistry and thermal equilibrium of reactant states. The current knowledge we have at hand to rationalize these findings comes mainly from crystallographic studies (presented herein) and previously performed molecular dynamics (MD) simulations. The MD data suggest a similar binding mode for both NADPH and NADH coenzymes in the active site of PETNR,[95] which makes it difficult to rationalize the differences in H-transfer chemistry and thermal conformation equilibrium presented above. Although the crystal structure of the PETNR:$NADH_4$ complex (PDB: 3KFT[95]) provides valuable insight into the structural proximity of reacting groups in the active site, π-π stacking between the symmetry-related adenosine moieties of $NADH_4$ in the two

PETNR:$NADH_4$ monomers present in the asymmetric unit of the crystal lattice results in the pyrophosphate and adenosine groups of $NADH_4$ being poorly coordinated by PETNR. The absence of such interactions limits predictions and analyses that can be made regarding the conformational preferences of $NADPH_4$ binding to PETNR. Despite numerous attempts, we have been unable to crystallize the PETNR:$NADPH_4$ complex, which limits further structural and computational investigations. Consequently, we pursued NMR studies of WT PETNR, and recently reported the ^{1}H, ^{15}N and ^{13}C sequential backbone resonance assignments of the holoenzyme.[202] Building on this recent work, we have now performed near-complete backbone resonance assignments of the ground state PETNR:$NADH_4$ and PETNR:$NADPH_4$ complexes at saturating concentrations of either $NADH_4$ or $NADPH_4$, which we further used to inspect differences in the binding modes between the coenzymes. Given the large size of PETNR (40 kDa), TROSY-based 3D heteronuclear experiments were acquired and analysed, which enabled a highly successful degree of assignment (97%) of the ^{1}H–^{15}N TROSY spectrum for each complex. Compared to the extent of assignment achieved for PETNR (333 residues), in the case of the PETNR:$NADH_4$ complex, 334 residues were successfully assigned, as H184 could be identified as a sharp and intense peak after ligand addition. Further assignment of one more residue of the flexible loop (D274) was also achieved, however residue R164 could not be assigned, most probably due to peak overlap. The PETNR:$NADPH_4$ complex was assigned to the greatest extent (335 residues), with all residues identified as in the PETNR:$NADH_4$ complex, as well as the additional assignment of residue R164.

In order to assess the impact of the NAD(P)H_4 coenzyme analogue binding on the PETNR structure, we comparatively analysed the ^{1}H-^{15}N TROSY spectrum of PETNR with ^{1}H-^{15}N TROSY spectra of the PETNR:$NADH_4$ and PETNR:$NADPH_4$ complexes. Overall, the changes in chemical shift for $^{1}H_N$ and ^{15}N are limited to similar residue segments for all complex comparisons (Figure S4.10). The differences in combined chemical shift between each complex and PETNR, and a visual mapping of these changes onto the crystal structure of the PETNR:$NADH_4$ complex (PDB: 3KFT[95]) is illustrated in Figure 4.6. It can be observed that, whilst the majority of the peaks are essentially not sensitive to coenzyme analogue binding, localized areas of PETNR are

noticeably affected by the addition of either $NADPH_4$ or $NADH_4$ (see Figure S4.11 for a structural overview of notably affected regions). Most of the changes that occur in PETNR upon binding of the coenzyme analogues are localized approximately 5 Å away from either $NADH_4$ or the FMN cofactor, with similarly affected sites for both the $NADPH_4$ and $NADH_4$ analogues. The regions that are affected significantly by binding of NAD(P)H_4 are depicted in Figure 4.6B. These encompass several loop regions (with maximum chemical shift differences recorded at residues T26, Y68, T104, Q241, G277, A302, Y351), a histidine "patch" that is known from crystallographic data to coordinate the $NADH_4$ coenzyme analogue[152] (denoted the H184 patch) and an α-helix found in close contact with the FMN cofactor (denoted the R324 helix). Coenzyme analogue binding is also observed to cause significant chemical shift changes in the β-hairpin flap (a region encompassing N126-T147), suggesting a major role of this structural motif in binding the NAD(P)H coenzyme in the active site. The significant differences in chemical shift between PETNR and the PETNR:NAD(P)H_4 complexes observed in the β-sheet containing A58 and the loop involving Y351 (which are known to coordinate the FMN cofactor[152]), along with differences located at the top of the β-barrel that is in close proximity to FMN, suggest that NAD(P)H_4 binding induces FMN repositioning within the active site for efficient H-transfer. This is supported by the formation of a charge-transfer complex between NAD(P)H_4 and FMN, resulting in changes to the electrostatic distribution within the system, which contributes to the observed differences in chemical shift. For T26, the large difference in chemical shift can be explained by the formation of a hydrogen bond between the sidechain hydroxyl group of T26 and the NH_2 group of the carboxamide function of the nicotinamide ring in NAD(P)H_4 and by perturbations in the hydrogen bond between the backbone amide proton of T26 and the N5 atom of FMN. For the resonances assigned in the G277 loop, the NMR data suggest that coenzyme analogue binding induces a dramatic reorganization of the loop. This effect is propagated into the α-helix from which the G277 loop emerges, which is also moderately affected by NAD(P)H_4 binding, even though it is positioned far away from the active site.

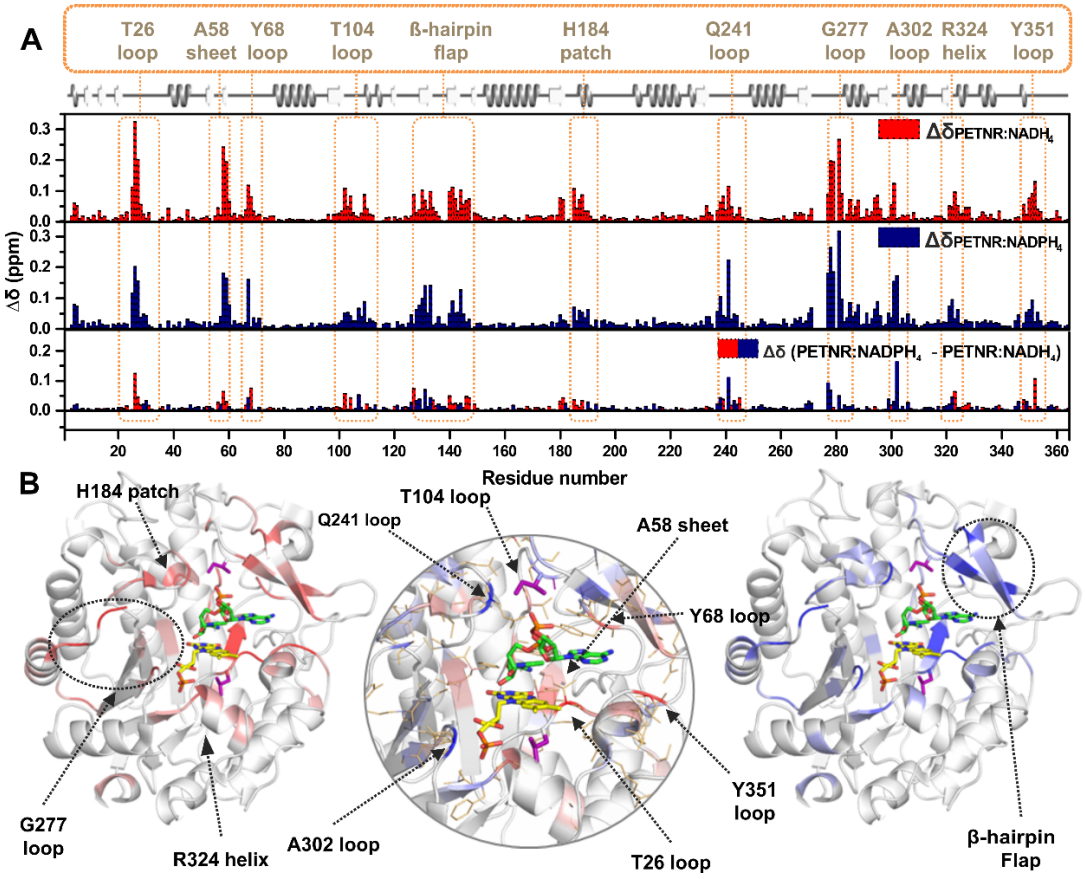

Figure 4.6. Observed changes in chemical shift for PETNR upon binding the $NADH_4$ or the $NADPH_4$ coenzyme analogues. A) Histograms of the residue-specific chemical shift changes for the backbone amide groups in PETNR upon binding $NADH_4$ (red) or $NADPH_4$ (blue). The absolute chemical shift changes were calculated using the following equation: $\Delta\delta_X = [(\delta_{HN}PETNR - \delta_{HN}X)^2 + (C(\delta_N PETNR - \delta_N X))^2]^{1/2}$, where δ_{HN} is the backbone amide proton chemical shift, δ_N is the backbone amide nitrogen chemical shift, C value is 0.12 (for rescaling of δ_N values), and X is either the PETNR:$NADH_4$ complex or the PETNR:$NADPH_4$ complex. The lower histogram shows the residue-specific chemical shift differences between the PETNR:$NADH_4$ complex and the PETNR:$NADPH_4$ complex, with red and blue bars indicating larger changes in PETNR upon binding $NADH_4$ or $NADPH_4$, respectively. The absolute chemical shift differences between the PETNR:NAD(P)H_4 complexes were calculated as $\Delta\delta = [(\Delta\delta_{PETNR:NADPH4} - \Delta\delta_{PETNR:NADH4})^2]^{1/2}$. The secondary structure of PETNR is shown at the top of the figure with gray helices denoting α-helices and white arrows indicating β-strands. Regions with significant $\Delta\delta$ values are highlighted with segment labels. B) Distributions of $\Delta\delta$ values plotted onto the structure of the PETNR:$NADH_4$ complex (PDB: 3KFT). Residues with significant $\Delta\delta$ values are coloured red ($\Delta\delta_{PETNR:NADH4}$ - left panel) and blue ($\Delta\delta_{PETNR:NADPH4}$ – right panel). The FMN cofactor is shown as yellow sticks, the $NADH_4$ coenzyme analogue is shown as green sticks and the mutation sites (L25 and I107) are depicted as purple sticks. The central panel encompasses a zoomed-in view of the active site and highlights the $\Delta\delta$ values between the two complexes (red – larger $\Delta\delta$ upon PETNR:$NADH_4$ complex formation; blue – larger $\Delta\delta$ upon PETNR:$NAPDH_4$ complex formation) and is a structural visualization

of the data in the lower histogram. Sidechains are shown as gold wireframes and regions with significant ΔΔδ values are highlighted with segment labels. Proline residues, unassigned residues and residues with Δδ < 0.04 ppm (the standard deviation) are left blank in the representation, while residues with Δδ ≥ 0.04 ppm are coloured as described above, with a stronger intensity of colour representing a higher Δδ value. In the central panel, no cut-off was applied for Δδ.

Overall, similar residue segments show differences in backbone amide ^{15}N chemical shifts between the PETNR:NADH$_4$ and PETNR:NADPH$_4$ complexes (Figure 4.7). Analysis of amide ^{15}N chemical shift changes ($\Delta\delta_N$) can provide valuable information on the location of conformational differences between the complexes, as they report mainly on changes in backbone torsion angles. The only structural difference between the coenzyme analogues is the presence of a 2'-phosphate group on the ribose ring of the adenosine moiety in NADPH$_4$. Therefore, $\Delta\delta_N$ values reported between these analogues reflect how PETNR specifically modifies its conformational and dynamic preferences to accommodate NADPH$_4$ binding in the active site.

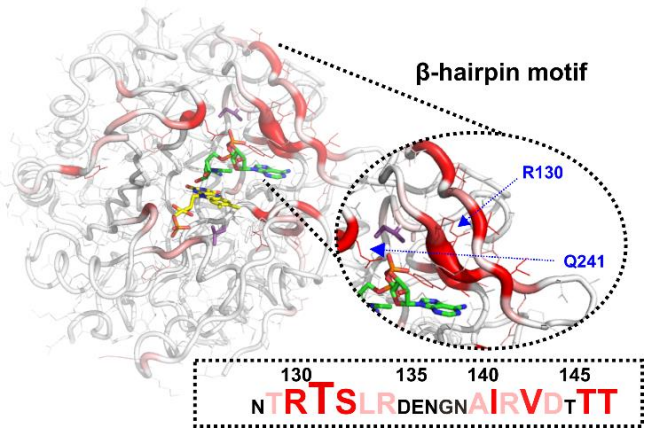

Figure 4.7. Structural mapping of absolute chemical shift differences for backbone amide ^{15}N atoms calculated as: $\Delta\delta_N = [(\delta_N\text{PETNR:NADPH}_4 - \delta_N\text{PETNR:NADH}_4)^2]^{1/2}$ plotted onto the structure of the PETNR:NADH$_4$ complex (PDB: 3KFT) (Figure S4.10). Residues with significant $\Delta\delta_N$ values are coloured red, with a stronger intensity of colour representing a higher $\Delta\delta_N$ value, with a cut-off of 0.1 ppm applied. The side-chains are shown as wireframes in the putty representation of the protein, the FMN cofactor is shown as yellow sticks, the NADH$_4$ coenzyme analogue is shown as green sticks and the mutation sites (L25 and I107) are depicted as purple sticks. The zoomed-in view of the β-hairpin flap highlights the $\Delta\delta_N$values between the two complexes, and identifies the location of R130 and Q241, which are residues with significant differences between the two complexes.

The residue with the largest $\Delta\delta_N$ value involves T131, present in a cluster of contiguous residues (T129-R134 and A140-T147 of the β-hairpin flap), which have significant ^{15}N chemical shift differences (Figure 4.7, Figure S4.10). Although the R130 side-chain and the putative location of the 2'-phosphate group are not within hydrogen bonding distance in the crystal structure of the PETNR:$NADH_4$ complex, it is likely that bond rotation would allow productive coordination of these groups in solution. Structural perturbations within the β-hairpin flap are propagated to Y68 and also to Q241 *via* a network of side-chain hydrogen bonds involving Y186, which are positioned directly over the face of the nicotinamide ring of NADH4 in close proximity to I107. Conformational differences within the β-hairpin flap are also propagated through side-chain hydrogen bonding with R134 to the L25-I31 and E348-G352 regions. For the D274-G277 loop with missing structural density in the crystal, chemical shift differences in the G278-E283 region indicate that the loop likely coordinates the coenzyme. Remarkably, chemical shift perturbations are also noted for G301-A302 and F322-G323 which are residues that coordinate the phosphate group present in FMN, indicating that conformational and dynamic preferences for $NADH_4$ and $NADPH_4$ coordination by PETNR are propagated through the charge transfer complex formed with FMN.

Based on the differences in chemical shift observed between PETNR and the PETNR:NAD(P)H_4 complexes, we can now rationalize, in part, the kinetic behaviour of the investigated variants. Residue L25 presents large differences in chemical shift for both PETNR:$NADH_4$ and PETNR:$NADPH_4$ complexes, and these observations are most readily explained by its close proximity to T26, which is a residue directly involved in FMN cofactor binding.[152] In the crystal structure, residue I107 is positioned ~8 Å away from the face of the $NADH_4$ nicotinamide ring and is sandwiched between Y68, Y186 and Q241, which make direct contact with the coenzyme analogue and a segment of the β-hairpin flap. I107 is slightly affected by $NADPH_4$ binding, but not by $NADH_4$ binding, suggesting that the presence of phosphate in the coenzyme analogue contributes to a more pronounced reorientation of the loop containing I107. Overall, the structural features in the vicinity of the FMN cofactor (and residue L25) are highly affected by both coenzymes,

with higher chemical shift changes occurring upon $NADH_4$ addition, while the regions affected more by $NADPH_4$ binding are situated in the vicinity of residue I107 (Figure 4.6B). The fact that residue I107 is not affected by $NADH_4$ binding, and H-transfer kinetics are also not majorly affected for the reduction with NADH (*i.e.* FMN reduction occurs in a single phase), as in contrast with $NADPH_4$, informs clearly about differences in the binding modes of the two coenzymes, which have consequences on the H-transfer mechanism. Along with the observed reorientation of Q241 side-chain in I107A variant, the NMR and thermodynamic data suggests extended vibrational coupling is present during H-transfer from NADPH to PETNR.

To further the analysis of the binding modes of the two coenzymes, we performed an analysis of the ^{1}H linewidth of peaks in the ^{1}H-^{15}N TROSY spectra (Figure S4.12), which enables detection of residues that have a significant exchange contribution to the transverse relaxation rate (R_2). Broadening of the linewidth suggests conformational exchange between two or more species on the µs-ms NMR timescale.[229] It can be observed that PETNR exhibits a high degree of conformational exchange on this timescale, with most of the regions affected being located around the active site (Figure S4.13). A reduction in the exchange contribution to R_2 can be observed for some residues following addition of $NADH_4$, such as those situated in the G277 loop. The minimization of this dynamic behaviour is even more pronounced in the case of the PETNR:$NADPH_4$ complex, for which most of these slow conformational exchange processes are removed. The data indicate that the $NADPH_4$ coenzyme mimic is interacting more tightly with PETNR than its non-phosphorylated counterpart, which explains the higher affinity of PETNR for NADPH than for NADH (Table 4.1). The mutations chosen for kinetic studies are located on the edge of these regions that exhibit µs-ms conformational exchange in PETNR. Residue I107 is not a dynamic centre, but it is located in a region with moderate dynamic behaviour in PETNR, while linewidths for residues in the vicinity of L25 are considerably broadened. Both regions around the targeted residues show a restriction in conformational exchange on addition of coenzyme, suggesting an important role of binding in controlling enzyme motions on the µs-ms timescale.

This study was undertaken to investigate how second sphere 'noncatalytic' residues influence vibrational modes linked to H-transfer and H-tunnelling in PETNR. The use of a combination of 'sharp' experimental tools (e.g. stopped-flow rapid kinetics, isotope/temperature dependence studies of H-transfer and NMR spectroscopy) allowed us to underpin a complex, coenzyme-specific kinetic and thermodynamic equilibrium during H-transfer in the investigated variants. The side-chain modifications (L25I, L25A, I107A and I107L PETNR) were designed based on their location within the active site (situated along the reaction coordinate in the PETNR:NAD(P)H complexes). The hypothesis that the targeted side-chains are not involved in major electrostatic interactions within the active site was confirmed through stationary UV-visible spectroscopy and crystallographic data. The side-chain modifications are very subtle, but they prompt changes to the conformational landscape of the enzyme that can be observed during the reductive half-reaction using stopped-flow techniques. Broadly, H-transfer rates are maintained through enthalpy-entropy compensation and any small changes in H-transfer rate can be correlated with truncation of the residue side-chains and their position in the active site. However, temperature dependence studies of H-transfer revealed a coenzyme-specific and complex thermodynamic equilibrium between different reactive configurations in PETNR–coenzyme complexes. We find that mutagenesis of these second sphere 'noncatalytic' residues (L25 and I107) affects differently the reactivity of PETNR with coenzymes NADPH and NADH. The thermal equilibrium between the multiple reactive states is considerably shifted in the case of alanine variants (L25A and I107A). Moreover, this equilibrium of MRCs is thermally activated and coenzyme-specific, as it does not occur in the FMN reduction of I107 variants with NADH. We attribute these differences to subtle, dynamic structural changes in the PETNR active site, the effects of which impact differently in the nonequivalent reactive geometries for PETNR:NADH and PETNR:NADPH complexes. This inference is confirmed in chemical shift data for PETNR:$NADH_4$ and PETNR:$NADPH_4$ complexes obtained from NMR analysis. Further NMR and computation studies focusing on the variants investigated herein could enable us to determine whether the thermodynamically-controlled MRCs are caused by shifts in the enzyme population

(changes in the conformational landscape of the enzyme) or/and perturbations of distance sampling of the donor-acceptor coordinate.

4.4. Concluding remarks

Enzymes have evolved to catalyse chemical reactions with extraordinary selectivity and specificity, and it is often assumed that predominantly one configuration of the enzyme-substrate complex will be the catalytically active one. This hypothesis has a strong physical basis for the reaction of WT enzymes with their natural substrates. However, when dealing with enzyme variants, the perturbation of the finely tuned enzyme structure by mutagenesis can change the conformational flexibility and geometries in the enzyme to the extent that multiple reactive conformations are populated. To date, kinetic studies of OYEs have allowed us to demonstrate that variants of two enzymes in this family (N189A variant of MR[87] and this study) exhibit shifted distributions of reactive conformational states, when compared to the corresponding WT enzymes. While the N189A variant of MR could be considered a disruptive mutation (N189 is intimately involved in coenzyme binding through H-bonding), it is not the case for the variants described in the current study. Herein, the synergistic use of complementary spectroscopic techniques has allowed us to unravel the nonequivalence of second sphere 'noncatalytic' residues in PETNR. The complex kinetic behaviour observed upon truncation of L25 and I107 side-chains indicates long-range cooperativity throughout the active site. We suggest that formation of MRCs could be a common feature when investigating variant enzymes, and other authors have pointed towards the existence of parallel reaction pathways during catalysis.[230,231]. Moreover, kinetic complexities on H-transfer caused by (distal) mutagenesis have been observed in dihydrofolate reductase catalysis,[82] and these effects have been correlated with protein dynamics contributions.[81,84,232–234] While we are aware of the experimental challenges that would allow us to visualize MRCs in a wider range of H-transfer enzymes, we believe that synergistic experimental approaches should aid interpretation of kinetic data. This study is an illustration of how the use of 'sharp' experimental tools can uncover details often masked in more traditional studies of H-transfer (e.g. those reliant only on the use

of steady-state turnover studies with isotopically-labelled substrates). These approaches are needed to identify these hidden complexities even for relatively simple reactions such as H-transfer. Similar approaches are therefore likely to be informative with other enzymes to understand the relative importance of small-scale dynamics in controlling enzymatic rates of reaction.

4.5. Supporting information

4.5.1. Experimental section

Materials. All reagents were of analytical grade and were purchased from Sigma-Aldrich (Dorset, UK), except for $NADP^+$, NADH and NADH, which were obtained from Melford Laboratories (Chelsworth, U.K.). All isotopically enriched compounds (^2H_2O, $^{15}NH_4Cl$ and $^2H_7$,$^{13}C_6$-D-glucose) used for ^2H,^{13}C,^{15}N-labelled PETNR overexpression were obtained from Goss Scientific Ltd. (Crewe, U.K.).

Preparation of deuterated and reduced coenzymes. (*R*)-[4-^{2}H]-NADPH and (*R*)-[4-^{2}H]-NADH were synthesized by enzymatic stereospecific reduction of $NADP^+$ or NAD^+ and purified as previously described (purity determination by ^{1}H NMR spectroscopy confirmed isotopic purity >98.5%).[235] NAD(P)H_4 was synthesized by reduction of NAD(P)H with hydrogen using palladium-activated charcoal, and isolated as described before.[235]

Overexpression and purification of variant enzymes. The desired mutations were introduced into the PETNR-containing pONR1 gene using the Stratagene QuikChange II Site-Directed Mutagenesis Kit (Stockport, UK), with custom primers ordered from Eurofins Genomics (Ebersberg, Germany). The correct mutations were confirmed by DNA sequencing (Eurofins Genomics), and the variant enzymes were overexpressed and purified as described before for WT enzyme.[152,162] ^2H,^{13}C,^{15}N-labelled PETNR samples that were used in NMR experiments were prepared as previously described.[202]

Extinction coefficients. Enzyme concentrations were determined using a molar extinction coefficient of 13.3 mM^{-1} cm^{-1} at 464 nm. NAD(P)H and (*R*)-[4-^{2}H]-NAD(P)H

concentrations were determined using a molar extinction coefficient of 6.22 mM^{-1} cm^{-1} at 340 nm, while $NAD(P)H_4$ concentrations were determined using a molar extinction coefficient of 16.8 mM^{-1} cm^{-1} at 289 nm.[235]

Stopped-flow spectroscopy. All kinetic measurements were performed using a Hi-Tech Scientific (TgK Scientific, Bradford on Avon, U.K.) stopped-flow spectrophotometer, which had the sample handling unit placed inside a Belle Technology anaerobic glovebox (<5 ppm of O_2). All buffer solutions (50 mM potassium phosphate buffer, pH 7.0) used for the measurements were degassed by bubbling nitrogen gas through the solution for 1 hour prior to transfer to the glovebox, and were left overnight to equilibrate in the glovebox and ensure removal of all oxygen traces. All concentration dependence measurements were performed at 25 °C, using a constant (~20 µM) enzyme concentration throughout, and with varying NADPH or NADH concentrations (0.1 – 20 mM and 0.3-50 mM final concentration, respectively). Temperature dependence measurements were performed using a constant enzyme concentration (20 µM) and a constant concentration of NADPH and NADH (10 mM and 25 mM final concentration, respectively), in order to ensure pseudo-first order kinetics for all variants throughout the whole temperature range (5-40 °C). All absorption traces were analysed and fitted with standard exponential decay functions, using OriginPro 9.1 (OriginLab Corporation, MA, USA). The reported observed rate constants represent the mean average of 3-6 individual measurements, and the error bars are plotted as ± 1 standard deviation.

Crystallography. The crystallization conditions used were similar to those previously reported.[152] Sitting drop vapor diffusion was used to obtain crystals by mixing 200 nl of 15 mg/ml protein (20 mM Tris/HCl, pH 8.0 at 4 °C) with 400 nl of a reservoir containing 25 % (w/v) PEG 3000, 17 % (v/v) isopropanol, 0.1 M trisodium citrate, 0.1 M cacodylic acid (pH 6.5). Plates were incubated at 21 °C and crystal formation was observed after 48 hours. Individual crystals were harvested and cryo-cooled by plunging into liquid nitrogen prior to data collection at Diamond Light Source. Single cryo-cooled crystals of each of the four PETNR variants were used to collect complete

data sets, which were subsequently scaled and integrated using Xia2.[236] Structures were solved by molecular replacement in Phaser[237] using a search model derived from the wild type PETNR structure (3P62). Iterative cycles of model building and refinement were performed using COOT and Phenix.[238,239] Validation with MOLPROBITY[240] and PDB-REDO[241] was integrated into the iterative rebuilding and refinement process. Complete data collection and refinement statistics are presented in Tables S4.1-S4.2.

NMR spectroscopy. Sequential backbone assignment of the PETNR:NAD(P)H_4 complexes was performed using an enzyme:ligand ratio of 1:10, to ensure the presence of a high population of saturated complex (K_d values for the PETNR:NADPH_4 and PETNR:NADH_4 complexes are 0.13 mM and 0.14 mM, respectively).[159] As the coenzyme analogues have a limited stability, as previously observed for the NAD(P)H coenzymes, the samples were prepared just prior to NMR spectral acquisition. All NMR experiments were conducted under identical conditions to those recently reported for the PETNR holoenzyme.[202] In summary, samples of approximately 1 mM ^{2}H,^{13}C,^{15}N-labelled PETNR, in 50 mM potassium phosphate buffer, pH 7.0, supplemented with 1 mM NaN_3 and containing 10 mM NAD(P)H_4 coenzyme analogue were used. All samples contained 10% (v/v) $^{2}H_2O$, added as an internal lock, and 0.5% (v/v) trimethylsilyl propanoic acid (TSP), used for chemical shift referencing. ^{1}H chemical shifts were referenced relative to the internal TSP signal, whereas ^{15}N and ^{13}C chemical shifts were indirectly referenced using the nuclei-specific gyromagnetic ratios.[217] NMR experiments were recorded at 298 K on an 800 MHz Bruker Avance III spectrometer (Bruker Corp., U.S.A.), equipped with a 5 mm $^{1}H/^{13}C/^{15}N$ TCI cryoprobe and a Z-field gradient coil, running Topspin v.3.2 (Bruker Corp., U.S.A.). The backbone assignment of the PETNR:NAD(P)H_4 complexes was achieved using ^{1}H-^{15}N TROSY HSQC and TROSY versions of HNCACB, HN(CO)CACB, HNCA, HN(CA)CO and HNCO triple resonance experiments.[168] NMR data were processed using Topspin v.3.2 software and analysed using CCpNmr Analysis v.2.4 software.[218] The chemical shift assignments for PETNR:NADPH_4 and PETNR:NADH_4 complexes have been deposited in the Biological Magnetic Resonance Bank (BMRB: http://www.bmrb.wisc.edu/) under the accession numbers 27469 and 27470, respectively.

4.5.2. Static UV-visible absorption spectroscopy data

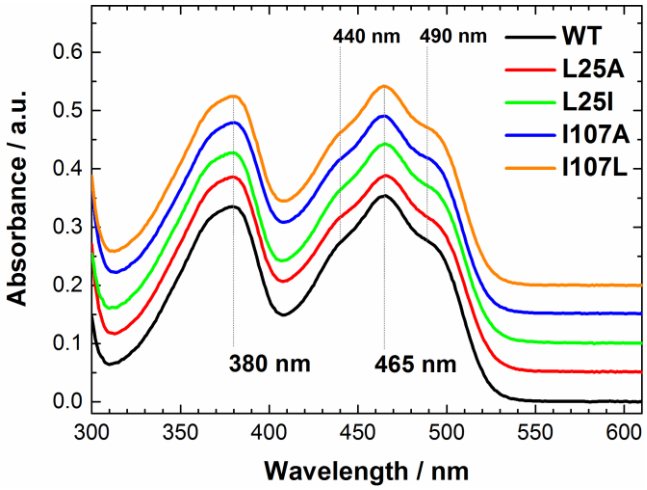

Figure S4.1. UV-visible absorption spectra of the PETNR variants. The broad absorbance peaks at 380 nm and 465 nm are characteristic of the oxidized form of PETNR-bound FMN, and it can be noted there are no observable changes in the shape of the spectra upon mutagenesis. For a better comparison, all spectra are vertically shifted, with the absorbance scale correlated with the WT PETNR data. Conditions: 30 µM enzyme, 50 mM potassium phosphate buffer (pH 7.0), 25 °C.

4.5.3. Crystallography data

Table S4.1. Data collection statistics for the crystal structures of L25A and L25I PETNR variants.

	L25A (PDB: 6GI8)	L25I (PDB: 6GI7)
Wavelength	0.9763	0.92
Resolution range	54.44 - 1.42 (1.471 - 1.42)	48.5 - 1.3 (1.346 - 1.3)
Space group	P 21 21 21	P 21 21 21
Unit cell	56.808 68.875 88.874 90 90 90	57.76 70.53 89.31 90 90 90
Total reflections	532239 (52383)	1623254 (156692)
Unique reflections	66485 (6534)	89476 (8544)
Multiplicity	8.0 (8.0)	18.1 (18.3)
Completeness (%)	99.97 (99.98)	98.93 (95.65)
Mean I/sigma(I)	15.88 (2.16)	22.94 (9.68)
Wilson B-factor	14.71	7.32
R-merge	0.08077 (0.917)	0.08843 (0.2971)
R-meas	0.08634 (0.9803)	0.09105 (0.3054)
R-pim	0.03014 (0.3435)	0.02141 (0.0697)
CC1/2	0.999 (0.682)	0.998 (0.985)
CC*	1 (0.9)	1 (0.996)
Reflections used in refinement	66464 (6534)	89319 (8544)
Reflections used for R-free	3377 (330)	4545 (446)
R-work	0.1323 (0.1969)	0.1108 (0.0947)
R-free	0.1798 (0.2504)	0.1396 (0.1351)
CC(work)	0.968 (0.903)	0.972 (0.976)
CC(free)	0.961 (0.797)	0.965 (0.961)
Number of non-hydrogen atoms	3409	3751
macromolecules	2855	3035
ligands	35	35
solvent	519	681
Protein residues	363	362
RMS(bonds)	0.016	0.012
RMS(angles)	1.62	1.56
Ramachandran favoured (%)	97.22	97.22
Ramachandran allowed (%)	2.78	2.78
Ramachandran outliers (%)	0	0
Rotamer outliers (%)	1.02	0.64
Clashscore	2.45	5.26
Average B-factor	19.19	10.56
macromolecules	16.95	8.09
ligands	12.34	6.21
solvent	31.96	21.81

Table S4.2. Data collection statistics for the crystal structures of I107A and I107L PETNR variants.

	I107A (PDB: 6GIA)	I107L (PDB: 6GI9)
Wavelength	0.92	0.9686
Resolution range	37.39 - 1.7 (1.761 - 1.7)	37.54 - 1.45 (1.502 - 1.45)
Space group	P 21 21 21	P 21 21 21
Unit cell	56.8716 69.1394 88.8937 90 90 90	57.32 70.32 88.78 90 90 90
Total reflections	134933 (13196)	227721 (22053)
Unique reflections	39076 (3865)	63458 (6292)
Multiplicity	3.5 (3.4)	3.6 (3.5)
Completeness (%)	99.39 (99.41)	98.68 (99.31)
Mean I/sigma(I)	14.92 (3.54)	13.19 (2.16)
Wilson B-factor	16.27	13.03
R-merge	0.05966 (0.4119)	0.06332 (0.6041)
R-meas	0.07095 (0.4883)	0.07426 (0.7131)
R-pim	0.03781 (0.2585)	0.03787 (0.3706)
CC1/2	0.99 (0.778)	0.998 (0.728)
CC*	0.997 (0.936)	1 (0.918)
Reflections used in refinement	39050 (3861)	63456 (6292)
Reflections used for R-free	1919 (194)	3221 (334)
R-work	0.1453 (0.1571)	0.1248 (0.2076)
R-free	0.2033 (0.2581)	0.1641 (0.2616)
CC(work)	0.970 (0.934)	0.973 (0.909)
CC(free)	0.935 (0.839)	0.968 (0.872)
Number of non-hydrogen atoms	3240	3393
macromolecules	2818	2850
ligands	35	35
solvent	387	508
Protein residues	362	363
RMS(bonds)	0.009	0.013
RMS(angles)	1.32	1.52
Ramachandran favoured (%)	96.39	98.06
Ramachandran allowed (%)	3.61	1.94
Ramachandran outliers (%)	0	0
Rotamer outliers (%)	0.69	1.36
Clashscore	1.06	1.4
Average B-factor	19.74	16.68
macromolecules	18.68	14.25
ligands	14.62	10.44
solvent	27.93	30.75

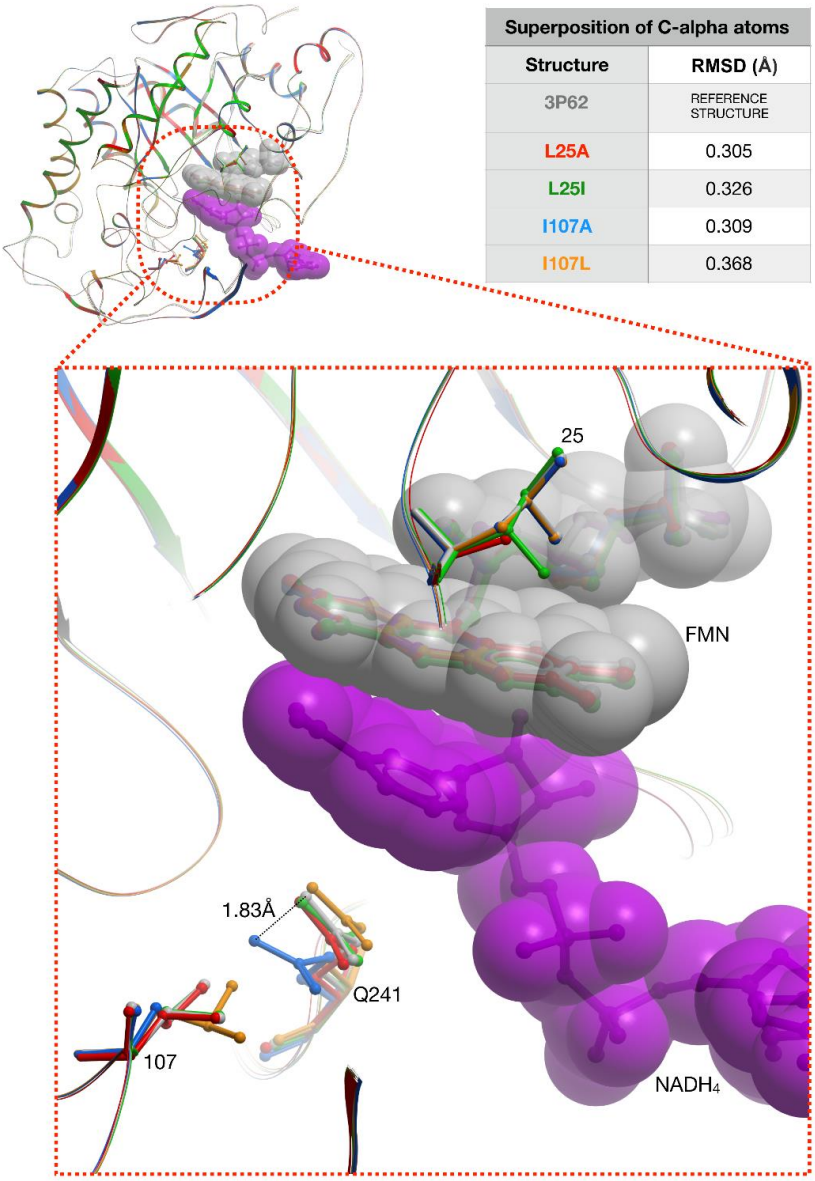

Figure S4.2. X-ray crystal structures of investigated PETNR variants. Each of the four variant PETNR crystal structures has been superimposed onto the WT PETNR structure (PDB: 3P62), and the C-alpha RMSD values are presented in the top right table. The C-alpha traces for each of the five structures are shown top left, coloured according to the convention adopted throughout this manuscript. To highlight the coenzyme binding region, the PETNR:$NADH_4$ complex structure (PDB: 3KFT) was also superimposed onto the WT structure (3P62) and $NADH_4$ from this structure is shown in purple CPK representation. The sites of mutation along with residue Q241 are shown in ball and stick representation. The side chain of Q241 has moved ~1.83Å relative to the position observed in the wild type structure for the I107A variant. Movement at Q241 will influence the spatial freedom available to the nicotinamide coenzyme. All variant structures show an alternative primary conformation at C5 of the FMN cofactor compared to that observed in WT PETNR. However, despite this variability, the hydrogen bonding networks of the FMN are maintained and consistent with those in WT PETNR.

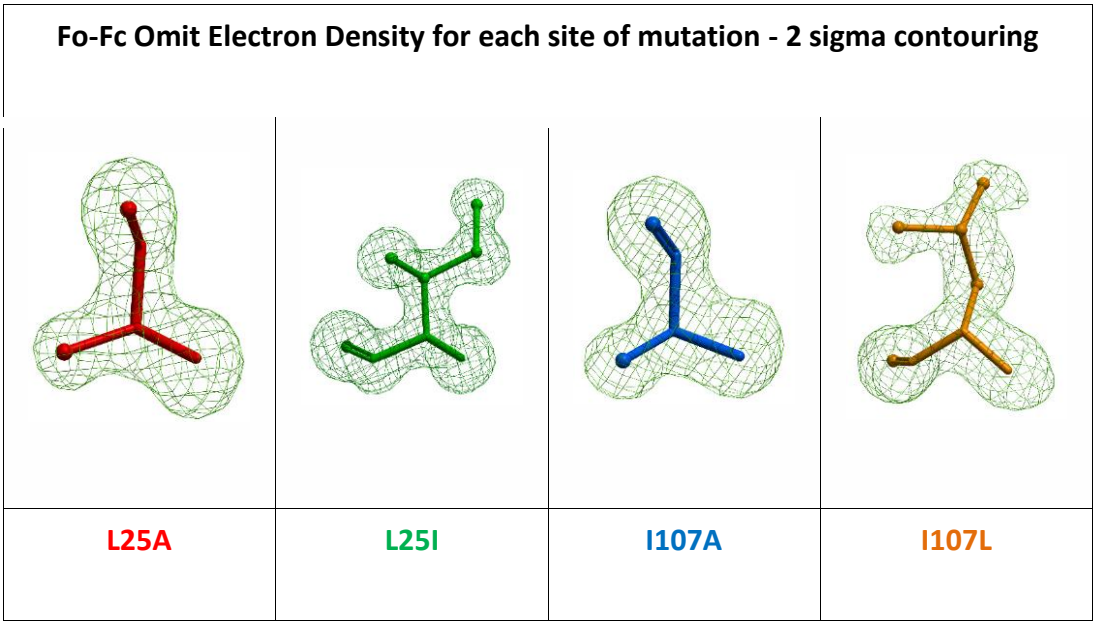

Figure S4.3. Electron density for each site of mutation in PETNR. Each of the four mutations are displayed in ball and stick representation and coloured according to the convention adopted throughout the manuscript.

4.5.4. Concentration dependence studies

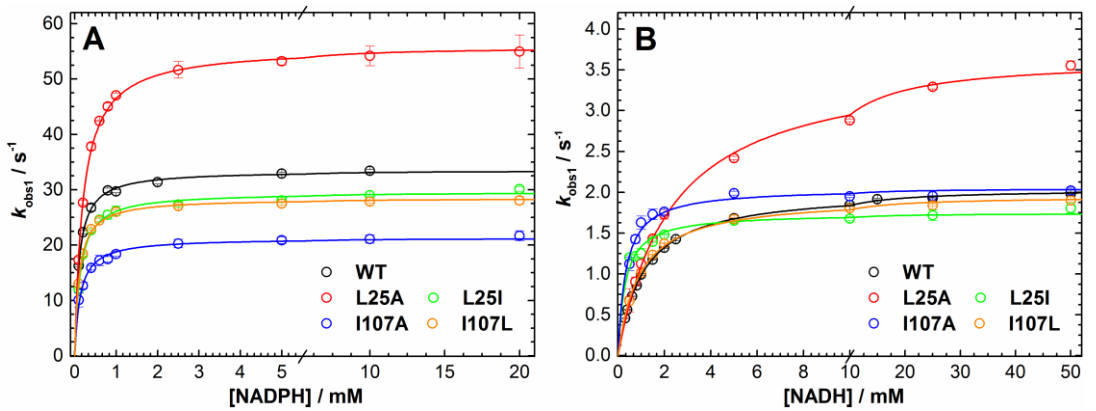

Figure S4.4. Concentration dependence of FMN reduction in the PETNR variants with NADPH (A) and NADH (B), recorded at 25 °C. Conditions: 50 mM potassium phosphate buffer (pH 7.0), 20 µM enzyme and varying coenzyme concentrations. In the cases where the reaction is multiphasic, only the fast observed rate constants (k_{obs1}) are represented and fitted. *Note:* For the variants exhibiting multiphasic behaviour at 25 °C (see below in Tables S4.3-S4.12), the slow observed rate constants (k_{obs2}) have constant values and amplitudes (within error) throughout the range of NAD(P)H concentrations studied, suggesting the K_s for k_{obs2} is very low (<10 µM). This observation ensures that further (i.e. temperature dependence) experiments are recorded under saturating conditions for all kinetic phases observed.

4.5.5. Tabulated rate constants from temperature dependence studies

Table S4.3. Temperature dependence of the observed rate constants (kobs) of FMN reduction for WT PETNR with NADPH and (R)-[4-2H]-NADPH.

	NADPH			**(*R*)-[4-^{2}H]-NADPH**		
T (°C)	k_{obs1} (s^{-1})	k_{obs2} (s^{-1})	A_2* (%)	k_{obs1} (s^{-1})	k_{obs2} (s^{-1})	A_2 (%)
5	11.31 ± 0.09	-	-	1.51 ± 0.01	-	-
10	15.23 ± 0.15	-	-	2.13 ± 0.01	-	-
15	20.32 ± 0.25	-	-	2.90 ± 0.01	-	-
20	26.28 ± 0.31	-	-	3.95 ± 0.02	-	-
25	33.74 ± 0.46	-	-	5.20 ± 0.04	-	-
30	41.64 ± 0.20	-	-	6.59 ± 0.04	-	-
35	50.46 ± 0.75	1.19 ± 0.92	1.41 ± 0.23	8.48 ± 0.03	1.22 ± 0.45	2.54 ± 0.53
40	58.49 ± 0.50	1.09 ± 0.16	2.29 ± 0.35	9.96 ± 0.18	1.11 ± 0.24	3.41 ± 0.65

*A_2 represents the change in amplitude corresponding to k_{obs2}, out of the total change in absorbance (A_{464nm}).

Table S4.4. Temperature dependence of the observed rate constants (k_{obs}) of FMN reduction for L25A PETNR with NADPH and (*R*)-[4-^{2}H]-NADPH.

	NADPH			**(*R*)-[4-^{2}H]-NADPH**		
T (°C)	k_{obs1} (s^{-1})	k_{obs2} (s^{-1})	A_2 (%)	k_{obs1} (s^{-1})	k_{obs2} (s^{-1})	A_2 (%)
5	19.18 ± 0.22	0.65 ± 0.215	2.93 ± 0.55	2.37 ± 0.01	-	-
10	26.03 ± 0.17	1.85 ± 0.64	2.70 ± 0.56	3.33 ± 0.03	-	-
15	34.93 ± 1.25	3.75 ± 3.25	4.36 ± 2.77	4.59 ± 0.03	-	-
20	43.51 ± 0.64	2.42 ± 0.48	3.58 ± 0.47	6.14 ± 0.04	-	-
25	53.77 ± 1.15	1.54 ± 0.45	4.73 ± 0.26	8.01 ± 0.22	0.03 ± 0.03	8.80 ± 4.08
30	59.63 ± 2.29	0.64 ± 1.50	7.50 ± 0.21	10.24 ± 0.05	0.16 ± 0.03	5.83 ± 0.60
35	68.39 ± 8.69	0.51 ± 0.17	16.48 ± 0.53	11.89 ± 0.07	0.17 ± 0.01	14.06 ± 0.45
40*	71.16 ± 6.56	0.26 ± 0.06	25.54 ± 0.91	12.39 ± 0.22	0.26 ± 0.02	31.19 ± 1.07

*A third phase is observed at 40 °C for the reaction with NADPH with k_{obs3} of 3.55 ± 1.03 and A_3 = 19.34 ± 0.54.

Table S4.5. Temperature dependence of the observed rate constants (k_{obs}) of FMN reduction for L25I PETNR with NADPH and (*R*)-[4-^{2}H]-NADPH.

	NADPH			**(*R*)-[4-^{2}H]-NADPH**		
T (°C)	**k_{obs1} (s^{-1})**	k_{obs2} (s^{-1})	A_2 (%)	**k_{obs1} (s^{-1})**	k_{obs2} (s^{-1})	A_2 (%)
5	10.12 ± 0.04	-	-	1.26 ± 0.02	-	-
10	13.47 ± 0.06	-	-	1.79 ± 0.01	-	-
15	18.07 ± 0.05	-	-	2.46 ± 0.01	-	-
20	24.33 ± 0.52	2.25 ± 2.63	3.28 ± 1.62	3.42 ± 0.03	0.19 ± 0.04	2.63 ± 0.15
25	30.24 ± 0.42	3.74 ± 1.20	3.96 ± 0.87	4.50 ± 0.02	0.27 ± 0.03	3.59 ± 0.27
30	36.74 ± 0.28	2.57 ± 0.62	4.00 ± 0.57	5.72 ± 0.06	0.28 ± 0.01	4.31 ± 0.37
35	43.84 ± 0.36	1.99 ± 0.12	5.72 ± 0.36	7.20 ± 0.07	0.42 ± 0.07	7.05 ± 0.36
40	49.82 ± 1.14	2.06 ± 0.19	10.89 ± 0.63	8.66 ± 0.09	0.66 ± 0.01	12.46 ± 0.45

Table S4.6. Temperature dependence of the observed rate constants (k_{obs}) of FMN reduction for I107A PETNR with NADPH and (*R*)-[4-^{2}H]-NADPH.

	NADPH			**(*R*)-[4-^{2}H]-NADPH**		
T (°C)	**k_{obs1} (s^{-1})**	k_{obs2} (s^{-1})	A_2 (%)	**k_{obs1} (s^{-1})**	k_{obs2} (s^{-1})	A_2 (%)
5	8.45 ± 0.08	1.46 ± 0.12	6.12 ± 0.67	1.01 ± 0.01	-	-
10	11.05 ± 0.13	2.60 ± 0.28	7.02 ± 0.79	1.43 ± 0.03	0.42 ± 0.26	4.21 ± 2.11
15	14.31 ± 0.34	3.29 ± 0.54	9.94 ± 2.01	1.90 ± 0.02	0.42 ± 0.16	3.81 ± 1.16
20	17.69 ± 0.14	3.29 ± 0.18	12.53 ± 0.12	2.39 ± 0.01	0.33 ± 0.05	3.56 ± 0.33
25	22.08 ± 0.55	4.31 ± 0.18	22.89 ± 1.963	2.87 ± 0.04	0.24 ± 0.03	5.16 ± 0.27
30	22.75 ± 0.34	3.90 ± 0.107	32.66 ± 0.61	3.19 ± 0.02	0.28 ± 0.03	8.70 ± 0.69
35	18.23 ± 0.58	3.57 ± 0.20	38.27 ± 1.59	3.31 ± 0.02	0.38 ± 0.01	15.07 ± 0.95
40	12.15 ± 0.43	2.42 ± 0.18	32.08 ± 1.75	3.08 ± 0.1	0.46 ± 0.10	20.99 ± 0.65

Table S4.7. Temperature dependence of the observed rate constants (k_{obs}) of FMN reduction for I107L PETNR with NADPH and (*R*)-[4-^{2}H]-NADPH.

	NADPH			**(*R*)-[4-^{2}H]-NADPH**		
T (°C)	**k_{obs1} (s^{-1})**	k_{obs2} (s^{-1})	A_2 (%)	**k_{obs1} (s^{-1})**	k_{obs2} (s^{-1})	A_2 (%)
5	9.05 ± 0.07	-	-	1.23 ± 0.03	-	-
10	12.34 ± 0.156	-	-	1.74 ± 0.01	-	-
15	16.65 ± 0.21	-	-	2.42 ± 0.01	-	-
20	21.84 ± 0.34	-	-	3.31 ± 0.02	-	-
25	27.36 ± 0.40	-	-	4.37 ± 0.02	-	-
30	33.87 ± 0.50	-	-	5.52 ± 0.04	-	-
35	43.71 ± 1.29	4.22 ± 1.79	6.81 ± 1.84	7.05 ± 0.13	1.05 ± 0.26	4.43 ± 1.03
40	47.70 ± 2.88	3.37 ± 0.90	12.22 ± 2.91	8.14 ± 0.12	1.19 ± 0.10	10.87 ± 0.74

Table S4.8. Temperature dependence of the observed rate constants (k_{obs}) of FMN reduction for WT PETNR with NADH and (*R*)-[4-^{2}H]-NADH.

	NADH			**(*R*)-[4-^{2}H]-NADH**		
T (°C)	k_{obs1} (s^{-1})	k_{obs2} (s^{-1})	A_2 (%)	k_{obs1} (s^{-1})	k_{obs2} (s^{-1})	A_2 (%)
5	0.73 ± 0.01	-	-	0.091 ± 0.001	-	-
10	0.92 ± 0.01	-	-	0.119 ± 0.001	-	-
15	1.17 ± 0.01	-	-	0.156 ± 0.001	-	-
20	1.51 ± 0.01	-	-	0.204 ± 0.002	-	-
25	1.95 ± 0.01	-	-	0.274 ± 0.001	-	-
30	2.53 ± 0.02	-	-	0.366 ± 0.002	-	-
35	3.30 ± 0.01	-	-	0.499 ± 0.011	-	-
40	4.25 ± 0.02	-	-	0.673 ± 0.005	-	-

Table S4.9. Temperature dependence of the observed rate constants (k_{obs}) of FMN reduction for L25A PETNR with NADH and (*R*)-[4-^{2}H]-NADH.

	NADH			**(*R*)-[4-^{2}H]-NADH**		
T (°C)	k_{obs1} (s^{-1})	k_{obs2} (s^{-1})	A_2 (%)	k_{obs1} (s^{-1})	k_{obs2} (s^{-1})	A_2 (%)
5	1.27 ± 0.01	-	-	0.162 ± 0.002	-	-
10	1.61 ± 0.01	-	-	0.211 ± 0.002	-	-
15	2.03 ± 0.01	-	-	0.275 ± 0.004	-	-
20	2.63 ± 0.03	-	-	0.360 ± 0.004	-	-
25	3.33 ± 0.07	0.09 ± 0.06	2.29 ± 0.92	0.495 ± 0.002	-	-
30	4.23 ± 0.06	0.08 ± 0.01	4.93 ± 0.85	0.612 ± 0.042	-	-
35	5.20 ± 0.11	0.11 ± 0.01	12.72 ± 0.74	0.885 ± 0.018	0.11 ± 0.03	15.60 ± 2.69
40*	6.74 ± 0.37	0.13 ± 0.01	20.40 ± 1.48	1.070 ± 0.054	0.17 ± 0.01	34.60 ± 0.91

*A third phase is observed at 40 °C for the reaction with NADH with k_{obs3} of 1.10 ± 0.0 and a %A of 19.01 ± 3.17.

Table S4.10. Temperature dependence of the observed rate constants (k_{obs}) of FMN reduction for L25I PETNR with NADH and (*R*)-[4-^{2}H]-NADH.

	NADH			**(*R*)-[4-^{2}H]-NADH**		
T (°C)	k_{obs1} (s^{-1})	k_{obs2} (s^{-1})	A_2 (%)	k_{obs1} (s^{-1})	k_{obs2} (s^{-1})	A_2 (%)
5	0.49 ± 0.01	-	-	0.062 ± 0.001	-	-
10	0.66 ± 0.01	-	-	0.083 ± 0.001	-	-
15	0.90 ± 0.01	-	-	0.113 ± 0.002	-	-
20	1.20 ± 0.01	-	-	0.160 ± 0.001	-	-
25	1.77 ± 0.06	0.36 ± 0.10	6.40 ± 2.07	0.223 ± 0.003	-	-
30	2.39 ± 0.06	0.39 ± 0.09	6.86 ± 1.61	0.306± 0.005	-	-
35	3.26 ± 0.07	0.49 ± 0.07	8.92 ± 1.01	0.418 ± 0.001	-	-
40	4.26 ± 0.13	0.58 ± 0.05	12.28 ± 1.93	0.604± 0.066	-	-

Table S4.11. Temperature dependence of the observed rate constants (k_{obs}) of FMN reduction for I107A PETNR with NADH and (*R*)-[4-^{2}H]-NADH.

	NADH			**(*R*)-[4-^{2}H]-NADH**		
T (°C)	k_{obs1} (s^{-1})	k_{obs2} (s^{-1})	A_2 (%)	k_{obs1} (s^{-1})	k_{obs2} (s^{-1})	A_2 (%)
5	0.42 ± 0.01	-	-	0.053 ± 0.001	-	-
10	0.62 ± 0.01	-	-	0.075 ± 0.003	-	-
15	0.92 ± 0.01	-	-	0.115 ± 0.001	-	-
20	1.35 ± 0.01	-	-	0.172 ± 0.005	-	-
25	1.97 ± 0.02	-	-	0.261 ± 0.007	-	-
30	2.75 ± 0.02	-	-	0.391 ± 0.004	-	-
35	3.63 ± 0.01	-	-	0.545 ± 0.008	-	-
40	4.29 ± 0.03	-	-	0.673± 0.013	-	-

Table S4.12. Temperature dependence of the observed rate constants (k_{obs}) of FMN reduction for I107L PETNR with NADH and (*R*)-[4-^{2}H]-NADH.

	NADH			**(*R*)-[4-^{2}H]-NADH**		
T (°C)	k_{obs1} (s^{-1})	k_{obs2} (s^{-1})	A_2 (%)	k_{obs1} (s^{-1})	k_{obs2} (s^{-1})	A_2 (%)
5	0.61 ± 0.01	-	-	0.073 ± 0.003	-	-
10	0.81 ± 0.01	-	-	0.102 ± 0.002	-	-
15	1.06 ± 0.01	-	-	0.136 ± 0.003	-	-
20	1.40 ± 0.01	-	-	0.185 ± 0.004	-	-
25	1.87 ± 0.01	-	-	0.263 ± 0.003	-	-
30	2.49 ± 0.01	-	-	0.357 ± 0.010	-	-
35	3.30 ± 0.03	-	-	0.504 ± 0.001	-	-
40	4.25 ± 0.02	-	-	0.685± 0.019	-	-

4.5.6. Additional kinetic analysis

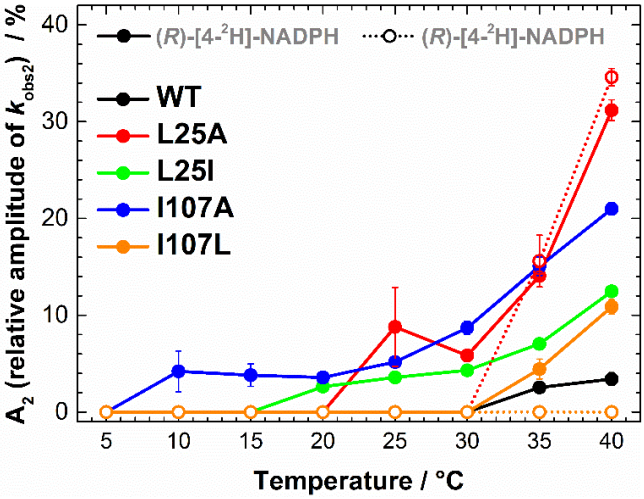

Figure S4.5. Manifestation of multiple reactive configurations as a function of temperature for the PETNR variants during FMN reduction with (*R*)-[4-^{2}H]-NADPH and (*R*)-[4-^{2}H]-NADH. For the variants exhibiting multiple reactive configurations, A_2 (the amplitude of slow observed rate, k_{obs2}) is increasing with increasing temperature, in the same manner as for the reduction of the variants with non-deuterated coenzymes.

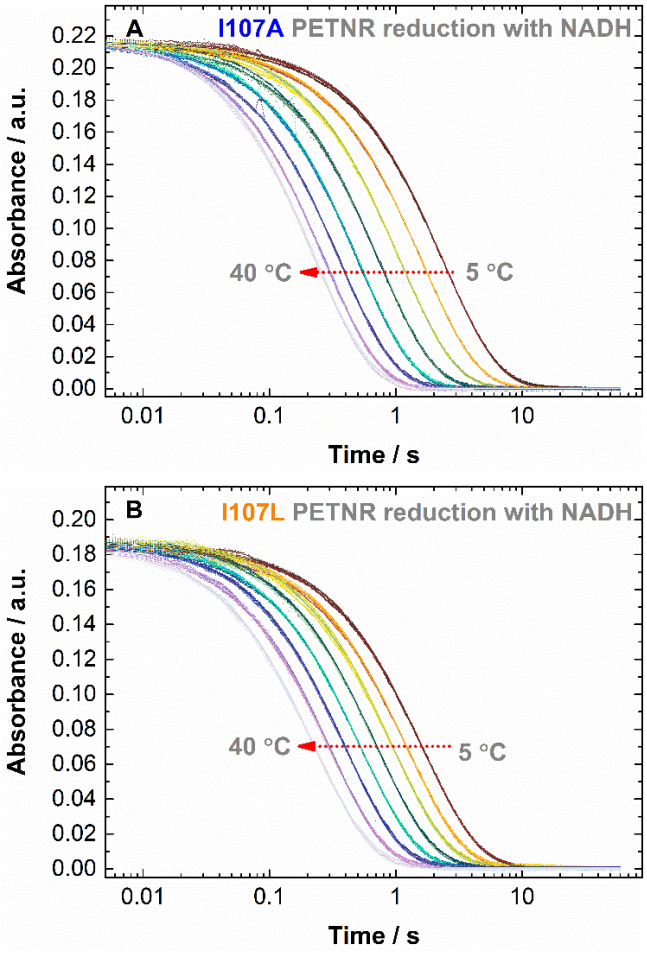

Figure S4.6. Raw kinetic transients showing the temperature dependence of the reduction of I107A (A) and I107L (B) with NADH coenzyme. The transients are represented as a scatter plot, with single exponential fitting functions depicted as thin lines of the same colour. Note that all transients fit to single exponential decay functions across the temperature range studied, and the total change in absorbance is constant, eliminating the possibility of other secondary reactive (or unreactive) species (this would lead to a decrease in the total change with increasing temperature, as the amplitude of the second phase would increase, which is not the case herein).

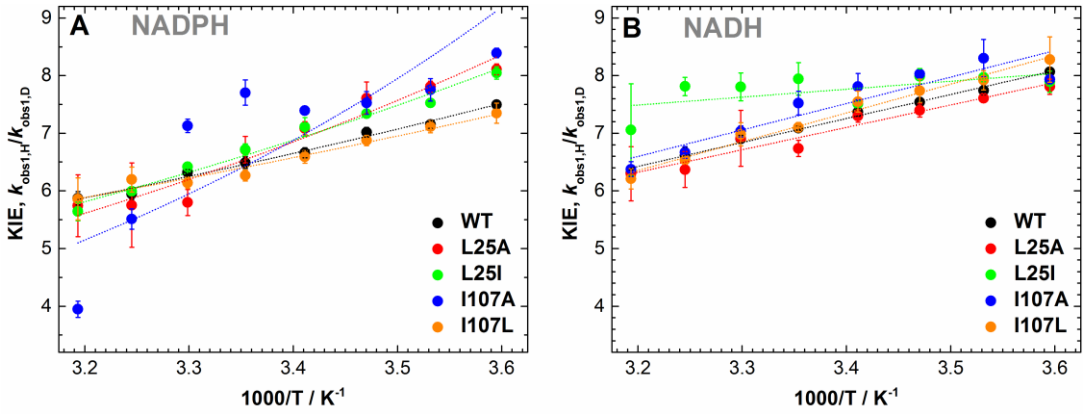

Figure S4.7. Temperature dependence of the observed primary kinetic isotope effects (KIEs) for FMN reduction in the PETNR variants with NADPH (A) and NADH (B). The solid lines are linear fits of each data set (for visual guidance). *Note:* The values presented in the current figure correspond to the KIE on the fast observed rate, k_{obs1}. See Figure S4.8 for KIEs on the slow observed rate, k_{obs2}.

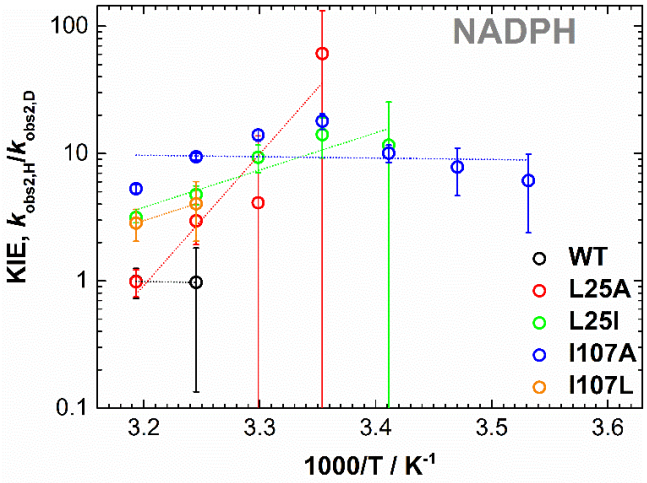

Figure S4.8. Temperature dependence of the KIEs for the slow observed rate (k_{obs2}) of FMN reduction in the PETNR variants with NADPH. The solid lines are linear fits of each data set (for visual guidance). While the presence of KIEs on k_{obs2} confirms (among other things) that the reduction of the enzyme occurs through different reactive configurations, with the multiphasic FMN reduction representing parallel pathways for H-transfer, the KIEs for k_{obs2} are not analysed further, as the interpretation is limited by the small amplitudes and low values for k_{obs2}, which give rise to very high errors. *Note (for NADH reactions):* Although during the reactions with (*R*)-[4-^{2}H]-NADH it is expected to observe multiple phases, fitting could only be typically done using single exponential functions, and no KIEs could be extracted. This is expected, as the second phases for the deuterated coenzyme would probably have rate constants < 0.05 s^{-1}.

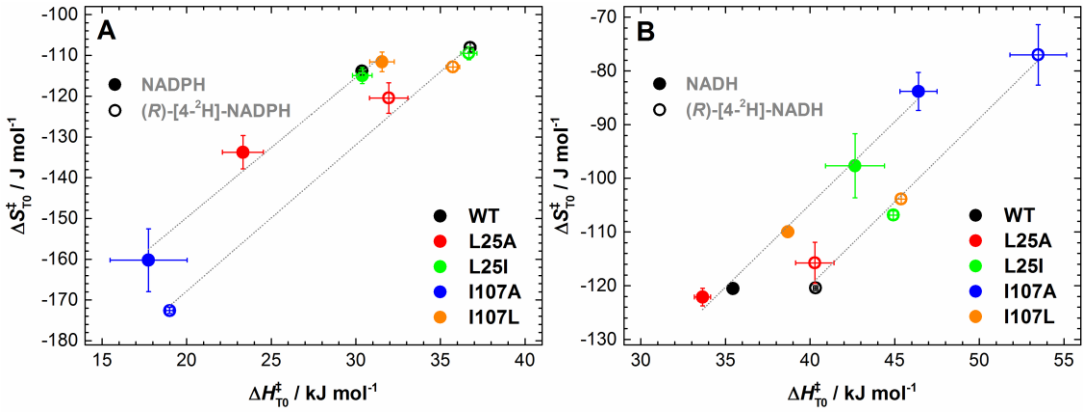

Figure S4.9. A) The relationship between the apparent activation enthalpy and entropy values determined for the reactions of NADPH and (*R*)-[4-^{2}H]-NADPH with the PETNR variants. The solid lines are linear fits of each data set to guide the eye. B) The same relationship illustrated for the reactions with NADH and (*R*)-[4-^{2}H]-NADH coenzymes.

4.5.7. Additional NMR analysis

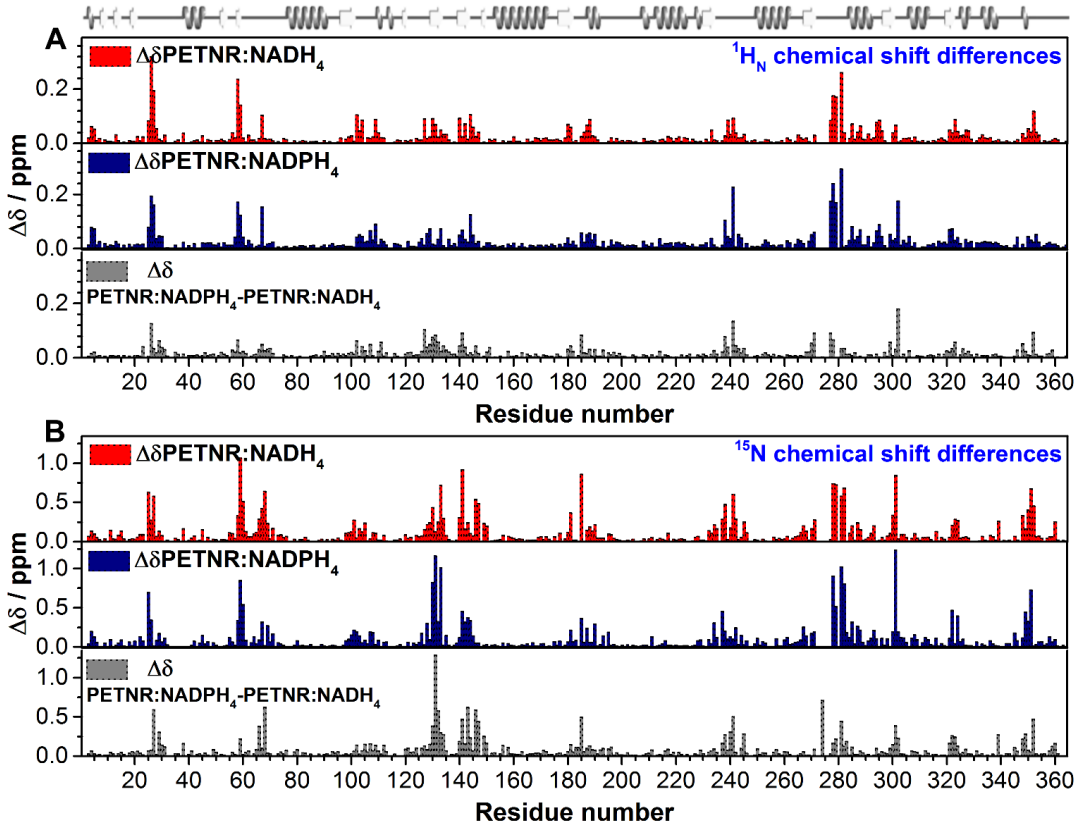

Figure S4.10. Histograms of (A) backbone amide proton ($^{1}H_N$) and (B) backbone amide nitrogen (^{15}N) residue-specific chemical shift changes that occur upon binding $NADH_4$ (red) and $NADPH_4$ (blue) to PETNR and the chemical shift differences between the PETNR:NAD(P)H_4 complexes (gray). The absolute chemical shift differences were calculated using the following equations: $\Delta\delta_X = [(\delta_X(\text{PETNR}) - \delta_X(\text{PETNR:NAD(P)H}_4))^2]^{1/2}$, where X = H_N or N; $\Delta\delta_X = [(\delta_X(\text{PETNR:NADPH}_4) - \delta_X(\text{PETNR:NADH}_4))^2]^{1/2}$, where X = H_N or N. The chemical shift assignments used for PETNR (holoenzyme) were previously deposited at BMRB (accession number 27224).[202]

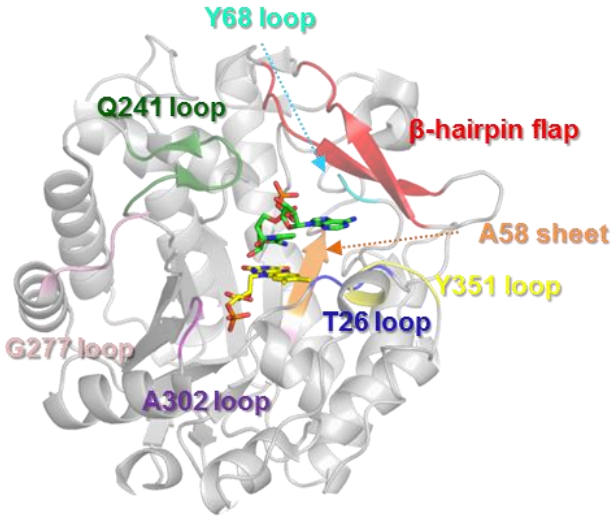

Figure S4.11. Structural representation of regions affected by NAD(P)H_4 binding to PETNR. The crystal structure of the PETNR:$NADH_4$ complex (PDB: 3KFT), with highlighted regions that are substantially affected by NAD(P)H_4 binding. The FMN cofactor is show as yellow sticks and the $NADH_4$ coenzyme analogue is shown as green sticks.

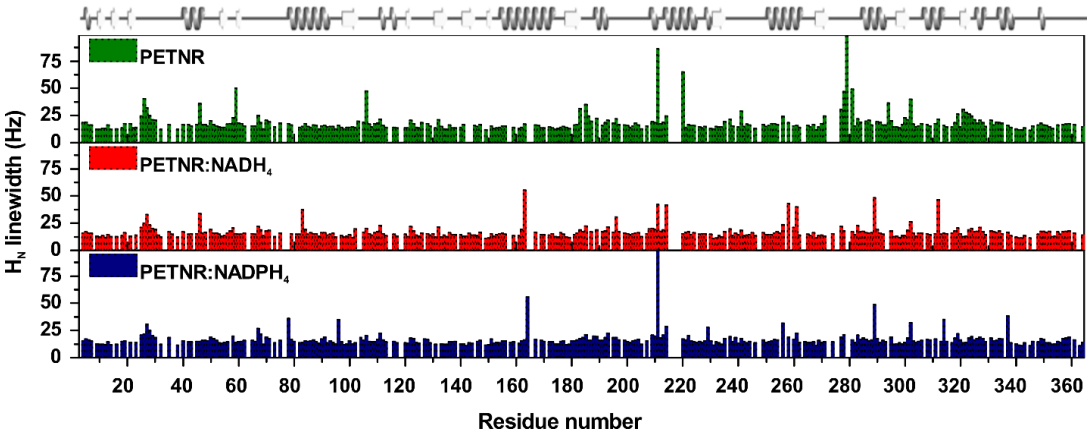

Figure S4.12. Distribution of ^{1}H linewidth values from ^{1}H-^{15}N TROSY spectra of PETNR and PETNR:NAD(P)H_4 complexes. The spectrum of each species was processed in an identical manner before analysis. Overlapped peaks were excluded from the data.

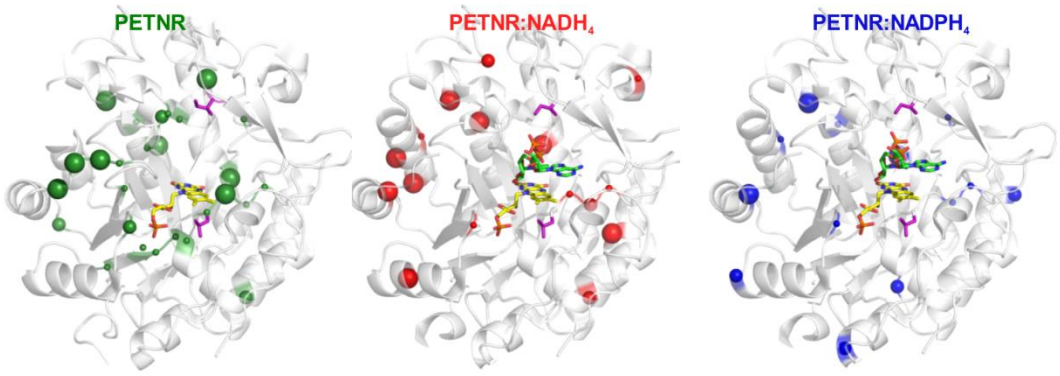

Figure S4.13. Line broadening analysis indicates regions affected by slow (µs-ms) dynamics in PETNR and the PETNR:NAD(P)H_4 complexes. Structural mapping of residues that exhibit line broadening depicted onto the crystal structure of PETNR (PDB:1H50) or PETNR:$NADH_4$ (PDB: 3KFT). The average linewidth and the standard deviation (σ) from the average for each residue-specific linewidth value were calculated (Figure S4.12). The residues that presented a ^{1}H linewidth value higher than the average value plus one standard deviation were considered broadened and are depicted as coloured spheres at the Cα position. Three different sizes were used for the spheres, with the largest size depicting residues with significant broadening (values higher than average value plus 3 × σ).

5. Selectivity through discriminatory induced fit enables switching of NAD(P)H coenzyme specificity in Old Yellow Enzyme ene-reductases

Publication status: *under review*

Authors: Andreea I. Iorgu, Tobias M. Hedison, Sam Hay, Nigel S. Scrutton

Running header: Probing ene-reductases specificity towards nicotinamide coenzymes

Contributions: A.I.I. wrote the paper, with contributions from all authors. A.I.I. conducted all experiments and data analysis. T.M.H. helped A.I.I. with data analysis and interpretation. A.I.I. designed the project, under supervision of S.H. and N.S.S.

5.1. Abstract

The vast majority of ene-reductases belong to the Old Yellow Enzyme (OYE) family of flavin-dependent oxidoreductases. OYEs use nicotinamide coenzymes as ancillary hydride donors to catalyse the reduction of a broad range of alkenes that bear an electron withdrawing group, making them of potential interest for use in industrial processes. Despite a vast number of previous investigations into the structure and catalytic mechanism of a large number of OYEs, a central question remains unanswered: *what determines coenzyme specificity in this large family of ene-reductases?* Herein, to investigate the role of specific residues in nicotinamide coenzyme selection, we have used available X-ray crystallographic and structural NMR data to rationally design variants of two OYEs, pentaerythritol tetranitrate reductase (PETNR) and morphinone reductase (MR). PETNR is a dual-specificity OYE, which reacts with both NADH and NADPH, while MR accepts only NADH as a hydride donor. Using stopped-flow spectroscopy, we investigated the coenzyme specificity in these enzymes by designing variants targeting a β-hairpin motif in an active site loop of both PETNR and MR. We found that R130 governs the kinetic preference of PETNR for NADPH and the neighbouring R142 coordinates the pyrophosphate linker of both coenzymes. We then used these findings to switch coenzyme specificity in MR, by replacing either E134 or L146 with an arginine, which led to increased affinity towards NADH and, moreover, enabled MR to also use NADPH as a reducing coenzyme. Thus, we have shown how structure-led design can address the long-standing question of coenzyme specificity in OYEs. This approach is general and can be further used towards improving and switching selectivity in other homologues of OYE family of ene-reductases.

5.2. Introduction

In recent years, there has been a shift from traditional synthetic methods to more environmentally friendly and sustainable approaches in the production of fine chemicals.[123–126] The development of novel chemoenzymatic approaches for manufacturing of high value chemicals is driven by ever increasing knowledge of enzyme structures and mechanisms, coupled with advances in metabolic engineering and synthetic biology. The asymmetric reduction of activated C=C bonds is one of the most widely employed chemical reactions in industry for which biocatalytic routes are intensively explored.[242,243] The stereoselective reduction of alkenes bearing an electron-withdrawing group is catalysed by a large family of enzymes, known under the umbrella term of "ene-reductases".[116–118] The majority of known ene-reductases are homologues of the Old Yellow Enzyme (OYE) family of oxidoreductases.[118,148] OYEs are a large family of flavin mononucleotide (FMN)-dependent enzymes based on the $(\alpha,\beta)_8$-barrel structural scaffold, which use NADH and/or NADPH nicotinamide coenzymes as ancillary hydride donors.[148,149,207,244] Extensive research has contributed to a wide range of catalysis applications employing OYEs, including their use in individual biocatalytic reactions[127] or as part of multiple enzymatic[128–132] and chemo-enzymatic cascade reactions,[133] and in whole cells biotransformation reactions.[134] These studies have also driven the development of effective nicotinamide coenzyme recycling systems,[245–247] biomimetic counterparts and the use of coenzyme-independent reduction methods.[225,248–251] The use of coenzyme biomimetics and coenzyme-free reduction systems is highly attractive for biocatalytic reduction of activated alkenes. However, their use is limited in cell factory engineering applications where natural coenzymes are required to drive flux through natural and engineered metabolic pathways, enable coenzyme cycling and to maintain redox balance. In these cases, there is a need to use self-sufficient closed-loop recycling systems and to have the ability to predictably engineer the coenzyme specificity of ene-reductase biocatalysts to meet pathway and cellular requirements. The broadening of substrate scope for asymmetric bioreductions and improvements in the chemo-, regio-, and stereoselectivity of target compounds has been extensively reported for engineering studies with

OYEs.[128,137,146,138–145] However, despite this achievements, there remains little understanding of the molecular basis of coenzyme discrimination in OYEs. Most OYEs use NADPH as the preferred hydride donor, but several display higher affinity and/or reactivity with NADH.[252–254] Conversely, others can use both nicotinamide coenzymes (NADH and NADPH) as hydride donors[225]. The sequence identity across different members of the OYE family is not generally conserved (< 15% conserved residues across all three classes of OYEs[148]), and quaternary structures range from monomers to dodecamers[148] (Figure S5.1). However, most OYE enzymes share a highly conserved monomer architecture, the $(\alpha,\beta)_8$-barrel structure (also known as a TIM fold[150,151]), with the FMN cofactor bound non-covalently at the C-terminal region of the β-strands (Figure 5.1 and Figure S5.2). Despite this similarity, the amino acid residues and/or structural motifs that direct coenzyme specificity are not known. In other dehydrogenases/reductases (e.g. based on the Rossmann fold), coenzyme discrimination is driven in part by interactions with the adenine 2'-phosphate (NADPH) or the adenine 2'-hydroxyl (NADH; see Figure 5.1 for numbering).[255,256] Recent studies have also suggested that coenzyme specificity could be engineered through heuristic-based approaches involving structure-guided, semi-rational strategies for enzyme engineering.[257] In the ene-reductases class, X-ray crystallographic data is available for several OYEs in complex with reduced coenzyme mimics (e.g. 1,4,5,6-tetrahydro-NAD(P) (NAD(P)H_4); Figure S5.2), but insight from these structures is limited. While the stacked arrangement of the nicotinamide moiety of NAD(P)H and the isoalloxazine ring of the FMN cofactor is conserved across these structures, the coenzyme 'tail' (Figure 5.1) is often disordered, or in different conformations (some artificially induced by coenzyme-coenzyme stacking interactions *in crystallo*). It is this 'tail' moiety that differs between NADH and NADPH, and thus, the interaction(s) of the enzyme with this moiety must underpin coenzyme selectivity.

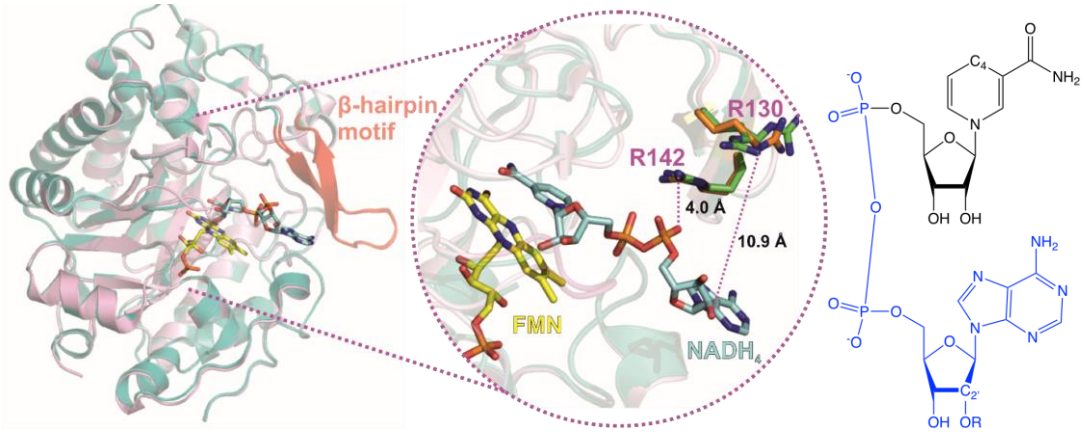

Figure 5.1. Overlaid structures of coenzyme-free and coenzyme-bound pentaerythritol tetranitrate reductase. The structures of oxidized PETNR (PDB:5LGX)[220] and PETNR:$NADH_4$ complex (PDB:3KFT)[95] are shown as pink and teal cartoons, respectively, with the β-hairpin structural motif highlighted in red. The middle panel encompasses a more detailed view of the active site and the β-hairpin motif, with the FMN cofactor (yellow), the $NADH_4$ coenzyme mimic (blue) and two arginine residues from the β-hairpin motif (green in holoenzyme, orange in coenzyme-bound PETNR) highlighted as sticks. NAD(P)H structure is shown in the right panel (R = H (NADH) or R = PO_3^{2-} (NADPH)), with the 'tail' moiety shown in blue and key atoms labelled.

In recent work, we have reported the first structural NMR studies of an OYE family member, pentaerythritol tetranitrate reductase (PETNR).[202] PETNR is a widely studied ene-reductase with a broad substrate scope. It is a monomeric 40 kDa enzyme, which uses both coenzymes NADH and NADPH, but reacting more quickly with NADPH.[95,162,166] Like all OYEs, the reaction catalysed by PETNR occurs by a single-site ping-pong mechanism comprising a reductive half-reaction (RHR; hydride transfer from the C4 *pro*-R hydrogen atom of NAD(P)H to the FMN N5 atom) and an oxidative half reaction (hydride transfer from the FMN N5 and proton transfer from solvent to an oxidizing substrate, typically an α,β unsaturated alkene).[157,159] A range of NMR chemical shift perturbations in the enzyme active site were observed upon coenzyme binding. However, these data also revealed a large reorientation of a β-hairpin structural motif (residues T129-T147; Figure 5.1) on coenzyme binding, suggestive of an induced fit mechanism. Major chemical shift perturbations were observed in particular for T131 and the neighboring R130, with more pronounced effects with $NADPH_4$ compared to $NADH_4$. (Section 4.3). This coenzyme-specific

binding by induced fit contrasts with a previous X-ray crystal structure, which now appears to be in an 'open' conformation.[95]

Informed by our NMR studies, we set out to determine the basis of coenzyme recognition in PETNR and to rationally tune and switch coenzyme specificity by protein engineering of PETNR and the related NADH-dependent morphinone reductase (MR).[153,254] We have identified the structural determinants of coenzyme specificity in these OYEs in a flexible and poorly conserved coenzyme-binding pocket, and suggested how protein engineering can be used to tune coenzyme specificity across other OYE oxidoreductases to facilitate future applications in biocatalysis and cell factory engineering.

5.3. Results and discussion

Residue R130 from the β-hairpin flap governs PETNR specificity towards NADPH. Recent ^{1}H-^{15}N TROSY NMR studies of the PETNR:NAD(P)H_4 complexes have suggested a potential role of R130 in differentiating between binding of the NADPH and NADH to PETNR. Apart from the perturbations observed in localized areas of the active site upon binding of either $NADH_4$ or $NADPH_4$, significant chemical shift perturbations are also observed in the β-hairpin structural motif (Figure 5.1, Section 4.3). Within this β-hairpin flap, significant differences in chemical shift were observed between the two complexes, indicating each of the coenzyme alters the orientation of the structural motif in different ways, possibly suggesting an interaction between R130 and the 2'-phosphate group of NADPH. However, upon inspection of the X-ray crystal structures of PETNR and $NADH_4$-bound PETNR (Figure 5.1), an interaction between R130 and the bound coenzyme would seem unlikely. The X-ray crystal structure of PETNR bound to $NADH_4$ indicates the side chain of R130 is facing the outer side of the active site channel and points away from the tail of the nicotinamide coenzyme. Specifically, the guanidino moiety of R130 is > 7 Å away from the pyrophosphate and > 10 Å away from the 2'-hydroxyl group of the bound $NADH_4$. To investigate the interaction of R130 with NAD(P)H, the neutral variants R130M, R130L and the negatively charged variant R130E were created. The RHR of each variant was characterised by stopped-flow spectroscopy. Coenzyme NADH and NADPH

concentration dependencies of the rate of FMN reduction at 25 °C were determined (Figures S5.3-S5.6), and the kinetic parameters obtained by fitting the observed rate constants to Eq 5.1 are shown in Figure 5.2.

$$k_{\mathrm{obs}} = k_{\mathrm{rev}} + \frac{k_{\mathrm{red}}\,[\mathrm{NAD(P)H}]}{K_{\mathrm{S}} + [\mathrm{NAD(P)H}]} \tag{5.1}$$

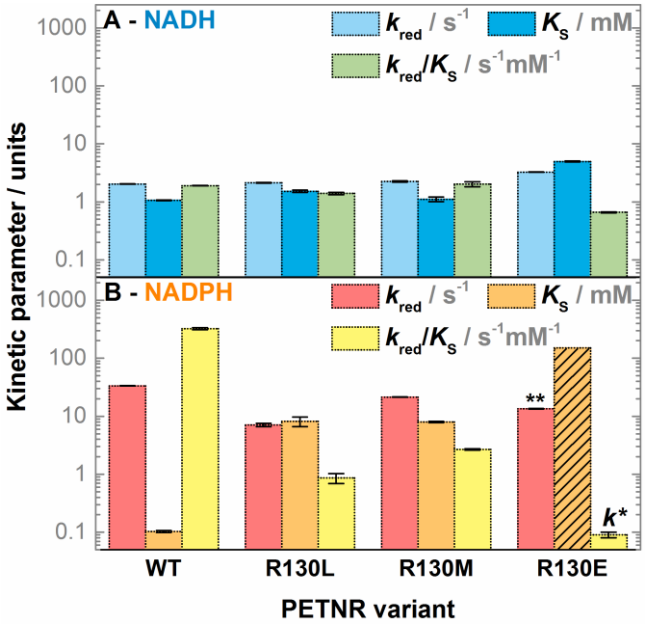

Figure 5.2. Observed kinetic parameters for the RHR of WT, R130L, R130M and R130E PETNR variants with (A) NADH and (B) NADPH. The kinetic parameters are represented as bars, with same the logarithmic *y* axis maintained for both panels for a better comparison. *The kinetics of FMN reduction in R130E PETNR with NADPH follow a second-order reaction, with a rate constant *k* represented instead of the k_{red}/K_S value. **In this case, the k_{red} constant has a theoretical value calculated by multiplying the second-order rate constant (*k*) by the maximum solubility limit of NADPH in solution (K_S ~ 150 mM), and the K_S value representing the solubility limit is shown as bars crossed out with black lines. Kinetic parameters for WT PETNR (data taken from Section 4) are shown for comparison.

Wild-type (WT) PETNR is reduced by both NADH and NADPH, with NADPH having a limiting rate constant (k_{red}) value 17-fold higher than NADH and 10-fold higher affinity towards NADPH (K_S of 0.1 mM) than for NADH. Consequently, NADPH is the preferred coenzyme for WT PETNR, with an overall efficiency for performing the RHR (k_{red}/K_S) 170× higher than NADH. However, by mutating the R130 site of PETNR, we can observe significant coenzyme-dependent changes to these kinetic parameters (Figure 5.2). The values of all kinetic parameters for the reactions of R130L, R130M

and R130E PETNR with NADH are broadly maintained and the only notable differences are the presence of two kinetic phases for the reduction of FMN in R130L and R130M PETNR (Figures S5.3-S5.6.) and a ~3-fold decrease in NADH affinity (K_S) and efficiency (k_{red}/K_S) for R130E. These results suggest that R130 does not play a major role in NADH binding to PETNR and it is likely that the modest changes observed in the kinetic parameters are a propagated effect of the substitution, i.e. causing other nearby residues with a functional role to adopt a different conformation, or creating a slight electrostatic repulsion in the case of R130E variant.

On the contrary, both R130L and R130M PETNR variants show noticeably decreased rates of hydride transfer in the reaction with NADPH, with the presence of a reversible rate of reaction (k_{rev} = 0.46 ± 0.11 s^{-1} for both variants) and a striking > 80-fold reduction in affinity values towards the phosphorylated coenzyme. This reduces the efficiency of the RHR (k_{red}/K_S) to values similar as for the reaction of WT, R130L and R130M PETNR with NADH. The most pronounced effect on the affinity of NADPH to PETNR is seen in the R130E variant. In this case, the substitution of the positively charged guanidino moiety with a negatively charged carboxylate moiety prevents the formation of a stable Michaelis complex. Instead, FMN reduction by NADPH in R130E PETNR is a second-order reaction, with a rate constant of 0.09 ± 0.01 s^{-1} mM^{-1}, and a theoretical k_{red} value of ~ 13.5 s^{-1} (assuming a maximum solubility of NADPH in buffer solution of 150 mM).

Since NADH and NADPH coenzymes are isostructural except for 2'-hydroxyl/phosphate group, the striking differences in affinity towards the coenzymes observed in the variants indicate that R130 likely coordinates the 2'-phosphate group of NADPH. Replacement of R130 with a neutral amino acid of similar length (Met or Leu) leads to essentially no discrimination between the two coenzymes, with similar k_{red}/K_S values for NADH and NADPH. This is mostly caused by changes in affinity, with the rates of FMN reduction by NADPH being higher than the ones for the reaction with NADH in all variants, suggesting the R130 site is mainly involved in binding preferentially the NADPH coenzyme, and having limited effect on

the arrangement of the nicotinamide for efficient H-transfer (i.e. not affecting the binding site of the nicotinamide moiety).

Residue R142 from the β-hairpin flap in PETNR coordinates the pyrophosphate group of the nicotinamide coenzyme(s). The observation that R130E showed a significant reduction in affinity towards NADH suggested that the R130E carboxylate may also perturb both NADH and NADPH binding through electrostatic repulsion with the pyrophosphate linker. Significant NMR chemical shift perturbations of I141 (also in the β-hairpin flap) have been observed upon NADH binding (Section 4.3), suggesting charged residue(s) in this loop are likely to be involved in coenzyme binding. The most likely candidate, R142, was next targeted for mutagenesis and we followed a similar strategy as for R130, substituting R142 with Leu and Glu before characterising the RHR of R142L and R142E using stopped-flow spectroscopy (Figures S5.7-S5.8). The kinetic parameters representing the FMN reduction in these variants are presented in Figure 5.3.

A notable feature of the reaction of R142L PETNR with both NADH and NADPH is the presence of two kinetic phases that contribute to the total change in amplitude at 465 nm. In the case of the reduction with NADH, one of the phases bears similar kinetic parameters as WT PETNR, and the other, which has a larger amplitude, manifests a reduced k_{red} (0.82 ± 0.06 s^{-1}) and an increased K_S (5.07 ± 1.87 mM), leading to a significantly impaired reaction efficiency. The reaction of R142L with NADPH is similar, with a minor phase showing kinetic parameters comparable to WT PETNR and a dominant kinetic phase, which is apparently second-order (k = 0.025 ± 0.001 s^{-1} mM^{-1}). The RHR of R142E PETNR with NADH is monophasic and almost completely impaired, with FMN reduction following a second-order reaction with k = 0.034 ± 0.002 s^{-1}, comparable to the dominant kinetic phase of R142L PETNR with NADPH. The reaction of R142E PETNR with NADPH is even more significantly impaired with a second-order k = 0.008 ± 0.002 s^{-1} mM^{-1}, consistent with an electrostatic clash between R142E and the NADPH 2' phosphate. For reference to the WT reactions, theoretical maximal first-order k_{red} values of ~ 5 s^{-1} and 0.4 s^{-1} can

be estimated for the RHRs of R142L PETNR with NADH and NADPH, respectively at saturating (150 mM) concentrations of NAD(P)H.

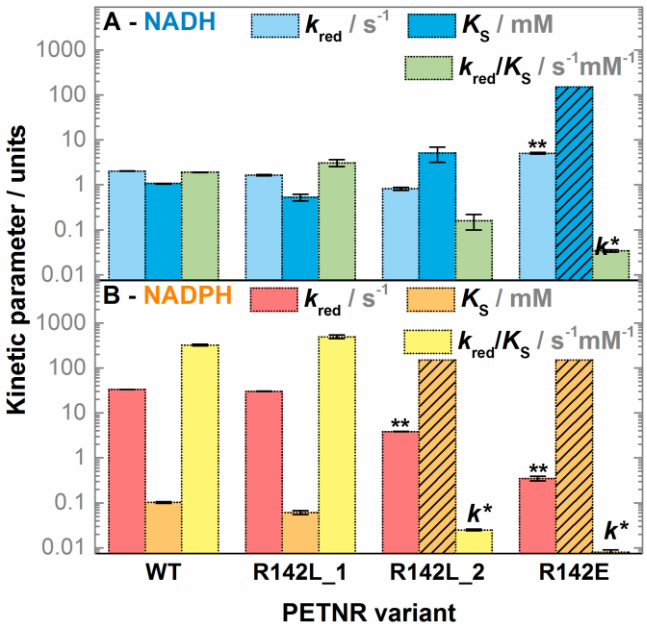

Figure 5.3. Observed kinetic parameters for the RHR of WT, R142L and R142E PETNR variants with (A) NADH and (B) NADPH. The R142L_1 and R142L_2 denote the two different kinetic phases observed for the FMN reduction in the R142L PETNR variant. The kinetic parameters are represented as bars, with the same *y* axis maintained for both panels for a better comparison. *In these cases, the kinetics of FMN reduction follow a second-order reaction, with a rate constant *k* represented instead of the k_{red}/K_S value. ** k_{red} constants are theoretical values, calculated by multiplying the second-order rate constant (*k*) by the maximum solubility limit of NAD(P)H in solution (K_S ~ 150 mM), and the K_S value representing the solubility limit is shown as bars crossed out with black lines.

The removal of the positive charge of the R142 side chain leads to notable reduction in the ability of the enzyme to bind both NADH and NADPH. These data are consistent with R142 stabilizing bound NAD(P)H through electrostatic interactions with the coenzyme pyrophosphate linker. The differences between the reactions of R142E PETNR with NADH and NADPH and the multiple kinetic phases observed in the reactions of R142L PETNR may arise through an alternative (and poorly reactive) coenzyme binding conformation where the pyrophosphate linker forms ionic bond(s) with R130. Again, these data are consistent with an induced fit mechanism.

In order to test whether the selectivity of PETNR towards the nicotinamides is governed by an induced fit mechanism controlled by the whole active site pocket

(and not just the β-hairpin flap), we extended investigations of RHR for other PETNR variants, by targeting three other active site residues (H181, D274, R324) that are hypothesized to have catalytic roles. The concentration dependence data for NADPH and NADH with the designed variants showed that the RHR of PETNR is affected by mutagenesis of the above active-site residues, but not in a coenzyme-specific manner. Thus, the data indicates that coenzyme specificity is not altered by mutagenesis of other functional residues in PETNR (see the relevant detailed section in the Supporting Information and Figures S5.9-S5.13).

Lessons from PETNR – towards switching coenzyme specificity of an NADH-dependent ene-reductase, MR. R130 is located in the β-hairpin flap, which is part of a large polypeptide excursion situated between the β3 strand and α3 helix of the TIM barrel structure of PETNR (Figure S5.1). The sequence identity of this loop is not conserved between members of the OYE family of ene-reductases, which explains why a common coenzyme-specific binding sequence motif has not been identified for OYEs. This leads to the question, *is there likely to be an equivalent residue(s) to R130 in other OYEs, and how would one identify such a residue(s) in order to engineer new coenzyme selectivity?*

MR is a dimeric member of the OYE family, which uses NADH in its RHR.[153,254] MR shares 51% sequence identity with PETNR and the X-ray crystal structures of the two OYEs are highly similar, with MR also possessing a β-hairpin flap in a similar position to PETNR. Upon comparison of the β-hairpin flaps of PETNR and MR, it is apparent that MR does not possess equivalent residues to PETNR's R130 and R142. Instead, MR possesses of an acidic residue (E134) in place of R130, and the neutral side chain of L146 at the same position as the guanidino group of R142 in PETNR (Figure 5.4A). We reasoned that as R130 confers coenzyme specificity in PETNR and that the R130E PETNR variant does not accept NADPH as hydride donor, MR is NADH-specific due to the presence of E134. To test this hypothesis, we created two MR variants, E134R and L146R. Again, the RHR of these variants was characterised using stopped-flow spectroscopy, with the resulting kinetic parameters presented in Figure 5.4B.

The RHR of WT MR with NADH proceeds with k_{red} = 55.44 ± 0.41 s^{-1} and K_S = 89 ± 4 µM.[59,157] The limiting rate of reaction of E134R and L146R MR with NADH are similar to WT with k_{red} = 44.64 ± 0.07 and 61.69 ± 0.22 s^{-1}, respectively. However, the introduction of an arginine at either site leads to a dramatic increase in binding affinity towards NADH, with estimated K_S values of 6 and 5 ± 1 µM for E134R and L146R, respectively. These are likely to be an upper limit due to experimental limitations of the experiment (Figure S5.14). Again, these results are consistent with coenzyme binding through ionic interactions between the NAD(P)H pyrophosphate moiety and the guanidine side chain(s) of arginine residues in the β-hairpin flap. The small differences in H-transfer rates (k_{red}) between MR variants may be attributed to subtle perturbations of the nicotinamide moiety of the NADH in each Michaelis complex.

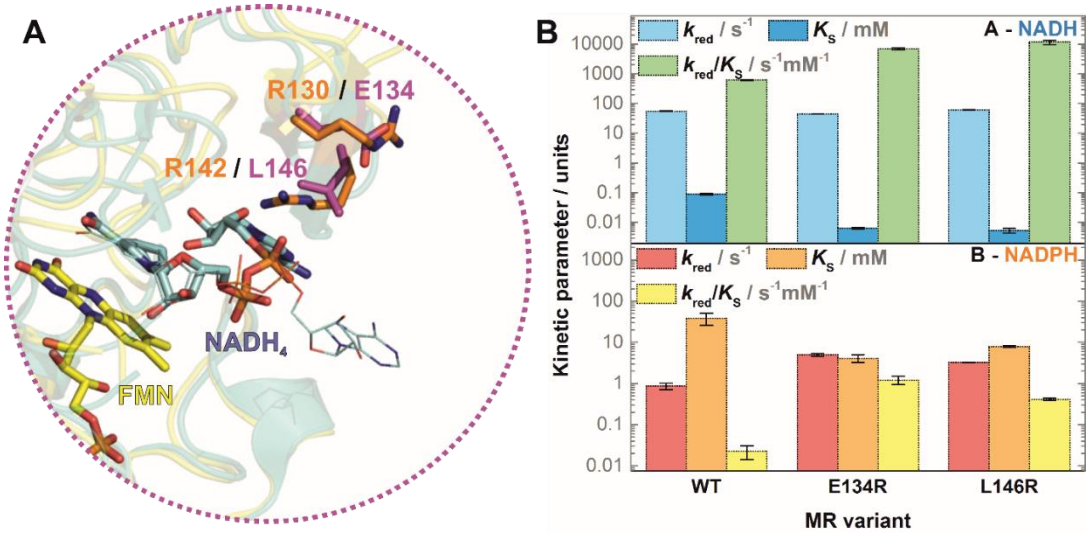

Figure 5.4. (A) Overlay of the X-ray crystal structures of PETNR:$NADH_4$ (teal cartoon, orange sticks, PDB code: 3KFT) and MR:$NADH_4$ complexes (yellow cartoon, magenta sticks, PDB code: 2R14) showing the active site and β-hairpin flap. The $NADH_4$ conformation in PDB: 3KFT is displayed in line form. (B) The observed kinetic parameters of FMN reduction in the MR variants with NADH (top) and NADPH (bottom) are represented as bars, with the same logarithmic *y* axis maintained for both panels for a better comparison.

Finally, we investigated whether NADPH could reduce any of the MR variants. While it was previously reported that WT MR does not react with NADPH,[254] we were able to observe slow RHR kinetics at very high concentrations of NADPH (k_{red} = 0.86 ± 0.15

s^{-1}, K_S = 38.5 ± 12.6 mM). Along with this slow phase, a minor fast phase was observed, which we attribute to a small amount of NADH impurity (0.05-0.1%) in the NADPH stock (Figure S5.15). The reactions of E134R and L146R MR with NADPH show greatly improved RHR kinetics, with reaction efficiencies, k_{red}/K_S = 55- and 20-fold greater than WT MR, respectively (Figure 5.4). As improvements in both k_{red} and K_S were observed, improved NADPH binding did not impair the rate of this reaction. Further, the E134R and L146R MR variants also manifest a 10- and 20-fold increase in k_{red}/K_S for the RHR with NADH, respectively, when compared to WT MR. Together, these results show that the introduction of an arginine at either of the targeted sites (R130 and R142 in PETNR) leads to improved RHR kinetics in MR.

This leads to an intriguing biological question: *why haven't PETNR and MR evolved to bind nicotinamide coenzymes more tightly?* First, we suggest that there is no evolutionary constraint to achieve values <100 µM, as NADH is often detected at concentrations above 100 µM *in vivo*.[258,259] Secondly, the very tight binding of NAD(P)H may also lead to tight binding of the $NAD(P)^+$ product, preventing its fast release from the active site and thus, slowing the rate of turnover. Finally, the β-hairpin flap may also have a role in binding the oxidative substrate, so improved NAD(P)H binding may only be possible if binding of the oxidative substrate can be compromised.

To test the last scenario, we investigated the steady state kinetics of E134R and L146R MR with NADH and the generic OYE substrate 2-cyclohexen-1-one. Similar kinetics to WT MR[153,157] were observed (Figure S5.16) and the oxidative half-reaction was rate-limiting in all cases. These results demonstrate that improved coenzyme affinity does not necessary lead to impaired oxidative kinetics in MR, and by extension to other OYEs. Also, as the E134R and L146R MR variants have greatly enhanced NADH affinity and an ability to work with NADPH, they are likely to offer real improvements to both *in vitro* and *in vivo* biocatalysis applications.

5.4. Conclusions

The construction of efficient metabolic pathways requires the ability to control enzymatic nicotinamide coenzyme utilization, but also to engineer or reverse coenzyme preference in oxidoreductases, one of the largest class of enzymes frequently used in biocatalytic processes. Efforts are made towards understanding and switching coenzyme preference of oxidoreductases, in particular for the dehydrogenase family.[255,257,260,261] Despite being targets for a vast number of biocatalytic processes, there is a lack of understanding regarding the molecular basis of NAD(P)H/specificity in OYEs, the largest group of enzymes in the ene-reductase class of oxidoreductases.

Herein, we have demonstrated that charged residues in the β-hairpin flap of two OYEs are largely responsible for the tight and selective binding of nicotinamide coenzymes in these ene-reductases. We show that the β-hairpin structural motif dictates the affinity of PETNR towards NADPH through electrostatic interactions between two arginine residues (R130 and R142) and the pyrophosphate linker and the 2'-phosphate group of the coenzyme. Inspection of conserved structural (but not sequence) motifs in MR and PETNR allowed the identification of two residues in MR (E134 and L146), which control binding affinity and coenzyme selectivity in this enzyme. Thus, we have shown how structure-led design can address the long-standing question of coenzyme specificity in two OYEs. The majority of OYE ene-reductases have a similar loop emerging between the between the β3 strand and α3 helix of the TIM barrel. While sequence similarity might not be conserved in this region, the approach used herein should allow tuning of nicotinamide affinity and selectivity in other members of the OYE family.

5.5. Experimental section

Materials. All commercial reagents were of analytical grade and were purchased from Sigma-Aldrich (Dorset, UK), unless otherwise stated. NADH and NADPH were procured from Melford Laboratories (Chelsworth, U.K.).

Cloning, overexpression and purification of variant enzymes. PETNR from *Enterobacter Cloacae PB2* and MR from *Pseudomonas putida* were overexpressed from C-terminal His_6-tagged constructs cloned into pET21a plasmids. The desired mutations were introduced into PETNR and MR genes using the Q5® Site-Directed Mutagenesis Kit from New England BioLabs (Hitchin, UK), with custom primers ordered from Eurofins Genomics (Ebersberg, Germany). The designed non-overlapping primers used for each variant are presented in Table S5.1. All mutations were confirmed by DNA sequencing (Eurofins Genomics). NiCo21(DE3) *E. coli* cells were used for overexpression of all variant enzymes. The His_6-tagged enzymes were isolated by affinity chromatography, using HisTrap HP nickel-charged IMAC columns from GE Healthcare (Little Chalfont, U.K.).

Extinction coefficients. NADH and NADPH concentrations were determined using a molar extinction coefficient of 6.22 mM^{-1} cm^{-1} at 340 nm.[235] PETNR and MR enzymes concentrations were determined using a molar extinction coefficient of 13.3 mM^{-1} cm^{-1} at 464 nm (the same value was used for all enzyme variants, as they presented the same UV-vis spectral features as the WT enzymes, with mutagenesis not affecting the characteristic spectra of PETNR/MR-bound FMN).

Stopped-flow spectroscopy. The RHR of the ene-reductases (PETNR and MR) with NADH and NADPH was investigated using a Hi-Tech Scientific (TgK Scientific, Bradford on Avon, U.K.) stopped-flow spectrophotometer, which had the sample handling unit placed inside a Belle Technology anaerobic glovebox (<5 ppm of O_2). All experiments were performed in 50 mM potassium phosphate buffer solution, pH 7.0, which was degassed prior to the experiments, as previously described (Section 4). All concentration dependence measurements were performed at 25 °C, using a ~20 µM enzyme (final concentration, after mixing of the two reactant solutions), and with

various NADPH or NADH concentrations (7-12 different concentrations for each concentration dependence, 0.1 – 25 mM final coenzyme concentration). FMN reduction was observed by continuously monitoring the decrease in absorbance at 464 nm (maximum peak for oxidized flavin-bound enzyme, same for both PETNR and MR). All transient kinetic traces were analysed and fitted with standard 1st, 2nd or 3rd-order exponential decay functions (depending on the number of phases observed), using OriginPro 9.1 (OriginLab Corporation, MA, USA). The reported observed rate constants (k_{obs}) represent the mean average of 3-6 individual measurements, with error bars plotted as ± 1 standard deviation. The limiting rate constant (k_{red}) and the apparent saturation constant (K_S) for the RHR of each mutant with NAD(P)H were determined by fitting the k_{obs} values at varying coenzyme concentration to a hyperbolic function (Eq 5.1).

Steady-state kinetics. The reduction of 2-cyclohexen-1-one using MR variants was followed by monitoring the oxidation of NADH (marked by the decrease in absorbance at 340 nm). All measurements were carried out at 25 °C in 50 mM potassium phosphate buffer solution, pH 7.0, using a saturating concentration of NADH (200 µM). All experiments were performed anaerobically, using a Hi-Tech Scientific stopped-flow spectrophotometer, by mixing a reactant solution consisting of 0.2 µM enzyme and 150 µM NADH (prepared prior to the stopped-flow mixing) with a reactant solution containing variable concentrations (0.5-50 mM) of 2-cyclohexen-1-one. All 2-cyclohexen-1-one reactant solutions were freshly prepared just before use, and 3-6 traces were recorded for each substrate concentration. All transient kinetic traces were fitted with a standard linear function, using OriginPro 9.1. The maximum velocity (V_{max}) and the Michaelis constant (K_M) were determined by fitting the initial reaction rates at varying 2-cyclohexen-1-one concentrations to the Michaelis-Menten equation (Eq 5.2).

$$V_0 = \frac{V_{\max}\,[\text{2-cyclohexen-1-one}]}{K_M + [\text{2-cyclohexen-1-one}]} \qquad (5.2)$$

5.6. Supporting information

5.6.1. Multiple sequence alignment of selected OYEs

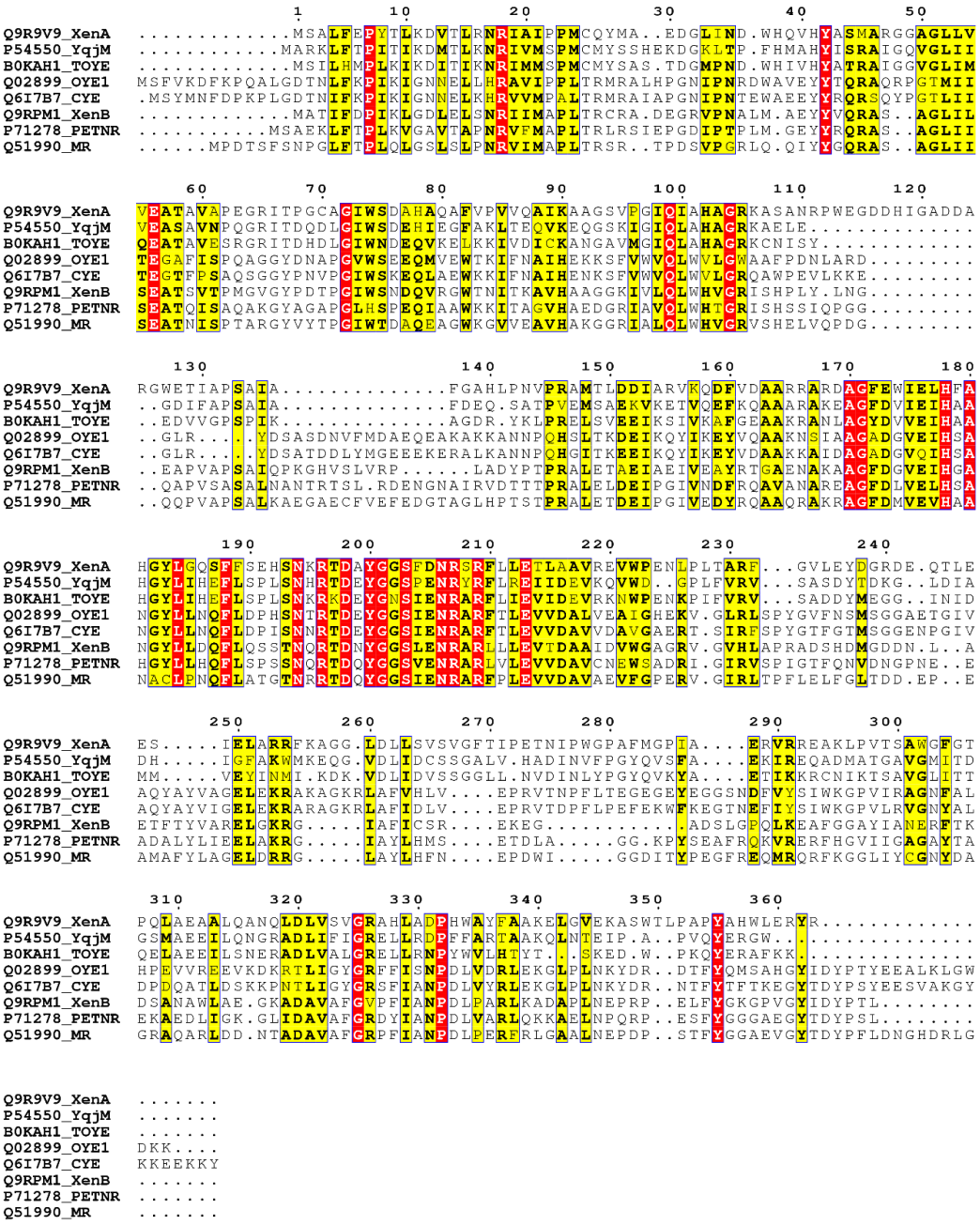

Figure S5.1. Multiple sequence alignment of selected ene-reductases from class I, II and III (as classified in [148]) of the OYE family. Residues highlighted in red are conserved among all selected OYEs, while those highlighted in yellow are only partially conserved/ sharing similar physico-chemical properties. The multiple sequence alignment was performed using the Clustal Omega web server,[262] and the alignment file was rendered using the ENDscript server.[263] Each line on the first column of the figure is showing the Uniprot accession code followed by the name of each ene-reductase.

5.6.1. Multiple structural alignment of selected OYEs

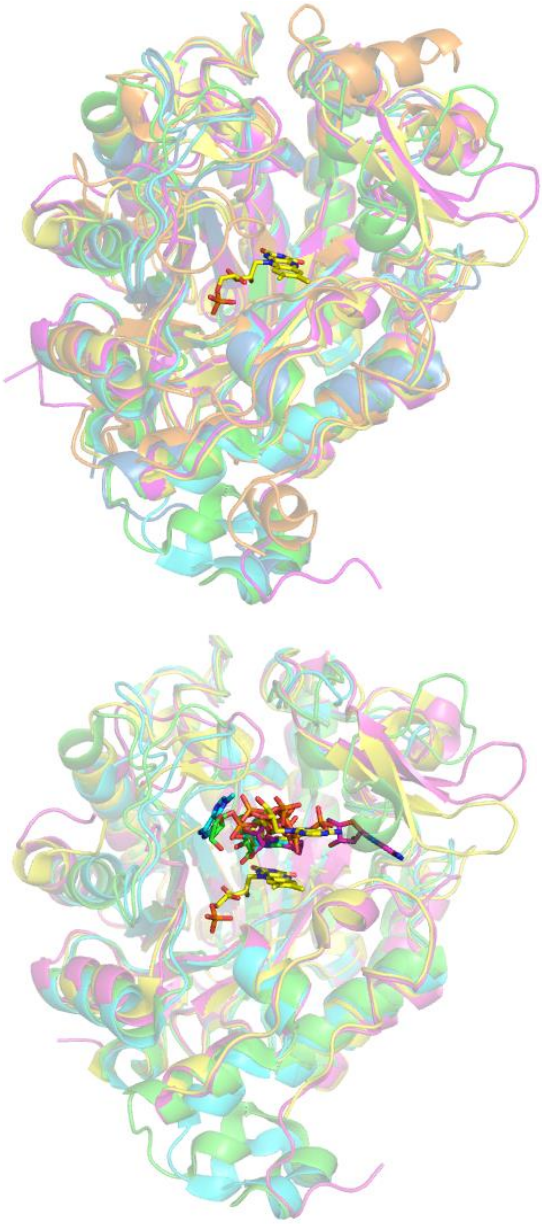

Figure S5.2. Multiple structural alignment of selected OYEs. OYEs are shown in coenzyme-free form in the left panel, with only one monomeric unit displayed for simplicity and one free FMN cofactor: XenA (green, PDB:3L5L), YqjM (blue, PDB:1Z41), TOYE (cyan, PDB:3KRU), OYE1 (orange, PDB:1OYA), PETNR (yellow, PDB:5LGX) and MR (magenta, PDB:1GWJ). The right panel illustrates the structures of coenzyme-bound OYEs (for which X-ray data are available): XenA:$NADPH_4$ (green, PDB:5CPM), TOYE:$NADH_4$ (cyan, PDB:3KRZ), PETNR:$NADH_4$ (yellow, PDB:5KFT) and MR:$NADH_4$ (magenta, PDB:2R14). For simplicity, only the FMN cofactor of PETNR (yellow) is shown as sticks in both panels. In the right panel, the bound coenzymes are represented as sticks, and coloured such as described above. As it can be observed, the NAD(P)H_4 binding conformation is highly different across each of the complexes.

5.6.3. Primer sequences used for mutagenesis

Table S5.1. Forward and reverse primers sequences used for site-directed mutagenesis of PETNR and MR.

Enzyme variant	Forward primer sequence	Reverse primer sequence
R130L PETNR	5′- **CTG**ACTTCCCTGCGCGATGAAAAC -3′	5′- GGTATTGGCGTTCAGGGCAGAGGC-3′
R130M PETNR	5′- **ATG**ACTTCCCTGCGCGATGAAAAC-3′	5′- GGTATTGGCGTTCAGGGCAGAGGC-3′
R130E PETNR	5′- **GAA**ACTTCCCTGCGCGATGAAAAC-3′	5′- GGTATTGGCGTTCAGGGCAGAGGC-3′
R142L PETNR	5′- **CTG**GTCGACACCACCACGCCAC-3′	5′- GATCGCATTACCGTTTTCATCGCG-3′
R142E PETNR	5′- **GAA**GTCGACACCACCACGCCA-3′	5′- GATCGCATTACCGTTTTCATCGCG-3′
R324M PETNR	5′- GCCTTTGGC**ATG**GACTACATTG-3′	5′- CACCGCGTCGATCAGGCC-3′
R324E PETNR	5′- GCCTTTGGC**GAA**GACTACATTG-3′	5′- CACCGCGTCGATCAGGCC-3′
H181N PETNR	5′- **AAC**TCTGCGCACGGTTACCTG-3′	5′- AAGCTCAACCAGGTCGAAGCC-3′
D274A PETNR	5′- **GCG**TTGGCAGGCGGCAAG-3′	5′- CGTCTCGGACATGTGCAGATAGGC-3′
E134R MR	5′- **CGT**TGCTTTGTCGAATTCGAA-3′	5′- CGCACCCTCAGCTTTCAGTG-3′
L146R MR	5′- **CGT**CATCCGACCTCTACGCCGC-3′	5′- ACCTGCGGTGCCGTCTTCGAA-3′

5.6.4. NADH and NADPH concentration dependence studies for the RHR of PETNR variants

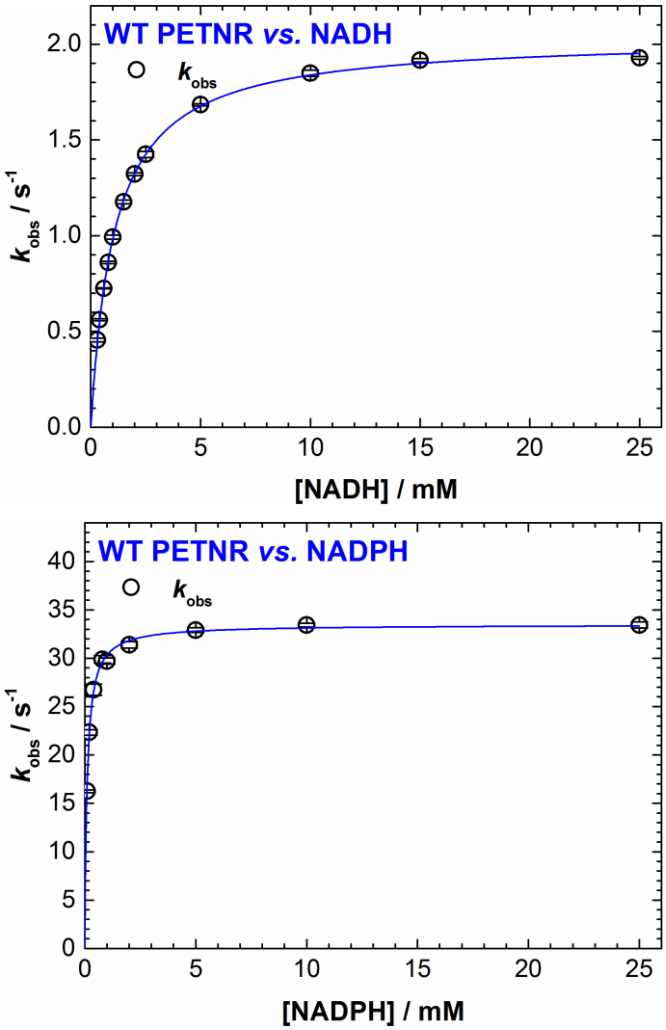

Figure S5.3. Concentration dependence of FMN reduction in WT PETNR variant with NADH (left panel) and NADPH (right panel) – data taken from Section 4.

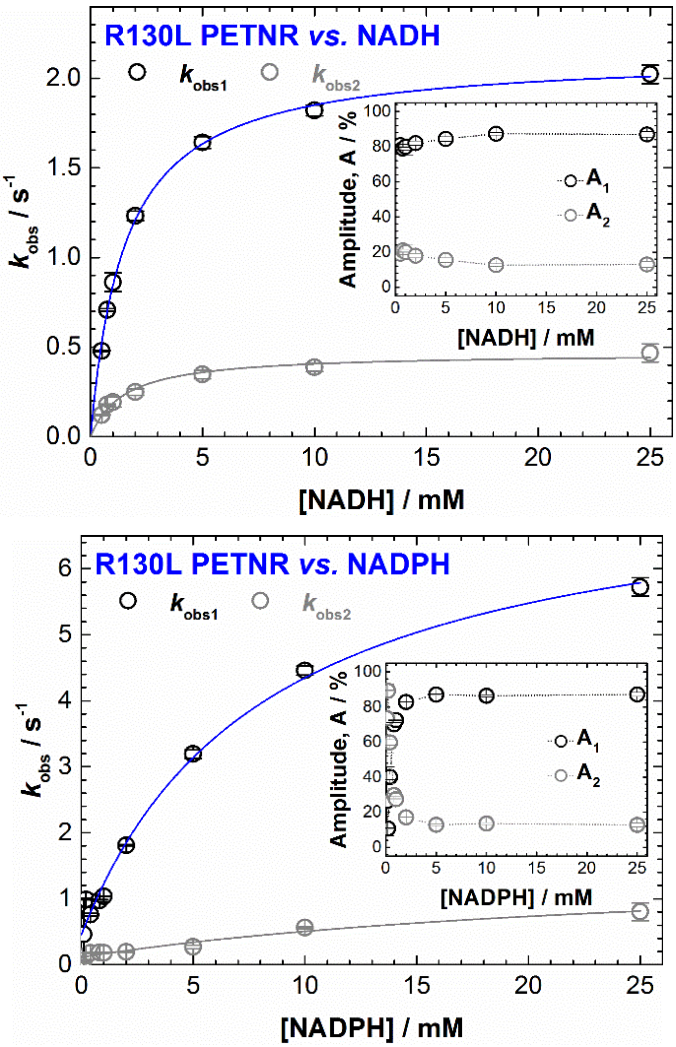

Figure S5.4. Concentration dependence of FMN reduction in R130L PETNR variant with NADH (left panel) and NADPH (right panel). *Inserts:* Concentration dependence of the amplitude of each observed kinetic phase. *Note:* the reactions are biphasic, and the observed rate constants for both phases could be fitted to a hyperbolic function. For the NADH reaction, the amplitudes of both phases remain largely unaffected throughout the whole concentration range, with values of 83 ± 3 % for A_1 and 17 ± 3 % for A_2, and similar K_S values of ~ 1.5 mM for both kinetic phases. For the NADPH reaction, the amplitude of the slow phase (k_{red2} = 1.47 ± 0.5 s-1, K_{S2} = 27.6 ± 16.4 mM) is decreasing with increasing NADPH concentration, with the fast phase being highly dominant for most of the concentration range studied.

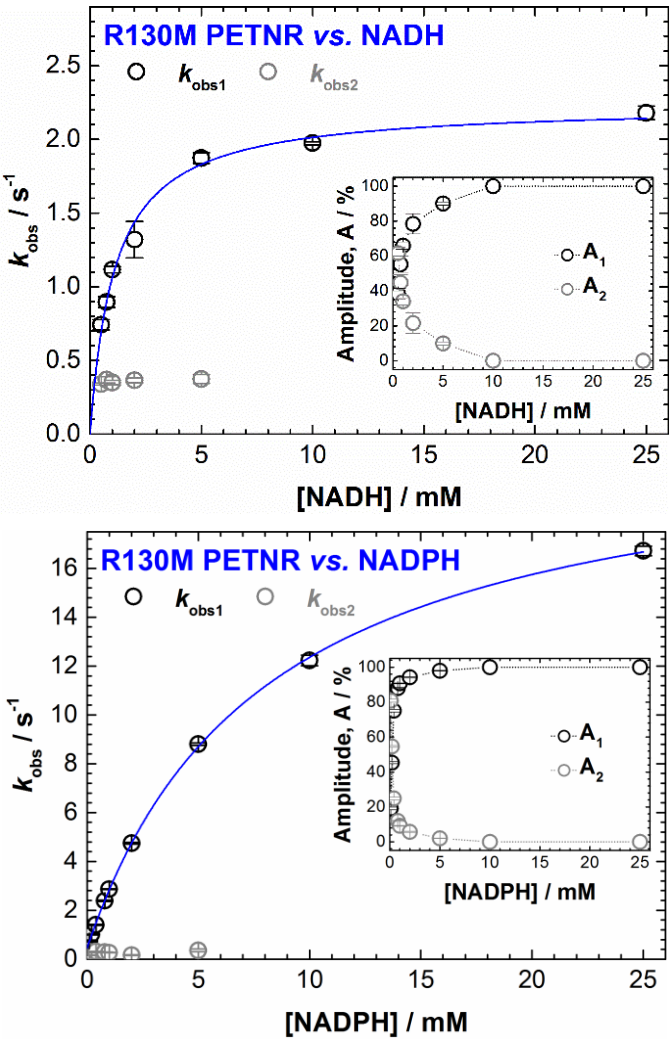

Figure S5.5. Concentration dependence of FMN reduction in R130M PETNR variant with NADH (left panel) and NADPH (right panel). *Inserts:* Concentration dependence of the amplitude of each observed kinetic phase. *Note:* the reactions are biphasic, with the slow phase (averaging 0.36 ± 0.01 s^{-1} and 0.26 ± 0.07 $s^{-}1$ for NADH and NADPH reactions, respectively) manifesting a decrease in amplitude with increase in NADH concentration; only the fast phase can be observed at coenzyme concentrations higher than the K_S of the fast phase.

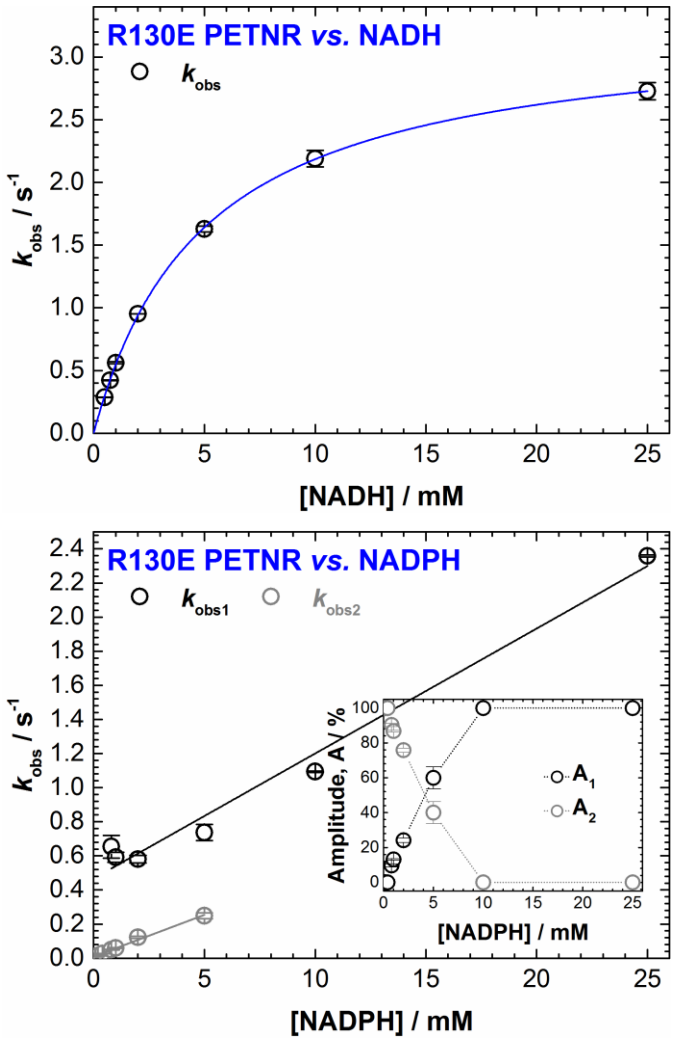

Figure S5.6. Concentration dependence of FMN reduction in R130E PETNR variant with NADH (left panel) and NADPH (right panel).*Insert for the left panel:* Concentration dependence of the amplitude of each observed kinetic phase. *Note:* for the NADPH reaction, both phases could only be fitted to a linear function, suggesting the reaction follows second-order kinetics; second-order rate constants (*k*) were determined from the slope of the linear fit of the concentration dependence of the observed rate constants; a theoretical k_{red} constant was calculated by multiplying *k* by the maximum solubility limit of NADPH in solution (K_S ~ 150 mM).

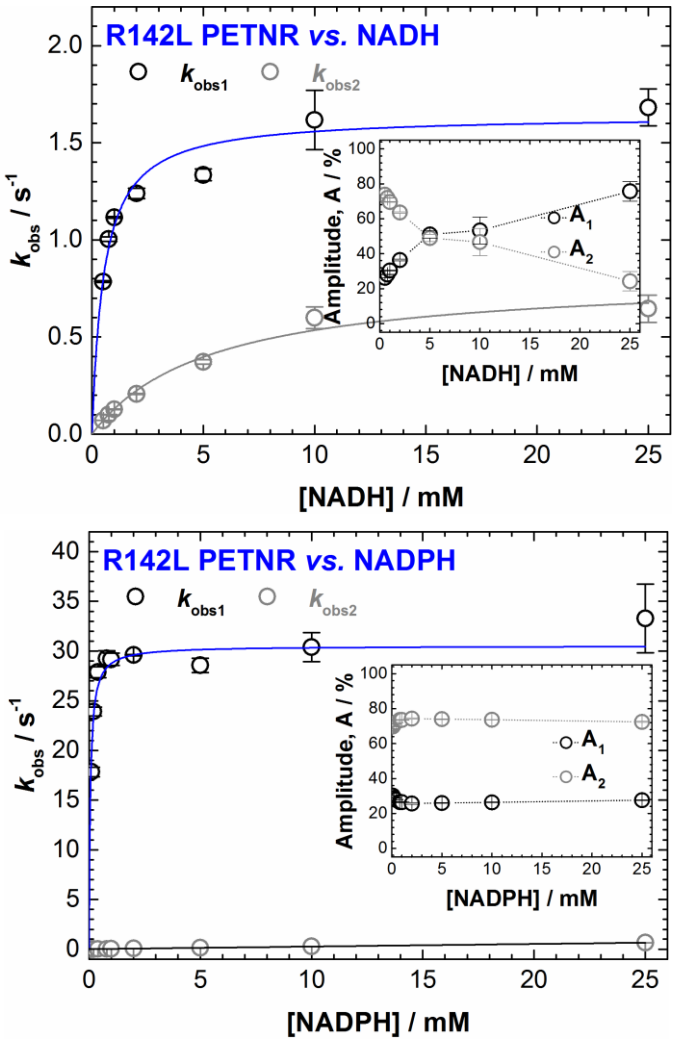

Figure S5.7. Concentration dependence of FMN reduction in R142L PETNR variant with NADH (left panel) and NADPH (right panel). *Inserts:* Concentration dependence of the amplitude of each observed kinetic phase. *Note:* the reactions are biphasic, and the observed rate constants for both phases could be fitted to a hyperbolic/linear functions. For the NADH reaction, the amplitude of the slow phase (k_{red2} = 0.81 s^{-1}, K_{S2} = 5.3 ± 1.0 mM) is decreasing with increasing NADH concentration. For the NADPH reaction, the amplitudes of both phases remain largely unaffected throughout the whole concentration range, with values of 27 ± 2 % for A_1 and 73 ± 2 % for A_2; the fast phase shows similar kinetic parameters to WT PETNR, while the slow dominant phase follows the kinetics of a second-order reaction, with k = 0.026 ± 0.001 s^{-1}).

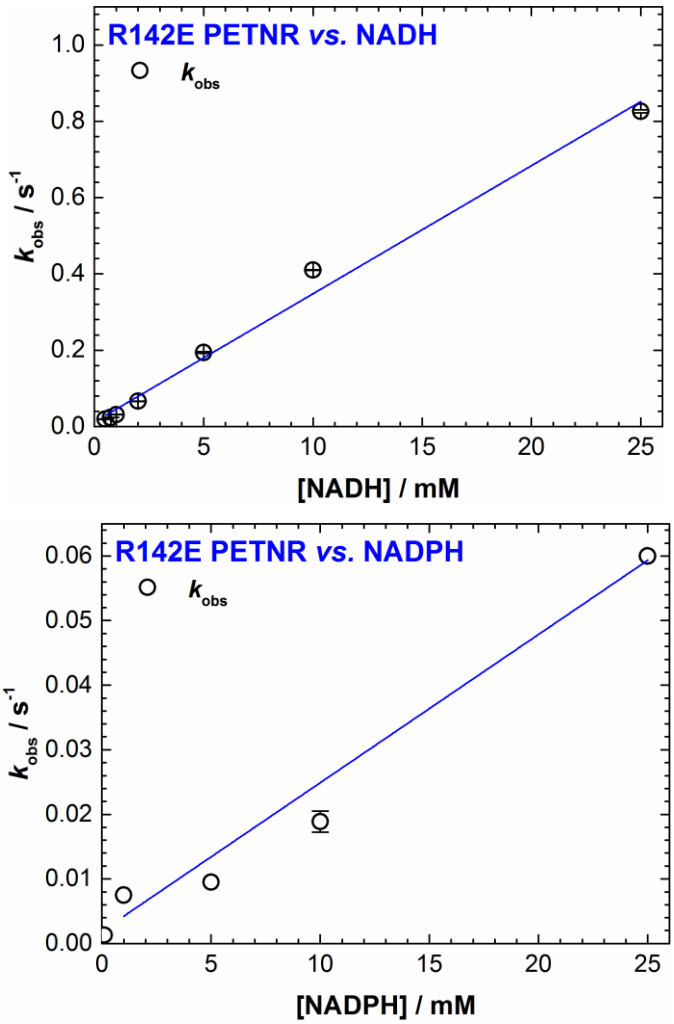

Figure S5.8. Concentration dependence of FMN reduction in R142E PETNR variant with NADH (left panel) and NADPH (right panel) *Note:* the observed rate constants could only be fitted to a linear function, suggesting the reaction follows second-order kinetics; second-order rate constants (*k*) were determined from the slope of the linear fit of the concentration dependence of the observed rate constants; a theoretical k_{red} constant was calculated by multiplying *k* by the maximum solubility limit of NADPH in solution (K_S ~ 150 mM).

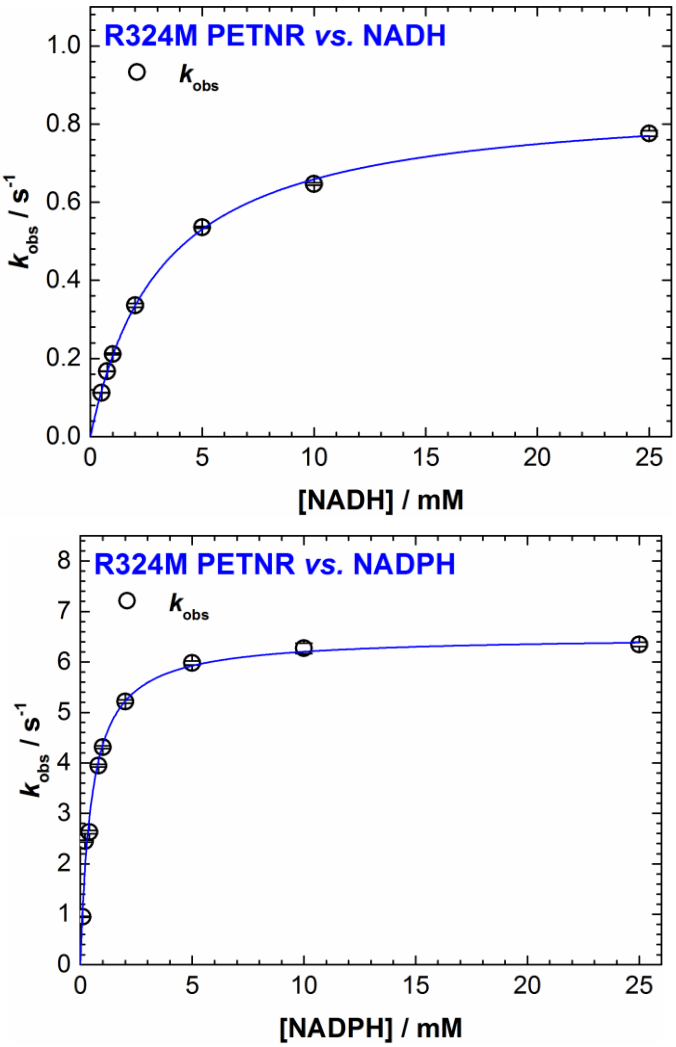

Figure S5.9. Concentration dependence of FMN reduction in R324M PETNR variant with NADH (left panel) and NADPH (right panel).

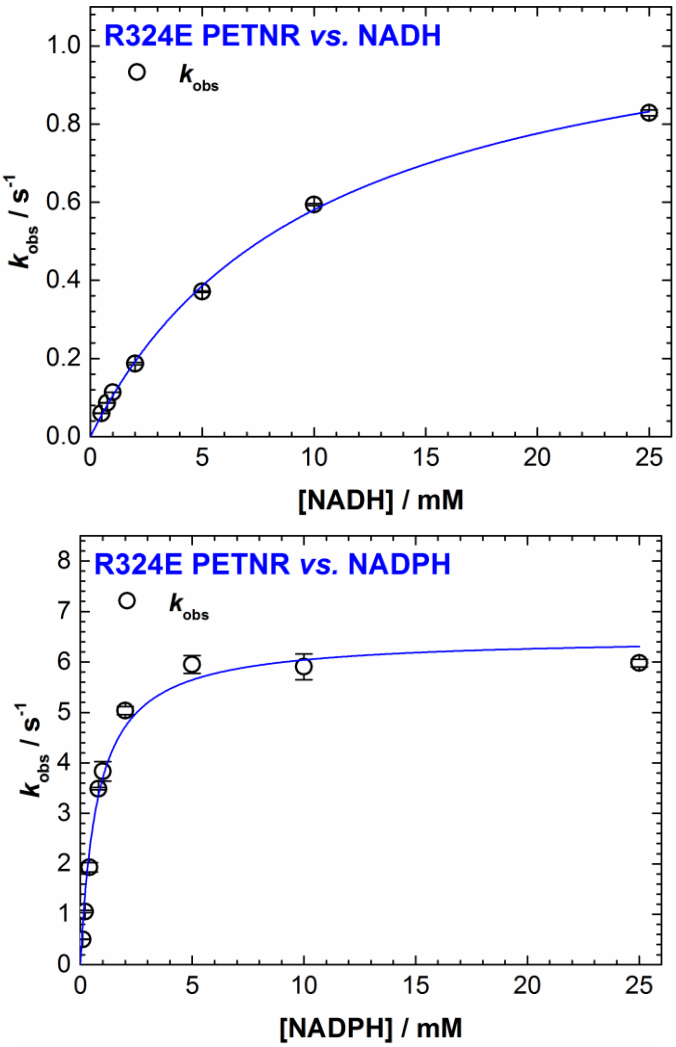

Figure S5.10. Concentration dependence of FMN reduction in R324E PETNR variant with NADH (left panel) and NADPH (right panel).

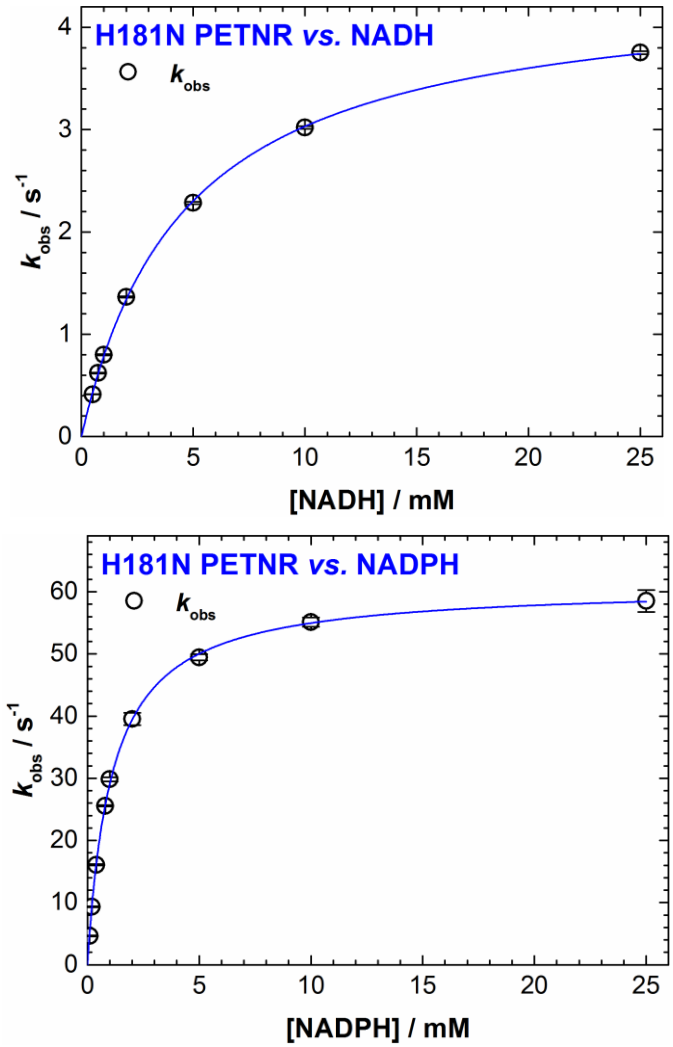

Figure S5.11. Concentration dependence of FMN reduction in H181N PETNR variant with NADH (left panel) and NADPH (right panel).

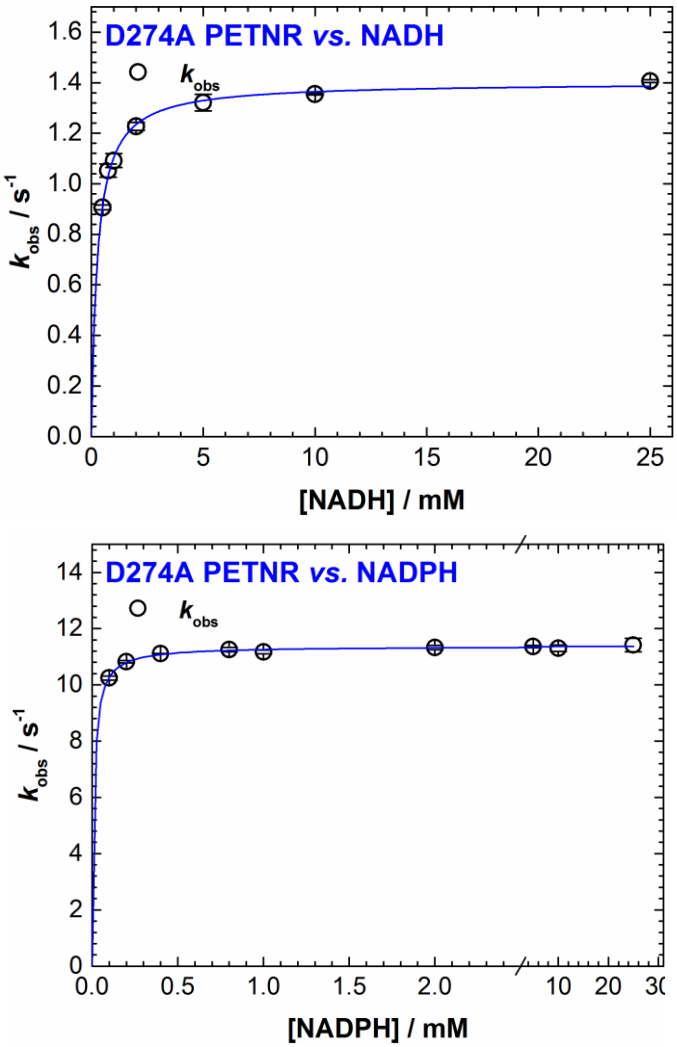

Figure S5.12. Concentration dependence of FMN reduction in D274A PETNR variant with NADH (left panel) and NADPH (right panel).

5.6.5. Extended kinetic investigations indicate no role for other (functional) residues in governing coenzyme specificity in PETNR

To expand our study, we have probed the effect of mutagenesis on other residues in PETNR that are hypothesized to have a role in binding the coenzyme or the FMN cofactor. We have thus selected an additional arginine residue (R324) that is known to be involved in coordinating the phosphate tail of the FMN cofactor,[137] and performed mutagenesis by substituting this arginine with a glutamate (R324E PETNR) and with a neutral amino acid (R324M). We further targeted a histidine residue (H181), and replaced it with an asparagine (H181N PETNR). The H181 site is highly conserved across many members of the ene-reductase family of enzymes, and known to play a pivotal role in binding both the reductive (nicotinamide coenzyme) and the oxidative (activated alkene) substrate, and is hypothesized to interact with the O(2) atom of the FMN isoalloxazine ring.[138,154,163] Another residue we have selected to study is D274, an aspartate residue located in a highly mobile loop that is missing structural density in the X-ray crystallographic structures and has been shown by NMR binding studies to dramatically reorganize upon coenzyme binding (Section 4.3). As the residue located in the loop that bears a charged functional group, and with a putative location that would probably electrostatically clash with the arrangement of $NADH_4$ (as seen from an the crystal structure of PETNR:$NADH_4$ complex), we probed the possible interactions of this residue with the H-transfer reaction coordinate changing its side chain for a neutral one (D274A PETNR). The three targeted residues are highlighted in Figure S.5.13A. We performed concentration dependence studies of the rate of FMN reduction with NADH and NADPH for all the above variants (Figures S5.9-S5.12), with the kinetic parameters of these reactions summarised in Figure S.5.13B.

It can be observed that the substitution of the R324 residue with either a methionine or a glutamate residues has a detrimental effect on H-transfer from the NAD(P)H coenzymes. The introduction of a methionine to the R324 site leads to a decrease in the k_{red} values, coupled with an increase in K_S values for the reduction of the enzyme by both NADPH and NADH coenzymes, causing a noticeable reduction in the

efficiency of hydride transfer from NAD(P)H to PETNR (as observed from the modest k_{red}/K_S values, compared to WT PETNR). The R324E variant shows the same behaviour during the RHR with both coenzymes, manifesting even lower binding affinity values than the R324M variant. The results suggest that removal of the positive R324 amino acid leads to impaired H-transfer rates (3-7x reduction in k_{red} values) and also poor binding of the coenzyme(s). Based on our data and available crystal structures, we suggest that the R324 site plays an important role in positioning the non-covalently bound FMN cofactor in a favourable configuration for efficient H-transfer, but is not involved in the selectivity of the nicotinamide coenzymes.

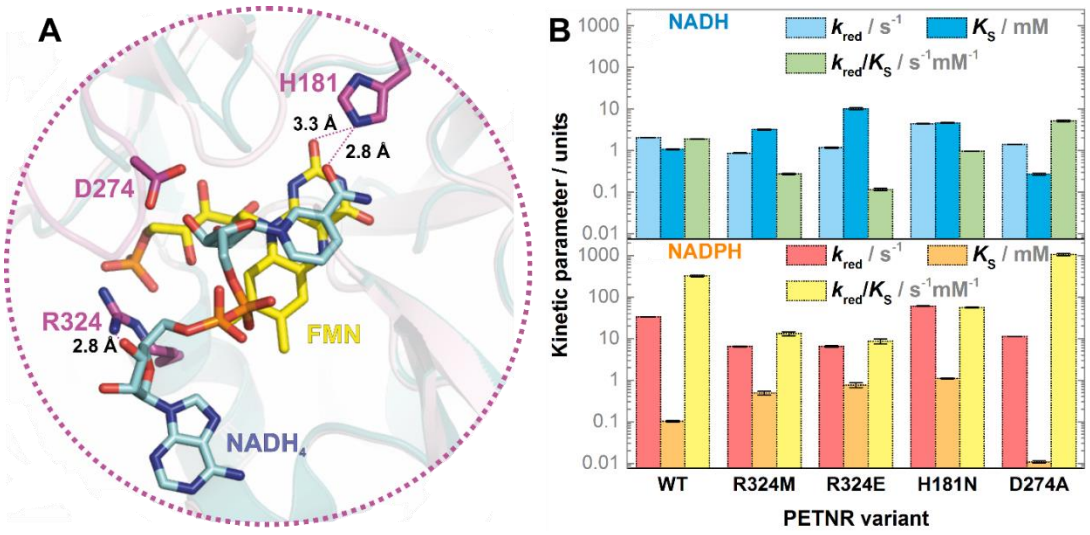

Figure S5.13. Localization of the residues targeted for mutagenesis within the active site of PETNR and observed kinetic parameters for the RHR of WT, R324M, R324E, H181N and D274A PETNR variants with NADH and NADPH. (A) An overlay of the structure of oxidized PETNR (shown in pink, PDB code: 5LGX) and the structure of PETNR:$NADH_4$ complex (teal, PDB code: 3KFT) is displayed, with a focus on the active site region encompassing the residues targeted for mutagenesis (represented as violet sticks). The FMN cofactor and the $NADH_4$ coenzyme mimic are shown as yellow and green sticks, respectively. (B) The observed kinetic parameters of FMN reduction in the above-mentioned PETNR variants with NADH (top) and NADPH (bottom) are represented as bars, with the same logarithmic *y* axis maintained for both panels for a better comparison.

Similar to the PETNR variants at the R324 site, the concentration dependence studies of the FMN reduction in H181N PETNR variant show that substitution of the arginine residue leads to noticeable increased K_S values for both NADH and NADPH

coenzymes, when compared to WT PETNR. However, H-transfer rates are actually positively affected by the mutation, with ~ 2-fold increase in k_{red} observed for both coenzymes (60.97 ± 0.34 s^{-1} and 4.43 ± 0.03 s^{-1} for NADPH and NADH reactions, respectively). Given that quantum mechanical tunnelling and fast dynamical effects have been proposed to play a role in the reaction of PETNR with various natural and synthetic nicotinamides,[65,95,96,166] we hypothesize that the observed effect of a considerably higher reaction rate for H181N variant could arise from a more optimal reaction geometry achieved during H-transfer in this variant. However, to fully understand the exact mechanism for the increase in the k_{red} values for this variant, additional kinetic measurements should be performed, making this variant an attractive target for the study of quantum mechanical tunnelling mechanism in PETNR. Lastly, the D274A variant is observed to be more efficient at performing the H-transfer step than WT PETNR. Specifically, our concentration dependent data for NADPH and NADH with D274A show that, while the limiting rate constant values are lowered by the side chain substitution, D274A variants exhibits very high affinity for NADPH (11 ± 1 μM), and also better binding of NADH (0.27 ± 0.01 mM) when compared to the WT enzyme.

Overall, the variants targeting the R324 and H181 sites show decreased efficiency for H-transfer with both NADH and NADPH, when compared to WT PETNR, while D274A PETNR variant is more competent for performing H-transfer (that is, when considering the overall k_{red}/K_S values). The main observation from the kinetic studies of these variants that target the active site of PETNR is that all 4 mutations introduced (R324M, R324E, H181N and D274A) affect the RHR of PETNR, but not in a coenzyme-specific manner. Thus, while mutagenesis of any of these residues has an observable effect on H-transfer catalysis, coenzyme specificity is not altered by any of these (functional) residues.

5.6.6. NADH and NADPH concentration dependence studies for the RHR of MR variants

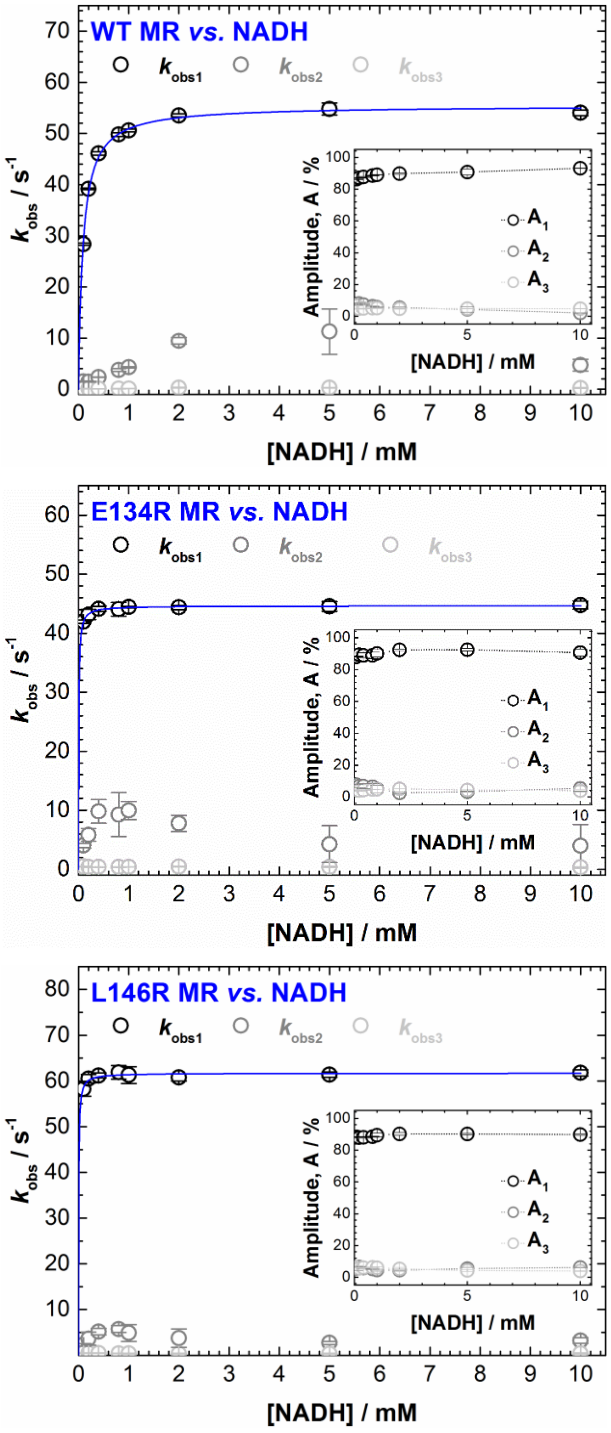

Figure S5.14. Concentration dependence of FMN reduction in WT MR, E134R MR and L146R MR variants with NADH. The reaction present multiphasic behaviour, as previously reported.[157] The two slow rates (k_{obs2} and k_{obs3}) contribute only to about 10% of the total amplitude change throughout the whole coenzyme concentration range (and are probably noncatalytic) – see Table S5.4 for all extracted kinetic parameters.

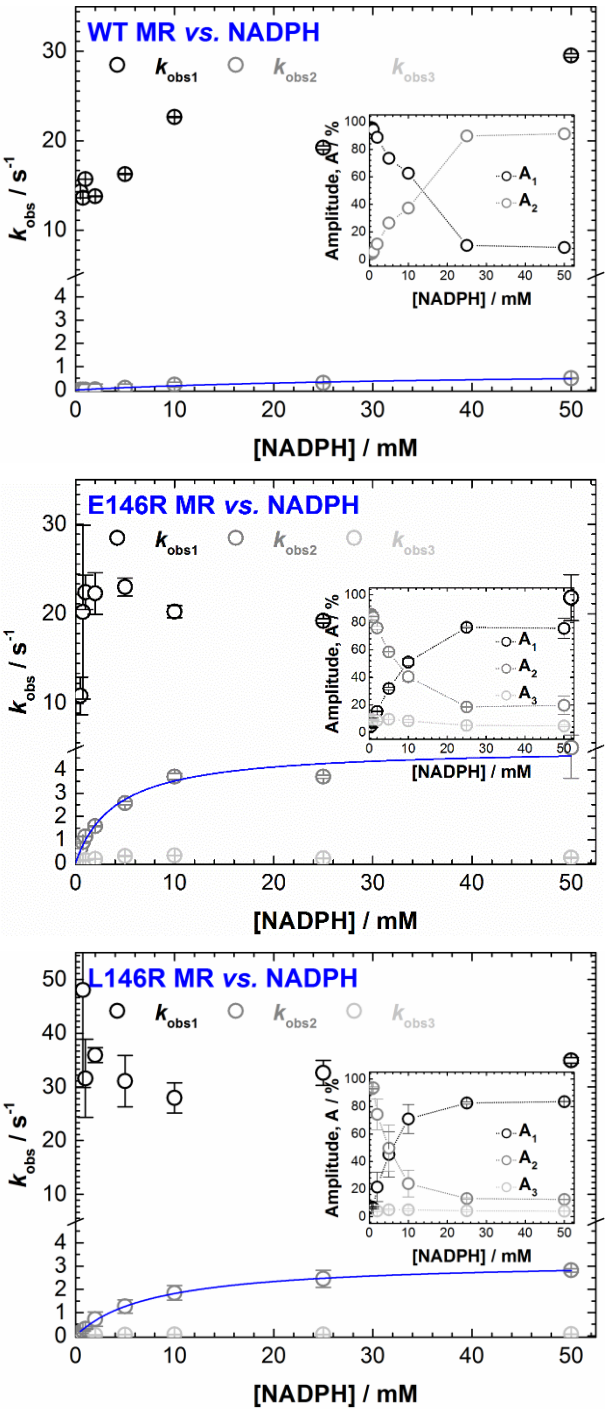

Figure S5.15. Concentration dependence of FMN reduction in WT MR, E134R MR and L146R MR variants with NADPH. The reaction present multiphasic behaviour, with up to three observed rate constants determined. The very slow rates (k_{obs2} and k_{obs3}) contribute only to about 10% of the total amplitude change throughout the whole coenzyme concentration range. The fast phase observed for WT MR (with an average k_{red} value 18.13 ± 5.54 s^{-1} and no detectable K_S value) shows a linear increase in contribution to the total change in amplitude with increase in NADPH concentration. A similar

phase was observed also in the reaction of NADPH with the other two variants (E134R and L146R), showing the same linear trend of increased contribution with increasing coenzyme concentration. Apart from a highly complex mechanism, which could not be readily explained, by applying Ockham's razor as a principle, a likely and feasible explanation for the presence of this phase is actually the contamination of a very small amount on NADH (~0.1%) impurity in the NADPH stock (which would explain the linear increase in contribution with increase in NADPH concentration and, thereby, of NADH impurity; moreover, the rates are similar to the k_{red} values describing the reaction of the variants with NADH, and the very tight binding of NADH to all the variants supports the observed results). See Table S5.5 for all extracted kinetic parameters.

5.6.7. Steady-state kinetics for the reaction of MR variants with 2-cyclohexen-1-one

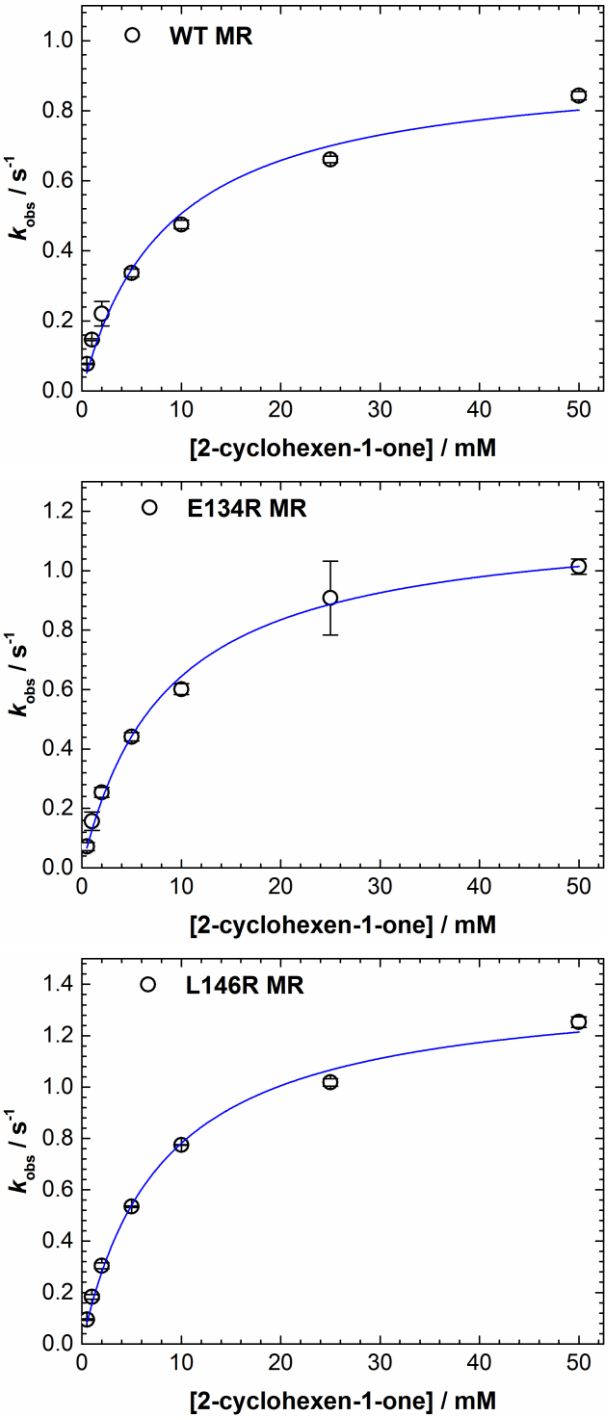

Figure S5.16. Steady-state kinetics for the reduction of 2-cyclohenexen-1-one with WT, E134R and L146R MR variants. Fitting the observed rate constants to the Michaelis-Menten equation yields similar kinetic parameter values for all three variants (WT MR: k_{cat} = 0.93 ± 0.06 s-1, K_M = 8.54 ± 1.64 mM, E134R MR: k_{cat} = 1.18 ± 0.04 s-1, K_M = 8.37 ± 0.84 mM, L146R MR: k_{cat} = 1.41 ± 0.05 s-1, K_M = 8.04 ± 0.77 mM, with the values being comparable to previously published data[153,157]).

5.6.8. Tabulated kinetic parameters for the RHR of PETNR and MR variants

Table S5.2. Kinetic parameters for the reductive half reaction of PETNR variants with NADH.

PETNR variant	k_{red} (s^{-1})	K_S (mM)	k_{rev} (s^{-1})	k_{red}/K_S (s^{-1} mM^{-1})	k (s^{-1} mM^{-1})	Additional comments
WT	2.03 ± 0.01	1.07 ± 0.01	-	1.90 ± 0.03	-	-
R130L	2.13 ± 0.03	1.53 ± 0.03	-	1.40 ± 0.06	-	2 phases*
R130M	2.24 ± 0.06	1.11 ± 0.10	-	2.01 ± 0.19	-	2 phases*
R130E	3.27 ± 0.02	4.95 ± 0.08	-	0.66 ± 0.01	-	-
R142L_1	1.64 ± 0.06	0.53 ± 0.09	-	3.09 ± 0.53		2 phases*
R142L_2	0.82 ± 0.06	5.07 ± 1.87	-	0.16 ± 0.06	-	-
R142E	-	-	-	-	0.034 ± 0.002	2^{nd}-order*
R324M	0.87 ± 0.01	3.18 ± 0.10	-	0.27 ± 0.01	-	-
R324E	1.17 ± 0.03	10.16 ± 0.59	-	0.12 ± 0.01	-	-
H181N	4.43 ± 0.03	4.63 ± 0.09	-	0.96 ± 0.02	-	-
D274A	1.40 ± 0.01	0.27 ± 0.01	-	5.20 ± 0.24	-	-

*For more details, see relevant figures in Section 4.6.4.

Table S5.3. Kinetic parameters for the reductive half reaction of PETNR variants with NADPH.

PETNR variant	k_{red} (s^{-1})	K_S (mM)	k_{rev} (s^{-1})	k_{red}/K_S (s^{-1} mM^{-1})	k (s^{-1} mM^{-1})	Additional comments
WT	33.43 ± 0.22	0.103 ± 0.004	-	324.6 ± 12.8	-	-
R130L	7.08 ± 0.45	8.20 ± 1.54	0.46 ± 0.11	0.9 ± 0.2	-	2 phases*
R130M	21.39 ± 0.18	7.97 ± 0.21	0.46 ± 0.05	2.7 ± 0.07	-	2 phases*
R130E	-	-	-	-	0.07 ± 0.01	2nd-order*
R142L_1	30.51 ± 0.15	0.061 ± 0.006	-	496.5 ± 47.2		2 phases*
R142L_2	-	-	-	-	0.025 ± 0.001	
R142E	-	-	-	-	0.002 ± 0.001	2nd-order*
R324M	6.51 ± 0.17	0.49 ± 0.05	-	13.2 ± 1.4	-	-
R324E	6.50 ± 0.22	0.75 ± 0.10	-	8.6 ± 1.1	-	-
H181N	60.97 ± 0.34	1.09 ± 0.02	-	55.7 ± 1.1	-	-
D274A	11.38 ± 0.02	0.011 ± 0.001	-	1055.3 ± 53.3	-	-

*For more details, see relevant figures in Section 4.6.4.

Table S5.4. Kinetic parameters for the reductive half reaction of MR variants with NADH.

MR variant	k_{red} (s^{-1})	K_S (mM)	k_{red}/K_S (s^{-1} mM^{-1})	k_{obs2}* (s^{-1})	k_{obs3}* (s^{-1})
WT	55.44 ± 0.41	0.089 ± 0.004	623.7 ± 29.9	4.85 ± 3.63	0.17 ± 0.09
E134R	44.64 ±0.07	0.006 ± 0.0001	6899.7 ± 472.5	2.40 ± 1.60	0.19 ± 0.09
L146R	61.69 ± 0.22	0.005 ± 0.001	11682.9 ± 2084.2	3.93 ± 1.22	0.43 ± 0.05

*k_{obs2} and k_{obs3} are average values observed throughout the whole concentration range, contributing by ~ 5% each to the total change in amplitude at 465 nm.

Table S5.5. Kinetic parameters for the reductive half reaction of MR variants with NADPH.

MR variant	k_{red}* (s^{-1})	K_S* (mM)	k_{red}/K_S (s^{-1} mM^{-1})	k_{obs1}** (s^{-1})	k_{obs3}*** (s^{-1})
WT	0.86 ± 0.15	38.5 ± 12.6	0.022 ± 0.008	18.13 ± 5.54	-
E134R	4.96 ±0.31	4.09 ± 0.88	1.21 ± 0.27	19.98 ± 3.93	0.18 ± 0.09
L146R	3.25 ± 0.06	7.85 ± 0.44	0.41 ± 0.02	38.17 ± 11.78	0.05 ± 0.01

*calculated from the hyperbolic fit of k_{obs2} values; **k_{obs1} is proposed to be a phase observed due to the presence of a small amount of NADH impurity in the NADPH stock (see more details in the Figure S5.14 caption); ***similar phase observed in the reaction with NADH.

6. Conclusions and future directions

Enzymes can be considered Nature's best catalysts, as they are able to catalyse extremely diverse biochemical reactions with extraordinary selectivity and specificity. Extremely efficient enzymes can achieve rates 21 orders of magnitude higher than for the non-catalysed solution reaction.[17–19] Concepts concerning the mode of action of enzymes have advanced a long way since the first proposition of the "lock-and-key" model by Fisher in 1894.[20] A plethora of studies has demonstrated that enzymes are highly dynamic entities, and motions ranging from fast (ps-ns) bond vibrations to slow (ms-s) conformational transitions can facilitate diverse catalytic steps.[50–53] New models of catalysis have been proposed recently, which recognise and incorporate dynamical contributions to catalysis,[27,78] but the physical basis of enzyme catalysis (a general understanding of how enzymes achieve their catalytic power) is still not fully understood, and it might not be universal for every enzyme. In this thesis, the physical basis of enzyme catalysis has been addressed through experiments designed to test dynamical contributions to H-transfer catalysis, and to unravel the molecular basis of coenzyme recognition in representative members belonging to the OYE family. In particular, the reactivity of PETNR (a model system for studying enzymatic H-transfer reactions) towards nicotinamide coenzymes has been addressed through site-directed mutagenesis of second sphere 'noncatalytic' residues (Section 4), complemented by novel structural NMR studies of the enzyme (Sections 3-4). The NMR data presented herein, along with previously reported X-ray crystallographic data, guided the rational design of PETNR and MR variants that were used to address the basis of coenzyme specificity in these two ene-reductases (Section 5). In this section, a summary of these findings, along with future perspectives, is presented.

In Section 2, methodologies for isotopic labelling of PETNR have been presented, along with aspects regarding the distribution of "heavy" (in particular ^{2}H) atoms within the enzyme upon production in *E. coli*. A very detailed method for determining optimal conditions upon which efficient deuterium-hydrogen (D-H) exchange of backbone amides can be achieved has been described. As the structure of PETNR

comprises of a $(\alpha,\beta)_8$-barrel structural scaffold (and, therefore, of a highly hydrophobic, solvent-inaccessible core) with a non-covalently bound FMN cofactor, re-protonation of amide backbone groups is challenging (but essential for structural NMR studies). This problem was addressed through the use of a denaturant (GuHCl), which would enabled destabilization of the protein structure and solvent access to the hydrophobic core. The unfolding behaviour of PETNR in presence of GuHCl was monitored using three different spectroscopic techniques (UV-vis, fluorescence and circular dichroism), which allowed determination of most advantageous conditions to be used for D-H exchange of backbone amide groups while maintaining structural integrity of the enzyme.

The near-complete, sequence-specific ^{1}H, $^{15}N_H$, $^{13}C_\alpha$, $^{13}C_\beta$ and $^{13}C'$ backbone resonance assignments of PETNR in its holoenzyme form were reported in Section 3. The assignment of the large 40 kDa PETNR was performed using heteronuclear multidimensional NMR spectroscopy. Given the wide dispersion and favourable line shape of the resonance in the ^{1}H-^{15}N TROSY spectrum of ^{2}H, ^{13}C, ^{15}N uniformly labelled PETNR, along with the optimal D-H backbone exchange of backbone amide groups (procedure described in Section 2), the sequential backbone assignment of the enzyme was achieved to a great extent (97% of backbone amide groups, along with the corresponding $^{13}C_\alpha$, $^{13}C_\beta$ and $^{13}C'$ resonances).

Taking advantage of the good quality of the ^{1}H-^{15}N TROSY spectrum of PETNR, the NMR studies were extended to encompass sequence-specific backbone resonance assignments of PETNR is complex with two coenzyme mimics, $NADH_4$ and $NADPH_4$ (as presented in Section 4). Similar degrees of assignment were achieved for both complexes, and this enabled analysis of differences in binding modes between the two coenzymes. It was observed that the changes in $^{1}H_N$ and ^{15}N chemical shifts upon coenzyme binding are limited to similar residue segments for both PETNR:$NADH_4$ and PETNR:$NADPH_4$ complexes, and are localised approximately 5 Å away from either $NAD(P)H_4$ or FMN cofactor (mostly restricted to the active site of the enzyme). Moreover, analysis of the ^{1}H linewidth of peaks in the ^{1}H-^{15}N TROSY spectra of the complexes showed how slow conformational exchange processes are removed upon

$NADPH_4$ addition to PETNR, and how minimization of the dynamic behaviour observed for PETNR holoenzyme is more pronounced in the case of PETNR:$NADPH_4$ complex than for PETNR:$NADH_4$ (consistent with the observed tighter binding of NADPH coenzyme).

Beside extended NMR studies on PETNR complexes, a wide range of kinetic and thermodynamic studies of four PETNR variants are illustrated in Section 4. Particularly, the H-transfer mechanism in PETNR was investigated through mutagenesis of second sphere 'noncatalytic' residues (L25 and I107). The data presented in this section comprises the first study investigating vibrational modes linked to H-transfer and H-tunnelling through mutagenesis probes in PETNR. The RHR of the variants (L25A, L25I, I107A and I107L) was studied using a combination of experimental tools (stopped-flow rapid kinetics coupled with isotope/temperature/concentration dependence studies of H-transfer), which were designed to probe for subtle kinetic changes that occur upon perturbation of the structure of PETNR through mutagenesis. It was observed that the side chain modifications, although very subtle, prompted changes to the conformational landscape of the enzyme that could be observed by monitoring the RHR with the NAD(P)H coenzymes. While X-ray crystallographic data confirmed no major structural perturbation is caused by mutagenesis of these residues, temperature dependence studies of H-transfer revealed a complex, coenzyme-specific kinetic and thermodynamic equilibrium during the enzymatic step in the investigated variants. Moreover, it was observed that mutagenesis of these second sphere 'noncatalytic' residues affected differently the reactivity of PETNR with coenzymes NADPH and NADH. In particular, the thermal equilibrium between the multiple reactive states is considerably shifted in the case of alanine variants (L25A and I107A), and is thermally activated and coenzyme-specific (e.g. it does not occur in the FMN reduction of I107 variants with NADH). These differences in kinetics and thermodynamic parameters could be attributed to subtle, dynamics structural changes in the PETNR active site, the effects of which impact differently in the nonequivalent reactive geometries for PETNR:NADH and PETNR:NADPH complexes (and this nonequivalence was confirmed through NMR studies). Overall, this section illustrated how the use of

'sharp' experimental tools can uncover details often masked in more traditional studies of H-transfer (e.g. such as those reliant on steady-state turnover measurements). Moreover, as a growing number of studies are reporting similar kinetic complexities on H-transfer caused by mutagenesis, the work undertaken indicates that development of MRCs (and parallel reaction pathways) could be a common feature when investigating variant enzymes.

In Section 5, a central question regarding the widely studied OYE family of enzymes was addressed: *What determines coenzyme specificity in this large family of ene-reductases?* As described in Section 4, NMR chemical shift data of PETNR complexes revealed a large reorientation of a β-hairpin structural motif (residues T129-T147) upon coenzyme binding. Significant chemical shift perturbations were observed in particular for T131 and the neighbouring R130, with more pronounced effects for $NADPH_4$, when compared to $NADH_4$. This is consistent with coenzyme-specific binding by an induced fit mechanism and contrasts with observations from a previous X-ray crystal structure of PETNR:$NADH_4$. The NMR data facilitated rational design of PETNR variants targeting the β-hairpin motif, which were investigated using stopped-flow spectroscopy. The mutagenesis studies indicated residue R130 governs the kinetic preference of PETNR for NADPH and the neighbouring R142 residue coordinates the pyrophosphate linker of both coenzymes. In particular, replacement of R130 with a neutral amino acid of similar length (such as in the case of R130L and R130M variants) led to no discrimination between the two coenzymes, with similar k_{red}/K_S values for NADH and NADPH. Thus, the data indicated that R130 likely coordinates the 2'-phosphate group of NADPH. Distinctly, the removal of the positive charge of R142 side chain (R124L and R142E variants) led to notable reduction in the ability of the enzyme to bind both NADH and NADPH, consistent with R142 having a role in stabilizing bound NAD(P)H through electrostatic interactions with the coenzyme pyrophosphate linker. Extended investigations of RHR were performed also for other PETNR variants, by targeting three other active site residues (H181, D274, R324) that are hypothesized to have catalytic roles. Stopped flow studies of these variants showed that the RHR of PETNR is affected by mutagenesis of the above active-site residues, but not in a coenzyme-specific manner, indicating that

coenzyme specificity is not altered by mutagenesis of other functional residues in PETNR. Finally, inspection of conserved structural (but not sequence) motifs in MR and PETNR allowed the identification of two residues in MR (E134 and L146) that could be responsible for controlling coenzyme specificity in this NADH-dependent enzyme. It was observed that, by replacing either E134 or L146 with an arginine, coenzyme specificity can be tuned in MR, leading to an increase in NADH affinity, along with recognition of NADPH. Overall, this study demonstrated how structure-led design can be used to tune PETNR and MR specificity towards nicotinamide coenzymes, and the approached described should be useful for other OYEs.

In summary, this thesis addressed the molecular basis of PETNR (and, to a more limited extent, MR) reactivity and specificity towards nicotinamide coenzymes through the use of a vast combination of experimental approaches (NMR spectroscopy, X-ray crystallography, mutagenesis, stopped-flow rapid kinetics, KIE studies coupled with concentration/temperature dependence studies). The findings presented herein constitute a good basis for more research avenues addressing H-transfer enzymatic catalysis, dynamical contributions to enzymatic catalysis and coenzyme specificity switching in the OYE family of ene-reductases. In particular, the availability of sequence-specific ^{1}H, $^{15}N_H$, $^{13}C_\alpha$, $^{13}C_\beta$ and $^{13}C'$ backbone resonance assignments of PETNR in three different states (holoenzyme, and in complex with $NADH_4$ and $NADPH_4$) opens many avenues for more details studies using NMR spectroscopy.

Taking advantage of the available residue-specific information, NMR experiments that measure R_1 and R_2 relaxation rates (along with NOE studies) could be undertaken to characterise backbone dynamics of PETNR. The contribution of fast protein motions to the H-transfer step catalysed by PETNR have been inferred from various temperature and pressure dependence studies.[95,96,157,166] Therefore, NMR relaxation experiments could prove very useful, as they could facilitate characterisation of the differences in fast (ps-ns) timescale motions between PETNR complexes, providing an atomistic characterisation of PETNR dynamics. Moreover, relaxation dispersion NMR experiments could be employed to detect conformational

exchange on a slower timescale. These experiments would provide more information regarding slow (µm-ms) conformational exchange processes, and they would constitute a more thorough analysis compared to the ^{1}H linewidth analysis studies provided in Section 4. An extension of the NMR studies could also include the assignment of side chain resonances (e.g. methyl groups), which would facilitate a whole new arrays of dynamic studies of PETNR.

As presented in Sections 1-2, differential labelling of PETNR was recently used to study the different contribution of protein and cofactor vibrational modes to catalysis. These types of differential labelling schemes could be used to study vibrational coupling of the reactive complex in PETNR using other state-of-the-art techniques, such as time-resolved infrared spectroscopy, a technique that can cover a wide large of timescales (ps-ms) and that is often used for studying protein dynamics.[264–266]

Extension of the work presented in Section 5 could include rational design of variants of other OYE ene-reductases, by targeting the loop emerging between the between the β3 strand and α3 helix of the TIM barrel structure. It would be interesting to demonstrate that this non-conserved region is mainly responsible for coenzyme specificity across all members of the OYE family.

Last, as dynamical contributions to enzymatic H-transfer catalysis in PETNR are mainly inferred from the temperature dependent KIE values obtained from measuring RHR kinetics, it would be insightful to measure (if possible) the kinetics of the uncatalysed reaction in solution (FMN reaction with NADH or NADPH). These experiments would be able to show whether the temperature dependence of the KIE is caused by enzymatic contributions or is intrinsic to the H-transfer chemical step.

7. References

(1) Bezanilla, F. How Membrane Proteins Sense Voltage. *Nat. Rev. Mol. Cell Biol.* **2008**, *9* (4), 323–332.

(2) Jeong, H.; Tombor, B.; Albert, R.; Ottval, Z. N.; Barabási, A. L. The Large Scale Organization of Metabolic Networks. *Nature* **2000**, *407* (6804), 651–654.

(3) Barabási, A. L.; Oltvai, Z. N. Network Biology: Understanding the Cell's Functional Organization. *Nat. Rev. Genet.* **2004**, *5* (2), 101–113.

(4) Baker, D. A Surprising Simplicity to Protein Folding. *Nature* **2000**, *405* (6782), 39–42.

(5) Bryngelson, J. D.; Onuchic, J. N.; Socci, N. D.; Wolynes, P. G. Funnels, Pathways, and the Energy Landscape of Protein Folding: A Synthesis. *Proteins* **1995**, *21* (3), 167–195.

(6) Dill, K. A.; Bromberg, S.; Yue, K.; Fiebig, K. M.; Yee, D. P.; Thomas, P. D.; Chan, H. S. Principles of Protein Folding -A Perspective from Simple Exact Models. *Protein Sci.* **1995**, *4*, 561–602.

(7) Dobson, C. M.; Sali, A.; Karplus, M. Protein Folding: A Perspective from Theory and Experiment. *Angew. Chemie Int. Ed.* **1998**, *37* (7), 868–893.

(8) Dill, K. A.; MacCallum, J. L. The Protein-Folding Problem, 50 Years On. *Science* **2012**, *338* (6110), 1042–1046.

(9) Dill, K. A.; Chan, H. S. From Levinthal to Pathways to Funnels. *Nat. Struct. Biol.* **1997**, *4* (1), 10–19.

(10) Kendrew, J. C.; Bodo, G.; Dintzis, H. M.; Parrish, R. G.; Wyckoff, H.; Phillips, D. C. A Three-Dimensional Model of the Myoglobin Molecule Obtained by X-Ray Analysis. *Nature* **1958**, *181* (4610), 662–666.

(11) Kendrew, J. C.; Dickerson, R. E.; Strandberg, B. E.; Hart, R. G.; Davies, D. R.; Phillips, D. C.; Shore, V. C. Structure of Myoglobin: A Three-Dimensional Fourier Synthesis at 2 Å Resolution. *Nature* **1960**, *185* (4711), 422–427.

(12) Perutz, M. F.; Rossmann, M. G.; Cullis, A. F.; Muirhead, H.; Will, G.; North, A. C. T. Structure of Hæmoglobin: A Three-Dimensional Fourier Synthesis at 5.5-Å Resolution, Obtained by X-Ray Analysis. *Nature* **1960**, *185* (4711), 416–422.

(13) Sillitoe, I.; Dawson, N.; Thornton, J.; Orengo, C. The History of the CATH Structural Classification of Protein Domains. *Biochimie* **2015**, *119*, 209–217.

(14) Li, B.; Fooksa, M.; Heinze, S.; Meiler, J. Finding the Needle in the Haystack: Towards Solving the Protein-Folding Problem Computationally. *Crit. Rev. Biochem. Mol. Biol.* **2018**, *53* (1), 1–28.

(15) Sjölander, K. Phylogenomic Inference of Protein Molecular Function: Advances and Challenges. *Bioinformatics* **2004**, *20* (2), 170–179.

(16) Friedberg, I. Automated Protein Function Prediction - The Genomic Challenge. *Brief. Bioinform.* **2006**, *7* (3), 225–242.

(17) Lad, C.; Williams, N. H.; Wolfenden, R. The Rate of Hydrolysis of Phosphomonoester Dianions and the Exceptional Catalytic Proficiencies of Protein and Inositol Phosphatases. *Proc. Natl. Acad. Sci.* **2003**, *100* (10), 5607–5610.

(18) Radzicka, A.; Wolfenden, R. A Proficient Enzyme. *Science* **1995**, *267* (5194), 90–93.

(19) Edwards, D. R.; Lohman, D. C.; Wolfenden, R. Catalytic Proficiency: The Extreme Case of S-O Cleaving Sulfatases. *J. Am. Chem. Soc.* **2012**, *134* (1), 525–531.

(20) Fischer, E. Einfluss Der Configuration Auf Die Wirkung Der Enzyme. *Berichte der Dtsch. Chem. Gesellschaft* **1894**, *27* (3), 2985–2993.

(21) Koshland, D. E. Application of a Theory of Enzyme Specificity to Protein Synthesis. *Proc. Natl. Acad. Sci.* **1958**, *44* (2), 98–104.

(22) Frauenfelder, H.; Sligar, S. G.; Wolynes, P. G. The Energy Landscapes and Motions of Proteins. *Science* **1991**, *254* (5038), 1598–1603.

(23) Henzler-Wildman, K. a; Thai, V.; Lei, M.; Ott, M.; Wolf-Watz, M.; Fenn, T.; Pozharski, E.; Wilson, M. a; Petsko, G. a; Karplus, M.; et al. Intrinsic Motions along an Enzymatic Reaction Trajectory. *Nature* **2007**, *450* (7171), 838–844.

(24) Nagel, Z. D.; Klinman, J. P. A 21st Century Revisionist's View at a Turning Point in Enzymology. *Nat. Chem. Biol.* **2009**, *5* (8), 543–550.

(25) Schwartz, S. D.; Schramm, V. L. Enzymatic Transition States and Dynamic Motion in Barrier Crossing. *Nat. Chem. Biol.* **2009**, *5*, 551.

(26) Villali, J.; Kern, D. Choreographing an Enzyme's Dance. *Curr. Opin. Chem. Biol.* **2010**, *14* (5), 636–643.

(27) Hay, S.; Scrutton, N. S. Good Vibrations in Enzyme-Catalysed Reactions. *Nat. Chem.* **2012**, *4* (3), 161–168.

(28) Hammes-Schiffer, S.; Benkovic, S. J. Relating Protein Motion to Catalysis. *Annu. Rev. Biochem.* **2006**, *75* (1), 519–541.

(29) Benkovic, S. J.; Hammes, G. G.; Hammes-Schiffer, S. Free-Energy Landscape of Enzyme Catalysis. *Biochemistry* **2008**, *47* (11), 3317–3321.

(30) Vendruscolo, M.; Dobson, C. M. Dynamics Visions of Enzymatic Reactions. *Science* **2006**, *313* (5793), 1586–1587.

(31) Kern, D.; Eisenmesser, E. Z.; Wolf-Watz, M. Enzyme Dynamics during Catalysis Measured by NMR Spectroscopy. *Methods Enzymol.* **2005**, *394*, 507–524.

(32) Nagel, Z. D.; Klinman, J. P. Tunneling and Dynamics in Enzymatic Hydride Transfer. *Chem. Rev.* **2006**, *106* (8), 3095–3118.

(33) Boehr, D. D.; Nussinov, R.; Wright, P. E. The Role of Dynamic Conformational Ensembles in Biomolecular Recognition. *Nat. Chem. Biol.* **2009**, *5* (11), 789–796.

(34) Boehr, D. D.; Wright, P. E. How Do Proteins Interact? *Science* **2008**, *320* (5882), 1429–1430.

(35) Dyson, H. J.; Wright, P. E. Intrinsically Unstructured Proteins and Their Functions. *Nat. Rev. Mol. Cell Biol.* **2005**, *6* (3), 197–208.

(36) Cui, Q.; Karplus, M. Allostery and Cooperativity Revisited. *Protein Sci.* **2008**, *17* (8), 1295–1307.

(37) Kern, D.; Zuiderweg, E. R. P. The Role of Dynamics in Allosteric Regulation. *Curr. Opin. Struct. Biol.* **2003**, *13* (6), 748–757.

(38) Eisenmesser, E. Z.; Millet, O.; Labeikovsky, W.; Korzhnev, D. M.; Wolf-Watz, M.; Bosco, D. a; Skalicky, J. J.; Kay, L. E.; Kern, D. Intrinsic Dynamics of an Enzyme Underlies Catalysis. *Nature* **2005**, *438* (7064), 117–121.

(39) Pauling, L. Molecular Architecture and Biological Reactions. *Chem. Eng. News* **1946**, *24* (10), 1375–1377.

(40) Schramm, V. L. Enzymatic Transition States and Transition State Analog Design. *Annu. Rev. Biochem.* **1998**, *67*, 693–720.

(41) Warshel, A. Electrostatic Origin of the Catalytic Power of Enzymes and the Role of Preorganized Active Sites. *J. Biol. Chem.* **1998**, *273* (42), 27035–27038.

(42) Gerlt, J. A.; Kreevoy, M. M.; Cleland, W. W.; Frey, P. A. Understanding Enzymic Catalysis: The Importance of Short, Strong Hydrogen Bonds. *Chem. Biol.* **1997**, *4* (4), 259–267.

(43) Cleland, W. W.; Frey, P. A.; Gerlt, J. A. The Low Barrier Hydrogen Bond in Enzymatic Catalysis.

J. Biol. Chem. **1998**, *273* (40), 25529–25532.

(44) Schramm, V. L. Enzymatic Transition States, Transition-State Analogs, Dynamics, Thermodynamics, and Lifetimes. *Annu. Rev. Biochem.* **2011**, *80* (1), 703–732.

(45) Imming, P.; Sinning, C.; Meyer, A. Drugs, Their Targets and the Nature and Number of Drug Targets. *Nat. Rev. Drug Discov.* **2006**, *5* (10), 821–834.

(46) Robertson, J. G. Enzymes as a Special Class of Therapeutic Target: Clinical Drugs and Modes of Action. *Curr. Opin. Struct. Biol.* **2007**, *17* (6), 674–679.

(47) Quaytman, S.; Schwartz, S. D. Comparison Studies of the Human Heart and Bacillus Stearothermophilus LDH by Transition Path Sampling. *J. Phys. Chem. A* **2009**, *113*, 1892–1897.

(48) Saen-Oon, S.; Quaytman-Machleder, S.; Schramm, V. L.; Schwartz, S. D. Atomic Detail of Chemical Transformation at the Transition State of an Enzymatic Reaction. *Proc. Natl. Acad. Sci.* **2008**, *105* (43), 16543–16548.

(49) Pearson, A. D.; Mills, J. H.; Song, Y.; Nasertorabi, F.; Han, G. W.; Baker, D.; Stevens, R. C.; Schultz, P. G. Trapping a Transition State in a Computationally Designed Protein Bottle. *Science* **2015**, *347* (6224), 863–867.

(50) Eisenmesser, E. Z.; Bosco, D. A.; Akke, M.; Kern, D. Enzyme Dynamics during Catalysis. *Science* **2002**, *295* (5559), 1520–1523.

(51) Agarwal, P. K. Enzymes: An Integrated View of Structure, Dynamics and Function. *Microb. Cell Fact.* **2006**, *5*, 2.

(52) Henzler-Wildman, K.; Kern, D. Dynamic Personalities of Proteins. *Nature* **2007**, *450* (7172), 964–972.

(53) Klinman, J. P.; Kohen, A. Evolutionary Aspects of Enzyme Dynamics. *J. Biol. Chem.* **2014**, *289* (44), 30205–30212.

(54) Zoi, I.; Suarez, J.; Antoniou, D.; Cameron, S. A.; Schramm, V. L.; Schwartz, S. D. Modulating Enzyme Catalysis through Mutations Designed to Alter Rapid Protein Dynamics. *J. Am. Chem. Soc.* **2016**, *138* (10), 3403–3409.

(55) Agarwal, P. K.; Billeter, S. R.; Rajagopalan, P. T. R.; Benkovic, S. J.; Hammes-Schiffer, S. Network of Coupled Promoting Motions in Enzyme Catalysis. *Proc. Natl. Acad. Sci.* **2002**, *99* (5), 2794–2799.

(56) Núñez, S.; Antoniou, D.; Schramm, V. L.; Schwartz, S. D. Promoting Vibrations in Human Purine Nucleoside Phosphorylase. A Molecular Dynamics and Hybrid Quantum Mechanical/Molecular Mechanical Study. *J. Am. Chem. Soc.* **2004**, *126* (48), 15720–15729.

(57) Hatcher, E.; Soudackov, A. V.; Hammes-Schiffer, S. Proton-Coupled Electron Transfer in Soybean Lipoxygenase: Dynamical Behavior and Temperature Dependence of Kinetic Isotope Effects. *J. Am. Chem. Soc.* **2007**, *129* (1), 187–196.

(58) Johannissen, L. O.; Hay, S.; Scrutton, N. S.; Sutcliffe, M. J. Proton Tunneling in Aromatic Amine Dehydrogenase Is Driven by a Short-Range Sub-Picosecond Promoting Vibration: Consistency of Simulation and Theory with Experiment. *J. Phys. Chem. B* **2007**, *111* (10), 2631–2638.

(59) Delgado, M.; Görlich, S.; Longbotham, J. E.; Scrutton, N. S.; Hay, S.; Moliner, V.; Tuñón, I. Convergence of Theory and Experiment on the Role of Preorganization, Quantum Tunneling, and Enzyme Motions into Flavoenzyme-Catalyzed Hydride Transfer. *ACS Catal.* **2017**, *7* (5), 3190–3198.

(60) Boehr, D. D.; Dyson, H. J.; Wright, P. E. An NMR Perspective on Enzyme Dynamics. *Chem. Rev.* **2006**, *106* (8), 3055–3079.

(61) Henzler-Wildman, K. A.; Lei, M.; Thai, V.; Kerns, S. J.; Karplus, M.; Kern, D. A Hierarchy of Timescales in Protein Dynamics Is Linked to Enzyme Catalysis. *Nature* **2007**, *450* (7171), 913–916.

(62) Wang, Z.; Antoniou, D.; Schwartz, S. D.; Schramm, V. L. Hydride Transfer in DHFR by Transition Path Sampling, Kinetic Isotope Effects, and Heavy Enzyme Studies. *Biochemistry* **2016**, *55* (1), 157–166.

(63) Harijan, R. K.; Zoi, I.; Antoniou, D.; Schwartz, S. D.; Schramm, V. L. Catalytic-Site Design for Inverse Heavy-Enzyme Isotope Effects in Human Purine Nucleoside Phosphorylase. *Proc. Natl. Acad. Sci.* **2017**, *114* (25), 6456–6461.

(64) Schramm, V. L.; Schwartz, S. D. Promoting Vibrations and the Function of Enzymes. Emerging Theoretical and Experimental Convergence. *Biochemistry* **2018**, *57* (24), 3299–3308.

(65) Geddes, A.; Paul, C. E.; Hay, S.; Hollmann, F.; Scrutton, N. S. Donor-Acceptor Distance Sampling Enhances the Performance of "Better than Nature" Nicotinamide Coenzyme Biomimetics. *J. Am. Chem. Soc.* **2016**, *138* (35), 11089–11092.

(66) Salna, B.; Benabbas, A.; Russo, D.; Champion, P. M. Tunneling Kinetics and Nonadiabatic Proton-Coupled Electron Transfer in Proteins: The Effect of Electric Fields and Anharmonic Donor-Acceptor Interactions. *J. Phys. Chem. B* **2017**, *121* (28), 6869–6881.

(67) Klinman, J. P.; Kohen, A. Hydrogen Tunneling Links Protein Dynamics to Enzyme Catalysis. *Annu. Rev. Biochem.* **2013**, *82* (1), 471–496.

(68) Kamerlin, S. C. L.; Warshel, A. At the Dawn of the 21st Century: Is Dynamics the Missing Link for Understanding Enzyme Catalysis. *Proteins Struct. Funct. Bioinforma.* **2010**, *78* (6), 1339–1375.

(69) Warshel, A.; Bora, R. P. Perspective: Defining and Quantifying the Role of Dynamics in Enzyme Catalysis. *J. Chem. Phys.* **2016**, *144* (18), 1–17.

(70) Pisliakov, A. V.; Cao, J.; Kamerlin, S. C. L.; Warshel, A. Enzyme Millisecond Conformational Dynamics Do Not Catalyze the Chemical Step. *Proc. Natl. Acad. Sci.* **2009**, *106* (41), 17359–17364.

(71) Hammes-Schiffer, S. Comparison of Hydride, Hydrogen Atom, and Proton-Coupled Electron Transfer Reactions. *Chemphyschem* **2002**, *3* (1), 33–42.

(72) Limbach, H.-H.; Miguel Lopez, J.; Kohen, A. Arrhenius Curves of Hydrogen Transfers: Tunnel Effects, Isotope Effects and Effects of Pre-Equilibria. *Philos. Trans. R. Soc. B Biol. Sci.* **2006**, *361* (1472), 1399–1415.

(73) Hay, S.; Johannissen, L. O.; Sutcliffe, M. J.; Scrutton, N. S. Barrier Compression and Its Contribution to Both Classical and Quantum Mechanical Aspects of Enzyme Catalysis. *Biophys. J.* **2010**, *98* (1), 121–128.

(74) Garcia-Viloca, M.; Gao, J.; Karplus, M.; Truhlar, D. G. How Enzymes Work: Analysis by Modern Rate Theory and Computer Simulations. *Science* **2004**, *303* (5655), 186–195.

(75) Kohen, A.; Cannio, R.; Bartolucci, S. Enzyme Dynamics and Hydrogen Tunnelling in a Thermophilic Alcohol Dehydrogenase. **1999**, No. June, 496–499.

(76) Chwartz, S. T. D. S. Large Kinetic Isotope Effects in Enzymatic Proton Transfer and the Role of Substrate Oscillations. **1997**, No. November 1997, 12360–12365.

(77) Cha, Y.; Murray, C. J.; Klinman, J. P. Hydrogen Tunneling in Enzyme Reactions. *Science* **1989**, *243* (4896), 1325–1330.

(78) Knapp, M. J.; Klinman, J. P. Environmentally Coupled Hydrogen Tunneling. *Eur. J. Biochem.* **2002**, *269* (13), 3113–3121.

(79) Kamerlin, S. C. L.; Warshel, A. An Analysis of All the Relevant Facts and Arguments Indicates That Enzyme Catalysis Does Not Involve Large Contributions from Nuclear Tunneling. *J. Phys. Org. Chem.* **2010**, *23* (7), 677–684.

(80) Ruiz-Pernía, J. J.; Behiry, E.; Luk, L. Y. P.; Loveridge, E. J.; Tuñón, I.; Moliner, V.; Allemann, R. K. Minimization of Dynamic Effects in the Evolution of Dihydrofolate Reductase. *Chem. Sci.* **2016**,

7 (5), 3248–3255.

(81) Wong, K. F.; Selzer, T.; Benkovic, S. J.; Hammes-Schiffer, S. Impact of Distal Mutations on the Network of Coupled Motions Correlated to Hydride Transfer in Dihydrofolate Reductase. *Proc. Natl. Acad. Sci.* **2005**, *102* (19), 6807–6812.

(82) Stojković, V.; Perissinotti, L. L.; Willmer, D.; Benkovic, S. J.; Kohen, A. Effects of the Donor-Acceptor Distance and Dynamics on Hydride Tunneling in the Dihydrofolate Reductase Catalyzed Reaction. *J. Am. Chem. Soc.* **2012**, *134* (3), 1738–1745.

(83) Bhabha, G.; Lee, J.; Ekiert, D. C.; Gam, J.; Wilson, I. a; Dyson, H. J.; Benkovic, S. J.; Wright, P. E. A Dynamic Knockout Reveals That Conformational Fluctuations Influence the Chemical Step of Enzyme Catalysis. *Science* **2011**, *332* (6026), 234–238.

(84) Wang, L.; Goodey, N. M.; Benkovic, S. J.; Kohen, A. Coordinated Effects of Distal Mutations on Environmentally Coupled Tunneling in Dihydrofolate Reductase. *Proc. Natl. Acad. Sci.* **2006**, *103* (43), 15753–15758.

(85) Knapp, M. J.; Rickert, K.; Klinman, J. P. Temperature-Dependent Isotope Effects in Soybean Lipoxygenase-1: Correlating Hydrogen Tunneling with Protein Dynamics. *J. Am. Chem. Soc.* **2002**, *124* (15), 3865–3874.

(86) Wang, Z.; Abeysinghe, T.; Finer-Moore, J. S.; Stroud, R. M.; Kohen, A. A Remote Mutation Affects the Hydride Transfer by Disrupting Concerted Protein Motions in Thymidylate Synthase. *J. Am. Chem. Soc.* **2012**, *134* (42), 17722–17730.

(87) Pudney, C. R.; Hay, S.; Pang, J.; Costello, C.; Leys, D.; Sutcliffe, M. J.; Scrutton, N. S. Mutagenesis of Morphinone Reductase Induces Multiple Reactive Configurations and Identifies Potential Ambiguity in Kinetic Analysis of Enzyme Tunneling Mechanisms. *J. Am. Chem. Soc.* **2007**, *129* (45), 13949–13956.

(88) Pudney, C. R.; McGrory, T.; Lafite, P.; Pang, J.; Hay, S.; Leys, D.; Sutcliffe, M. J.; Scrutton, N. S. Parallel Pathways and Free-Energy Landscapes for Enzymatic Hydride Transfer Probed by Hydrostatic Pressure. *Chembiochem* **2009**, *10* (8), 1379–1384.

(89) Hay, S.; Sutcliffe, M. J.; Scrutton, N. S. Promoting Motions in Enzyme Catalysis Probed by Pressure Studies of Kinetic Isotope Effects. *Proc. Natl. Acad. Sci.* **2007**, *104* (2), 507–512.

(90) Hay, S.; Johannissen, L. O.; Hothi, P.; Sutcliffe, M. J.; Scrutton, N. S. Pressure Effects on Enzyme-Catalyzed Quantum Tunneling Events Arise from Protein-Specific Structural and Dynamic Changes. *J. Am. Chem. Soc.* **2012**, *134* (23), 9749–9754.

(91) Silva, R. G.; Murkin, A. S.; Schramm, V. L. Femtosecond Dynamics Coupled to Chemical Barrier Crossing in a Born-Oppenheimer Enzyme. *Proc. Natl. Acad. Sci.* **2011**, *108* (46), 18661–18665.

(92) Suarez, J.; Schramm, V. L. Isotope-Specific and Amino Acid-Specific Heavy Atom Substitutions Alter Barrier Crossing in Human Purine Nucleoside Phosphorylase. *Proc. Natl. Acad. Sci.* **2015**, *112* (36), 11247–11251.

(93) Wang, Z.; Singh, P.; Czekster, C. M.; Kohen, A.; Schramm, V. L. Protein Mass-Modulated Effects in the Catalytic Mechanism of Dihydrofolate Reductase: Beyond Promoting Vibrations. *J. Am. Chem. Soc.* **2014**, *136* (23), 8333–8341.

(94) Francis, K.; Sapienza, P. J.; Lee, A. L.; Kohen, A. The Effect of Protein Mass Modulation on Human Dihydrofolate Reductase. *Biochemistry* **2016**, *55* (7), 1100–1106.

(95) Pudney, C. R.; Hay, S.; Levy, C.; Pang, J.; Sutcliffe, M. J.; Leys, D.; Scrutton, N. S. Evidence to Support the Hypothesis That Promoting Vibrations Enhance the Rate of an Enzyme Catalyzed H-Tunneling Reaction. *J. Am. Chem. Soc.* **2009**, *131* (47), 17072–17073.

(96) Longbotham, J. E.; Hardman, S. J. O. O.; Görlich, S.; Scrutton, N. S.; Hay, S. Untangling Heavy Protein and Cofactor Isotope Effects on Enzyme-Catalyzed Hydride Transfer. *J. Am. Chem. Soc.* **2016**, *138* (41), 13693–13699.

(97) Vaughn, M. B.; Zhang, J.; Spiro, T. G.; Dyer, R. B.; Klinman, J. P. Activity-Related Microsecond

Dynamics Revealed by Temperature-Jump Förster Resonance Energy Transfer Measurements on Thermophilic Alcohol Dehydrogenase. *J. Am. Chem. Soc.* **2018**, *140* (3), 900–903.

(98) Mattevi, A. To Be or Not to Be an Oxidase: Challenging the Oxygen Reactivity of Flavoenzymes. *Trends Biochem. Sci.* **2006**, *31* (5), 276–283.

(99) Piano, V.; Palfey, B. A.; Mattevi, A. Flavins as Covalent Catalysts: New Mechanisms Emerge. *Trends Biochem. Sci.* **2017**, *42* (6), 457–469.

(100) MacHeroux, P.; Kappes, B.; Ealick, S. E. Flavogenomics - A Genomic and Structural View of Flavin-Dependent Proteins. *FEBS J.* **2011**, *278* (15), 2625–2634.

(101) Gruber, C. W.; Čemažar, M.; Heras, B.; Martin, J. L.; Craik, D. J. Protein Disulfide Isomerase: The Structure of Oxidative Folding. *Trends Biochem. Sci.* **2006**, *31* (8), 455–464.

(102) Weber, S. Light-Driven Enzymatic Catalysis of DNA Repair: A Review of Recent Biophysical Studies on Photolyase. *Biochim. Biophys. Acta* **2005**, *1707* (1), 1–23.

(103) Tomiki, T.; Saitou, N. Phylogenetic Analysis of Proteins Associated in the Four Major Energy Metabolism Systems: Photosynthesis, Aerobic Respiration, Denitrification, and Sulfur Respiration. *J. Mol. Evol.* **2004**, *59* (2), 158–176.

(104) Mansoorabadi, S. O.; Thibodeaux, C. J.; Liu, H. W. The Diverse Roles of Flavin Coenzymes - Nature's Most Versatile Thespians. *J. Org. Chem.* **2007**, *72* (17), 6329–6342.

(105) Joosten, V.; van Berkel, W. J. H. Flavoenzymes. *Curr. Opin. Chem. Biol.* **2007**, *11* (2), 195–202.

(106) Massey, V. Introduction: Flavoprotein Structure and Mechanism. *FASEB J.* **1995**, *9* (7), 473–475.

(107) Payne, K. A. P.; White, M. D.; Fisher, K.; Khara, B.; Bailey, S. S.; Parker, D.; Rattray, N. J. W.; Trivedi, D. K.; Goodacre, R.; Beveridge, R.; et al. New Cofactor Supports α,β-Unsaturated Acid Decarboxylation via 1,3-Dipolar Cycloaddition. *Nature* **2015**, *522* (7557), 497–501.

(108) White, M. D.; Payne, K. A. P.; Fisher, K.; Marshall, S. A.; Parker, D.; Rattray, N. J. W.; Trivedi, D. K.; Goodacre, R.; Rigby, S. E. J.; Scrutton, N. S.; et al. UbiX Is a Flavin Prenyltransferase Required for Bacterial Ubiquinone Biosynthesis. *Nature* **2015**, *522* (7557), 502–506.

(109) Leys, D.; Scrutton, N. S. Sweating the Assets of Flavin Cofactors: New Insight of Chemical Versatility from Knowledge of Structure and Mechanism. *Curr. Opin. Struct. Biol.* **2016**, *41*, 19–26.

(110) Wang, P. H.; Khusnutdinova, A. N.; Luo, F.; Xiao, J.; Nemr, K.; Flick, R.; Brown, G.; Mahadevan, R.; Edwards, E. A.; Yakunin, A. F. Biosynthesis and Activity of Prenylated FMN Cofactors. *Cell Chem. Biol.* **2018**, *25* (5), 560–570.e6.

(111) Ghisla, S.; Massey, V. Mechanisms of Flavoprotein-catalyzed Reactions. *Eur. J. Biochem.* **1989**, *181* (1), 1–17.

(112) König, B.; Kümmel, S.; Svobodová, E.; Cibulka, R. Flavin Photocatalysis. In *Chemical Photocatalysis*; 2013; pp 45–66.

(113) Heelis, P. F. The Photophysical and Photochemical Properties of Flavins (Isoalloxazines). *Chem. Soc. Rev.* **1982**, *11* (1), 15–39.

(114) Fraaije, M. W.; Mattevi, A. Flavoenzymes : Diverse Catalysts with Recurrent Features. **2000**, *0004* (1999), 126–132.

(115) Romero, E.; Gómez Castellanos, J. R.; Gadda, G.; Fraaije, M. W.; Mattevi, A. Same Substrate, Many Reactions: Oxygen Activation in Flavoenzymes. *Chem. Rev.* **2018**, *118* (4), 1742–1769.

(116) Toogood, H. S.; Scrutton, N. S. New Developments in 'Ene'-Reductase Catalysed Biological Hydrogenations. *Curr. Opin. Chem. Biol.* **2014**, *19* (1), 107–115.

(117) Knaus, T.; Toogood, H. S.; Scrutton, N. S. Ene-Reductases and Their Applications. In *Green Biocatalysis*; Wiley Online Books; 2016.

(118) Toogood, H. S.; Scrutton, N. S. Discovery, Characterization, Engineering, and Applications of Ene-Reductases for Industrial Biocatalysis. *ACS Catal.* **2018**, *8* (4), 3532–3549.

(119) Rohdich, F.; Wiese, A.; Feicht, R.; Simon, H.; Bacher, A. Enoate Reductases of Clostridia. Cloning, Sequencing, and Expression. *J. Biol. Chem.* **2001**, *276* (8), 5779–5787.

(120) Mordaka, P. M.; Hall, S. J.; Minton, N.; Stephens, G. Recombinant Expression and Characterisation of the Oxygensensitive 2-Enoate Reductase from Clostridium Sporogenes. *Microbiology* **2018**, *164* (2), 122–132.

(121) Nordling, E.; Jörnvall, H.; Persson, B. Medium-Chain Dehydrogenases/Reductases (MDR): Family Characterizations Including Genome Comparisons and Active Site Modelling. *Eur. J. Biochem.* **2002**, *269* (17), 4267–4276.

(122) Moummou, H.; Kallberg, Y.; Tonfack, L. B.; Persson, B.; van der Rest, B. The Plant Short-Chain Dehydrogenase (SDR) Superfamily: Genome-Wide Inventory and Diversification Patterns. *BMC Plant Biol.* **2012**, *12*, 219.

(123) Wenda, S.; Illner, S.; Mell, A.; Kragl, U. Industrial Biotechnology—the Future of Green Chemistry? *Green Chem.* **2011**, *13* (11), 3007–3047.

(124) Muñoz Solano, D.; Hoyos, P.; Hernáiz, M. J.; Alcántara, A. R.; Sánchez-Montero, J. M. Industrial Biotransformations in the Synthesis of Building Blocks Leading to Enantiopure Drugs. *Bioresour. Technol.* **2012**, *115*, 196–207.

(125) Clouthier, C. M.; Pelletier, J. N. Expanding the Organic Toolbox: A Guide to Integrating Biocatalysis in Synthesis. *Chem. Soc. Rev.* **2012**, *41* (4), 1585–1605.

(126) Blamey, J. M.; Fischer, F.; Meyer, H. P.; Sarmiento, F.; Zinn, M. Enzymatic Biocatalysis in Chemical Transformations: A Promising and Emerging Field in Green Chemistry Practice. In *Biotechnology of Microbial Enzymes: Production, Biocatalysis and Industrial Applications*; Elsevier Inc., 2016; pp 347–403.

(127) Waller, J.; Toogood, H. S.; Karuppiah, V.; Rattray, N. J. W.; Mansell, D. J.; Leys, D.; Gardiner, J. M.; Fryszkowska, A.; Ahmed, S. T.; Bandichhor, R.; et al. Structural Insights into the Ene-Reductase Synthesis of Profens. *Org. Biomol. Chem.* **2017**, *15* (20), 4440–4448.

(128) Reich, S.; Nestl, B. M.; Hauer, B. Loop-Grafted Old Yellow Enzymes in the Bienzymatic Cascade Reduction of Allylic Alcohols. *ChemBioChem* **2016**, *17* (7), 561–565.

(129) Skalden, L.; Peters, C.; Ratz, L.; Bornscheuer, U. T. Synthesis of (1R,3R)-1-Amino-3-Methylcyclohexane by an Enzyme Cascade Reaction. *Tetrahedron* **2016**, *72* (46), 7207–7211.

(130) Peters, C.; Kölzsch, R.; Kadow, M.; Skalden, L.; Rudroff, F.; Mihovilovic, M. D.; Bornscheuer, U. T. Identification, Characterization, and Application of Three Enoate Reductases from Pseudomonas Putida in In Vitro Enzyme Cascade Reactions. *ChemCatChem* **2014**, *6* (4), 1021–1027.

(131) Oberleitner, N.; Peters, C.; Rudroff, F.; Bornscheuer, U. T.; Mihovilovic, M. D. In Vitro Characterization of an Enzymatic Redox Cascade Composed of an Alcohol Dehydrogenase, an Enoate Reductases and a Baeyer-Villiger Monooxygenase. *J. Biotechnol.* **2014**, *192*, 393–399.

(132) Knaus, T.; Mutti, F. G.; Humphreys, L. D.; Turner, N. J.; Scrutton, N. S. Systematic Methodology for the Development of Biocatalytic Hydrogen-Borrowing Cascades: Application to the Synthesis of Chiral α-Substituted Carboxylic Acids from α-Substituted α,β-Unsaturated Aldehydes. *Org. Biomol. Chem.* **2015**, *13* (1), 223–233.

(133) Litman, Z. C.; Wang, Y.; Zhao, H.; Hartwig, J. F. Cooperative Asymmetric Reactions Combining Photocatalysis and Enzymatic Catalysis. *Nature* **2018**, *560* (7718), 355–359.

(134) Castiglione, K.; Fu, Y.; Polte, I.; Leupold, S.; Meo, A.; Weuster-Botz, D. Asymmetric Whole-Cell Bioreduction of (R)-Carvone by Recombinant Escherichia Coli with in Situ Substrate Supply and Product Removal. *Biochem. Eng. J.* **2017**, *117*, 102–111.

(135) Toogood, H. S.; Cheallaigh, A. N.; Tait, S.; Mansell, D. J.; Jervis, A.; Lygidakis, A.; Humphreys,

L.; Takano, E.; Gardiner, J. M.; Scrutton, N. S. Enzymatic Menthol Production: One-Pot Approach Using Engineered Escherichia Coli. *ACS Synth. Biol.* **2015**, *4* (10), 1112–1123.

(136) Sun, J.; Lin, Y.; Shen, X.; Jain, R.; Sun, X.; Yuan, Q.; Yan, Y. Aerobic Biosynthesis of Hydrocinnamic Acids in Escherichia Coli with a Strictly Oxygen-Sensitive Enoate Reductase. *Metab. Eng.* **2016**, *35*, 75–82.

(137) Hulley, M. E.; Toogood, H. S.; Fryszkowska, A.; Mansell, D.; Stephens, G. M.; Gardiner, J. M.; Scrutton, N. S. Focused Directed Evolution of Pentaerythritol Tetranitrate Reductase by Using Automated Anaerobic Kinetic Screening of Site-Saturated Libraries. *Chembiochem* **2010**, *11* (17), 2433–2447.

(138) Toogood, H. S.; Fryszkowska, A.; Hulley, M.; Sakuma, M.; Mansell, D.; Stephens, G. M.; Gardiner, J. M.; Scrutton, N. S. A Site-Saturated Mutagenesis Study of Pentaerythritol Tetranitrate Reductase Reveals That Residues 181 and 184 Influence Ligand Binding, Stereochemistry and Reactivity. *Chembiochem* **2011**, *12* (5), 738–749.

(139) Daugherty, A. B.; Horton, J. R.; Cheng, X.; Lutz, S. Structural and Functional Consequences of Circular Permutation on the Active Site of Old Yellow Enzyme. *ACS Catal.* **2015**, *5* (2), 892–899.

(140) Daugherty, A. B.; Govindarajan, S.; Lutz, S. Improved Biocatalysts from a Synthetic Circular Permutation Library of the Flavin-Dependent Oxidoreductase Old Yellow Enzyme. *J. Am. Chem. Soc.* **2013**, *135* (38), 14425–14432.

(141) Yu, Y.; Lutz, S. Circular Permutation: A Different Way to Engineer Enzyme Structure and Function. *Trends Biotechnol.* **2011**, *29* (1), 18–25.

(142) Amato, E. D.; Stewart, J. D. Applications of Protein Engineering to Members of the Old Yellow Enzyme Family. *Biotechnol. Adv.* **2015**, *33* (5), 624–631.

(143) Bougioukou, D. J.; Kille, S.; Taglieber, A.; Reetz, M. T. Directed Evolution of an Enantioselective Enoate-Reductase: Testing the Utility of Iterative Saturation Mutagenesis. *Adv. Synth. Catal.* **2009**, *351* (18), 3287–3305.

(144) Nett, N.; Duewel, S.; Richter, A. A.; Hoebenreich, S. Revealing Additional Stereocomplementary Pairs of Old Yellow Enzymes by Rational Transfer of Engineered Residues. *ChemBioChem* **2017**, *18* (7), 685–691.

(145) Mueller, N. J. J.; Stueckler, C.; Hauer, B.; Baudendistel, N.; Housden, H.; Bruce, N. C. C.; Faber, K. The Substrate Spectra of Pentaerythritol Tetranitrate Reductase, Morphinone Reductase, N-Ethylmaleimide Reductase and Estrogen-Binding Protein in the Asymmetric Bioreduction of Activated Alkenes. *Adv. Synth. Catal.* **2010**, *352* (2-3), 387–394.

(146) Horita, S.; Kataoka, M.; Kitamura, N.; Nakagawa, T.; Miyakawa, T.; Ohtsuka, J.; Nagata, K.; Shimizu, S.; Tanokura, M. An Engineered Old Yellow Enzyme That Enables Efficient Synthesis of (4R,6R)-Actinol in a One-Pot Reduction System. *ChemBioChem* **2015**, *16* (3), 440–445.

(147) Warburg, O.; Christian, W. Ein Zweites Sauerstoffübertragendes Ferment Und Sein Absorptionsspektrum. *Naturwissenschaften* **1932**, *20* (37), 688.

(148) Scholtissek, A.; Tischler, D.; Westphal, A.; van Berkel, W.; Paul, C. Old Yellow Enzyme-Catalysed Asymmetric Hydrogenation: Linking Family Roots with Improved Catalysis. *Catalysts* **2017**, *7* (5), 130.

(149) Toogood, H. S.; Gardiner, J. M.; Scrutton, N. S. Biocatalytic Reductions and Chemical Versatility of the Old Yellow Enzyme Family of Flavoprotein Oxidoreductases. *ChemCatChem* **2010**, *2* (8), 892–914.

(150) Wierenga, R. K. The TIM-Barrel Fold: A Versatile Framework for Efficient Enzymes. *FEBS Lett.* **2001**, *492* (3), 193–198.

(151) Lolis, E.; Alber, T.; Davenport, R. C.; Rose, D.; Hartman, F. C.; Petsko, G. A. Structure of Yeast Triosephosphate Isomerase at 1.9-.ANG. Resolution. *Biochemistry* **1990**, *29* (28), 6609–6618.

(152) Barna, T. M.; Khan, H.; Bruce, N. C.; Barsukov, I.; Scrutton, N. S.; Moody, P. C. E.; Messiha, H. L.; Petosa, C.; Bruce, N. C.; Scrutton, N. S.; et al. Crystal Structure of Pentaerythritol Tetranitrate Reductase: "Flipped" Binding Geometries for Steroid Substrates in Different Redox States of the Enzyme. *J. Mol. Biol.* **2001**, *310* (2), 433–447.

(153) Barna, T.; Messiha, H. L.; Petosa, C.; Bruce, N. C.; Scrutton, N. S.; Moody, P. C. E. Crystal Structure of Bacterial Morphinone Reductase and Properties of the C191A Mutant Enzyme. *J. Biol. Chem.* **2002**, *277* (34), 30976–30983.

(154) Fox, K. M.; Karplus, P. a. Old Yellow Enzyme at 2 A Resolution: Overall Structure, Ligand Binding, and Comparison with Related Flavoproteins. *Structure* **1994**, *2* (11), 1089–1105.

(155) Brown, B. J.; Deng, Z.; Karplus, P. A.; Massey, V. On the Active Site of Old Yellow Enzyme Turnover . Solution of the Crystal Structure of OYE1 From. *Biochemistry* **1998**, *273* (49), 32753–32762.

(156) Kohli, R. M. The Oxidative Half-Reaction of Old Yellow Enzyme. THE ROLE OF TYROSINE 196. *J. Biol. Chem.* **1998**, *273* (49), 32763–32770.

(157) Basran, J.; Harris, R. J.; Sutcliffe, M. J.; Scrutton, N. S. H-Tunneling in the Multiple H-Transfers of the Catalytic Cycle of Morphinone Reductase and in the Reductive Half-Reaction of the Homologous Pentaerythritol Tetranitrate Reductase. *J. Biol. Chem.* **2003**, *278* (45), 43973–43982.

(158) Massey, V.; Schopfer, L. M. Reactivity of Old Yellow Enzyme with α-NADPH and Other Pyridine Nucleotide Derivatives. *J. Biol. Chem.* **1986**, *261* (3), 1215–1222.

(159) Pudney, C. R.; Hay, S.; Scrutton, N. S. Bipartite Recognition and Conformational Sampling Mechanisms for Hydride Transfer from Nicotinamide Coenzyme to FMN in Pentaerythritol Tetranitrate Reductase. *FEBS J.* **2009**, *276* (17), 4780–4789.

(160) Khan, H.; Harris, R. J.; Barna, T.; Craig, D. H.; Bruce, N. C.; Munro, A. W.; Moody, P. C. E.; Scrutton, N. S. Kinetic and Structural Basis of Reactivity of Pentaerythritol Tetranitrate Reductase with NADPH, 2-Cyclohexenone, Nitroesters, and Nitroaromatic Explosives. *J. Biol. Chem.* **2002**, *277* (24), 21906–21912.

(161) Pudney, C. R.; Johannissen, L. O.; Sutcliffe, M. J.; Hay, S.; Scrutton, N. S. Direct Analysis of Donor-Acceptor Distance and Relationship to Isotope Effects and the Force Constant for Barrier Compression in Enzymatic H-Tunneling Reactions. *J. Am. Chem. Soc.* **2010**, *132* (32), 11329–11335.

(162) French, C. E.; Nicklin, S.; Bruce, N. C. Sequence and Properties of Pentaerythritol Tetranitrate Reductase from Enterobacter Cloacae PB2. *J. Bacteriol.* **1996**, *178* (22), 6623–6627.

(163) Fryszkowska, A.; Toogood, H.; Sakuma, M.; Gardiner, J. M.; Stephens, G. M.; Scrutton, N. S.; Gill, M.; Stephens, G. M.; Scrutton, N. S. Asymmetric Reduction of Activated Alkenes by Pentaerythritol Tetranitrate Reductase: Specificity and Control of Stereochemical Outcome by Reaction Optimisation. *Adv. Synth. Catal.* **2009**, *351* (17), 2976–2990.

(164) Fryszkowska, A.; Toogood, H. S.; Mansell, D.; Stephens, G.; Gardiner, J. M.; Scrutton, N. S. A Surprising Observation That Oxygen Can Affect the Product Enantiopurity of an Enzyme-Catalysed Reaction. *FEBS J.* **2012**, *279* (22), 4160–4171.

(165) Hay, S.; Scrutton, N. S. Incorporation of Hydrostatic Pressure into Models of Hydrogen Tunneling Highlights a Role for Pressure-Modulated Promoting Vibrations. *Biochemistry* **2008**, *47* (37), 9880–9887.

(166) Pudney, C. R.; Guerriero, A.; Baxter, N. J.; Johannissen, L. O.; Waltho, J. P.; Hay, S.; Scrutton, N. S. Fast Protein Motions Are Coupled to Enzyme H-Transfer Reactions. *J. Am. Chem. Soc.* **2013**, *135* (7), 2512–2517.

(167) Clore, G. M.; Gronenborn, A. M. NMR Structure Determination of Proteins and Protein Complexes Larger than 20 KDa. *Curr. Opin. Chem. Biol.* **1998**, *2* (5), 564–570.

(168) Gardner, K. H.; Kay, L. E. The Use of 2H, 13C, 15N Multidimensional NMR to Study the Structure and Dynamics of Proteins. *Annu. Rev. Biophys. Biomol. Struct.* **1998**, *27*, 357–406.

(169) Clore, M. G.; Ronenborn, A. M. New Methods of Structure Refinement for Macromolecular Structure Determination by NMR. *Proc. Natl. Acad. Sci.* **1998**, *95* (11), 5891–5898.

(170) Kay, L. E.; Torchia, D. A.; Bax, A. Backbone Dynamics of Proteins As Studied by 15N Inverse Detected Heteronuclear NMR Spectroscopy : Application to Staphylococcal Nuclease. *Biochemistry* **1989**, *28* (23), 8972–8979.

(171) Xue, Y.; Ward, J. M.; Yuwen, T.; Podkorytov, I. S.; Skrynnikov, N. R. Microsecond Time-Scale Conformational Exchange in Proteins: Using Long Molecular Dynamics Trajectory To Simulate NMR Relaxation Dispersion Data. *J. Am. Chem. Soc.* **2012**, *134* (2), 2555–2562.

(172) Lipsitz, R. S.; Tjandra, N. Residual Dipolar Couplings in NMR Structure Analysis. *Annu. Rev. Biophys. Biomol. Struct.* **2004**, *33* (1), 387–413.

(173) Prestegard, J. H.; Bougault, C. M.; Kishore, a. I. Residual Dipolar Couplings in Structure Determination of Biomolecules. *Chem. Rev.* **2004**, *104* (8), 3519–3540.

(174) Blackledge, M. Recent Progress in the Study of Biomolecular Structure and Dynamics in Solution from Residual Dipolar Couplings. *Prog. Nucl. Magn. Reson. Spectrosc.* **2005**, *46* (1), 23–61.

(175) Meier, S.; Cho, K.; Grzesiek, S.; Bru, R.; Bouvignies, G.; Bernado, P.; Blackledge, M. Identification of Slow Correlated Motions in Proteins Using Residual Dipolar and Hydrogen-Bond Scalar Couplings. *Proc. Natl. Acad. Sci.* **2005**, *102* (39), 13885–13890.

(176) Guerriero, A. Variable Pressure NMR Analyses to Assess Compressive Motion in PETNR and Catalytically Germane PETNR:Ligand Complexes, The University of Manchester, 2011.

(177) Geddes, A. C. A Study of H-Transfer Kinetics and Catalytic Protein Dynamics in Ene-Reductase Enzymes of the OYE Family, The University of Manchester, 2016.

(178) Markley, J. L.; Putter, I.; Jardetzky, O. High-Resolution Nuclear Magnetic Resonance Spectra of Selectively Deuterated Staphylococcal Nuclease. *Science* **1968**, *161* (3847), 1249–1251.

(179) Farmer, B. T.; Venters, R. A. NMR of Perdeuterated Large Proteins. *Mod. Tech. Protein NMR* **2002**, *16*, 75–120.

(180) Crespi, H. L.; Katz, J. J. High Resolution Proton Magnetic Resonance Studies of Fully Deuterated and Isotope Hybrid Proteins. *Nature* **1969**, *224* (5219), 560–562.

(181) Katz, J. J.; Crespi, H. L. Deuterated Organisms: Cultivation and Uses. *Science* **1966**, *151* (3715), 1187–1194.

(182) Rosano, G. L.; Ceccarelli, E. A. Recombinant Protein Expression in Escherichia Coli: Advances and Challenges. *Front. Microbiol.* **2014**, *5*, 172.

(183) Skora, L.; Shrestha, B.; Gossert, A. D. Isotope Labeling of Proteins in Insect Cells. *Methods Enzymol.* **2015**, *565*, 245–288.

(184) Sastry, M.; Bewley, C. A.; Kwong, P. D. Effective Isotope Labeling of Proteins in a Mammalian Expression System. *Methods Enzymol.* **2015**, *565*, 289–307.

(185) Staunton, D.; Schlinkert, R.; Zanetti, G.; Colebrook, S. A.; Campbell, I. D. Cell-Free Expression and Selective Isotope Labelling in Protein NMR. *Magn. Reson. Chem.* **2006**, *44*, S2-9.

(186) Takeda, M.; Kainosho, M. Cell-Free Protein Production for NMR. *Methods Mol. Biol.* **2012**, *831*, 71–84.

(187) Duff, A. P.; Wilde, K. L.; Rekas, A.; Lake, V.; Holden, P. J. Robust High-Yield Methodologies For2H And2H/15N/13C Labeling of Proteins for Structural Investigations Using Neutron Scattering and NMR. *Methods Enzymol.* **2015**, *565*, 3–25.

(188) Peuker, S.; Andersson, H.; Gustavsson, E.; Maiti, K. S.; Kania, R.; Karim, A.; Niebling, S.;

Pedersen, A.; Erdelyi, M.; Westenhoff, S. Efficient Isotope Editing of Proteins for Site-Directed Vibrational Spectroscopy. *J. Am. Chem. Soc.* **2016**, *138* (7), 2312–2318.

(189) Lin, M. T.; Fukazawa, R.; Miyajima-Nakano, Y.; Matsushita, S.; Choi, S. K.; Iwasaki, T.; Gennis, R. B. Escherichia Coli Auxotroph Host Strains for Amino Acid-Selective Isotope Labeling of Recombinant Proteins. *Methods Enzymol.* **2015**, *565*, 45–66.

(190) Michel, E.; Allain, F. H. T. Selective Amino Acid Segmental Labeling of Multi-Domain Proteins. *Methods Enzymol.* **2015**, *565*, 389–422.

(191) Haertlein, M.; Moulin, M.; Devos, J. M.; Laux, V.; Dunne, O.; Trevor Forsyth, V. Biomolecular Deuteration for Neutron Structural Biology and Dynamics. *Methods Enzymol.* **2016**, *566*, 113–157.

(192) Chahrour, O.; Cobice, D.; Malone, J. Stable Isotope Labelling Methods in Mass Spectrometry-Based Quantitative Proteomics. *J. Pharm. Biomed. Anal.* **2015**, *113*, 2–20.

(193) Heinrich, F. Deuteration in Biological Neutron Reflectometry. *Methods Enzymol.* **2016**, *566*, 211–230.

(194) Antoniou, D.; Ge, X.; Schramm, V. L.; Schwartz, S. D. Mass Modulation of Protein Dynamics Associated with Barrier Crossing in Purine Nucleoside Phosphorylase. *J. Phys. Chem. Lett.* **2012**, *3* (23), 3538–3544.

(195) Toney, M. D.; Castro, J. N.; Addington, T. A. Heavy-Enzyme Kinetic Isotope Effects on Proton Transfer in Alanine Racemase. *J. Am. Chem. Soc.* **2013**, *135* (7), 2509–2511.

(196) Luk, L. Y. P.; Javier Ruiz-Pernia, J.; Dawson, W. M.; Roca, M.; Loveridge, E. J.; Glowacki, D. R.; Harvey, J. N.; Mulholland, A. J.; Tunon, I.; Moliner, V.; et al. Unraveling the Role of Protein Dynamics in Dihydrofolate Reductase Catalysis. *Proc. Natl. Acad. Sci.* **2013**, *110* (41), 16344–16349.

(197) Wang, Z.; Chang, E. P.; Schramm, V. L. Triple Isotope Effects Support Concerted Hydride and Proton Transfer and Promoting Vibrations in Human Heart Lactate Dehydrogenase. *J. Am. Chem. Soc.* **2016**, *138* (45), 15004–15010.

(198) Kipp, D. R.; Silva, R. G.; Schramm, V. L. Mass-Dependent Bond Vibrational Dynamics Influence Catalysis by HIV-1 Protease. *J. Am. Chem. Soc.* **2011**, *133* (48), 19358–19361.

(199) Krzemińska, A.; Moliner, V.; Świderek, K. Dynamic and Electrostatic Effects on the Reaction Catalyzed by HIV-1 Protease. *J. Am. Chem. Soc.* **2016**, *138* (50), 16283–16298.

(200) Kholodar, S. A.; Ghosh, A. K.; Kohen, A. Measurement of Enzyme Isotope Effects. *Methods Enzymol.* **2017**, *596*, 43–83.

(201) Świderek, K.; Javier Ruiz-Pernía, J.; Moliner, V.; Tuñón, I. Heavy Enzymes-Experimental and Computational Insights in Enzyme Dynamics. *Curr. Opin. Chem. Biol.* **2014**, *21*, 11–18.

(202) Iorgu, A. I.; Baxter, N. J.; Cliff, M. J.; Waltho, J. P.; Hay, S.; Scrutton, N. S. 1H,15N And13C Backbone Resonance Assignments of Pentaerythritol Tetranitrate Reductase from Enterobacter Cloacae PB2. *Biomol. NMR Assign.* **2018**, *12* (1), 79–83.

(203) Pudney, C. R.; Hay, S.; Sutcliffe, M. J.; Scrutton, N. S. α-Secondary Isotope Effects as Probes of "Tunneling-Ready" Configurations in Enzymatic H-Tunneling: Insight from Environmentally Coupled Tunneling Models. *J. Am. Chem. Soc.* **2006**, *128* (43), 14053–14058.

(204) Studier, F. W. Protein Production by Auto-Induction in High Density Shaking Cultures. *Protein Expr. Purif.* **2005**, *41* (1), 207–234.

(205) Sambrook, J.; Fritsch, E. F.; Maniatis, T. *Molecular Cloning: A Laboratory Manual*; Cold Spring Harbor Laboratory Press, 1989.

(206) Nietlispach, D.; Clowes, R. T.; Broadhurst, R. W.; Ito, Y.; Keeler, J.; Kelly, M.; Ashurst, J.; Oschkinat, H.; Domaille, P. J.; Laue, E. D. An Approach to the Structure Determination of Larger Proteins Using Triple Resonance NMR Experiments in Conjunction with Random Fractional

Deuteration. *J. Am. Chem. Soc.* **1996**, *118* (2), 407–415.

(207) Williams, R. E.; Bruce, N. C. "New Uses for an Old Enzyme" – the Old Yellow Enzyme Family of Flavoenzymes. *Microbiology* **2002**, *148*, 1607–1614.

(208) Hardman, S. J. O.; Pudney, C. R.; Hay, S.; Scrutton, N. S. Excited State Dynamics Can Be Used to Probe Donor-Acceptor Distances for H-Tunneling Reactions Catalyzed by Flavoproteins. *Biophys. J.* **2013**, *105* (11), 2549–2558.

(209) Hay, S.; Pudney, C. R.; Scrutton, N. S. Structural and Mechanistic Aspects of Flavoproteins: Probes of Hydrogen Tunnelling. *FEBS J.* **2009**, *276* (15), 3930–3941.

(210) Harijan, R. K.; Zoi, I.; Antoniou, D.; Schwartz, S. D.; Schramm, V. L. Inverse Enzyme Isotope Effects in Human Purine Nucleoside Phosphorylase with Heavy Asparagine Labels. *Proc. Natl. Acad. Sci.* **2018**, *115* (27), E6209–E6216.

(211) Venditti, V.; Fawzi, N. L.; Clore, G. M. An Efficient Protocol for Incorporation of an Unnatural Amino Acid in Perdeuterated Recombinant Proteins Using Glucose-Based Media. *J. Biomol. Nmr* **2012**, *52* (3), 191–195.

(212) Arcus, V. L.; Pudney, C. R. Change in Heat Capacity Accurately Predicts Vibrational Coupling in Enzyme Catalyzed Reactions. *FEBS Lett.* **2015**, *589* (17), 2200–2206.

(213) Arcus, V. L.; Prentice, E. J.; Hobbs, J. K.; Mulholland, A. J.; Van Der Kamp, M. W.; Pudney, C. R.; Parker, E. J.; Schipper, L. A. On the Temperature Dependence of Enzyme-Catalyzed Rates. *Biochemistry* **2016**, *55* (12), 1681–1688.

(214) Khan, H.; Barna, T.; Bruce, N. C.; Munro, A. W.; Leys, D.; Scrutton, N. S. Proton Transfer in the Oxidative Half-Reaction of Pentaerythritol Tetranitrate Reductase. Structure of the Reduced Enzyme-Progesterone Complex and the Roles of Residues Tyr186, His181 and His184. *FEBS J.* **2005**, *272* (18), 4660–4671.

(215) Fryszkowska, A.; Toogood, H.; Sakuma, M.; Stephens, G. M.; Gardiner, J. M.; Scrutton, N. S. Active Site Modifications in Pentaerythritol Tetranitrate Reductase Can Lead to Improved Product Enantiopurity, Decreased by-Product Formation and Altered Stereochemical Outcome in Reactions with α,β-Unsaturated Nitroolefins. *Catal. Sci. Technol.* **2011**, *1* (6), 948–957.

(216) Hyberts, S. G.; Robson, S. A.; Wagner, G. Exploring Signal-to-Noise Ratio and Sensitivity in Non-Uniformly Sampled Multi-Dimensional NMR Spectra. *J. Biomol. NMR* **2013**, *55* (2), 167–178.

(217) Markley, J. L.; Bax, A.; Arata, Y.; Hilbers, C. W.; Kaptein, R.; Sykes, B. D.; Wright, P. E.; Wüthrich, K. Recommendations for the Presentation of NMR Structures of Proteins and Nucleic Acids – IUPAC-IUBMB-IUPAB Inter-Union Task Group on the Standardization of Data Bases of Protein and Nucleic Acid Structures Determined by NMR Spectroscopy. *J. Biomol. NMR* **1998**, *12* (1), 1–23.

(218) Vranken, W. F.; Boucher, W.; Stevens, T. J.; Fogh, R. H.; Pajon, A.; Llinas, M.; Ulrich, E. L.; Markley, J. L.; Ionides, J.; Laue, E. D. The CCPN Data Model for NMR Spectroscopy: Development of a Software Pipeline. *Proteins Struct. Funct. Bioinforma.* **2005**, *59* (4), 687–696.

(219) Sprangers, R.; Kay, L. E. Quantitative Dynamics and Binding Studies of the 20S Proteasome by NMR. *Nature* **2007**, *445* (7128), 618–622.

(220) Kwon, H.; Smith, O.; Raven, E. L.; Moody, P. C. E. E. Combining X-Ray and Neutron Crystallography with Spectroscopy. *Acta Crystallogr. Sect. D Struct. Biol.* **2017**, *73* (2), 141–147.

(221) Shen, Y.; Bax, A. Protein Backbone and Sidechain Torsion Angles Predicted from NMR Chemical Shifts Using Artificial Neural Networks. *J. Biomol. NMR* **2013**, *56* (3), 227–241.

(222) Warshel, A.; Sharma, P. K.; Kato, M.; Xiang, Y.; Liu, H.; Olsson, M. H. M. Electrostatic Basis for Enzyme Catalysis. *Chem. Rev.* **2006**, *106* (8), 3210–3235.

(223) Klinman, J. P. Dynamically Achieved Active Site Precision in Enzyme Catalysis. *Acc. Chem. Res.* **2015**, *48* (2), 449–456.

(224) Warshel, A.; Bora, R. P. Perspective: Defining and Quantifying the Role of Dynamics in Enzyme Catalysis Perspective: Found in Translation: Quantum Chemical Tools for Grasping Non-Covalent Interactions Perspective: Defining and Quantifying the Role of Dynamics in Enzyme Catalysis. *J. Chem. Phys. J. Chem. Phys. J. Chem. Phys. J. Chem. Phys.* **2016**, *144* (144), 180901–140901.

(225) Knaus, T.; Paul, C. E.; Levy, C. W.; De Vries, S.; Mutti, F. G.; Hollmann, F.; Scrutton, N. S. Better than Nature: Nicotinamide Biomimetics That Outperform Natural Coenzymes. *J. Am. Chem. Soc.* **2016**, *138* (3), 1033–1039.

(226) Nguyen, V.; Wilson, C.; Hoemberger, M.; Stiller, J. B.; Agafonov, R. V.; Kutter, S.; English, J.; Theobald, D. L.; Kern, D. Evolutionary Drivers of Thermoadaptation in Enzyme Catalysis. *Science* **2017**, *355* (6322), 289–294.

(227) Firestone, R. S.; Cameron, S. A.; Karp, J. M.; Arcus, V. L.; Schramm, V. L. Heat Capacity Changes for Transition-State Analogue Binding and Catalysis with Human 5′-Methylthioadenosine Phosphorylase. *ACS Chem. Biol.* **2017**, *12* (2), 464–473.

(228) Van Der Kamp, M. W.; Prentice, E. J.; Kraakman, K. L.; Connolly, M.; Mulholland, A. J.; Arcus, V. L. Dynamical Origins of Heat Capacity Changes in Enzyme-Catalysed Reactions. *Nat. Commun.* **2018**, *9* (1), 1–7.

(229) Williamson, M. P. Using Chemical Shift Perturbation to Characterise Ligand Binding. *Prog. Nucl. Magn. Reson. Spectrosc.* **2013**, *73*, 1–16.

(230) Nagel, Z. D.; Dong, M.; Bahnson, B. J.; Klinman, J. P. Impaired Protein Conformational Landscapes as Revealed in Anomalous Arrhenius Prefactors. *Proc. Natl. Acad. Sci.* **2011**, *108* (26), 10520–10525.

(231) Roston, D.; Cheatum, C. M.; Kohen, A. Hydrogen Donor-Acceptor Fluctuations from Kinetic Isotope Effects: A Phenomenological Model. *Biochemistry* **2012**, *51* (34), 6860–6870.

(232) Cameron, C. E.; Benkovic, S. J. Evidence for a Functional Role of the Dynamics of Glycine-121 of Escherichia Coli Dihydrofolate Reductase Obtained from Kinetic Analysis of a Site-Directed Mutant. *Biochemistry* **1997**, *36* (50), 15792–15800.

(233) Rajagopalan, P. T. R.; Lutz, S.; Benkovic, S. J. Coupling Interactions of Distal Residues Enhance Dihydrofolate Reductase Catalysis: Mutational Effects on Hydride Transfer Rates. *Biochemistry* **2002**, *41* (42), 12618–12628.

(234) Boehr, D. D.; Schnell, J. R.; McElheny, D.; Bae, S. H.; Duggan, B. M.; Benkovic, S. J.; Dyson, H. J.; Wright, P. E. A Distal Mutation Perturbs Dynamic Amino Acid Networks in Dihydrofolate Reductase. *Biochemistry* **2013**, *52* (27), 4605–4619.

(235) Pudney, C. R.; Hay, S.; Scrutton, N. S. Practical Aspects on the Use of Kinetic Isotope Effects as Probes of Flavoprotein Enzyme Mechanisms. *Methods Mol. Biol.* **2014**, *1146*, 161–175.

(236) Winter, G. Xia2: An Expert System for Macromolecular Crystallography Data Reduction. *J. Appl. Crystallogr.* **2010**, *43* (1), 186–190.

(237) McCoy, A. J.; Grosse-Kunstleve, R. W.; Adams, P. D.; Winn, M. D.; Storoni, L. C.; Read, R. J. Phaser Crystallographic Software. *J. Appl. Crystallogr.* **2007**, *40* (4), 658–674.

(238) Emsley, P.; Lohkamp, B.; Scott, W. G.; Cowtan, K. Features and Development of Coot. *Acta Crystallogr. Sect. D Biol. Crystallogr.* **2010**, *66* (4), 486–501.

(239) Afonine, P. V.; Grosse-Kunstleve, R. W.; Echols, N.; Headd, J. J.; Moriarty, N. W.; Mustyakimov, M.; Terwilliger, T. C.; Urzhumtsev, A.; Zwart, P. H.; Adams, P. D. Towards Automated Crystallographic Structure Refinement with Phenix.Refine. *Acta Crystallogr. Sect. D Biol. Crystallogr.* **2012**, *68* (4), 352–367.

(240) Chen, V. B.; Arendall, W. B.; Headd, J. J.; Keedy, D. A.; Immormino, R. M.; Kapral, G. J.; Murray,

L. W.; Richardson, J. S.; Richardson, D. C. MolProbity: All-Atom Structure Validation for Macromolecular Crystallography. *Acta Crystallogr. Sect. D Biol. Crystallogr.* **2010**, *66* (1), 12–21.

(241) Joosten, R. P.; Long, F.; Murshudov, G. N.; Perrakis, A. The *PDB_REDO* Server for Macromolecular Structure Model Optimization. *IUCrJ* **2014**, *1* (4), 213–220.

(242) Stuermer, R.; Hauer, B.; Hall, M.; Faber, K. Asymmetric Bioreduction of Activated C=C Bonds Using Enoate Reductases from the Old Yellow Enzyme Family. *Curr. Opin. Chem. Biol.* **2007**, *11* (2), 203–213.

(243) Winkler, C. K.; Faber, K.; Hall, M. Biocatalytic Reduction of Activated C[Dbnd]C-Bonds and beyond: Emerging Trends. *Curr. Opin. Chem. Biol.* **2018**, *43*, 97–105.

(244) Williams, R. E.; Rathbone, D. A.; Scrutton, N. S.; Bruce, N. C. Biotransformation of Explosives by the Old Yellow Enzyme Family of Flavoproteins. *Appl. Environ. Microbiol.* **2004**, *70* (6), 3566–3574.

(245) Hummel, W.; Gröger, H. Strategies for Regeneration of Nicotinamide Coenzymes Emphasizing Self-Sufficient Closed-Loop Recycling Systems. *J. Biotechnol.* **2014**, *191*, 22–31.

(246) Kara, S.; Schrittwieser, J. H.; Gargiulo, S.; Ni, Y.; Yanase, H.; Opperman, D. J.; van Berkel, W. J. H.; Hollmann, F. Complete Enzymatic Oxidation of Methanol to Carbon Dioxide: Towards More Eco-Efficient Regeneration Systems for Reduced Nicotinamide Cofactors. *Adv. Synth. Catal.* **2015**, *357* (8), 1687–1691.

(247) Toogood, H. S.; Knaus, T.; Scrutton, N. S. Alternative Hydride Sources for Ene-Reductases: Current Trends. *ChemCatChem* **2014**, *6* (4), 951–954.

(248) Paul, C. E.; Gargiulo, S.; Opperman, D. J.; Lavandera, I.; Gotor-Fernández, V.; Gotor, V.; Taglieber, A.; Arends, I. W. C. E.; Hollmann, F. Mimicking Nature: Synthetic Nicotinamide Cofactors for C═C Bioreduction Using Enoate Reductases. *Org. Lett.* **2013**, *15* (1), 180–183.

(249) Stueckler, C.; Reiter, T. C.; Baudendistel, N.; Faber, K. Nicotinamide-Independent Asymmetric Bioreduction of CC-Bonds via Disproportionation of Enones Catalyzed by Enoate Reductases. *Tetrahedron* **2010**, *66* (3), 663–667.

(250) Lee, S. H.; Choi, D. S.; Pesic, M.; Lee, Y. W.; Paul, C. E.; Hollmann, F.; Park, C. B. Cofactor-Free, Direct Photoactivation of Enoate Reductases for the Asymmetric Reduction of C=C Bonds. *Angew. Chemie Int. Ed.* **2017**, *56* (30), 8681–8685.

(251) Peers, M. K.; Toogood, H. S.; Heyes, D. J.; Mansell, D.; Coe, B. J.; Scrutton, N. S. Light-Driven Biocatalytic Reduction of α,β-Unsaturated Compounds by Ene Reductases Employing Transition Metal Complexes as Photosensitizers. *Catal. Sci. Technol.* **2016**, *6* (1), 169–177.

(252) Brigé, A.; Van Den Hemel, D.; Carpentier, W.; De Smet, L.; Van Beeumen, J. J. Comparative Characterization and Expression Analysis of the Four Old Yellow Enzyme Homologues from Shewanella Oneidensis Indicate Differences in Physiological Function. *Biochem. J.* **2006**, *394* (1), 335–344.

(253) Snape, J. R.; Walkley, N. A.; Morby, A. P.; Nicklin, S.; White, G. F. Purification, Properties, and Sequence of Glycerol Trinitrate Reductase from Agrobacterium Radiobacter. *J. Bacteriol.* **1997**, *179* (24), 7796 LP-7802.

(254) French, C. E.; Bruce, N. C. Purification and Characterization of Morphinone Reductase from Pseudomonas Putida M10. *Biochem. J.* **1994**, *301 (Pt 1*, 97–103.

(255) Scrutton, N. S.; Berry, A.; Perham, R. N. Redesign of the Coenzyme Specificity of a Dehydrogenase by Protein Engineering. *Nature* **1990**, *343* (6253), 38–43.

(256) Mittl, P. R. E.; Berry, A.; Scrutton, N. S.; Perham, R. N.; Schulz, G. E. Anatomy of an Engineered NAD-Binding Site. *Protein Sci.* **2018**, *3* (9), 1504–1514.

(257) Cahn, J. K. B.; Werlang, C. A.; Baumschlager, A.; Brinkmann-Chen, S.; Mayo, S. L.; Arnold, F. H. A General Tool for Engineering the NAD/NADP Cofactor Preference of Oxidoreductases. *ACS*

Synth. Biol. **2017**, *6* (2), 326–333.

(258) Wimpenny, J. W. T.; Firth, A.; Wimpenny JW; Firth A. Levels of Nicotinamide Adenine Dinucleotide and Reduced Nicotinamide Adenine Dinucleotide in Facultative Bacteria and the Effect of Oxygen. *J. Bacteriol.* **1972**, *111* (1), 24–32.

(259) Yamada, K.; Hara, N.; Shibata, T.; Osago, H.; Tsuchiya, M. The Simultaneous Measurement of Nicotinamide Adenine Dinucleotide and Related Compounds by Liquid Chromatography/Electrospray Ionization Tandem Mass Spectrometry. *Anal. Biochem.* **2006**, *352* (2), 282–285.

(260) Pire, C.; Esclapez, J.; Díaz, S.; Pérez-Pomares, F.; Ferrer, J.; Bonete, M. J. Alteration of Coenzyme Specificity in Halophilic NAD(P)+ Glucose Dehydrogenase by Site-Directed Mutagenesis. *J. Mol. Catal. B Enzym.* **2009**, *59* (4), 261–265.

(261) Chen, R.; Greer, A. F.; Dean, A. M.; Hurley, J. H. Engineering Secondary Structure to Invert Coenzyme Specificity in Isopropylmalate Dehydrogenase. *Tech. Protein Chem.* **1997**, *8* (C), 809–816.

(262) McWilliam, H.; Li, W.; Uludag, M.; Squizzato, S.; Park, Y. M.; Buso, N.; Cowley, A. P.; Lopez, R. Analysis Tool Web Services from the EMBL-EBI. *Nucleic Acids Res.* **2013**, *41* (Web Server issue), W597-600.

(263) Robert, X.; Gouet, P. Deciphering Key Features in Protein Structures with the New ENDscript Server. *Nucleic Acids Res.* **2014**, *42* (W1), 320–324.

(264) Vos, M. H.; Liebl, U. Time-Resolved Infrared Spectroscopic Studies of Ligand Dynamics in the Active Site from Cytochrome c Oxidase. *Biochim. Biophys. Acta - Bioenerg.* **2015**, *1847* (1), 79–85.

(265) Kötting, C.; Güldenhaupt, J.; Gerwert, K. Time-Resolved FTIR Spectroscopy for Monitoring Protein Dynamics Exemplified by Functional Studies of Ras Protein Bound to a Lipid Bilayer. *Chem. Phys.* **2012**, *396* (1), 72–83.

(266) Noguchi, T.; Suzuki, H.; Tsuno, M.; Sugiura, M.; Kato, C. Time-Resolved Infrared Detection of the Proton and Protein Dynamics during Photosynthetic Oxygen Evolution. *Biochemistry* **2012**, *51* (15), 3205–3214.

Appendix

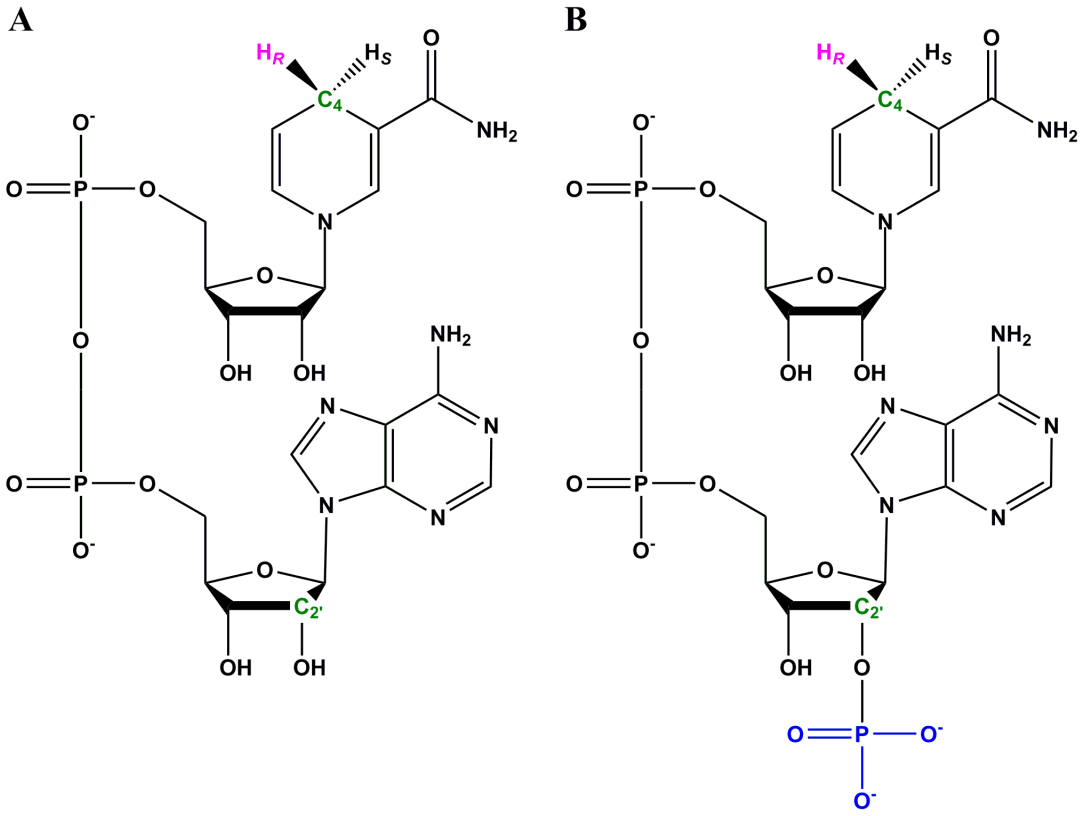

Figure A1. Chemical structures of NADH (A) and NADPH (B). Note that the only structural difference between the two coenzymes is the presence of a 2'-phosphate group (shown in blue) on the ribose ring of the adenosine moiety in NADPH. Key atoms (C_4, $C_{2'}$, and *pro*-R H) are highlighted.

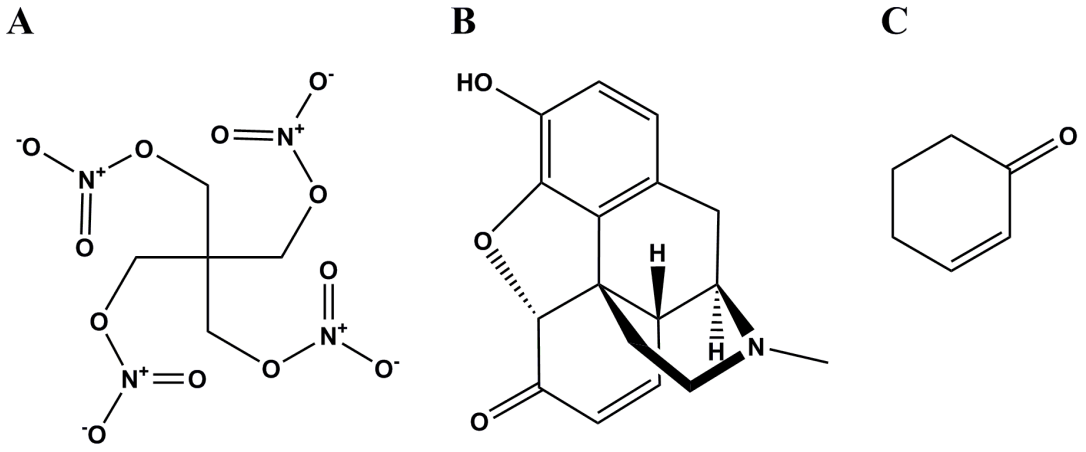

Figure A2. Chemical structures of pentaerythritol tetranitrate (A), morphinone (B) and 2-cyclohenexen-1-one (C).

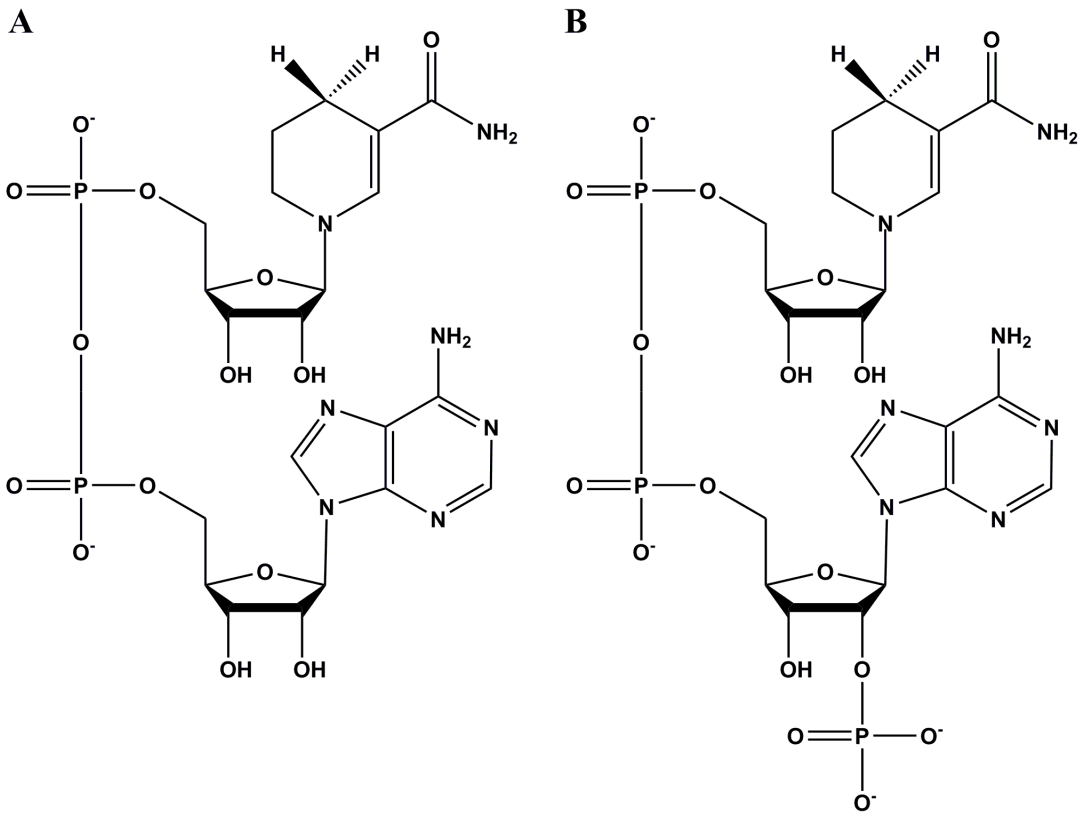

Figure A3. Chemical structures of $NADH_4$ (A) and $NADPH_4$ (B).